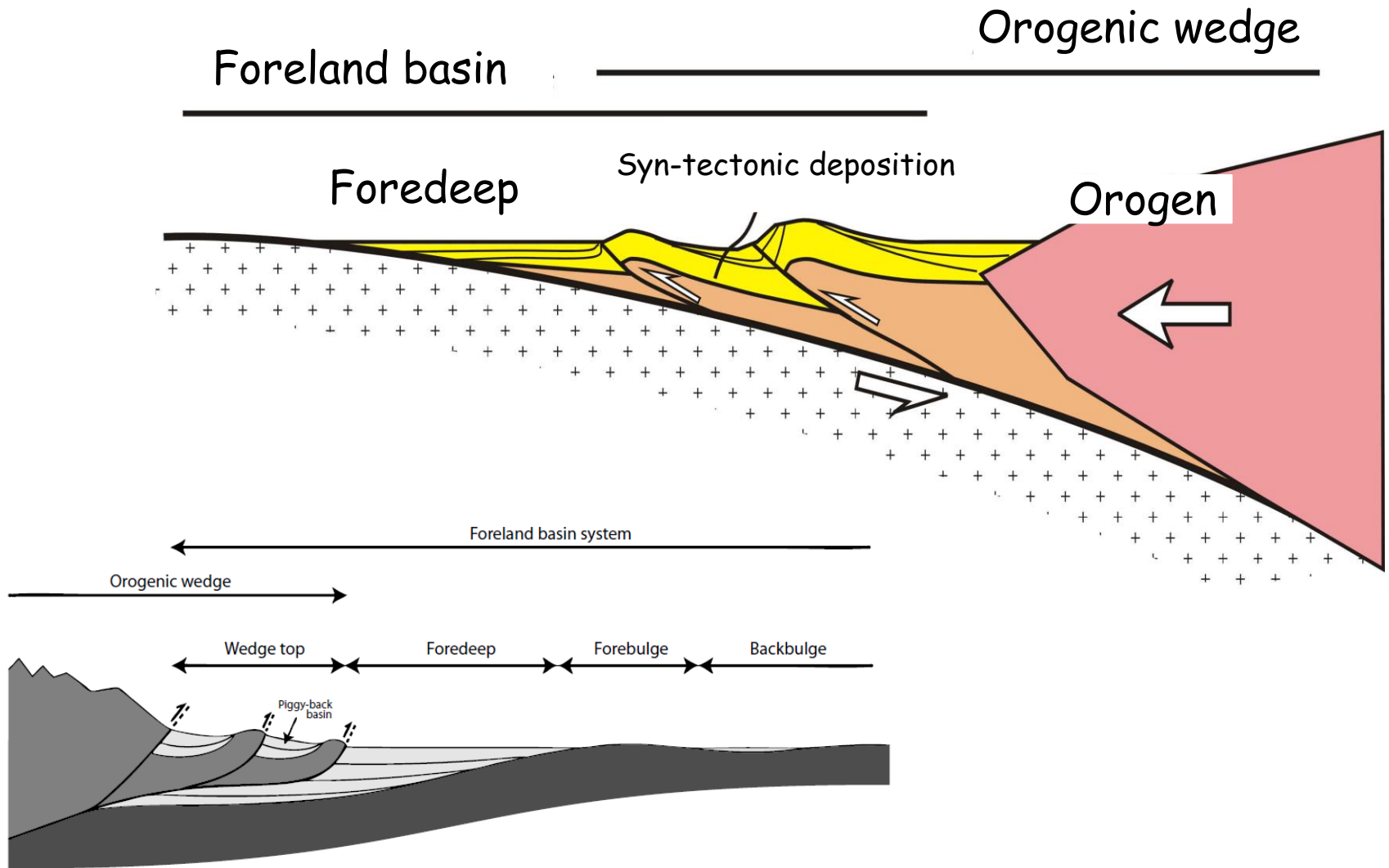


Geometry, kinematics and mechanics of foreland fold-thrust belts : insights from a multisource and multiscale study of the active Zagros fold-thrust belt (Iran).

Prof. Olivier LACOMBE

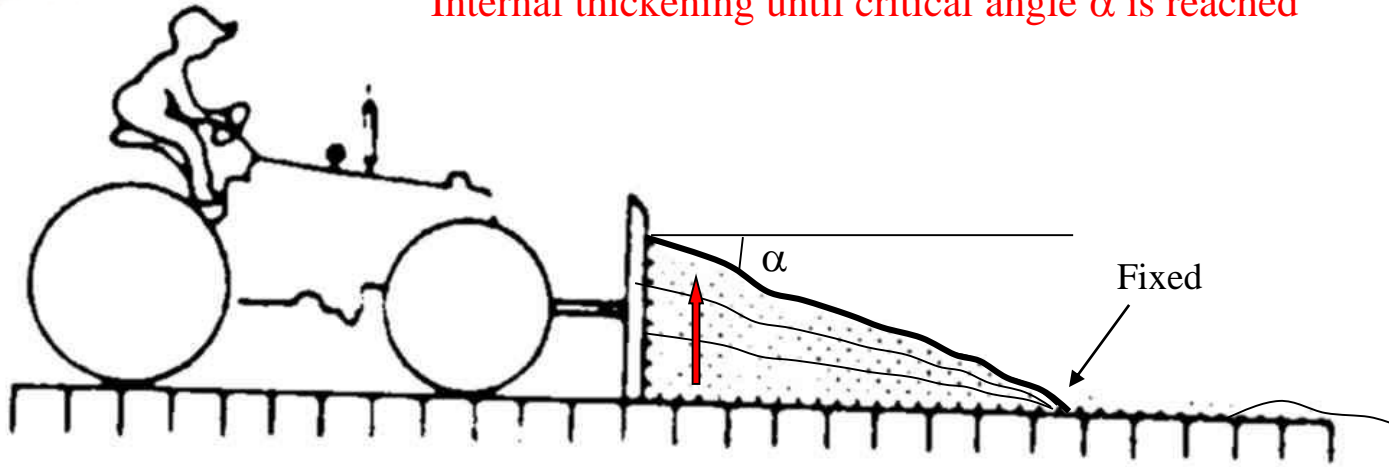


The fold-and-thrust belt / foreland system

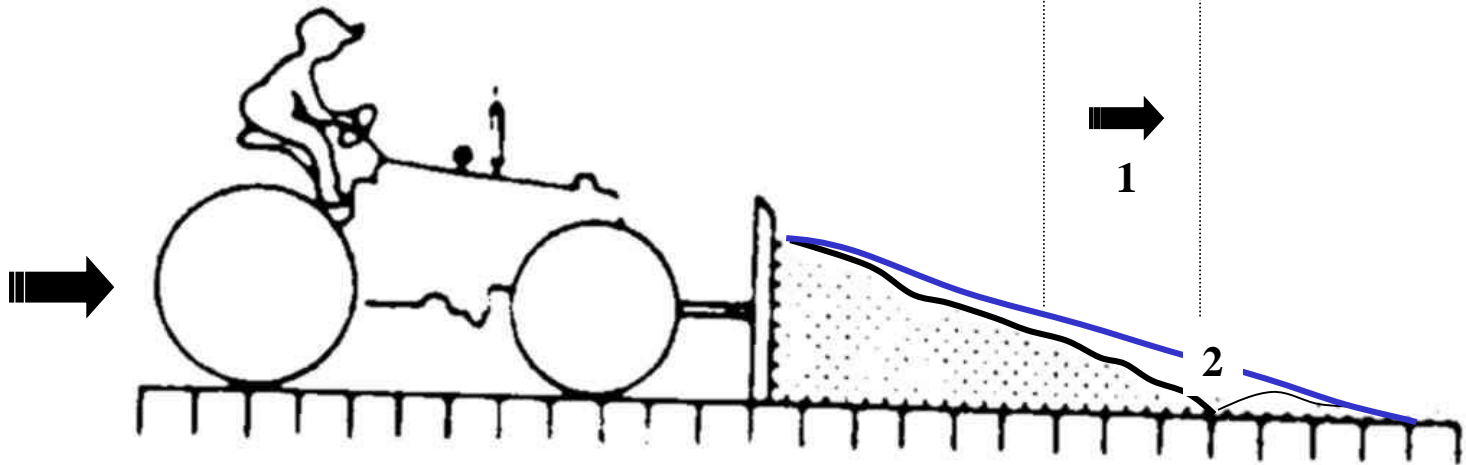


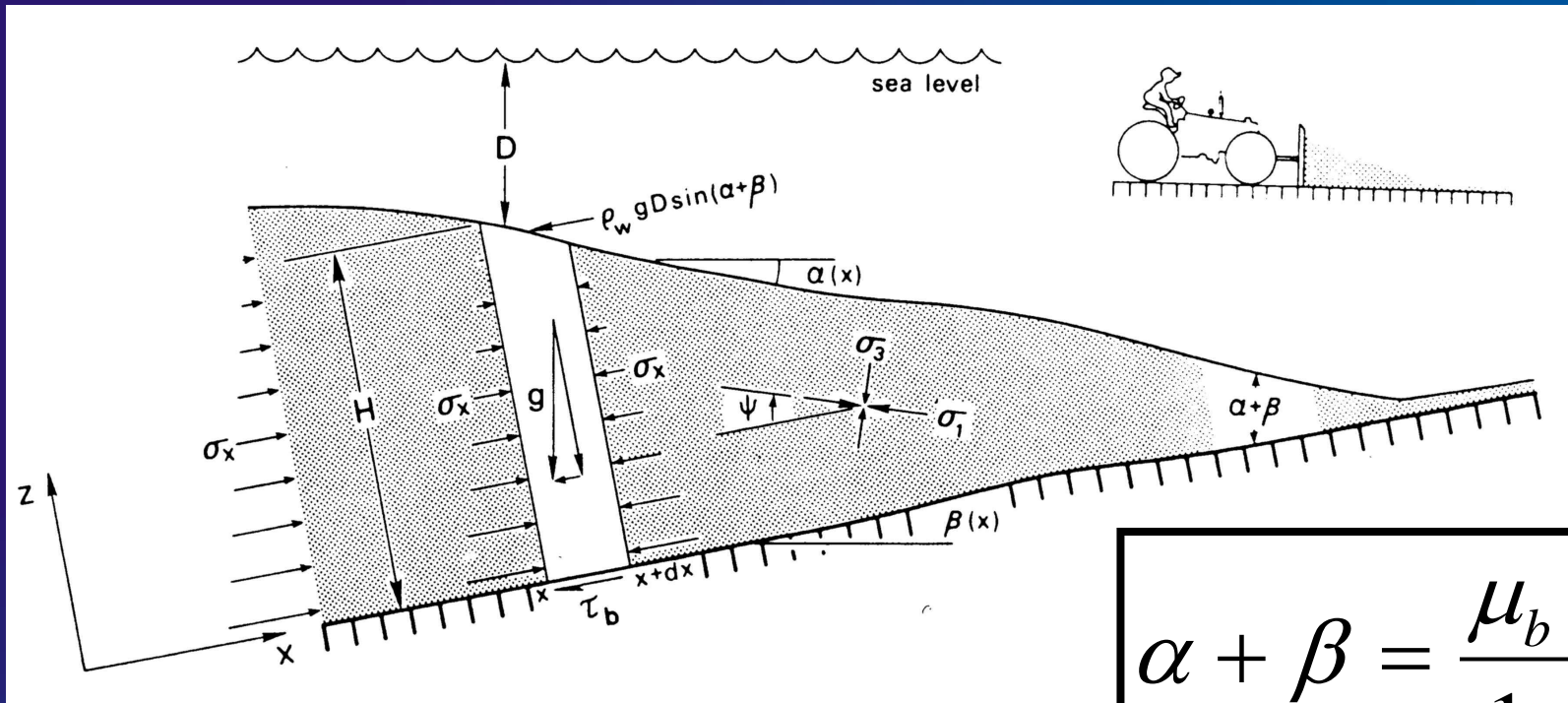


Internal thickening until critical angle α is reached



1. Basal sliding without internal thickening, then
2. New snow is incorporated in the wedge, α is lowered, then
3. The wedge will deform internally until α is reached again, and so on





$$\alpha + \beta = \frac{\mu_b + \beta}{1 + K}$$

for a non-cohesive sub-aerial wedge

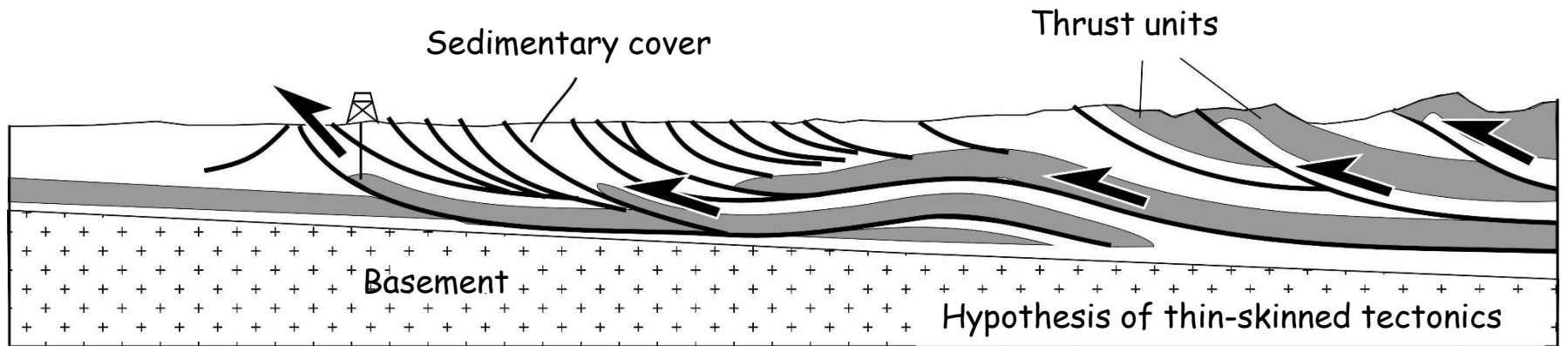
$$\rho g H \beta + \rho_w g D (\alpha + \beta) + \tau_b + \frac{d}{dx} \int_0^H \sigma_x dz = 0$$

Weight of sedimentary column (lithostatic pressure)

Weight of water column

Basal frictional shear strength

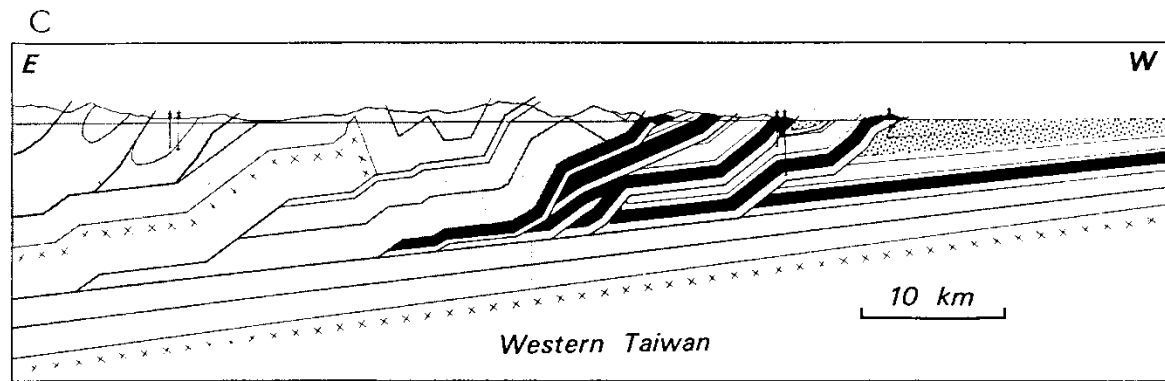
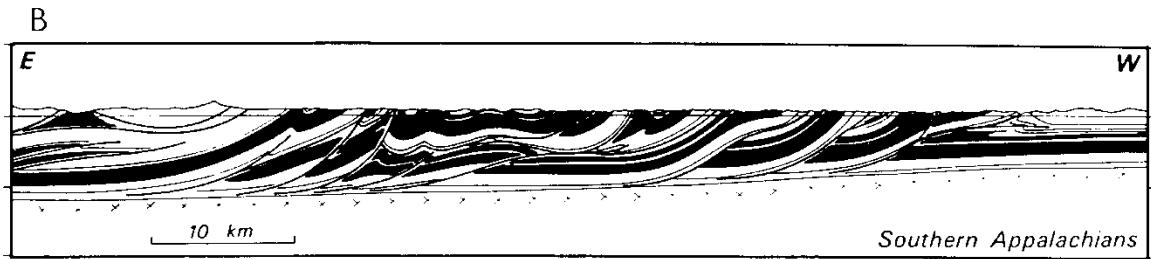
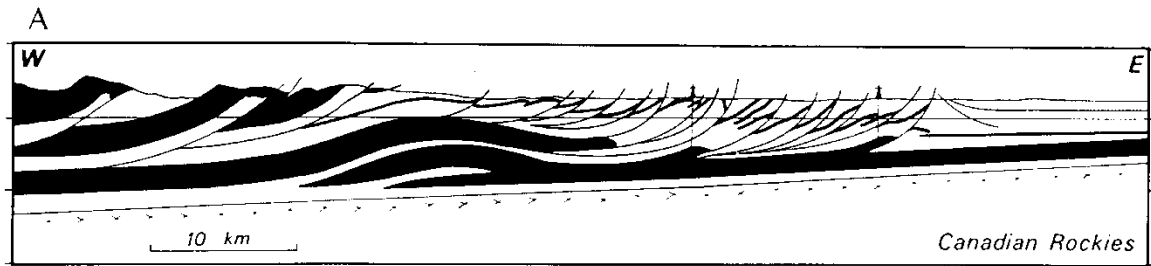
Sum of lateral push forces

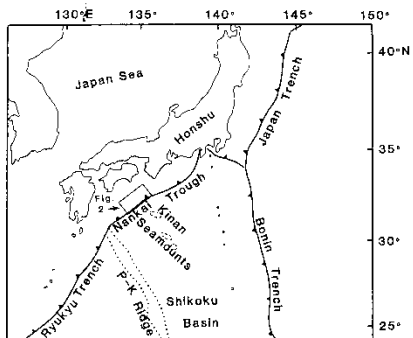
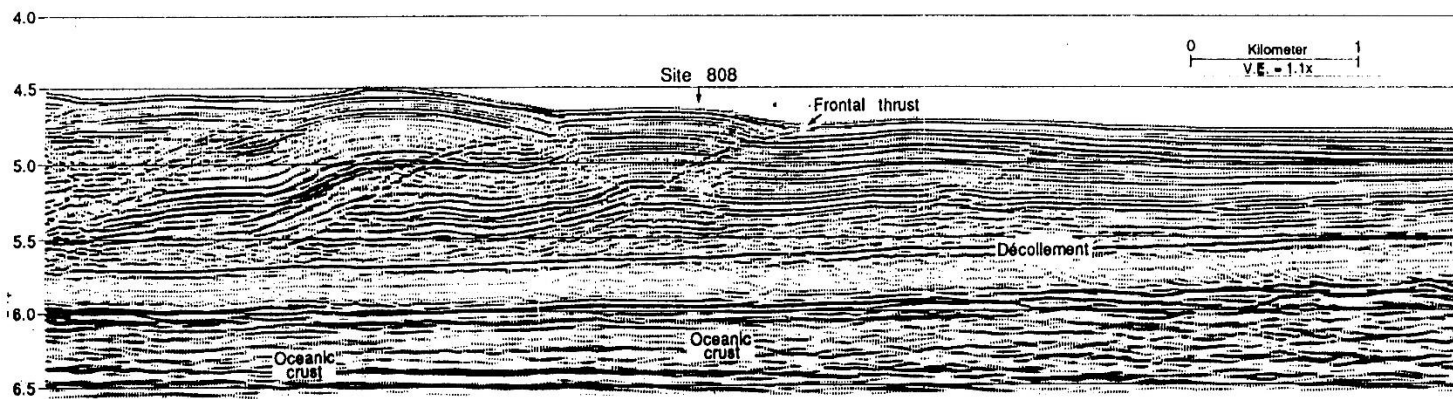


Shortening is accommodated in the upper part of the crust above a basal décollement dipping toward the hinterland

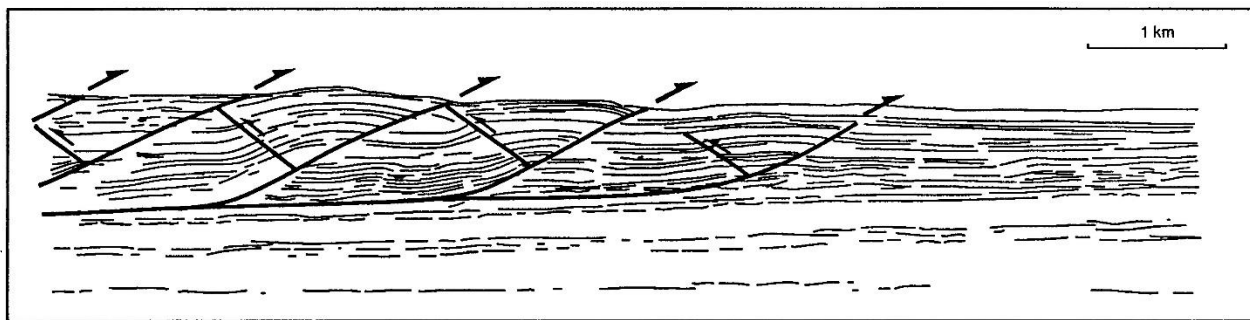
Implicit assumption of « thin-skinned » tectonic style

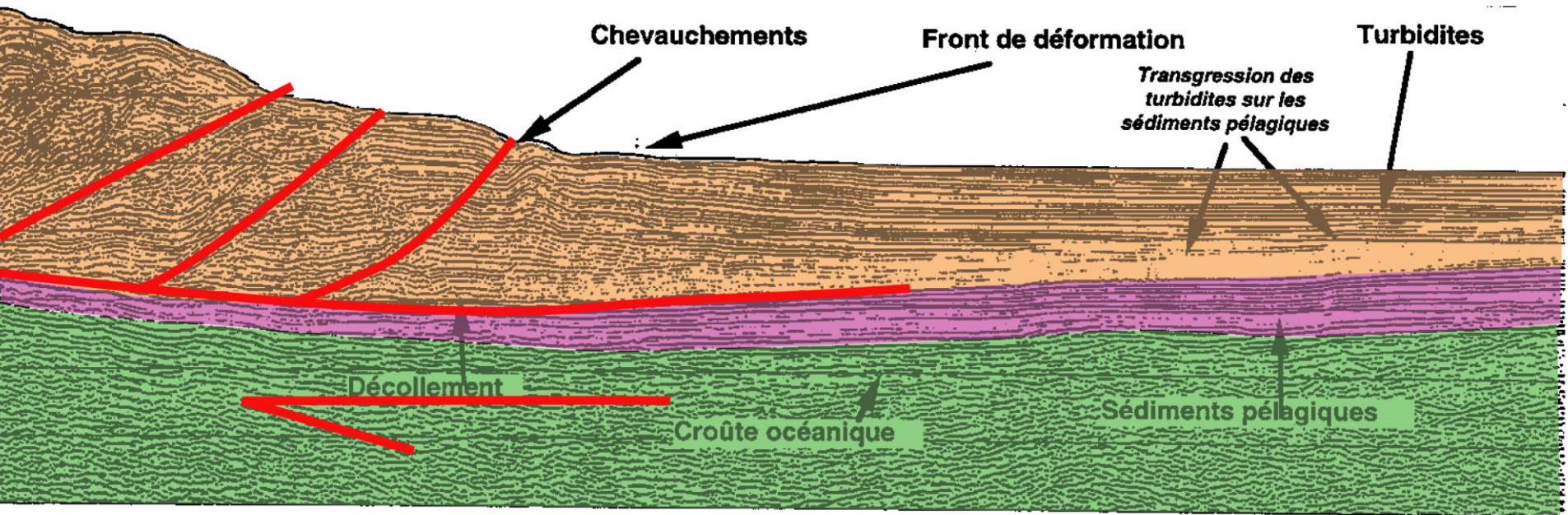
Topographic slope and dip of basal décollement define the orogenic wedge



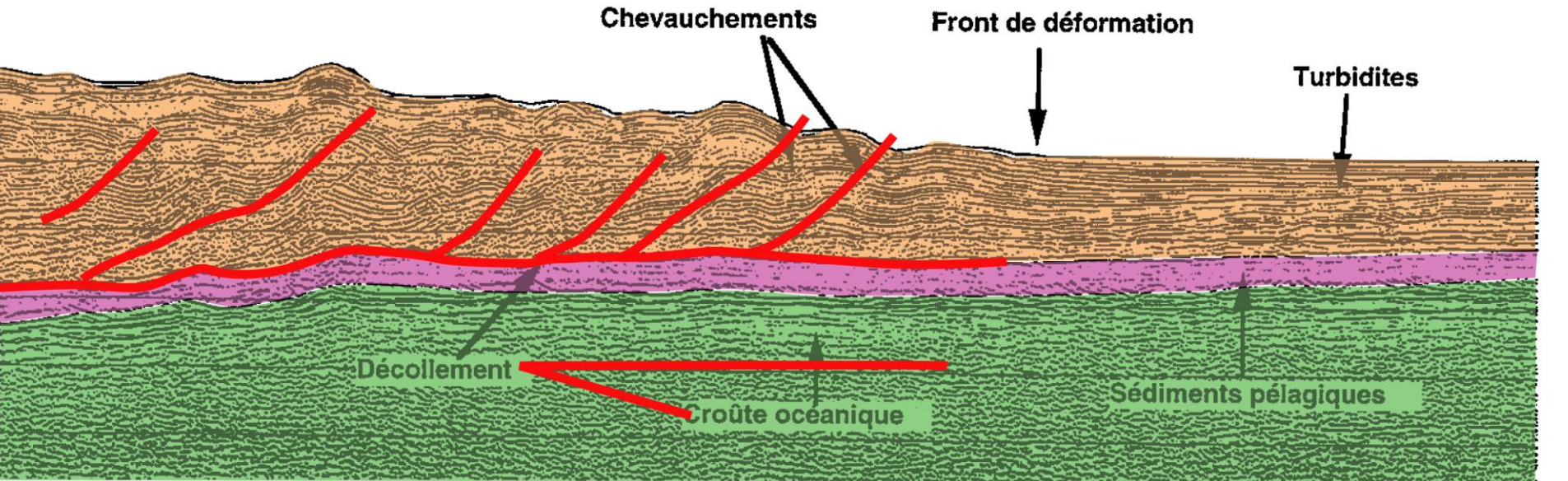


Regional tectonic map showing setting of the Nankai Trough study area (box labeled as Figure 2).





1 km



Conditions de fracturation et état critique

Dans le prisme

➔ **Critère de néorupture (Mohr-Coulomb)**

$$\tau_i = C_o + \mu_c \sigma_n$$

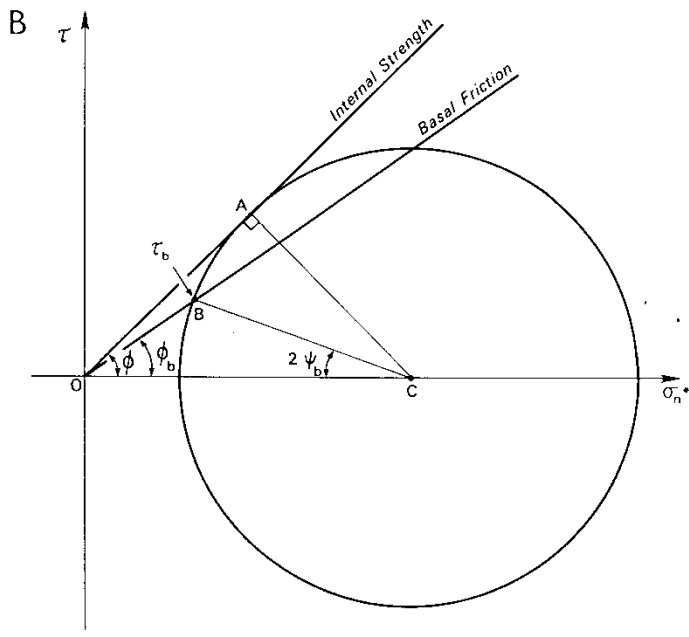
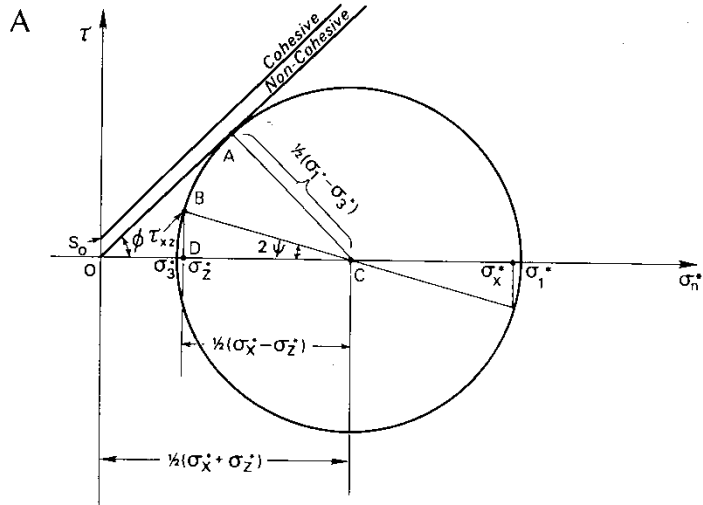
$$\tau_b = C_f + \mu_f \sigma_n$$

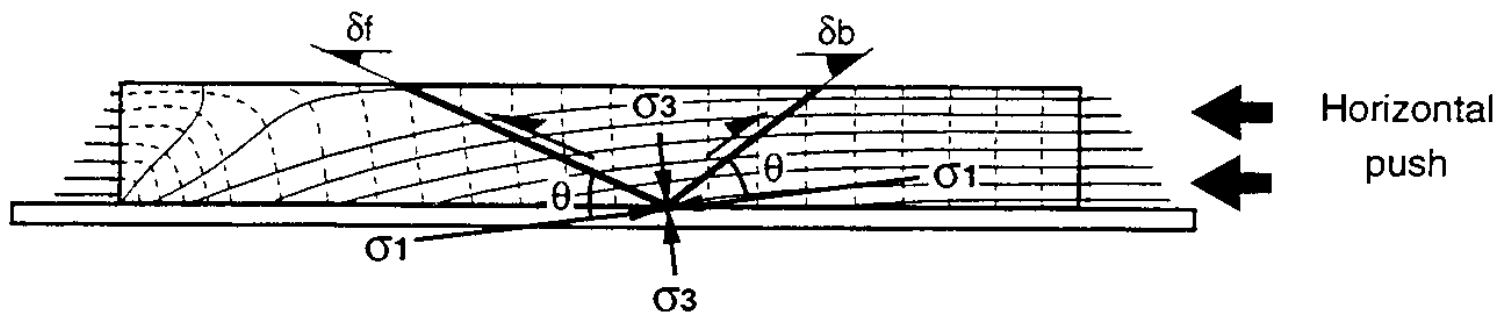
$$\text{avec } \mu_f < \mu_c$$

Le prisme est à l'état critique lorsque le cercle tangente la droite de néorupture

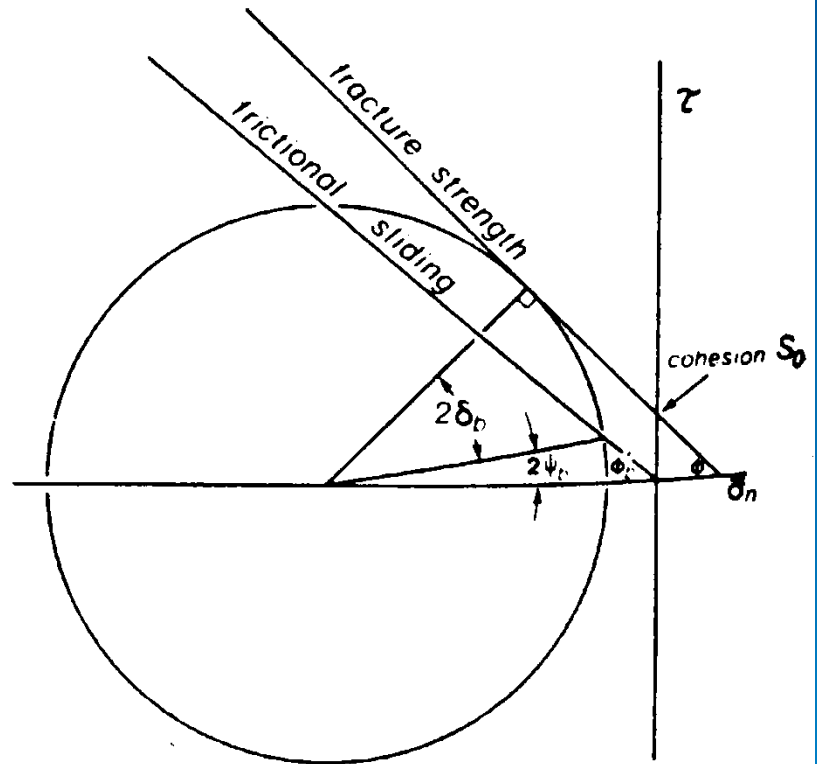
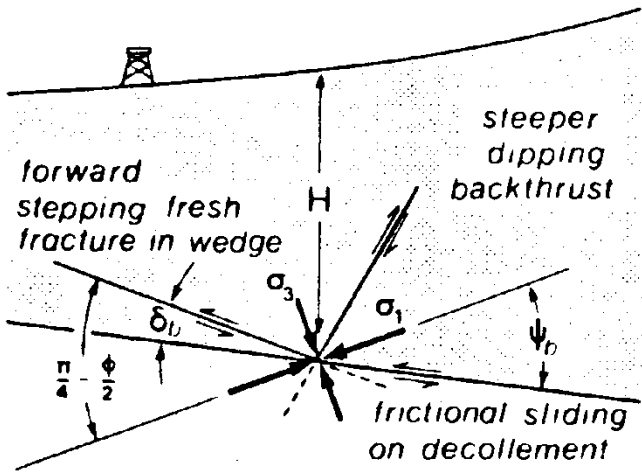
Base du prisme

➔ **Critère de friction**





$$\text{tg } 2\theta = 2 \cdot \tau_b / (\sigma_h - \sigma_v)$$



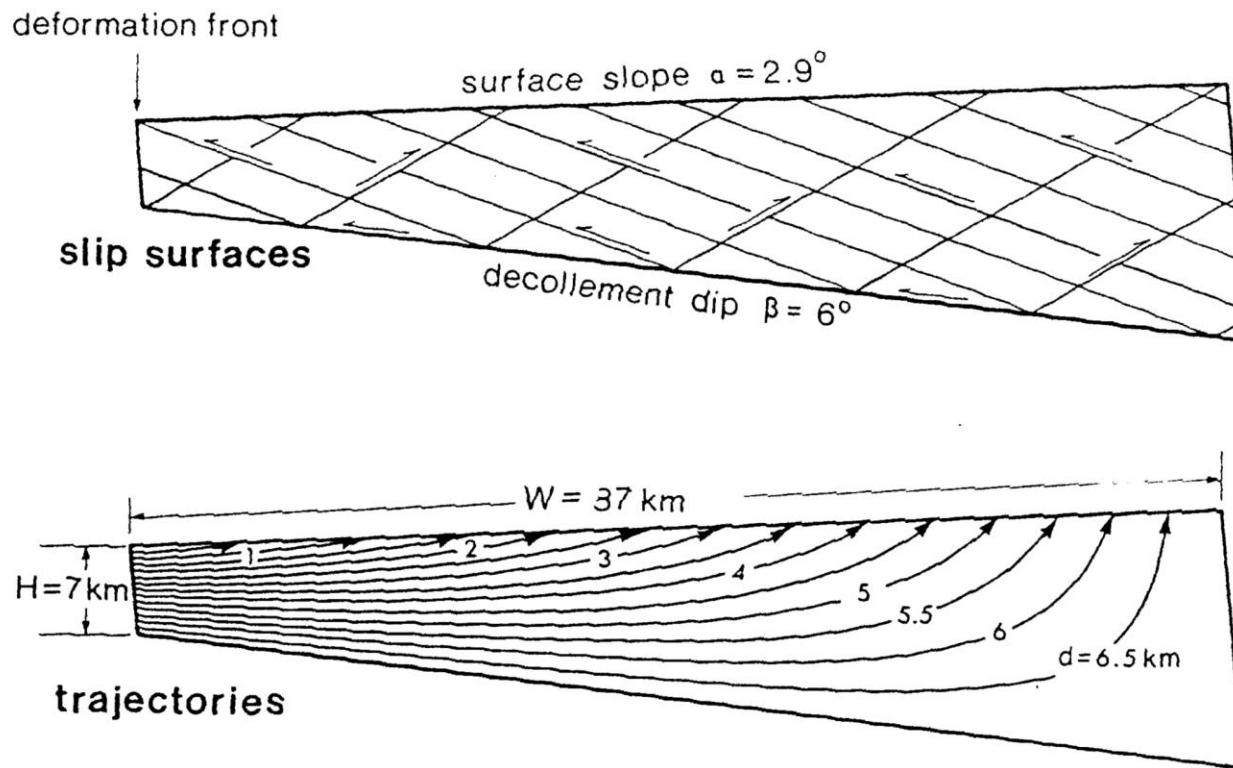
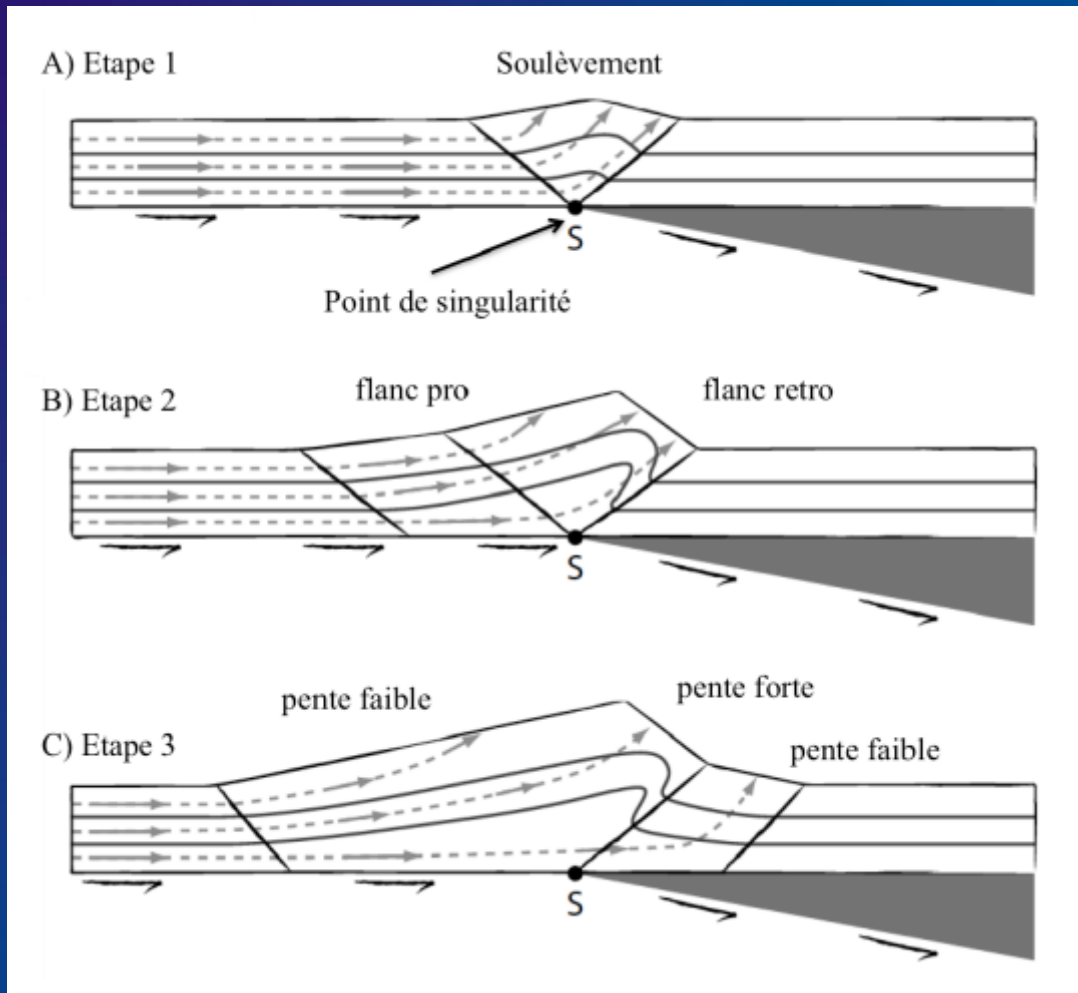
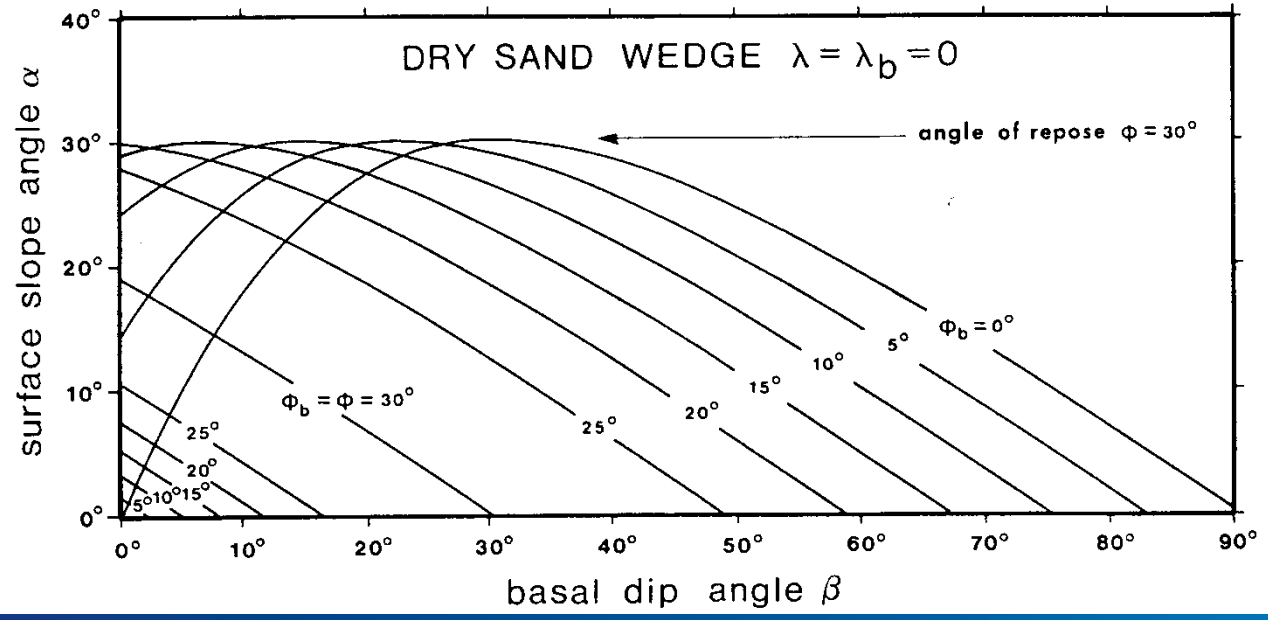
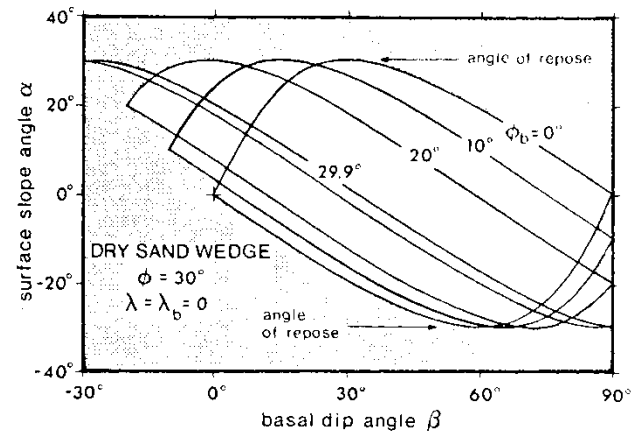
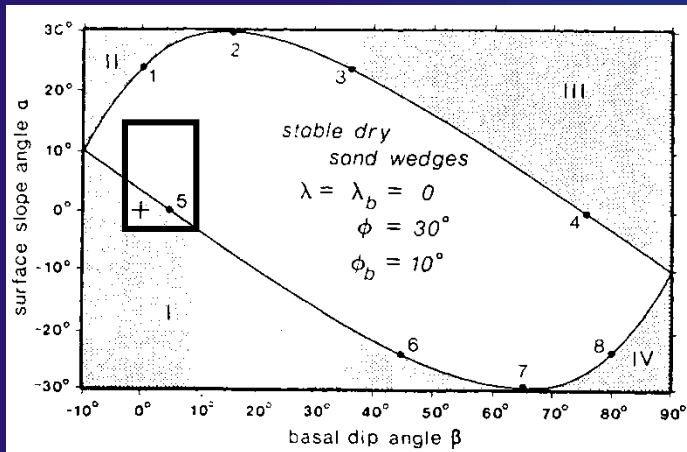


Figure 14. Theoretical slip surfaces and rock trajectories in the critically tapered Taiwan wedge, assuming $\mu = 0.85$.

Dahlen et Suppe, 1988

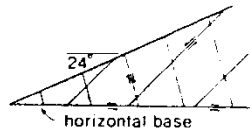




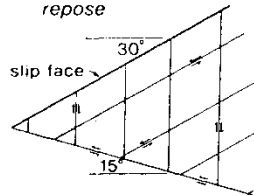


EXAMPLES OF CRITICAL DRY SAND WEDGES

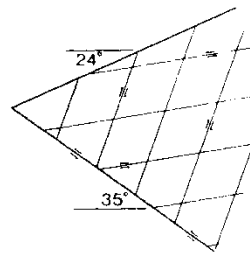
1. normal faulting and downslope flow



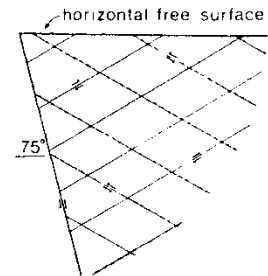
2. surface at angle of repose



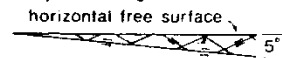
3. combined normal and thrust faulting



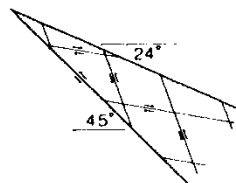
4. thrust faulting



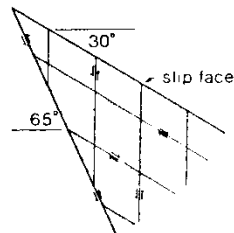
5. accretionary wedge fails by thrusting



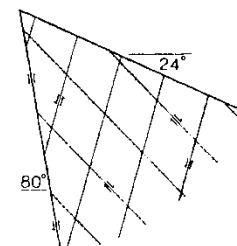
6. combined normal and thrust faulting

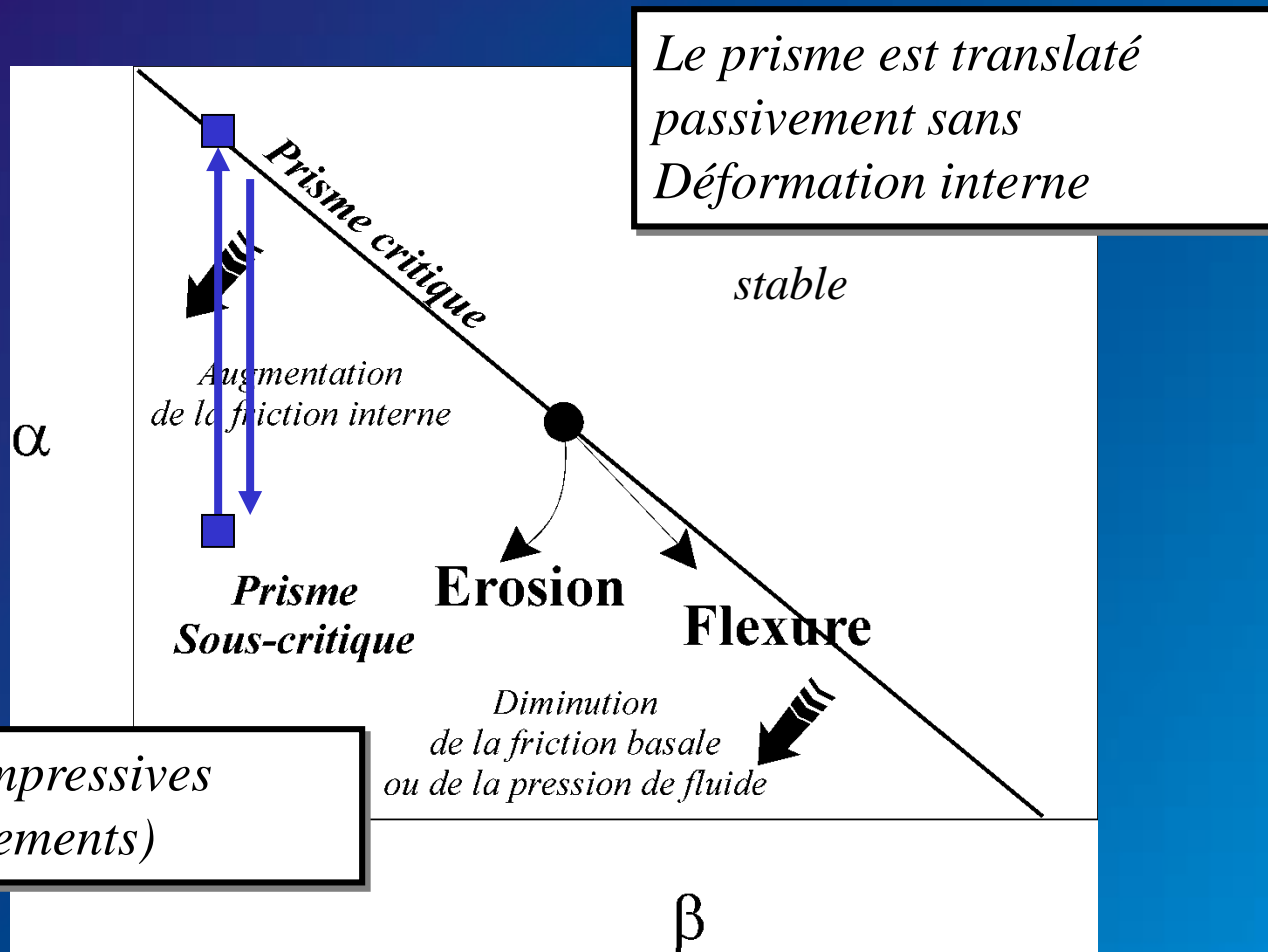


7. surface at angle of repose



8. normal faulting

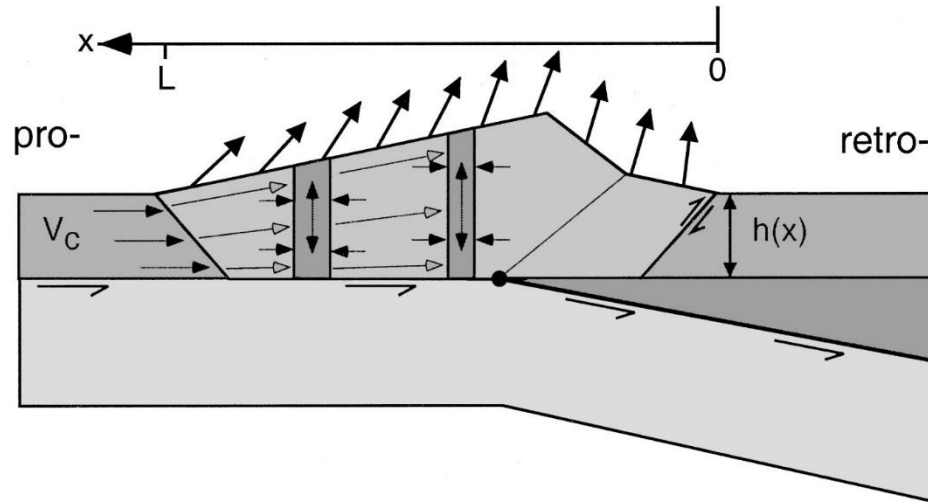




Le prisme est translaté passivement sans Déformation interne

Déformations compressives (Plis et chevauchements)

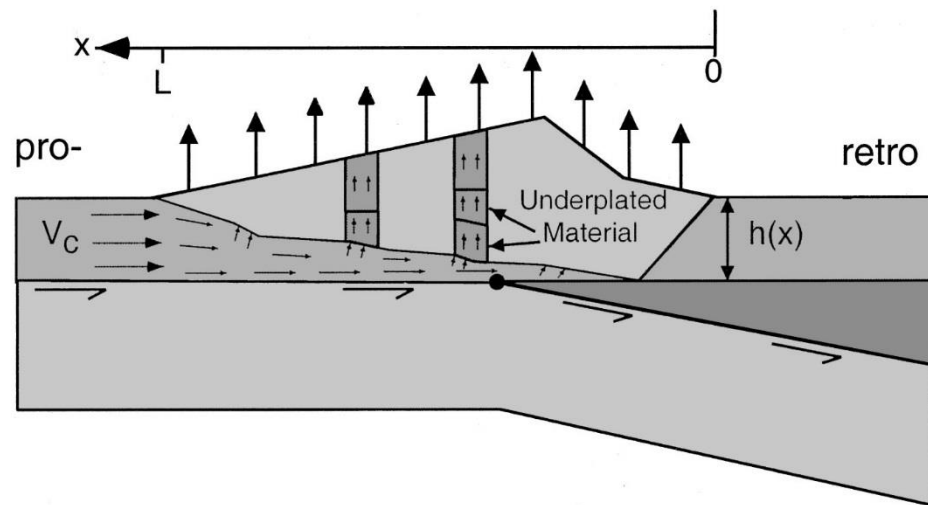
A. Frontal Accretion



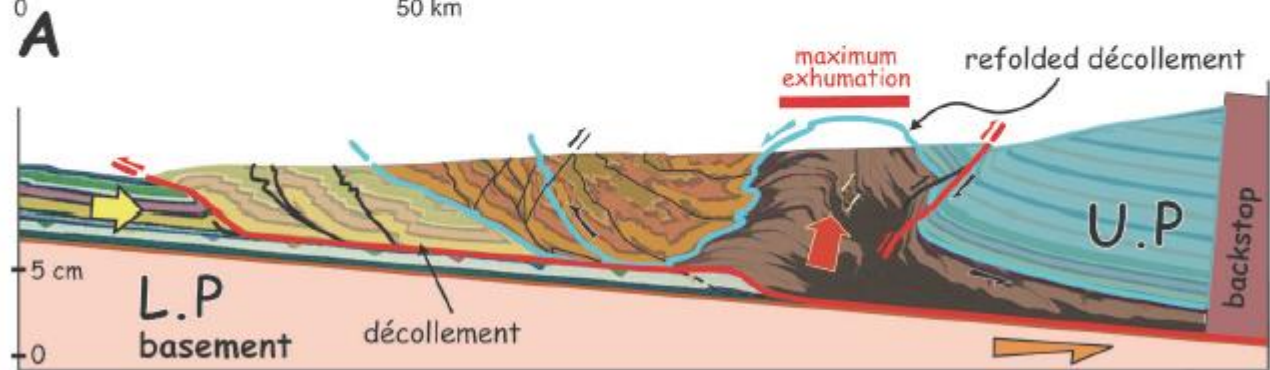
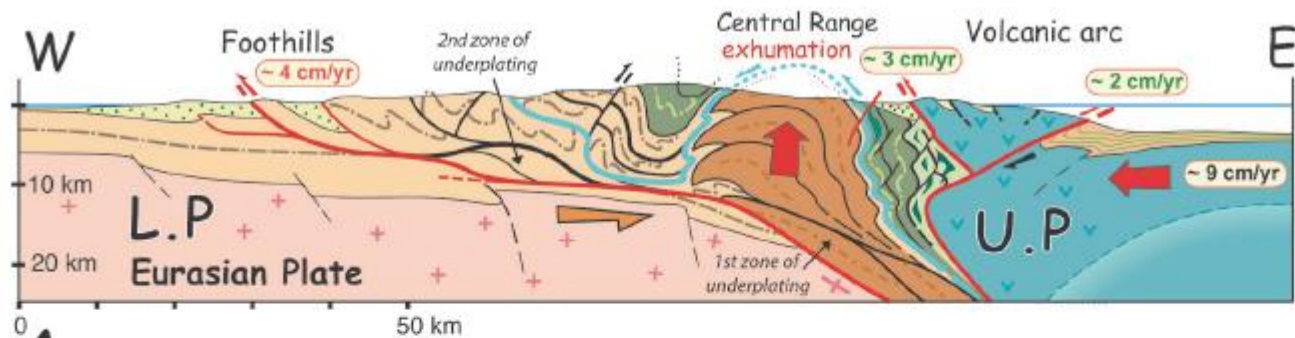
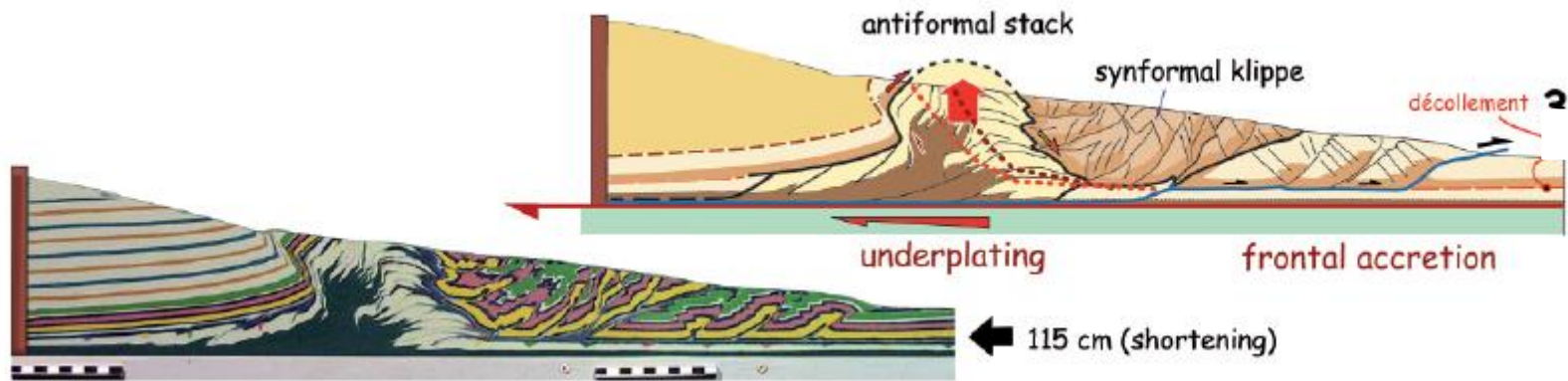
End-member kinematic models of orogenic wedge growth.

A) Frontal accretion. Wedge shortens such that a vertical column extends vertically and shortens horizontally. Vertical component of surface velocity is relatively constant.

B. Underplating

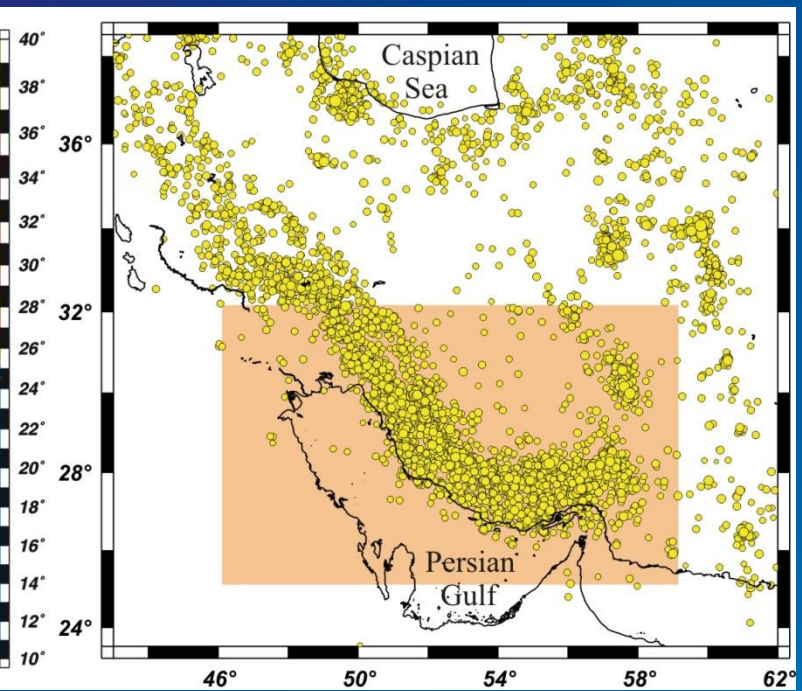
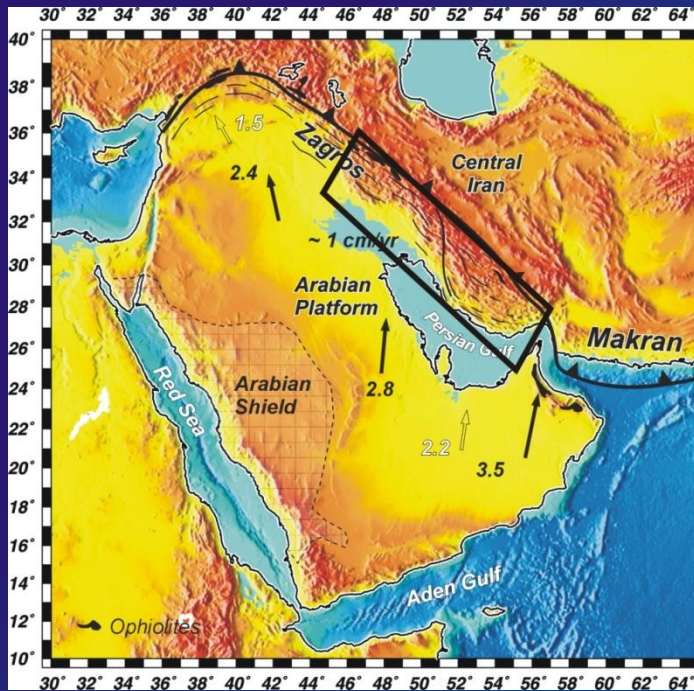


B) Underplating. Wedge does not shorten horizontally and thus has no horizontal velocity. Columns of rock move vertically at a constant rate in response to addition of new material at the base of the wedge.



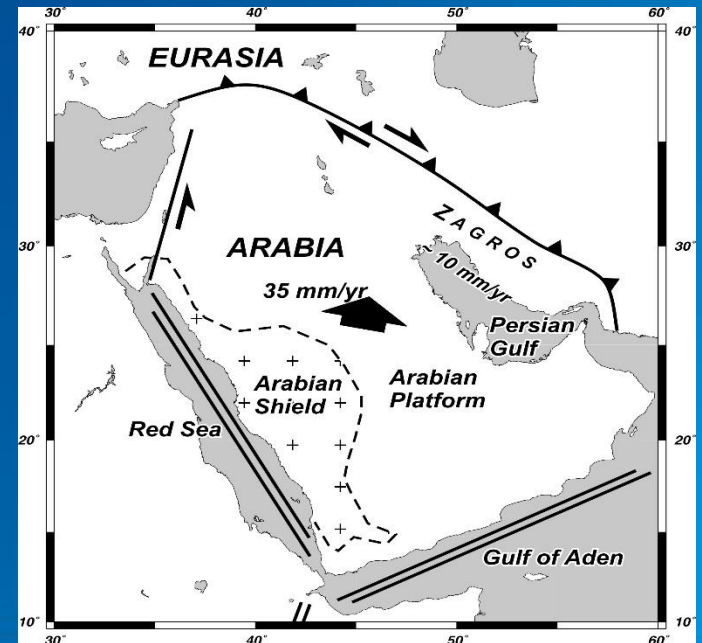
B Tectonic units: frontal imbricate, synformal thrust stack, underplated units, antiformal stack, U.P. = Upper Plate, L.P. = Lower Plate

**Geodynamic and kinematic setting of the Zagros
fold-and-thrust belt**

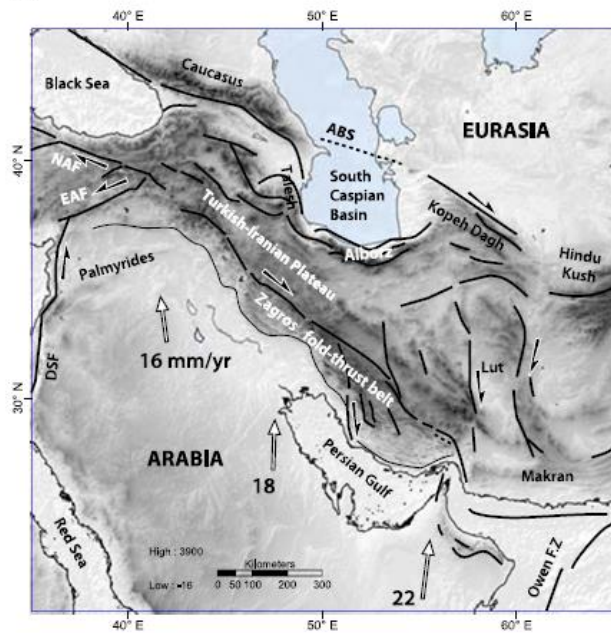


The Zagros belt results from the collision between Arabia and Central Iran, beginning in (Oligo ?)-Miocene times and continuing today.

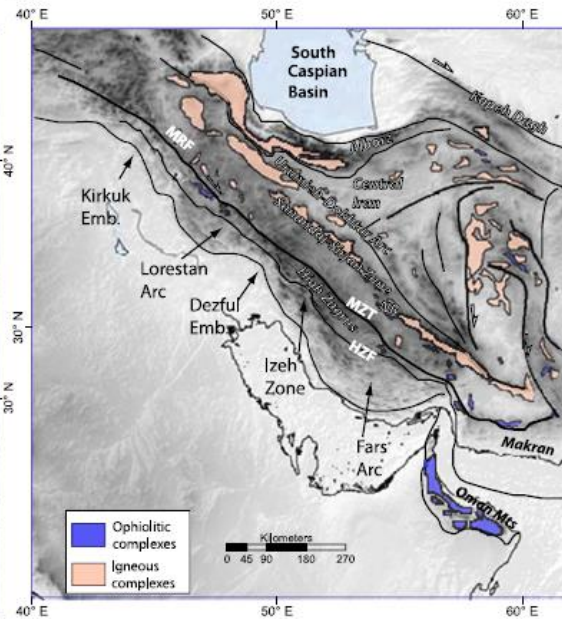
About one third of the 22-25 mm/yr Arabia-Eurasia convergence is currently accommodated in the Zagros
(Vernant et al., 2004)



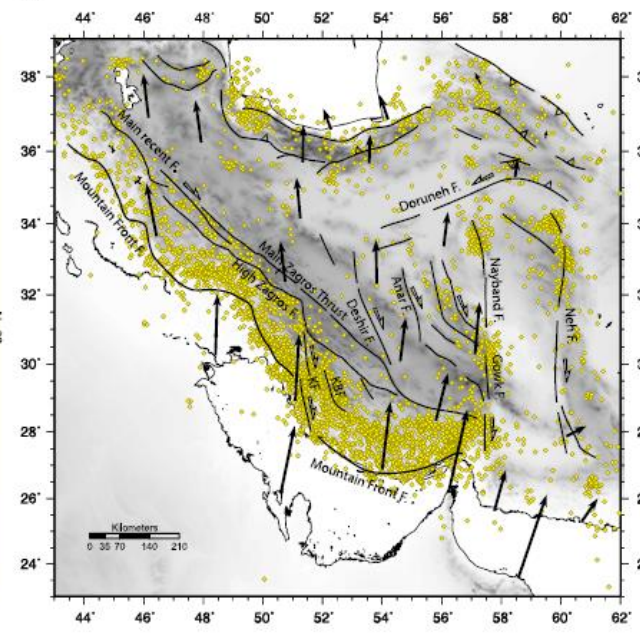
A



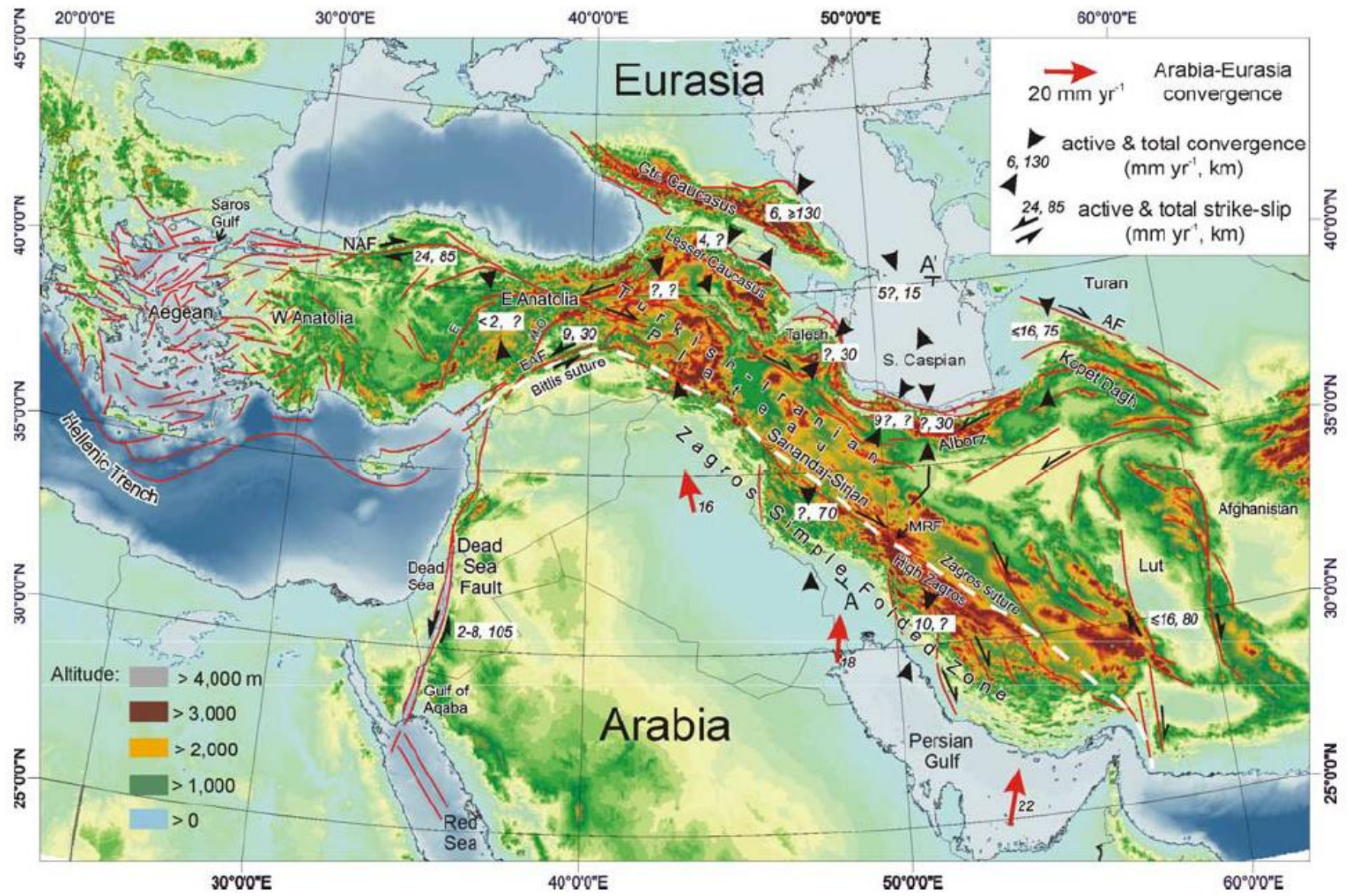
B



C



Mouthereau et al. 2012





MINISTRY OF MINES AND METALS
GEOLOGICAL SURVEY OF IRAN
**GEOLOGICAL MAP
OF
IRAN**

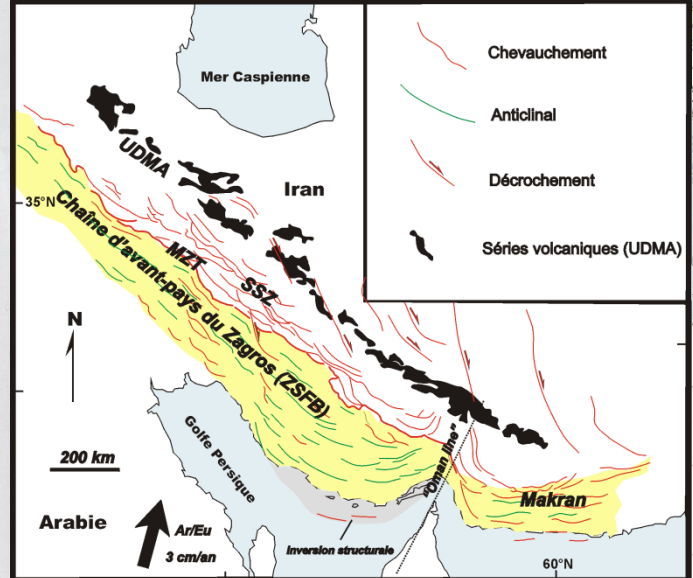
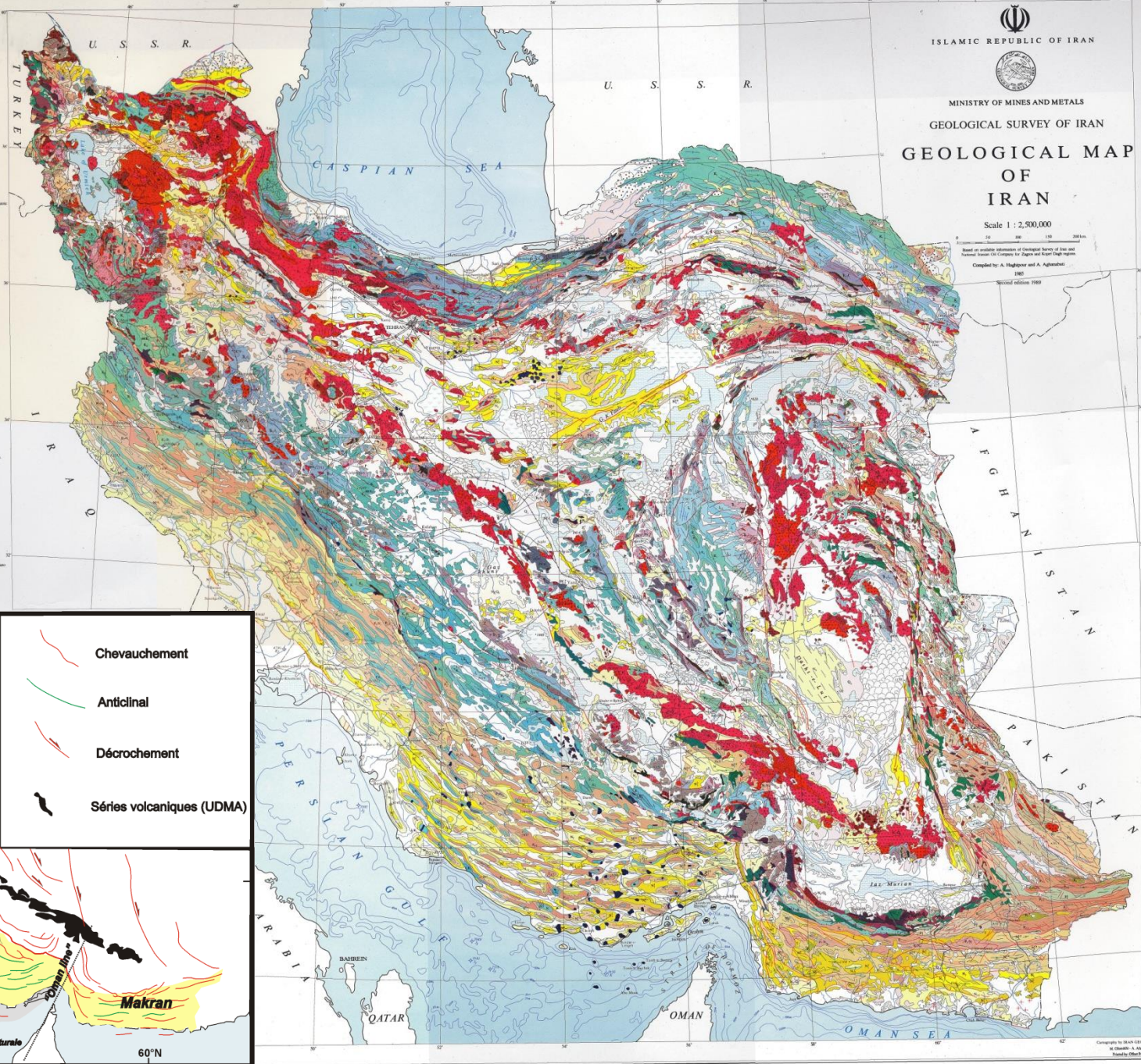
Scale 1 : 2,500,000

Based on available information of Geological Survey of Iran and
National Survey of Iran and Geographical Survey of Iran
Compiled by: A. Haghighat and A. Aghajani
1985
Second edition 1989

LEGEND

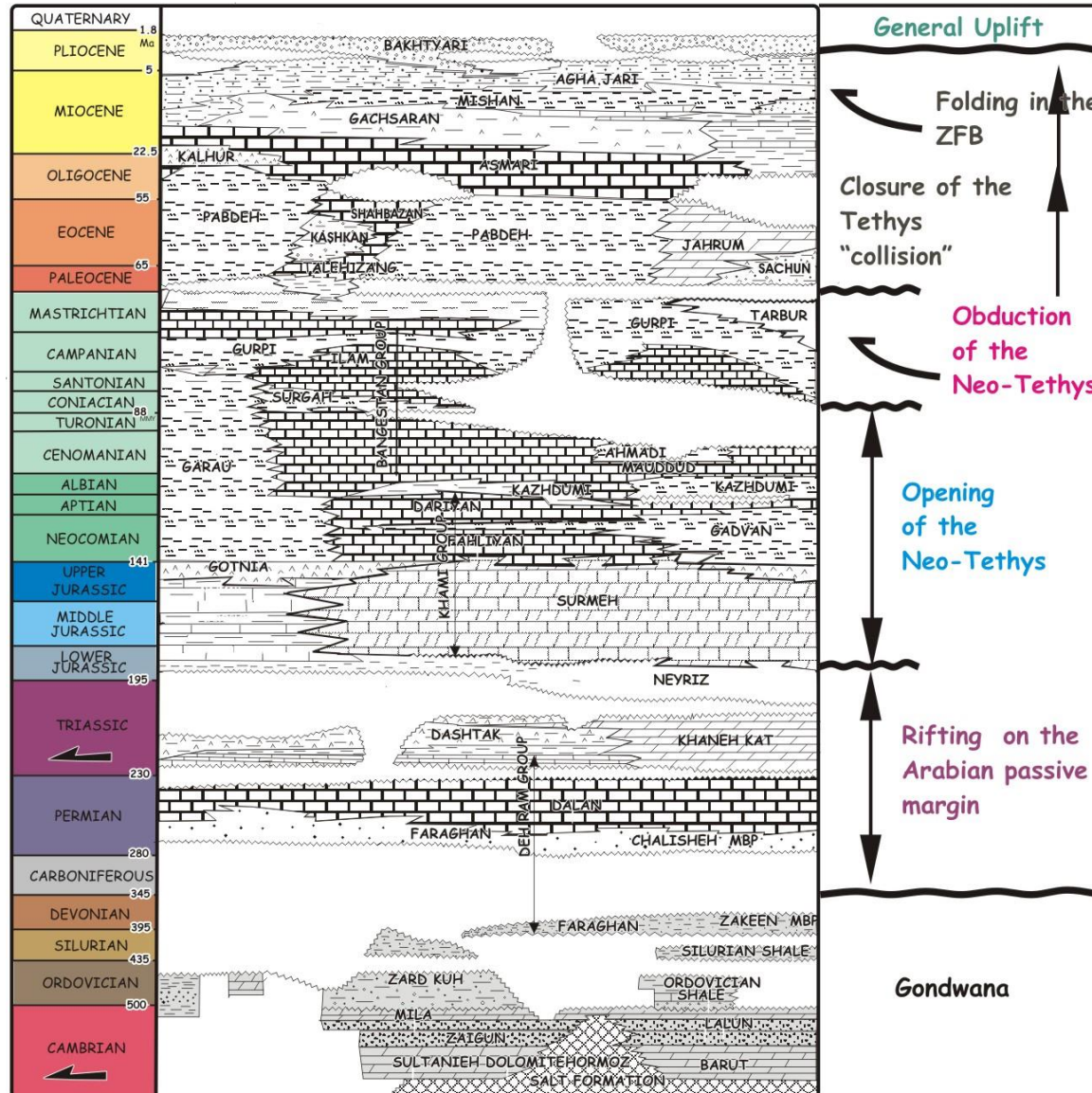
Quaternary: Recent	Q	Q ₁ Pleistocene	Q ₂ Holocene
Pliocene	P		
Pliocene	P		
Upper Miocene	M ₃		
Lower Middle Miocene	M ₂		
Oligocene	O		
Upper Eocene	E ₃		
Middle Eocene	E ₂		
Lower Eocene	E ₁		
Eocene	E		
Palaeocene	Pc		
Upper Cretaceous	C ₃		
Lower Cretaceous	C ₂		
Upper Jurassic	J ₃		
Middle Jurassic	J ₂		
Lower Jurassic	J ₁		
Upper Triassic	T ₃		
Middle Triassic	T ₂		
Lower Triassic	T ₁		
Triassic	T		
Permian	P		
Carboniferous	C		
Devonian	D		
Shinarump	S		
Ordovician-Steirer	O-S		
Carboniferous	C		
Upper Permian-Carboniferous	P-C		
Lower Permian-Carboniferous	P-C		

IGNEOUS ROCKS	
Granite	Granite
Diorite	Diorite
Gabbro	Gabbro
Basalt	Basalt
Andesite	Andesite
Trachyte	Trachyte
Basaltic andesite	Basaltic andesite
Diabase	Diabase
Chert	Chert
Quartzite	Quartzite
Siltstone	Siltstone
Shale	Shale
Concretion	Concretion
Unconformity	Unconformity
Subvolcanic Concretion	Subvolcanic Concretion
Metamorphic facies	Metamorphic facies
Unconformity	Unconformity
Low grade	Low grade
Medium grade	Medium grade
High grade	High grade
Overthrust	Overthrust

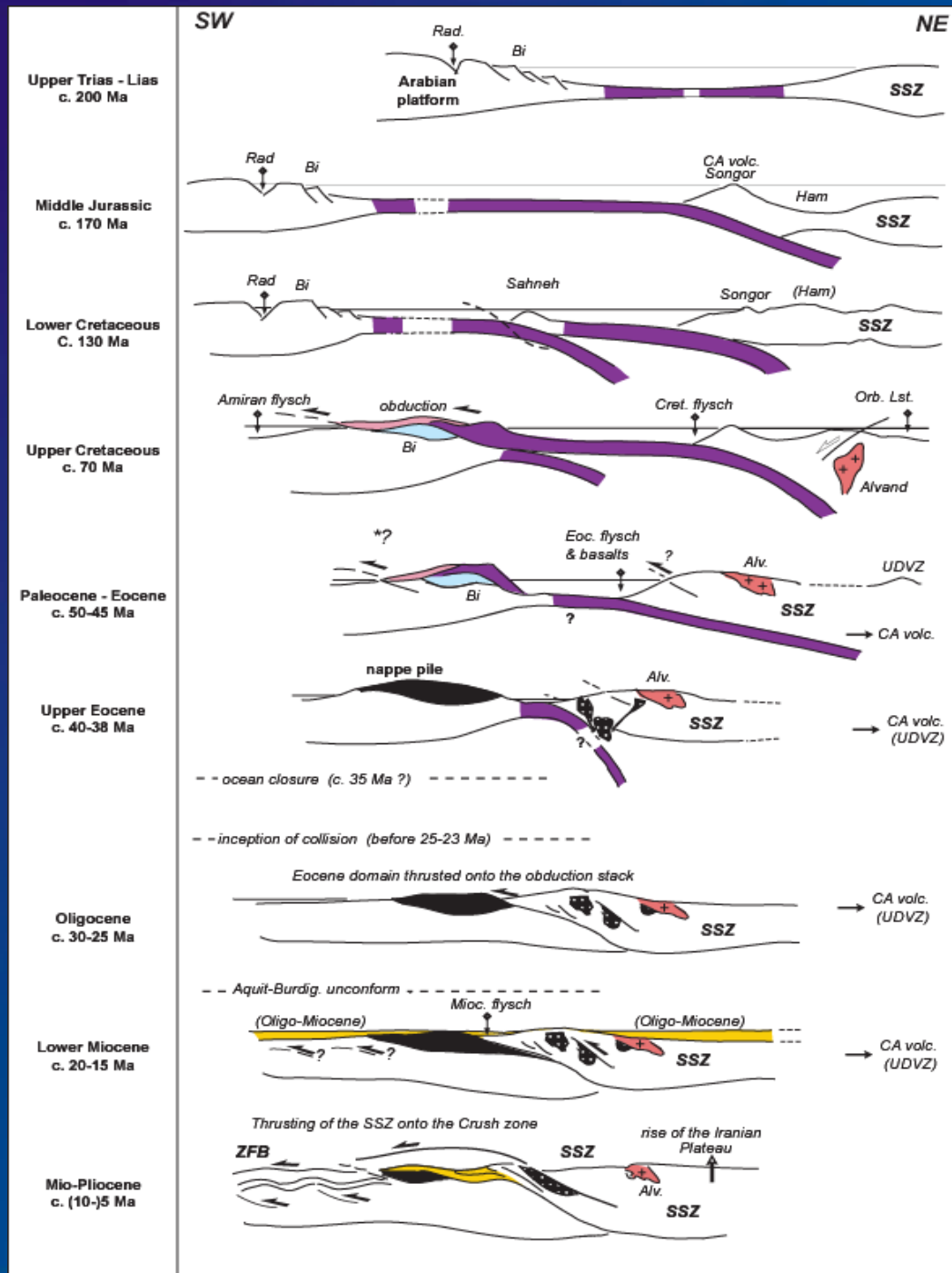


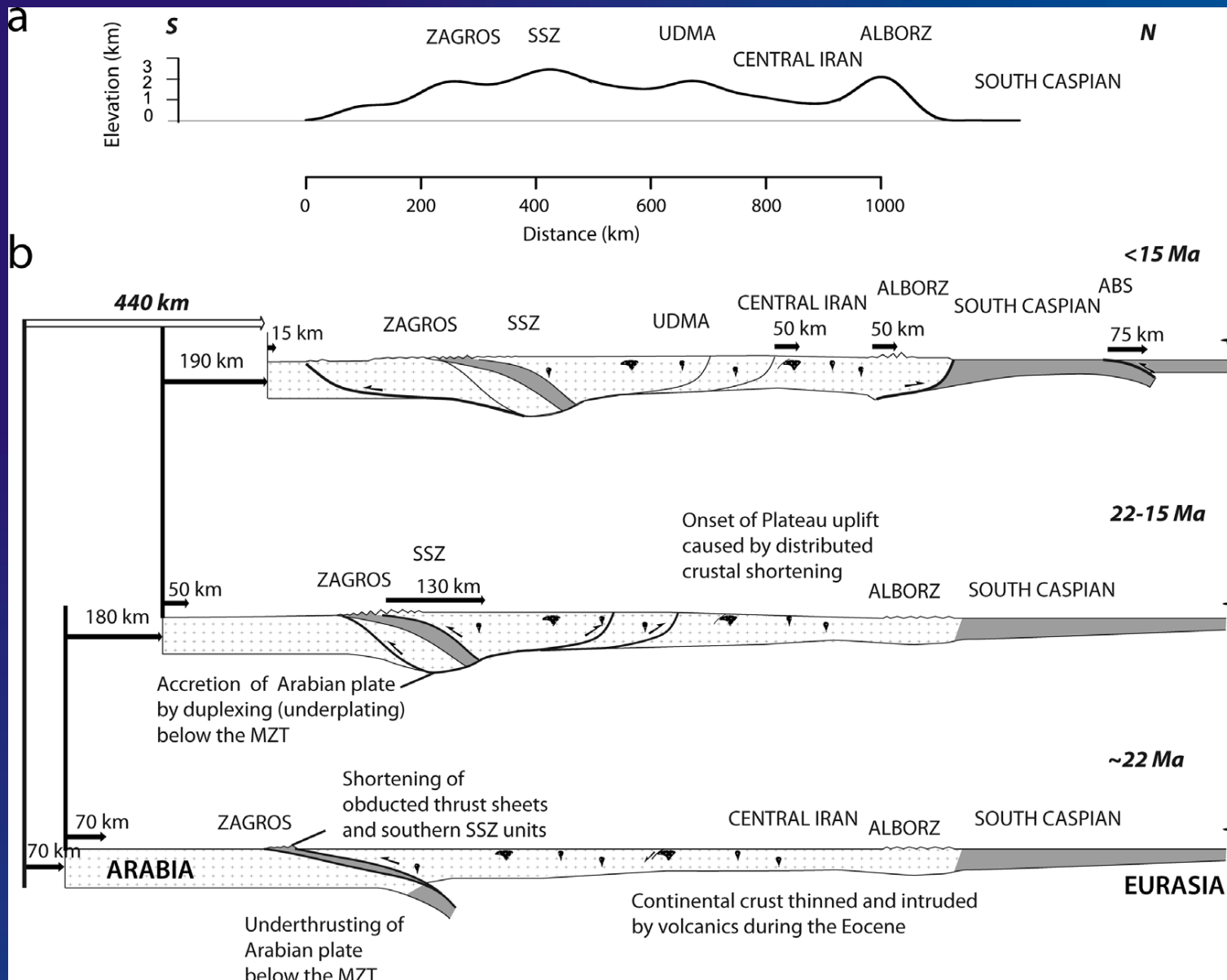
Copyright © IRAN 2000/00/00/00
W. G. Carter, A. Haghighat, A. Aghajani
Printed by Shiraz Press, Shiraz, Iran

Lithofacies and stratigraphy in the Zagros basin



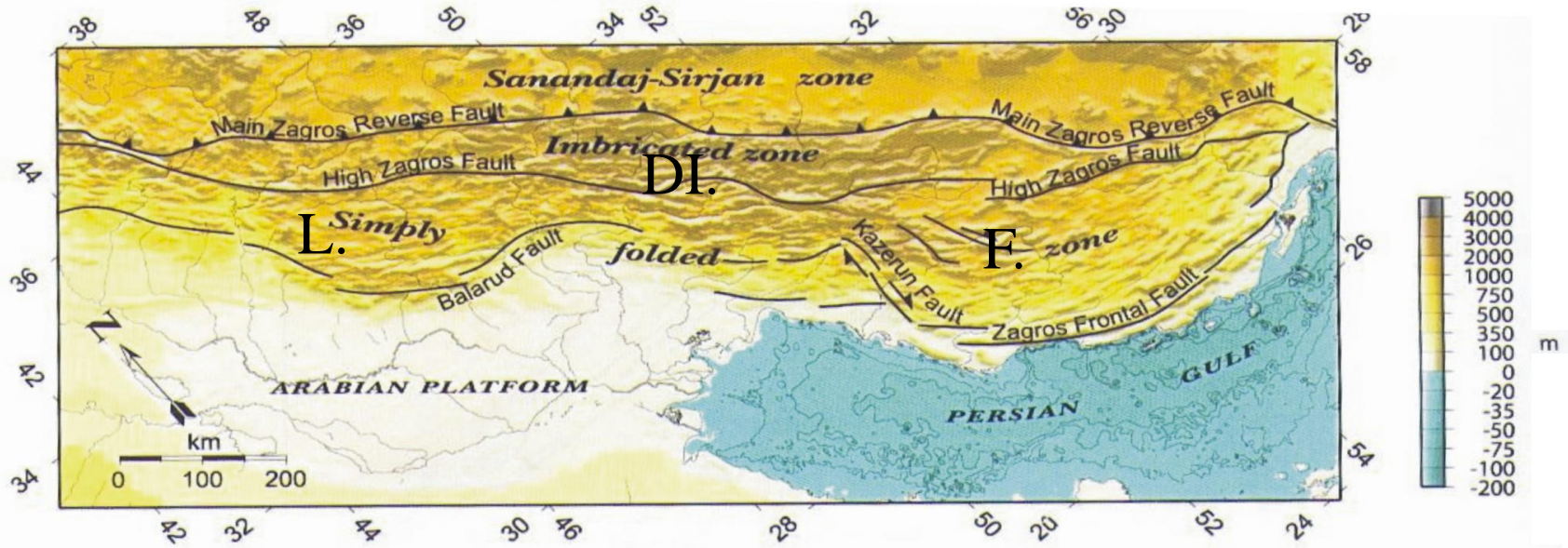
(Agard et al., 2005)



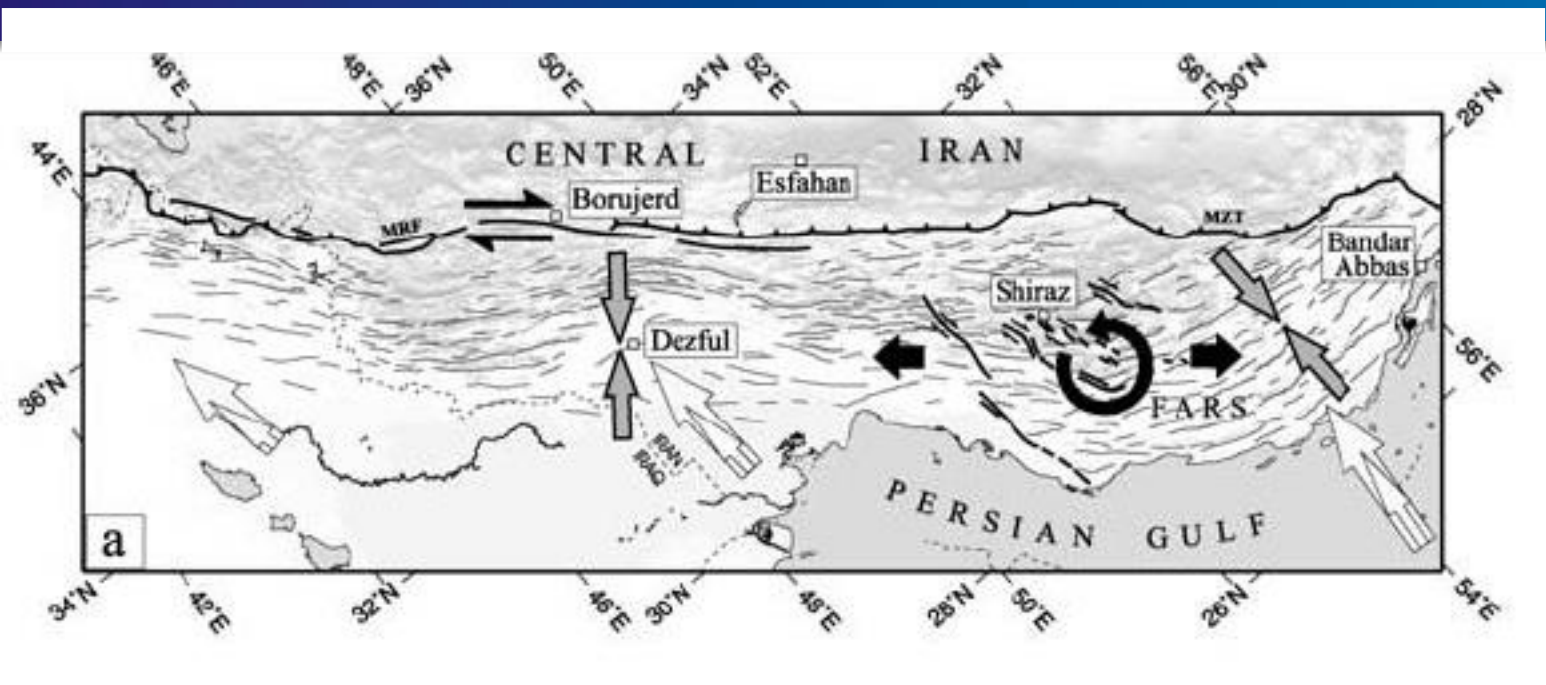
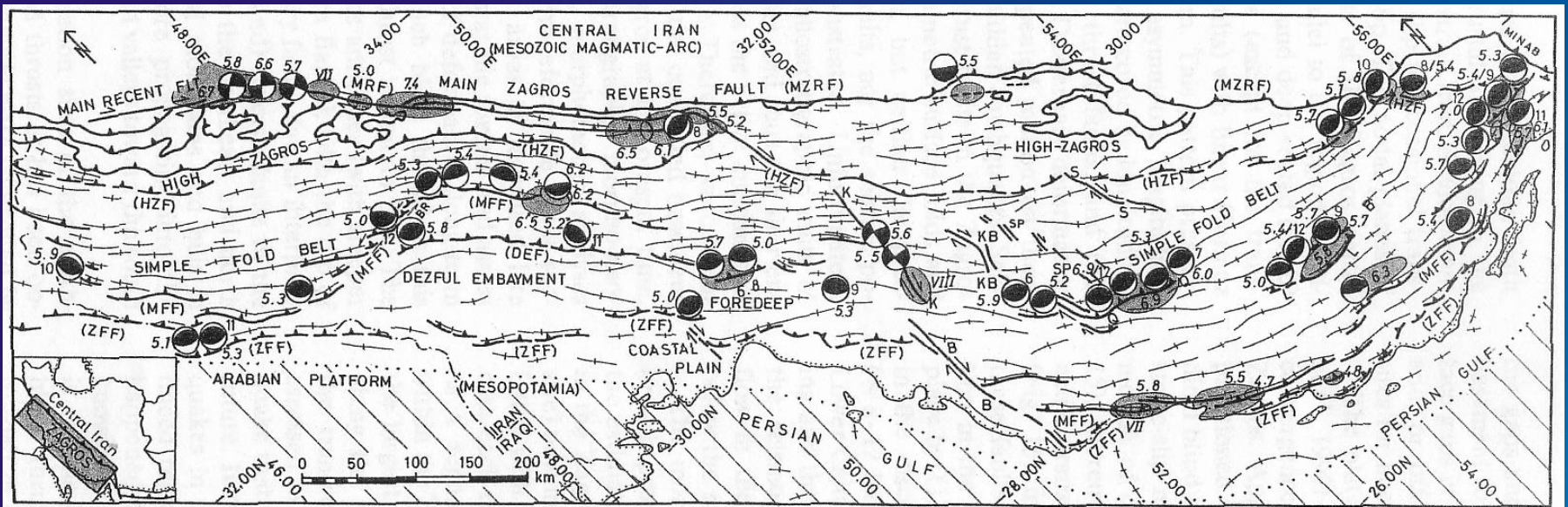


(Mouthereau, 2011)

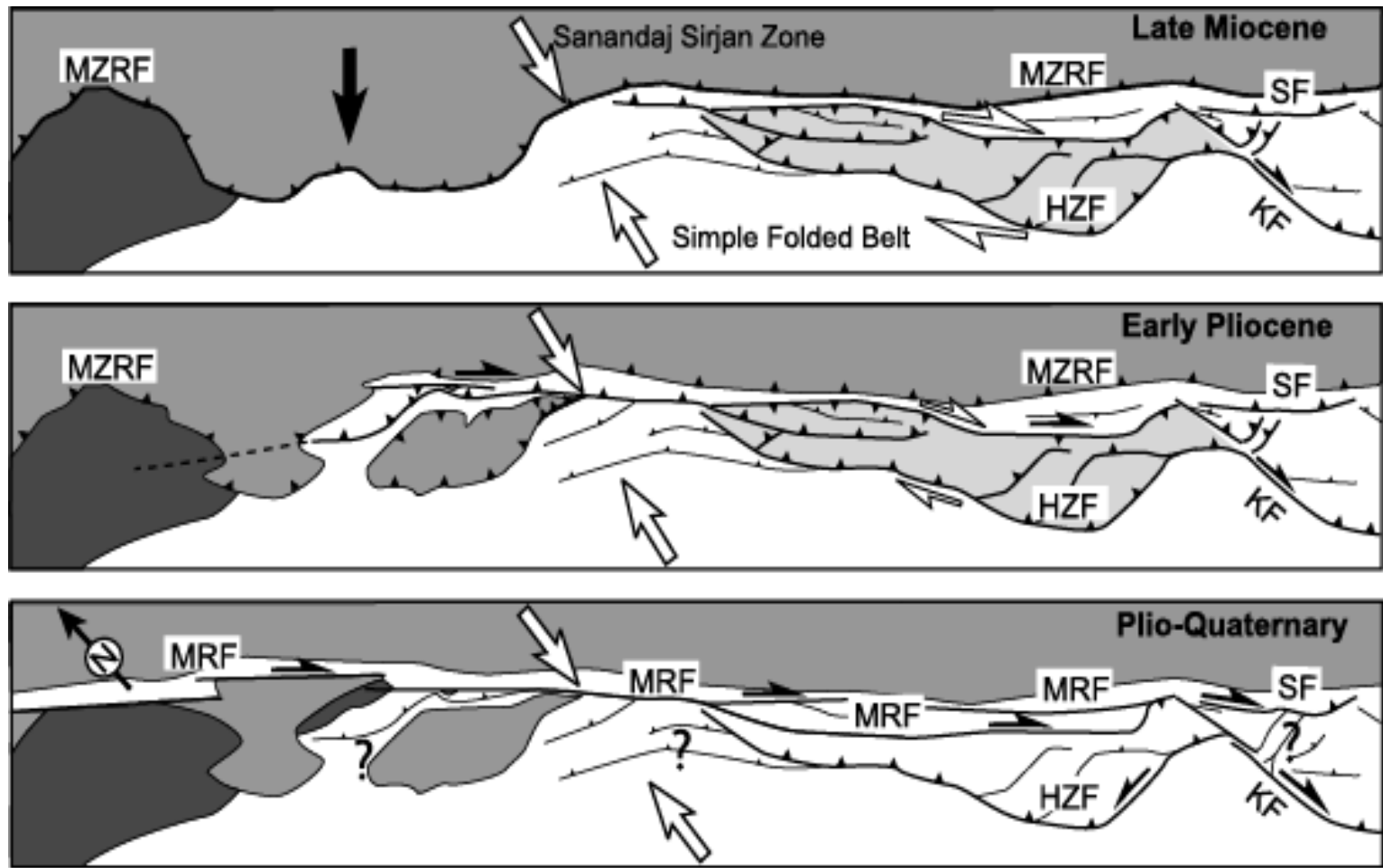




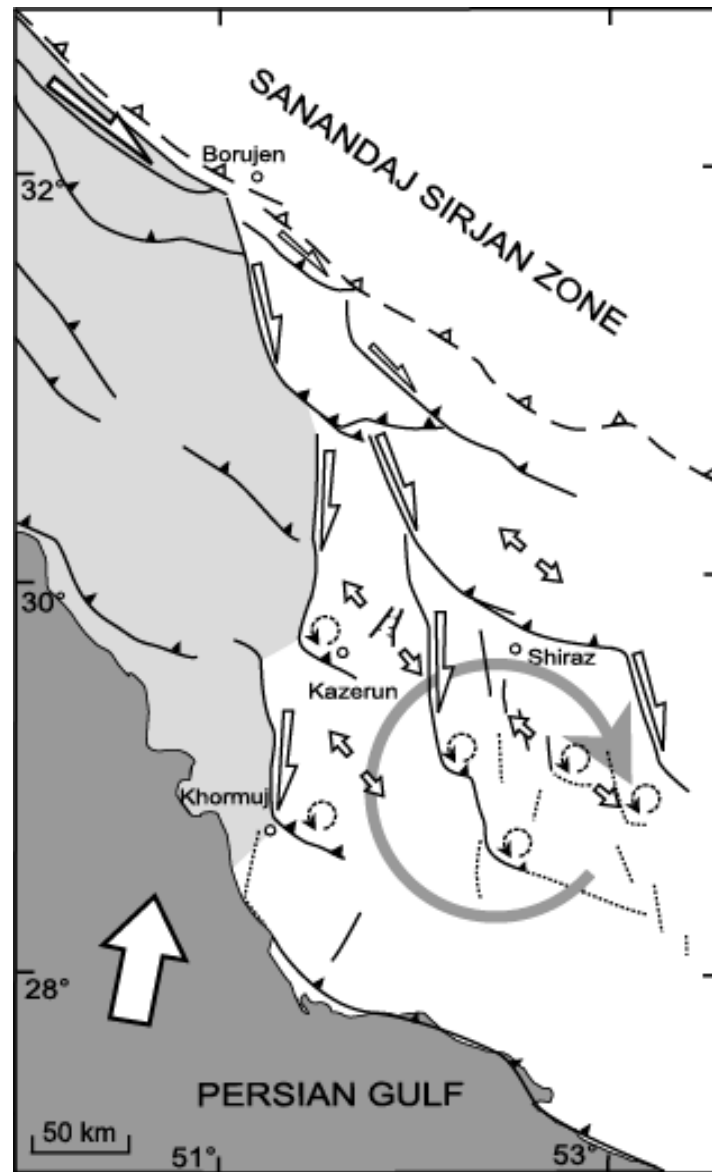
(Berberian, 1995)






(Berberian, 1995; Talebian and Jackson, 2004)



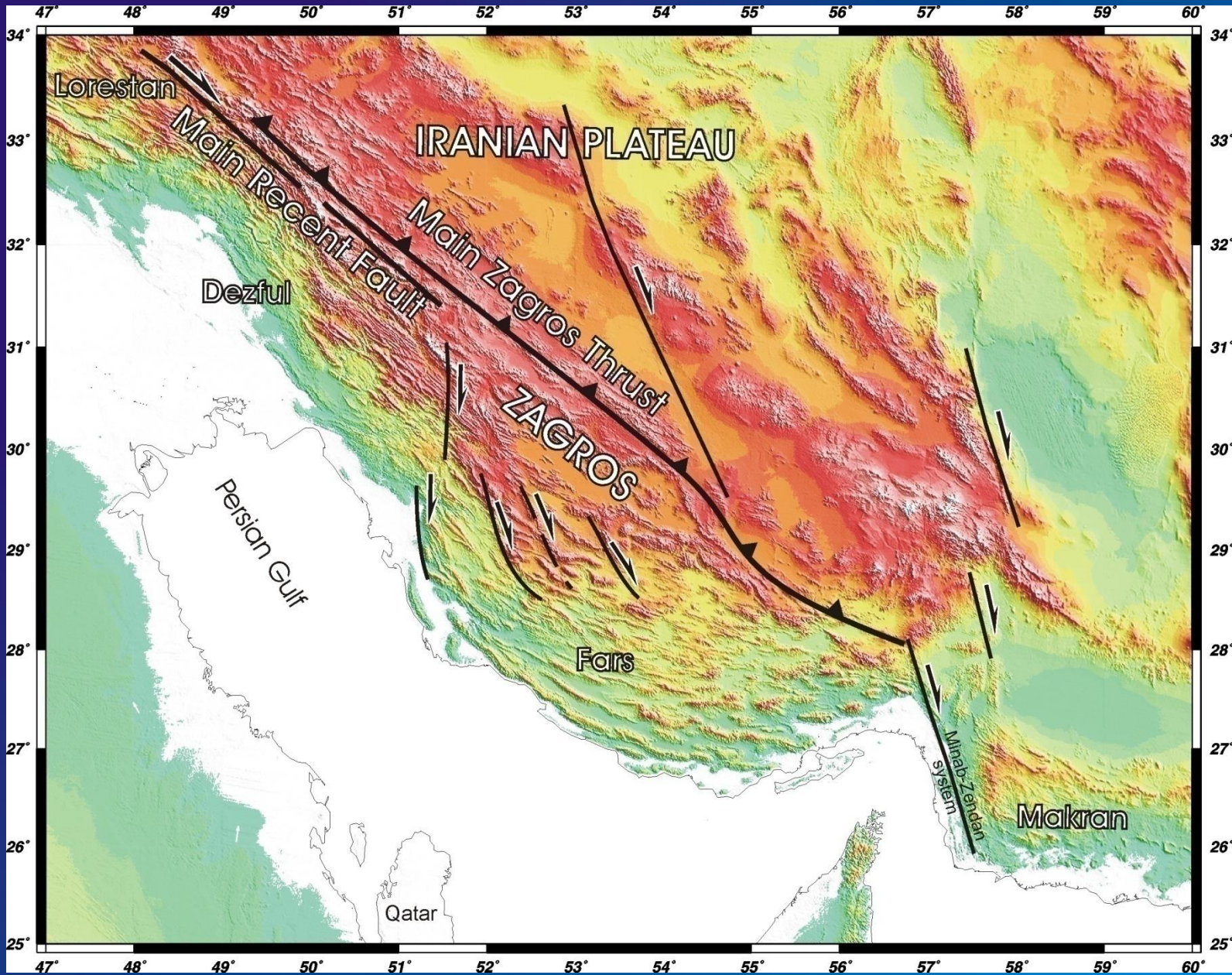
(Authemayou et al., 2006)

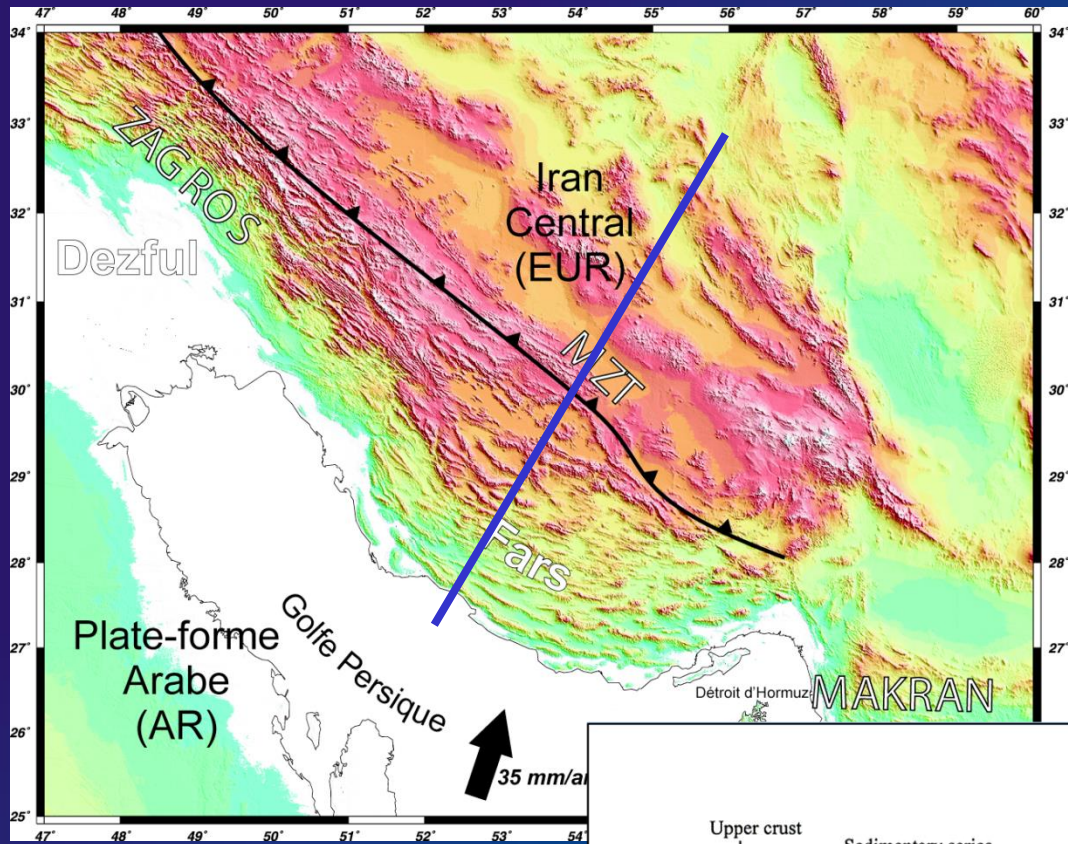


-  Along-strike belt stretching
-  Anticlockwise block rotation between dextral strike-slip faults in the basement
-  Clockwise rotation in the cover by lateral pinch-out of the Hormuz salt detachment horizon

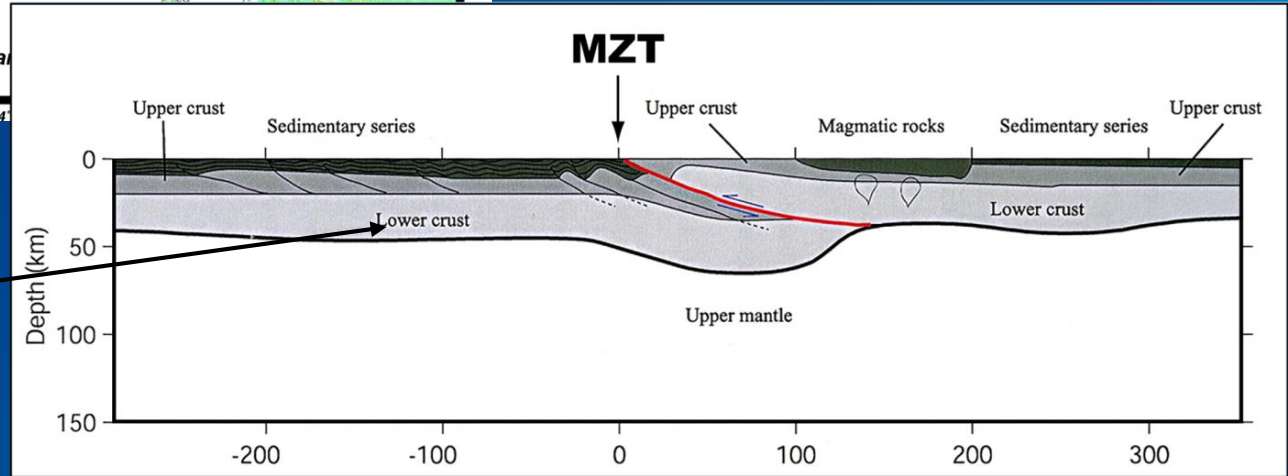
(Authemayou et al., 2006)

**Geological setting of the Zagros
fold-and-thrust belt**

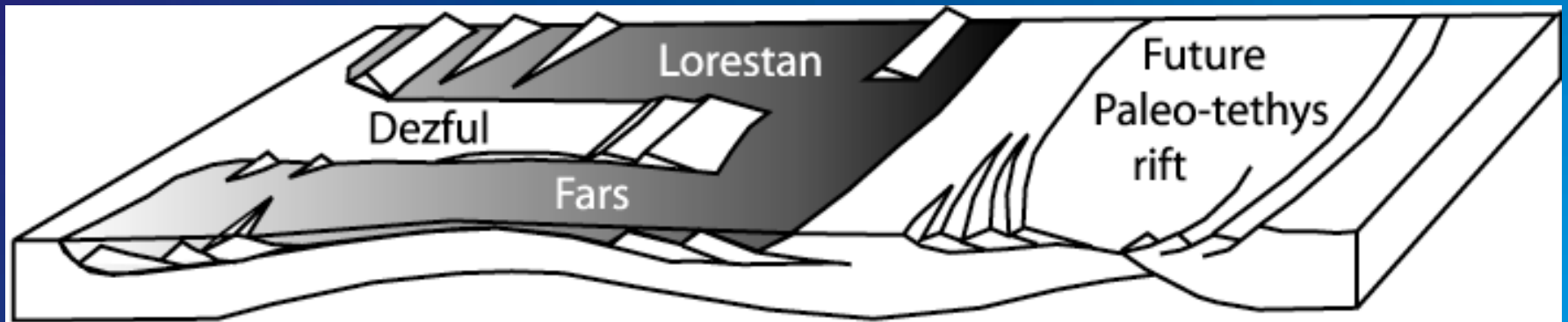
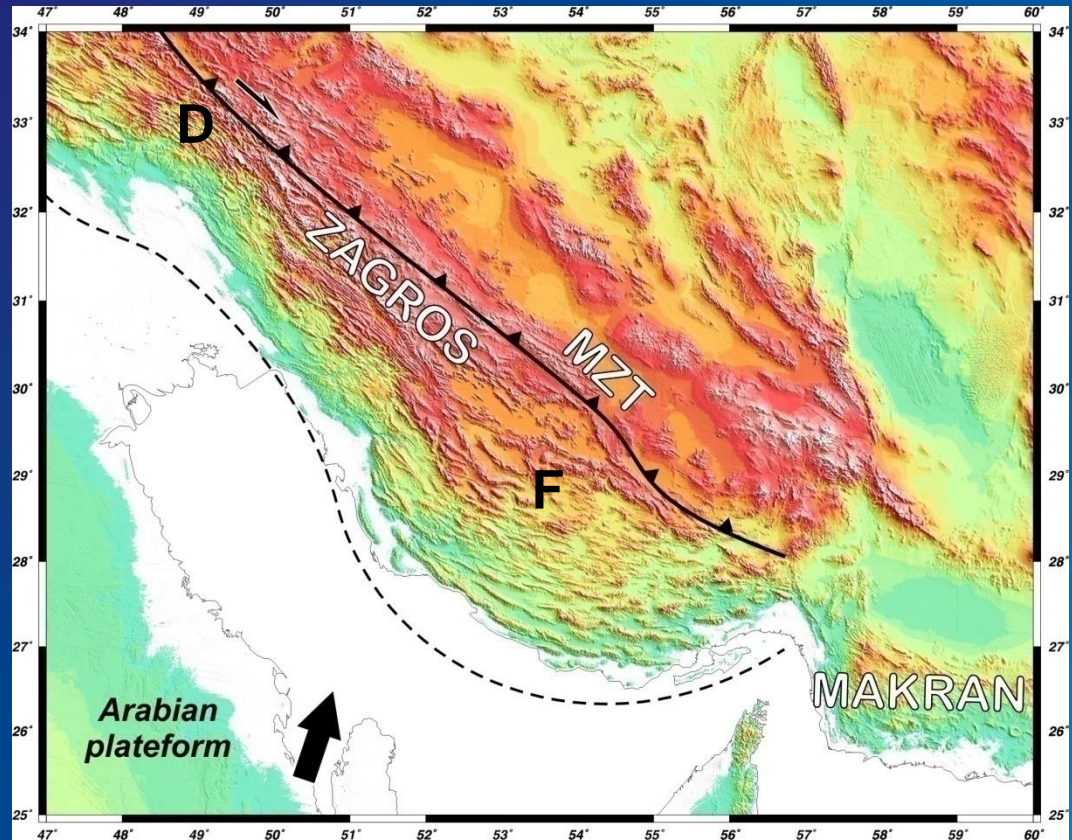




Little thickening below the Zagros

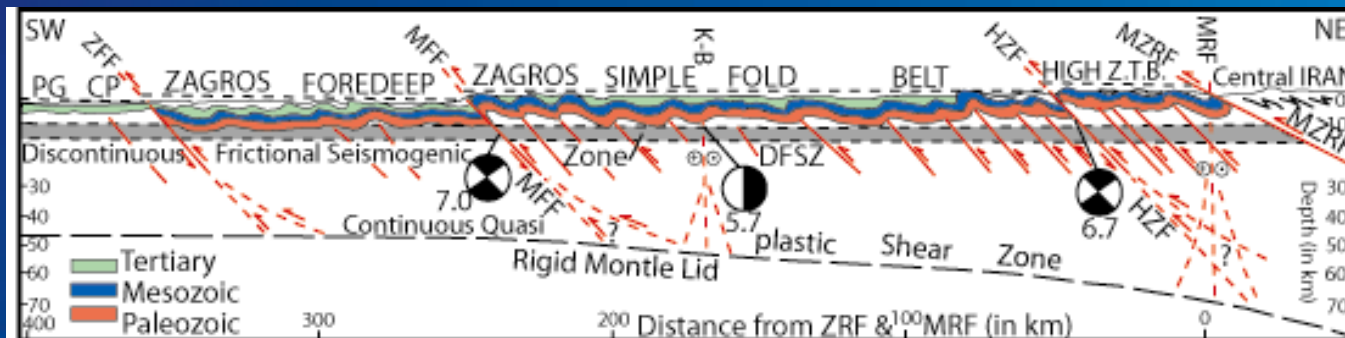


Along-strike segmentation is usually related either to variations in frictional properties of the basal décollement (Cambrian Salts) and/or to the distribution of pre-orogenic basins in the Arabian margin

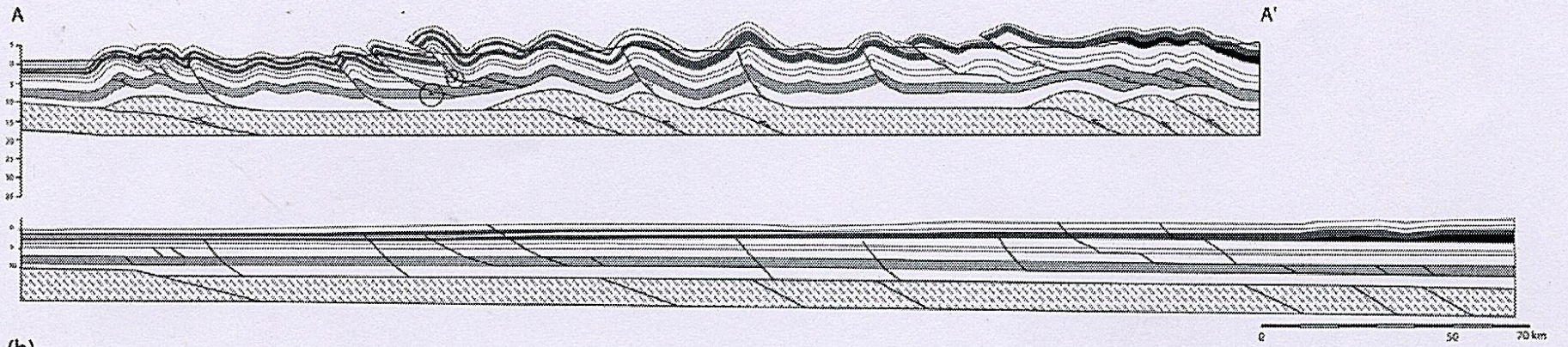




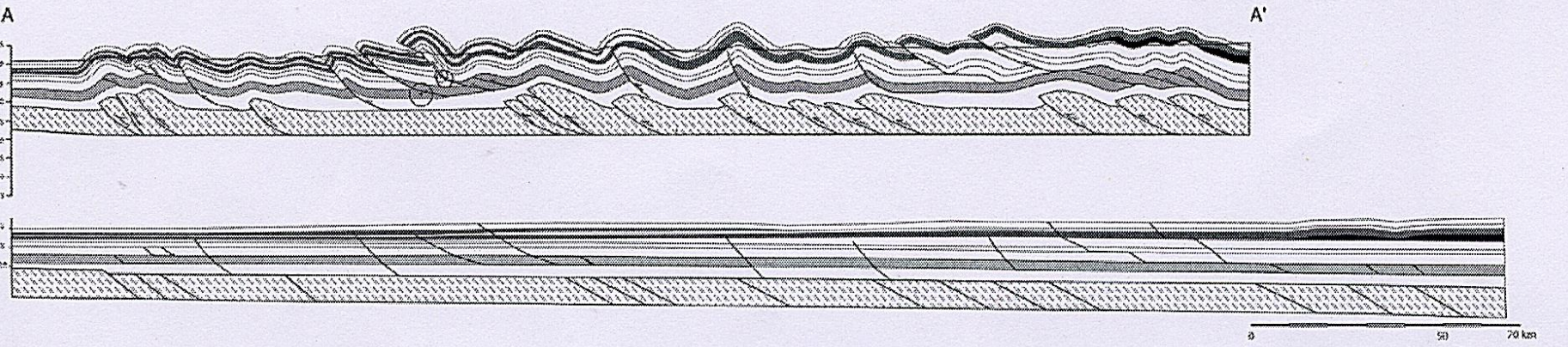
(Berberian, 1995)



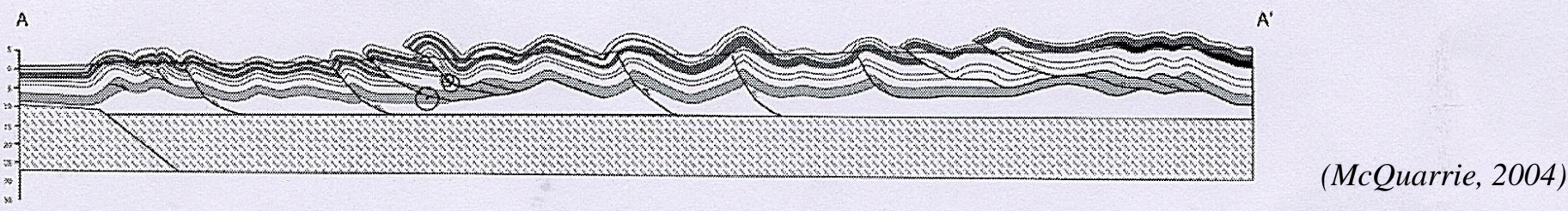
(a)



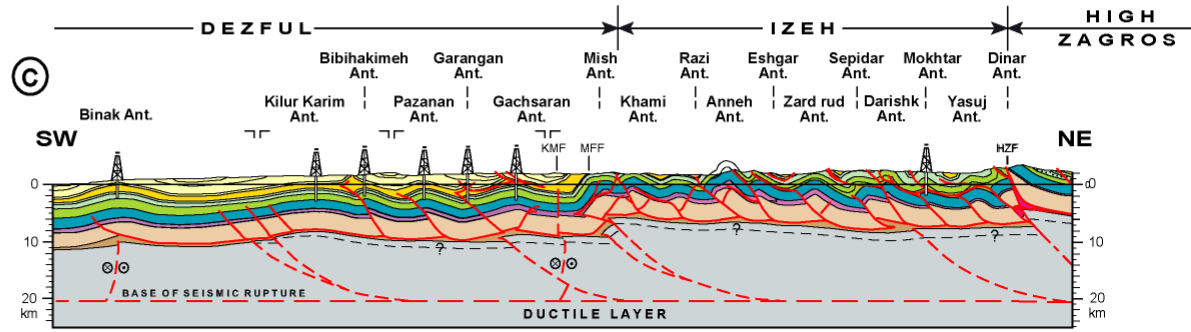
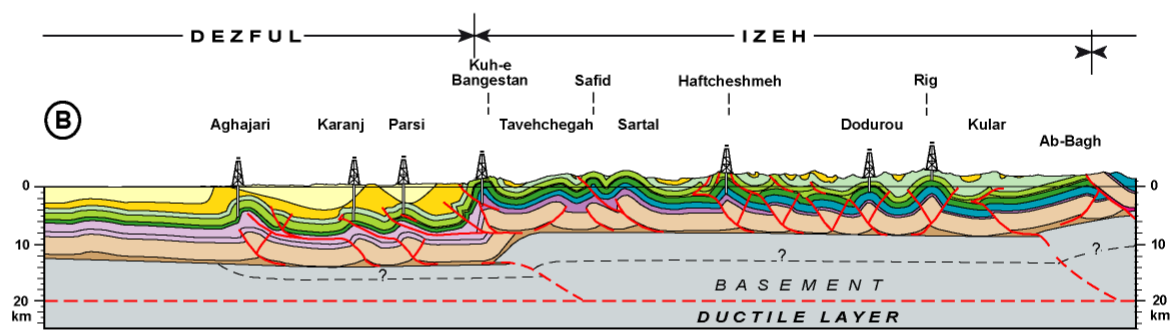
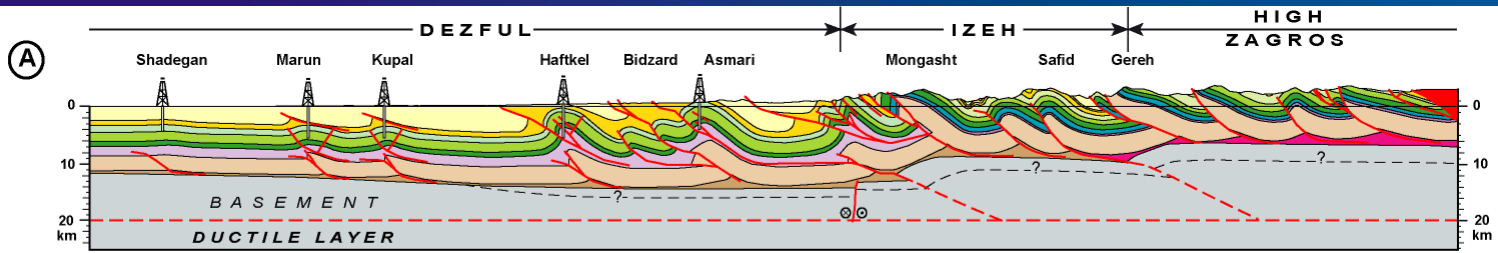
(b)



(c)



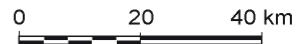
(McQuarrie, 2004)

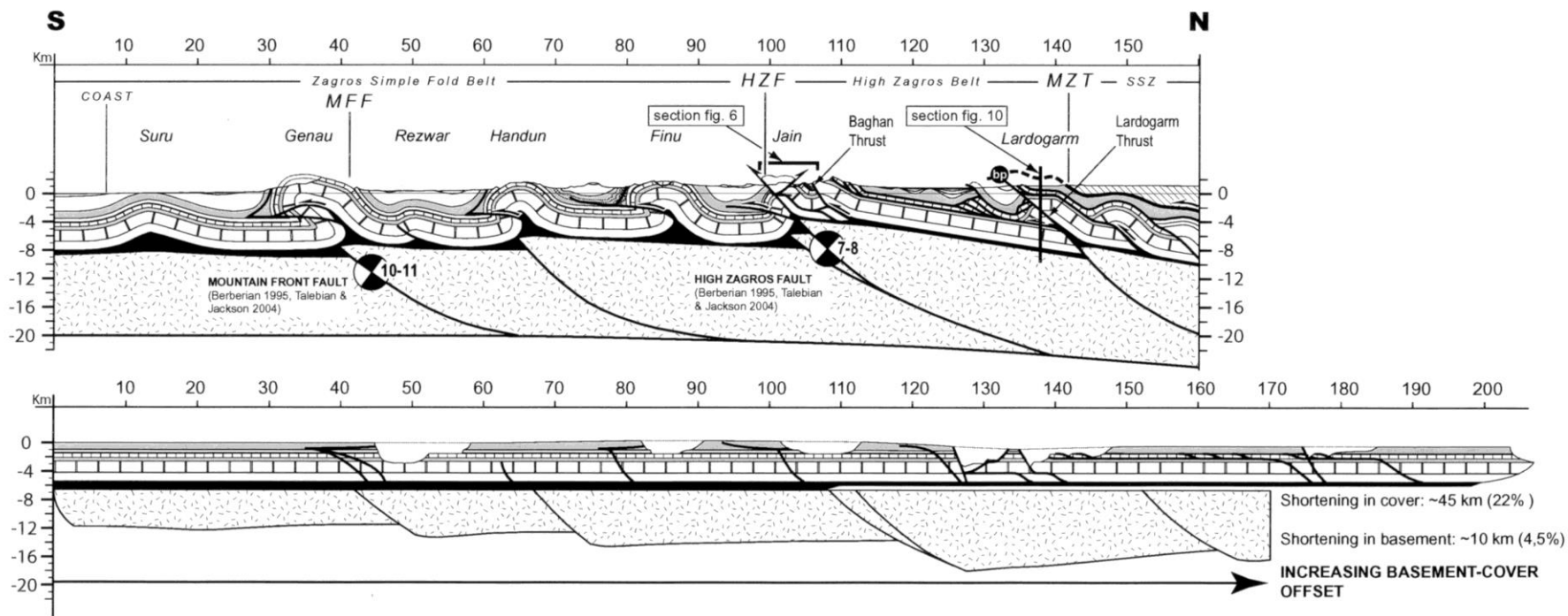


LEGEND

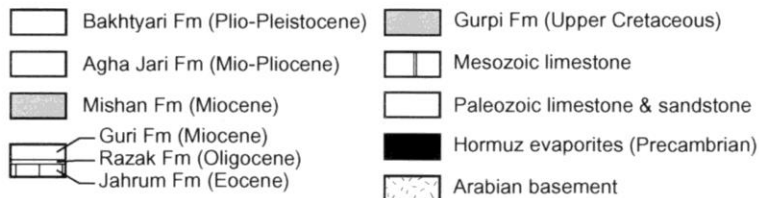
- Mishan, Aghajari, Bakhtiyari fms.
- MIDDLE MIOCENE : salt and evaporite (Gachsaran fm.)
- Pabdeh, Gurpi, Asmari fms.
- a : Kazhdumi Sarvak fms.
b : Sarvak fm.
- Fahliyan, Gadvan, Dariyan fms.
- MIDDLE JURASSIC and LOWER to MIDDLE CRETACEOUS SEDIMENT (Mus and Adaiyah, Alan, Sargelu, Gotnia, Garau fms.)
- JURASSIC
- TRIASSIC, JURASSIC to LOWER CRETACEOUS SEDIMENTS (Dashtak, Mus, Adaiyah, Alan, Sargelu, Gotnia, Garau fms.)
- TRIASSIC
- PALEOZOIC
- LOWER PALEOZOIC : shale or evaporite
- LATE PROTEROZOIC - LOWER PALEOZOIC (Hormuz salt)
- BASEMENT
- METAMORPHIC ROCKS

(after Sherkati & Letouzey 2004)





SIMPLE FOLD & HIGH ZAGROS BELTS



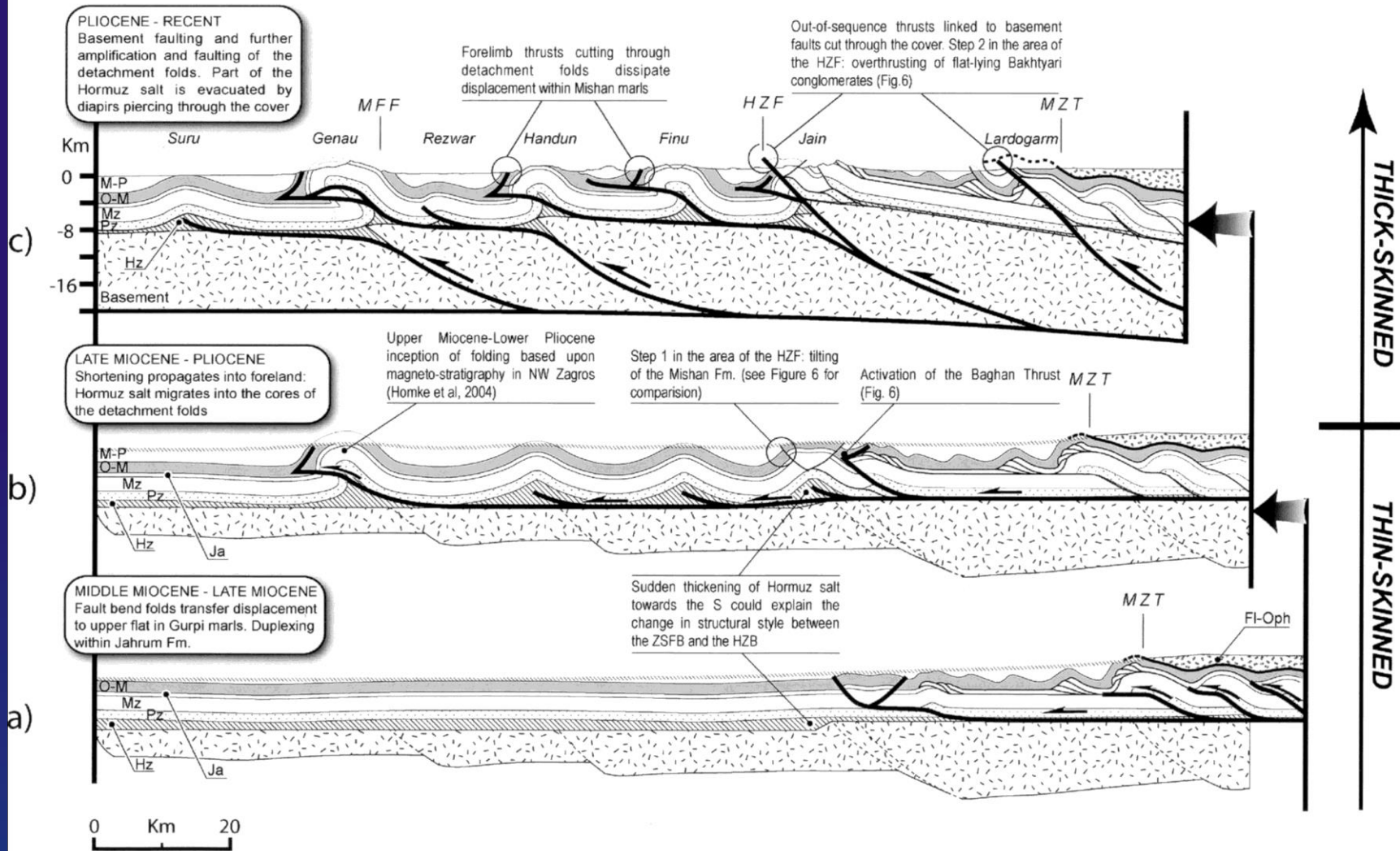
Published focal mechanisms, with centroid depths in Km



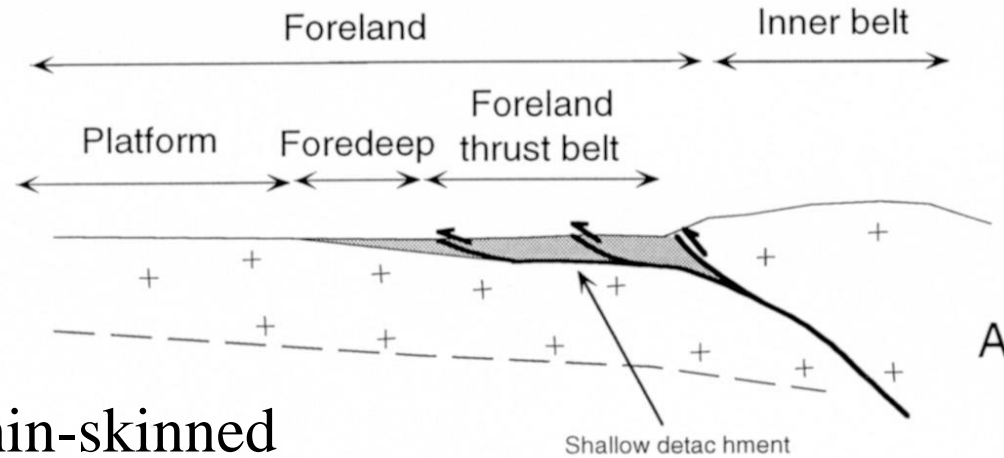
Eroded branch point between Lardogarm Thrust and MZT

SANANDAJ-SIRJAN ZONE

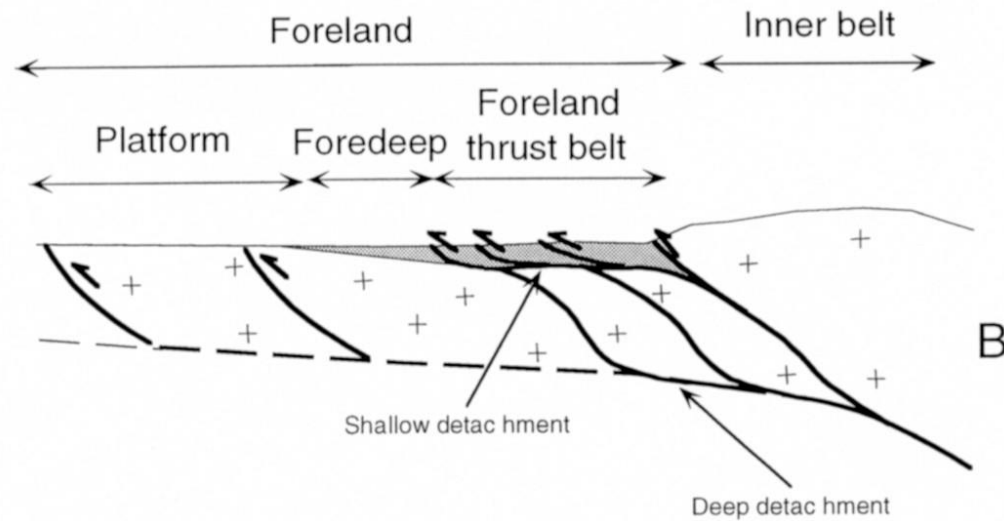




(Molinaro et al., 2005)

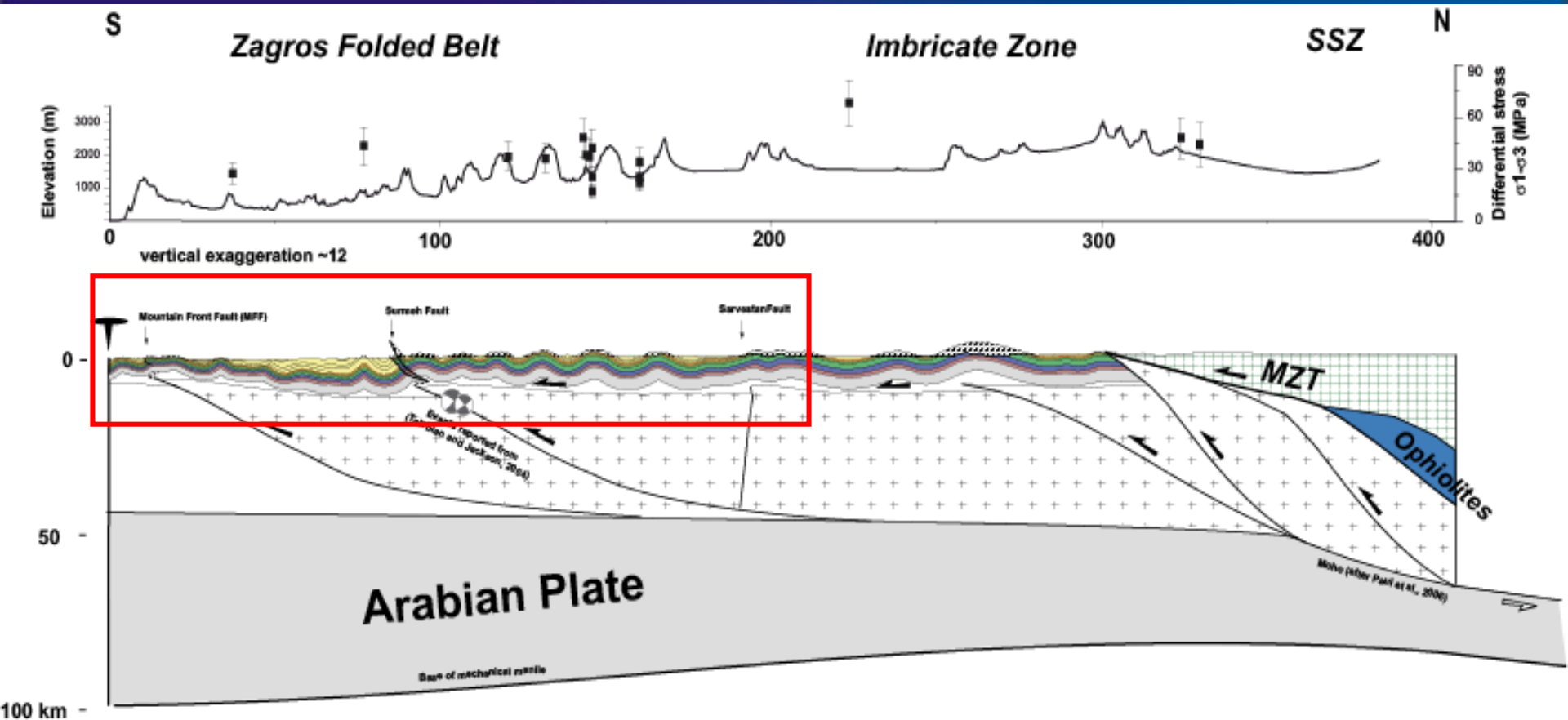


(Lacombe and Mouthereau, 2002)

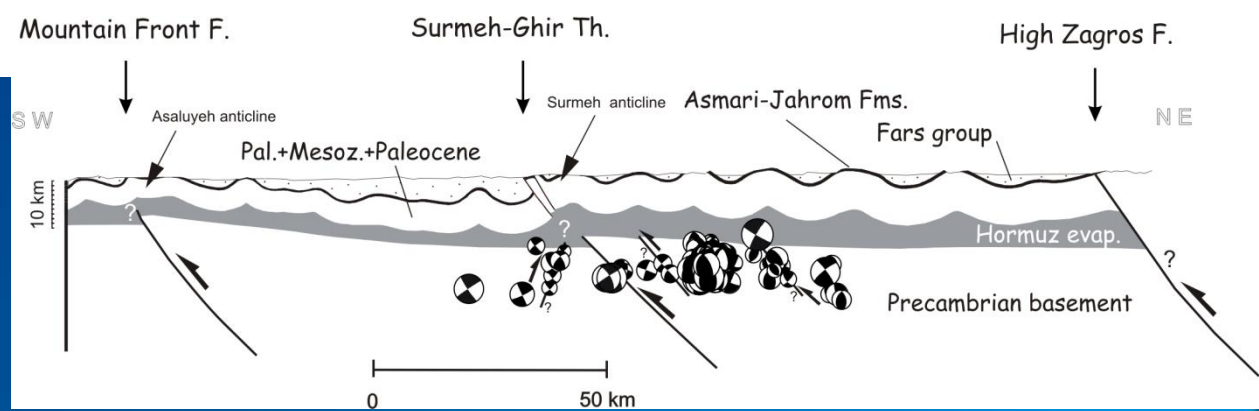


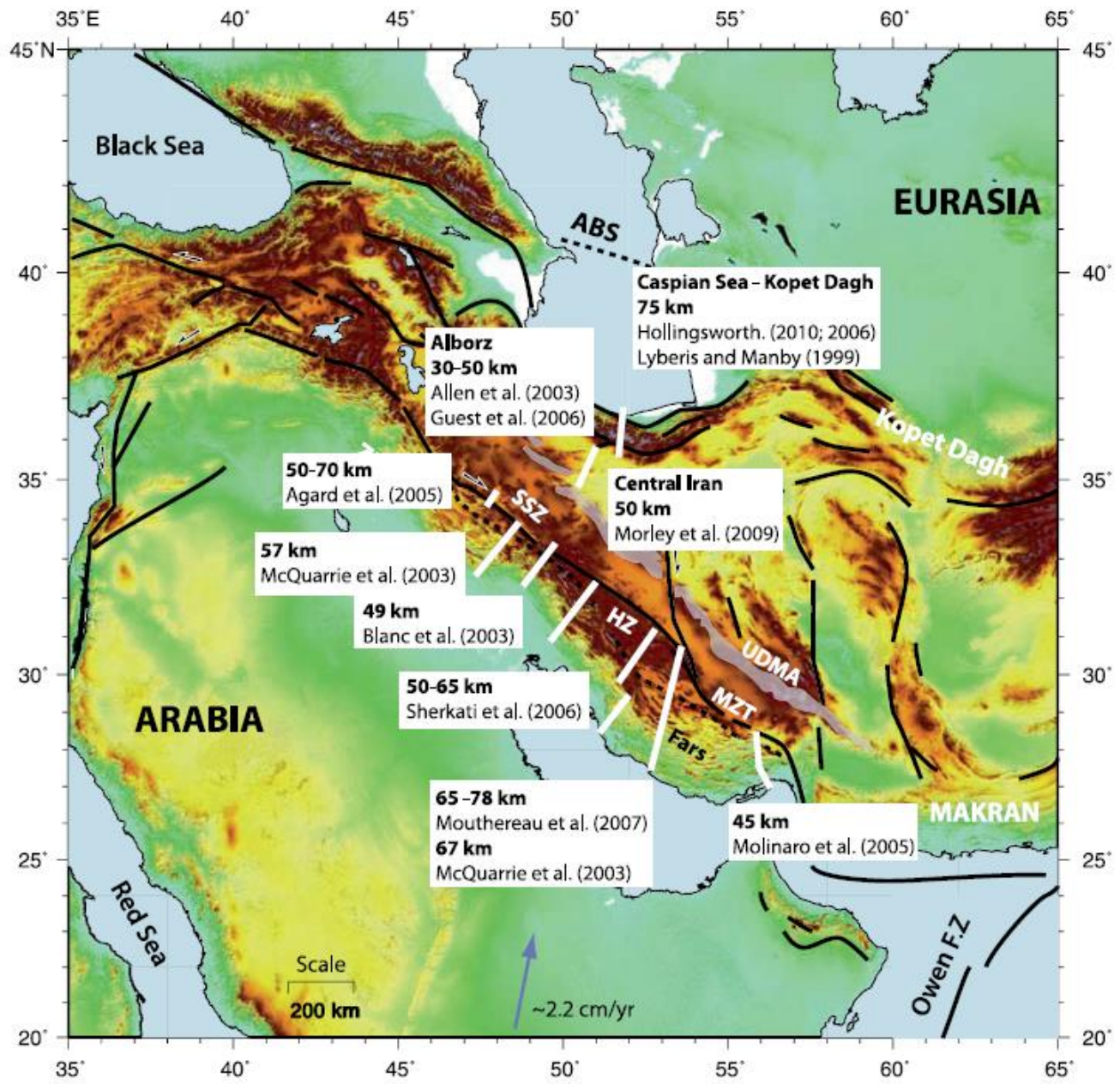
Thick-skinned ?

Thin-skinned + thick-skinned ?

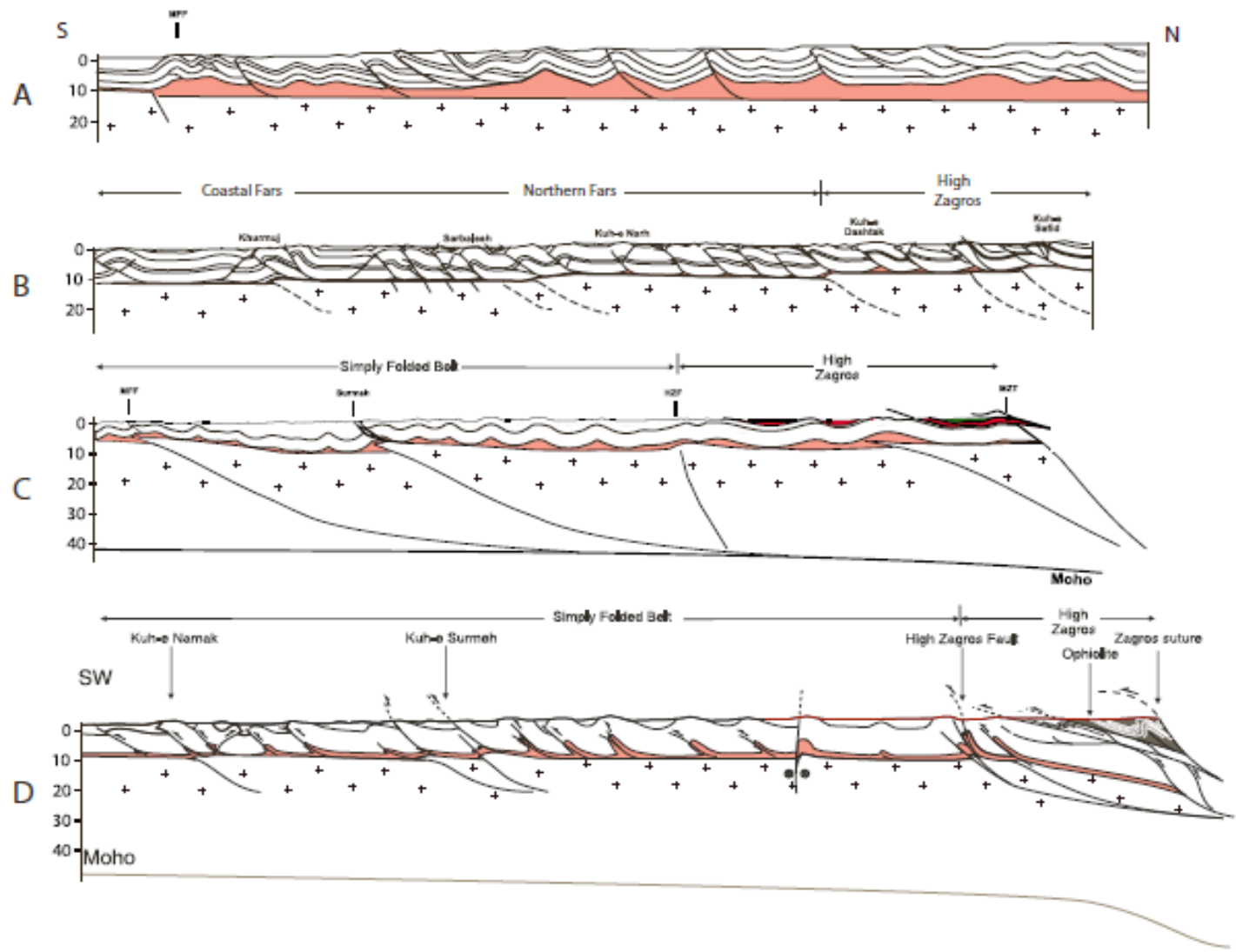


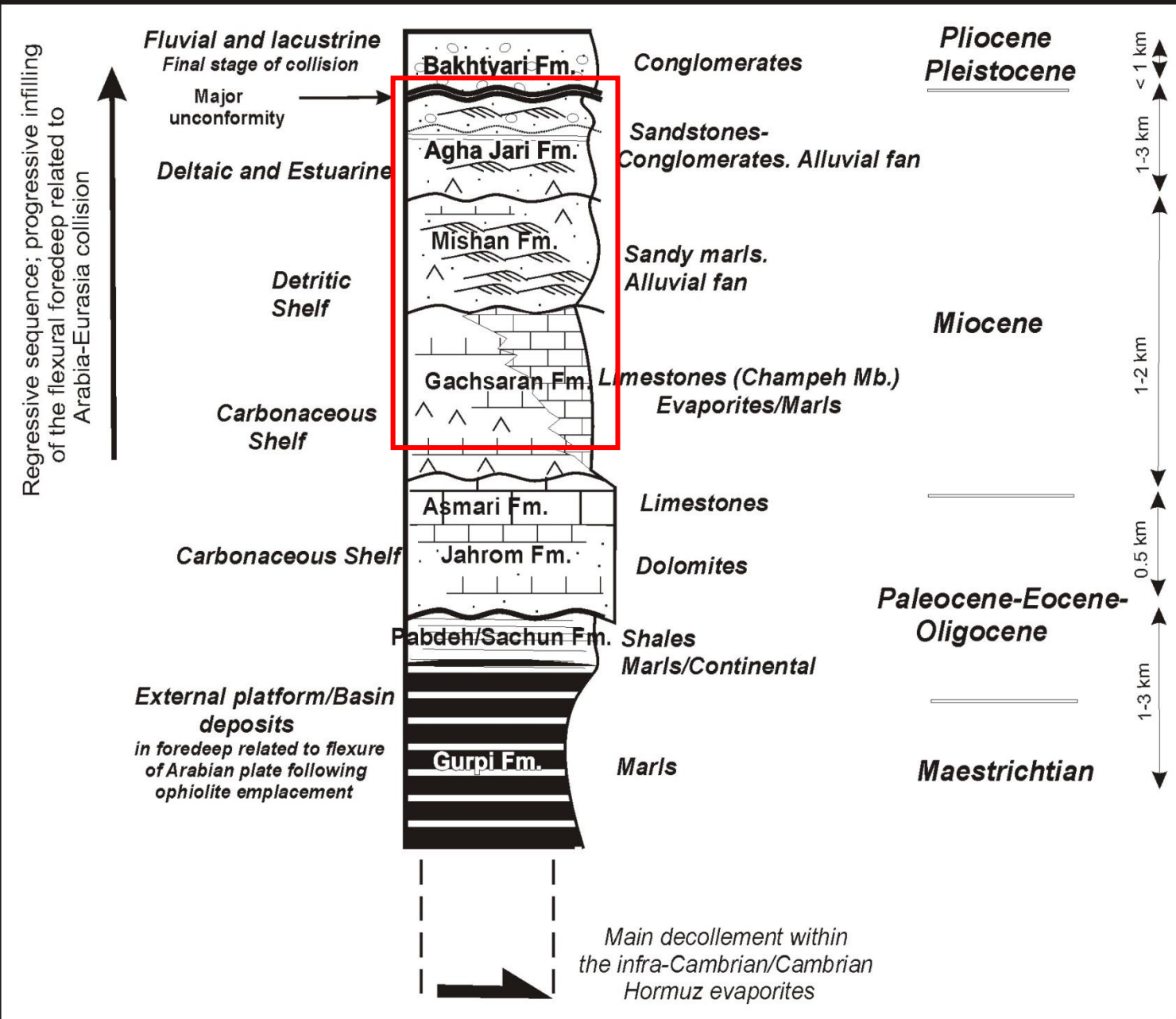
(Mouthereau et al., 2007;
Lacombe et al., 2006)





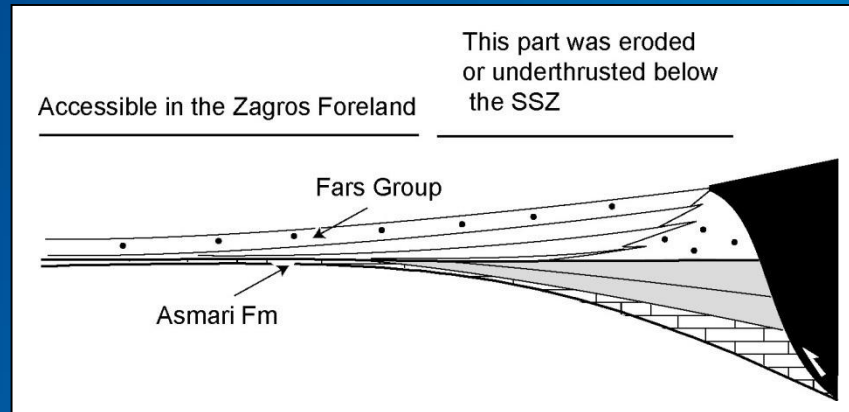
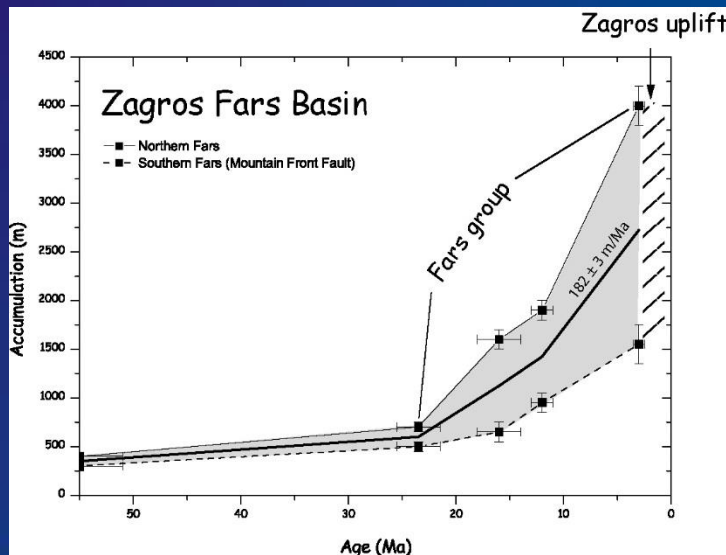
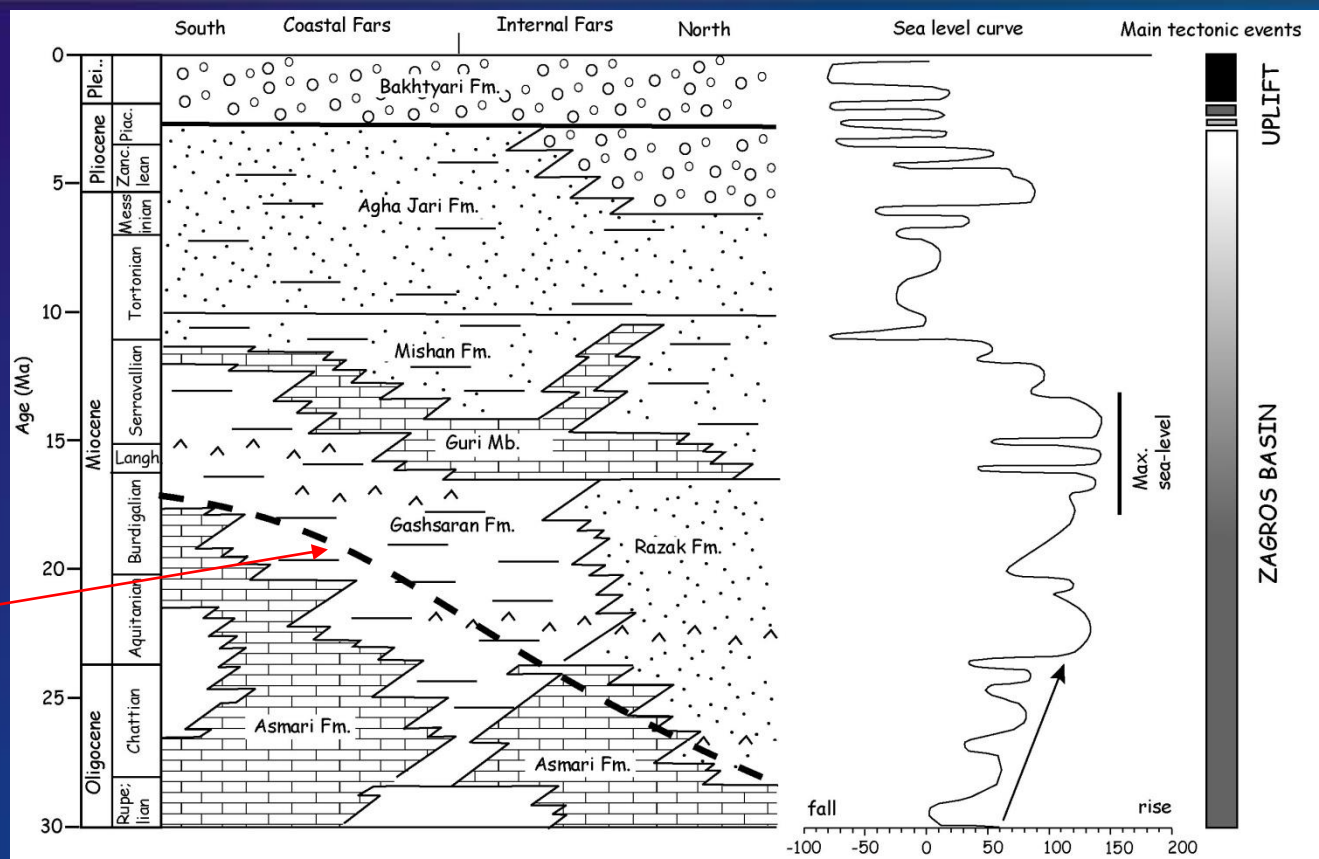
(Mouthereau et al., 2012)





Miocene foreland sequences :
Thick regressive siliciclastic sequence of the Fars Group

Progressive southward onlap through time of the shallowing-upward synorogenic deposits (Razak-Gashsaran Fm) onto the carbonates of the Asmari Fm in the context of flexural basin development.

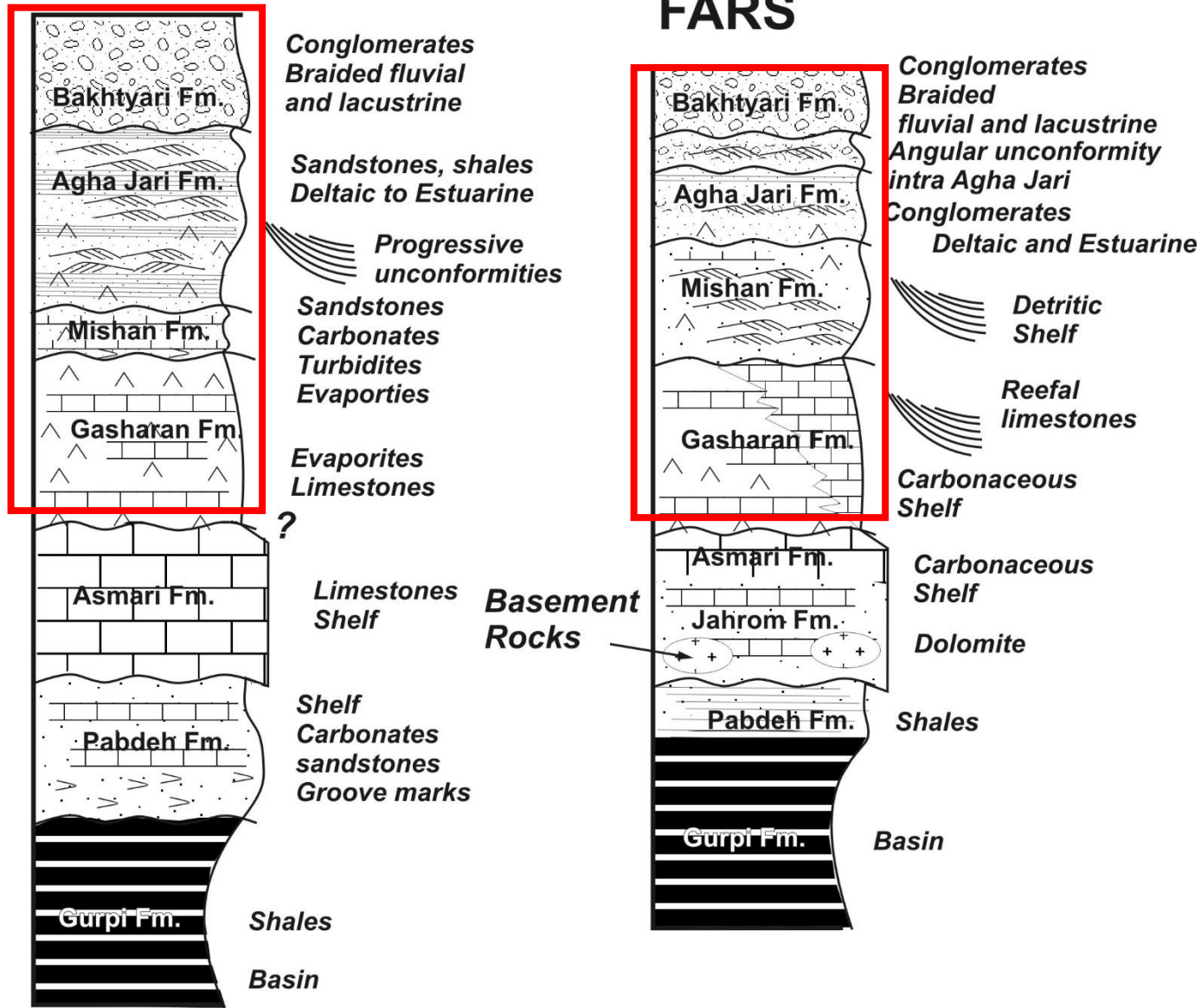


(Mouthereau et al., 2007)

DEZFUL

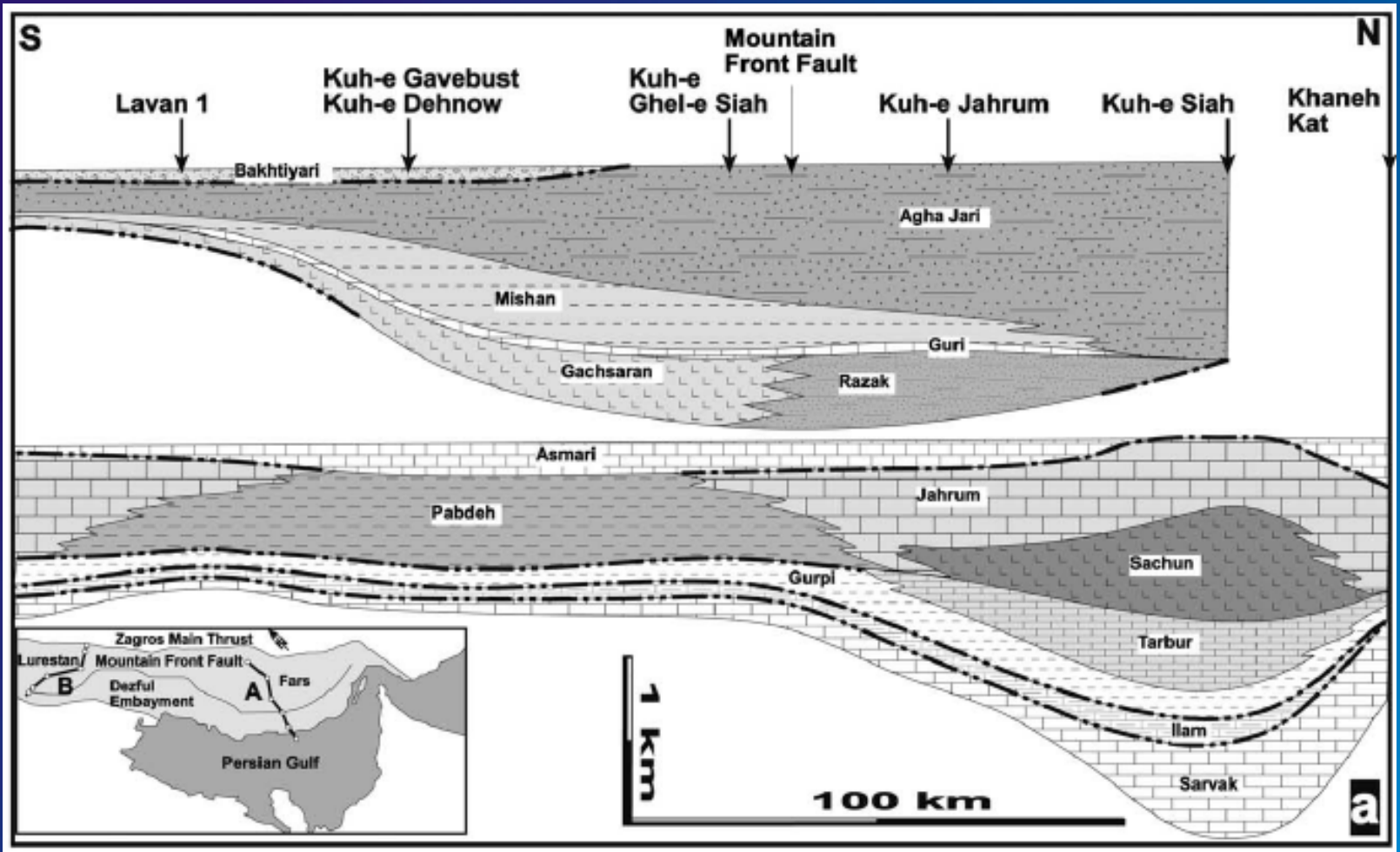
FARS

Regressive sequence



Infill of the foreland basin

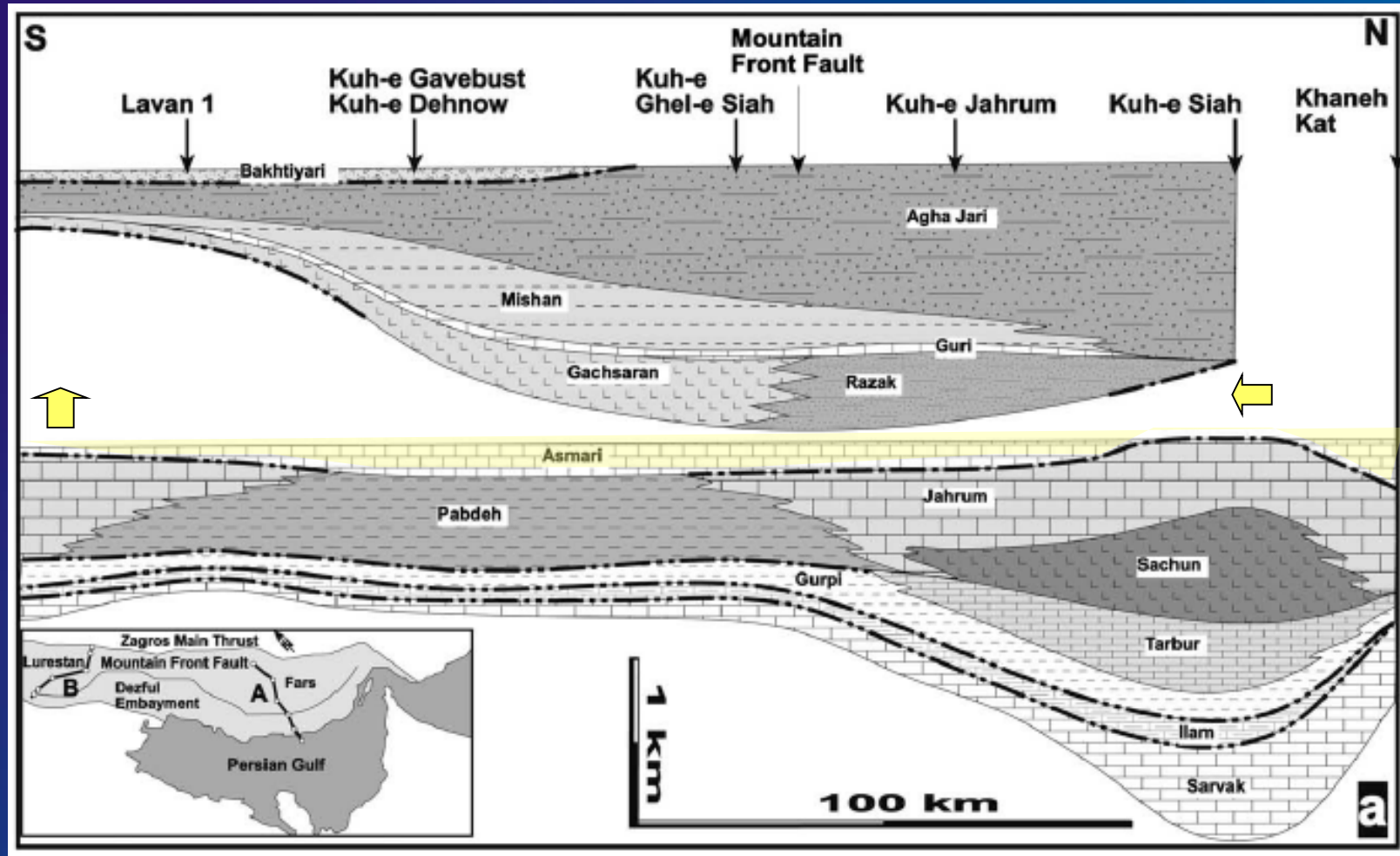
Miocene foreland sequence : thick regressive siliciclastic sequence of the Fars Group



(Sepher and Cosgrove, 2004)

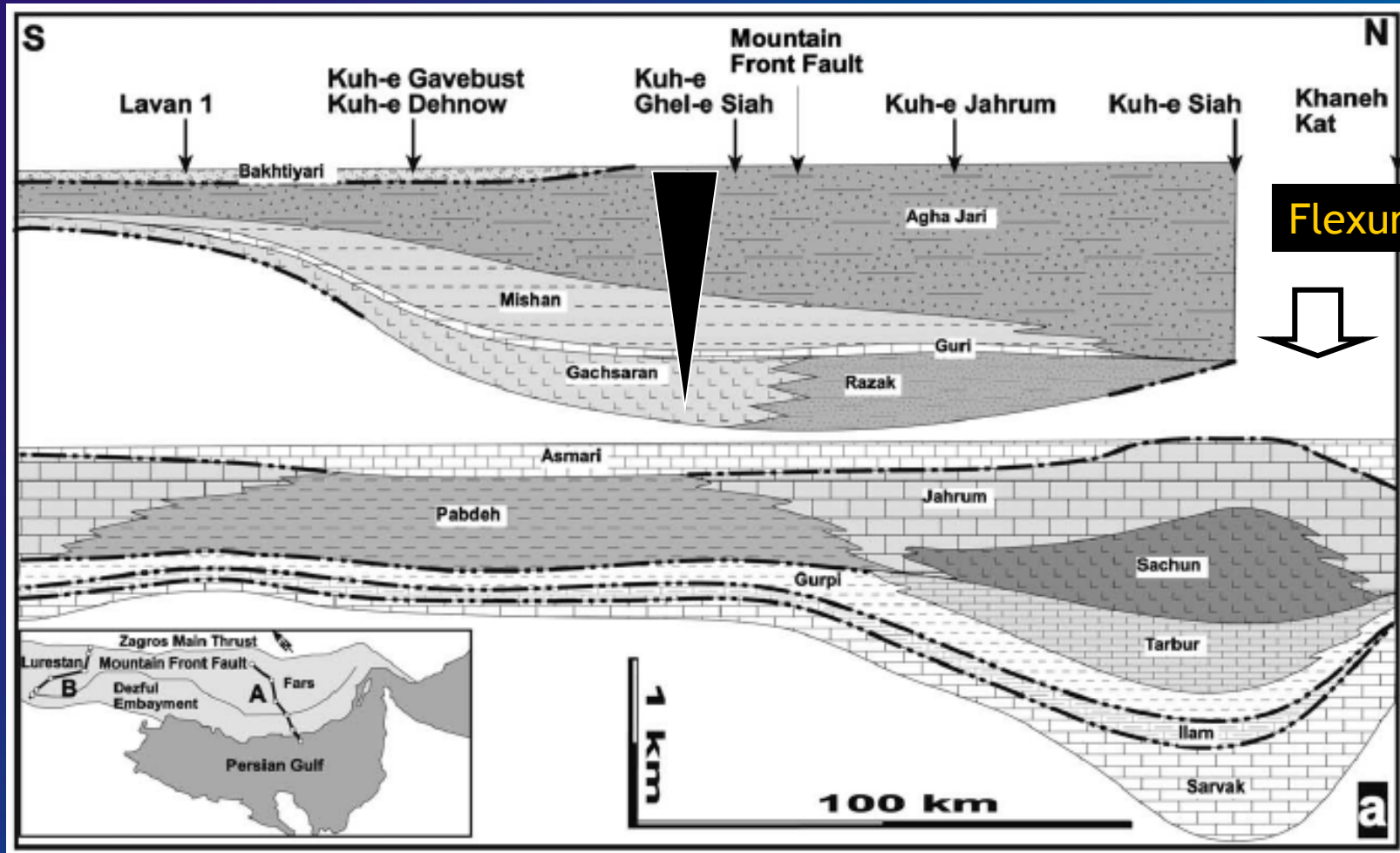
Oligocene- lower Miocene

- Major transgression on the Plateau and the northern Zagros : deposition of miocene flyschs to the north and carbonates to the south.
- No evidence of folding at that time



Miocene. Fars Group

- Regression and filling of the foreland flexural basin; coarsening-upward sequence
- Zagros : migration of the basin, strong subsidence, clasts

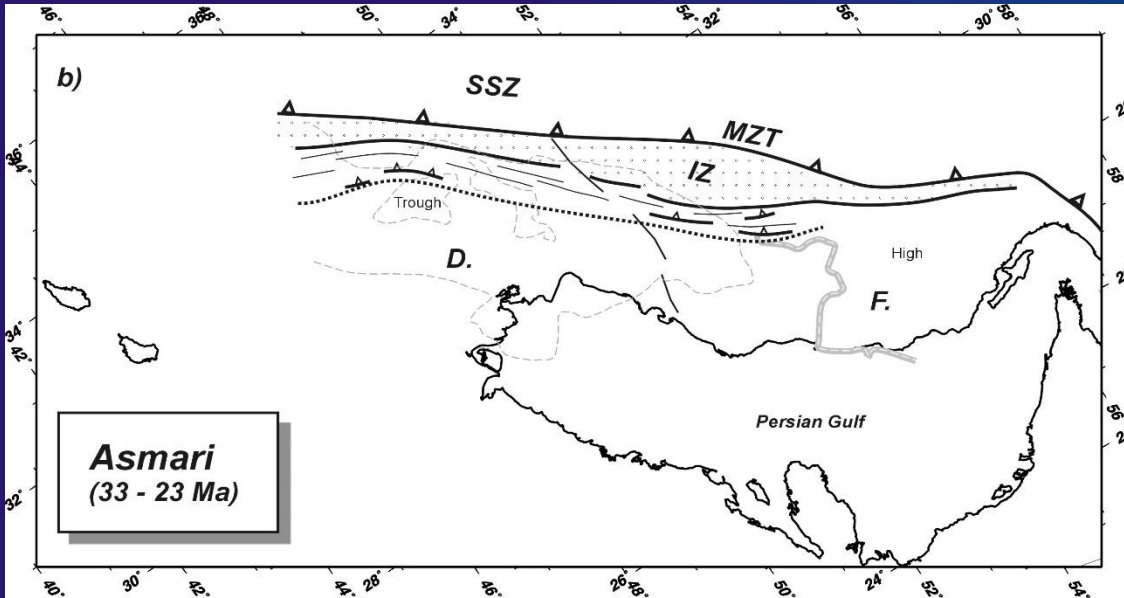


(Sepher and Cosgrove, 2004)

Oldest folding event recorded in the Fars - Oligocene

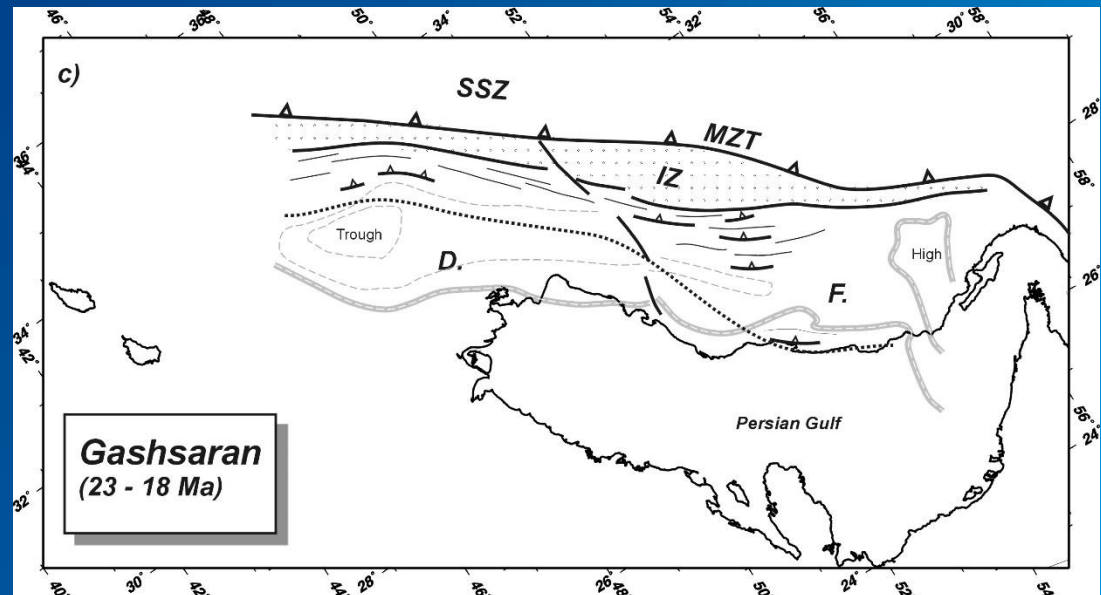
(adapted from Mottiei, 1993)

Migration of the collision southward
Maximum subsidence in the Dezful

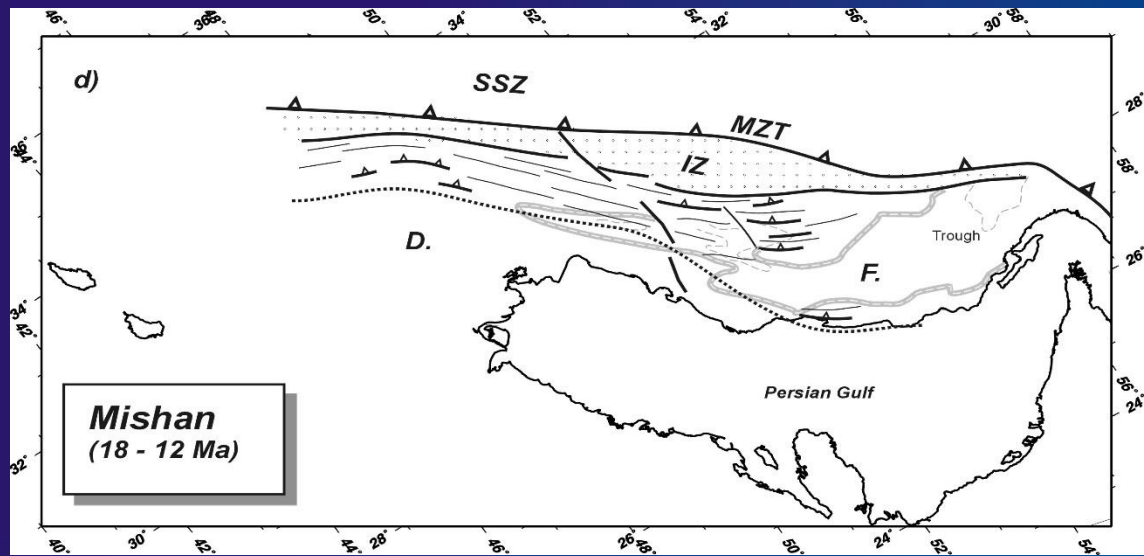


Initiation of deformation in the southern Fars (Gulf Coast)

Migration of the collision southward
Maximum subsidence parallel to the MZT - the flexural basin was formed



Development of the upper Fars and active folding near the Gulf Coast (formation of an intramountain trough)

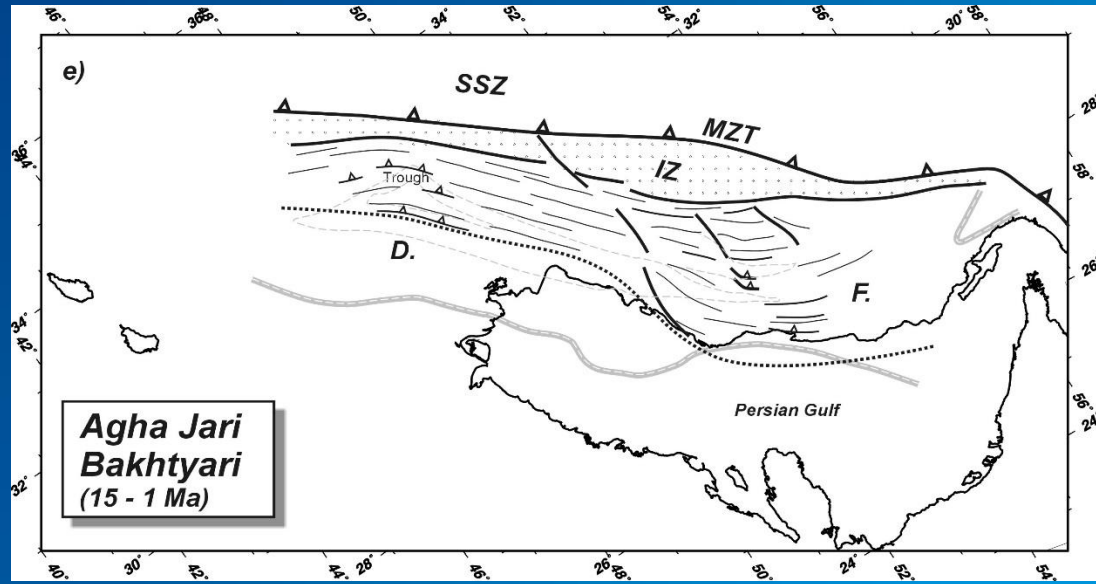


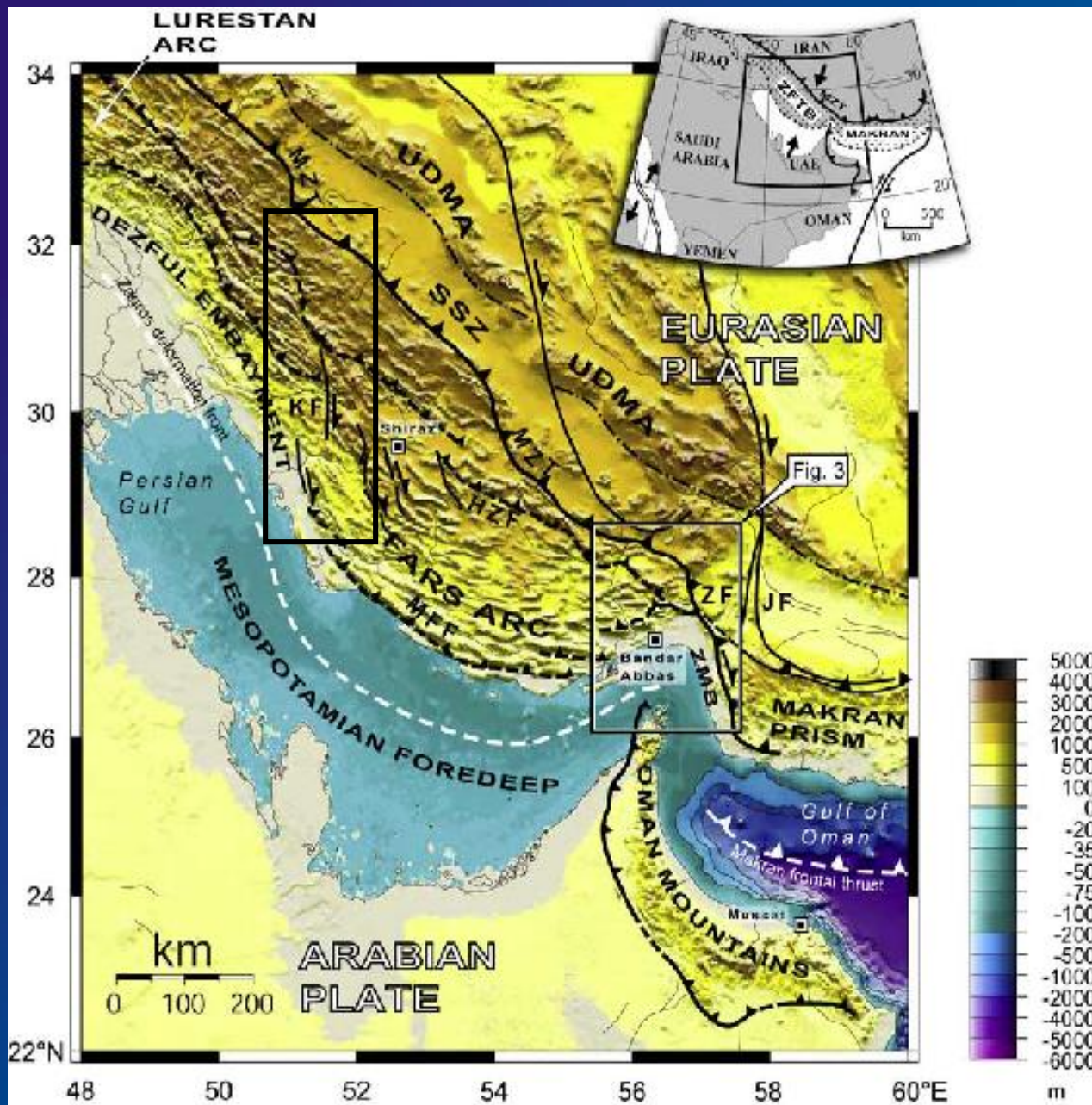
Migration of the collision southward
Maximum subsidence toward a southern trough

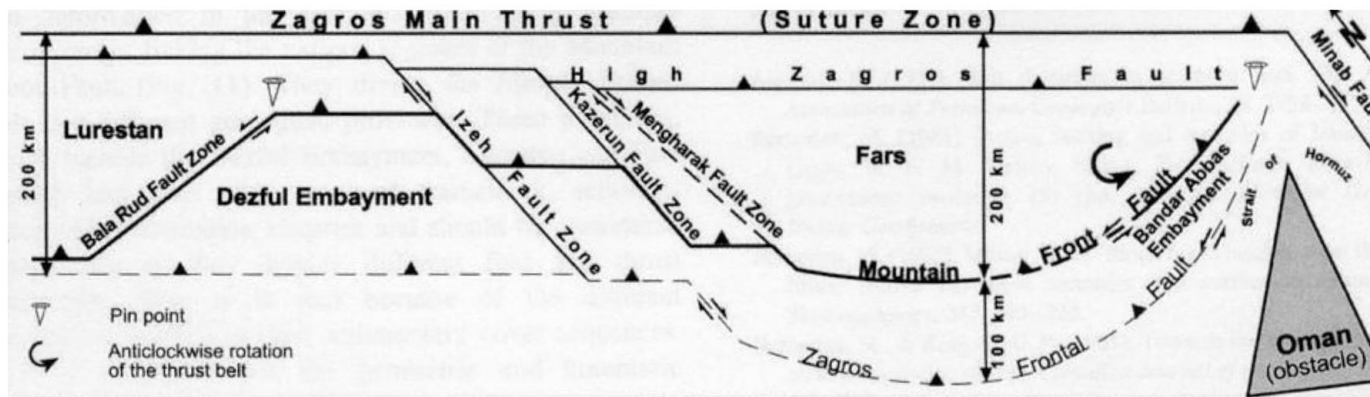
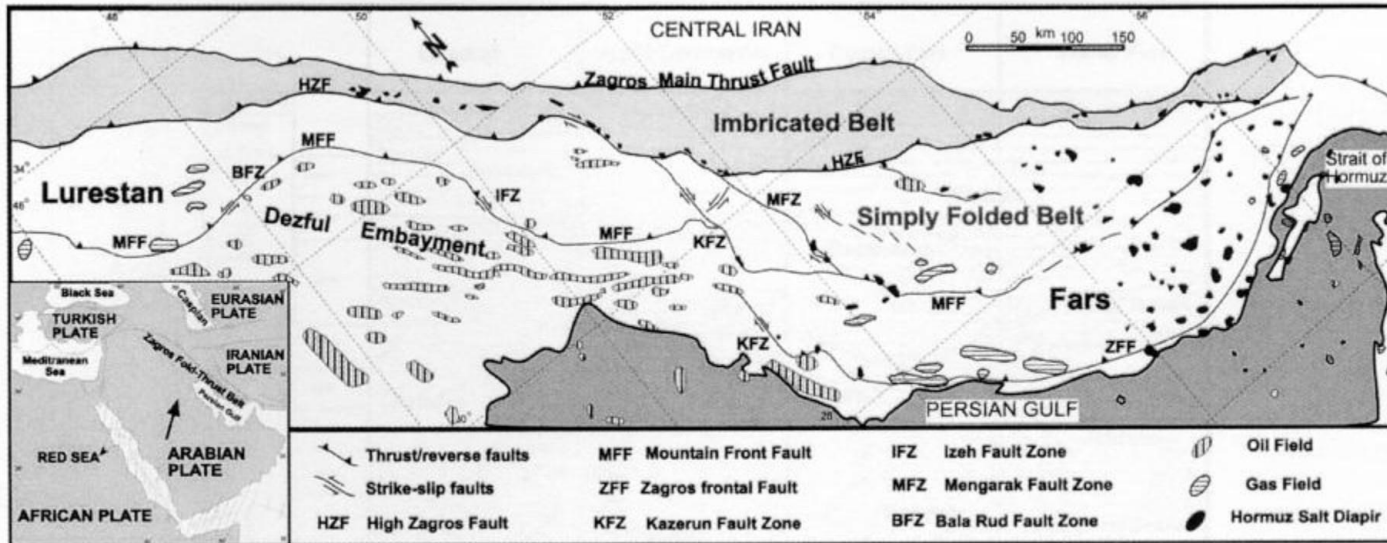
(adapted from Mottiei, 1993)

Renewed subsidence in the Dezful and achievement of the present structure of the ZSFB

Migration of the deformation front toward the Arabian shelf
Maximum subsidence domain propagated into the Arabian shelf consistently

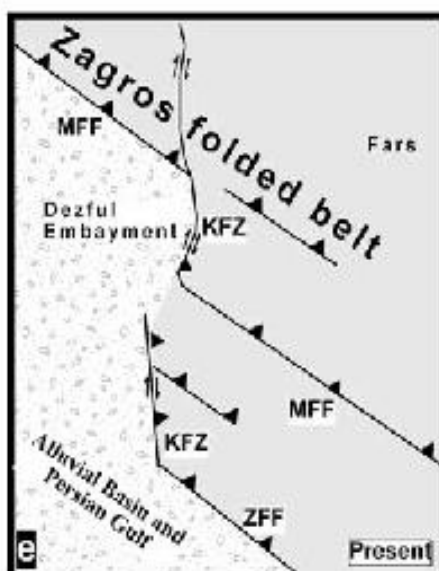
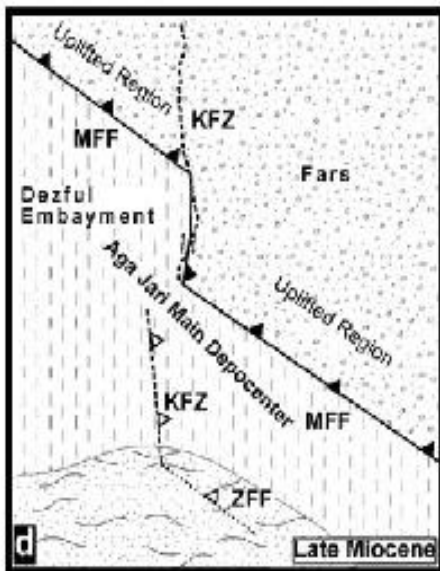
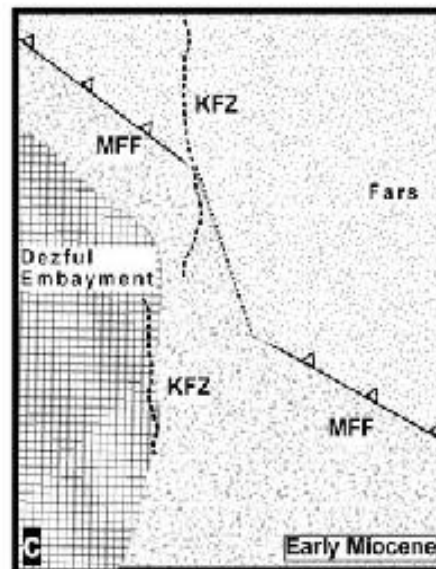
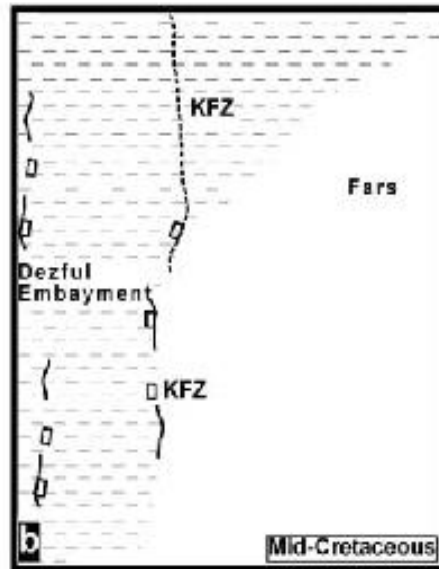
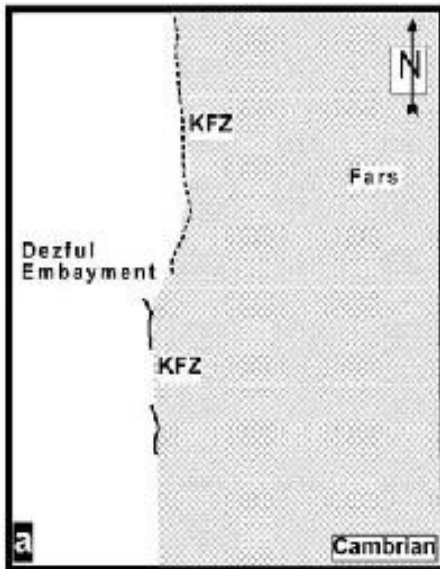






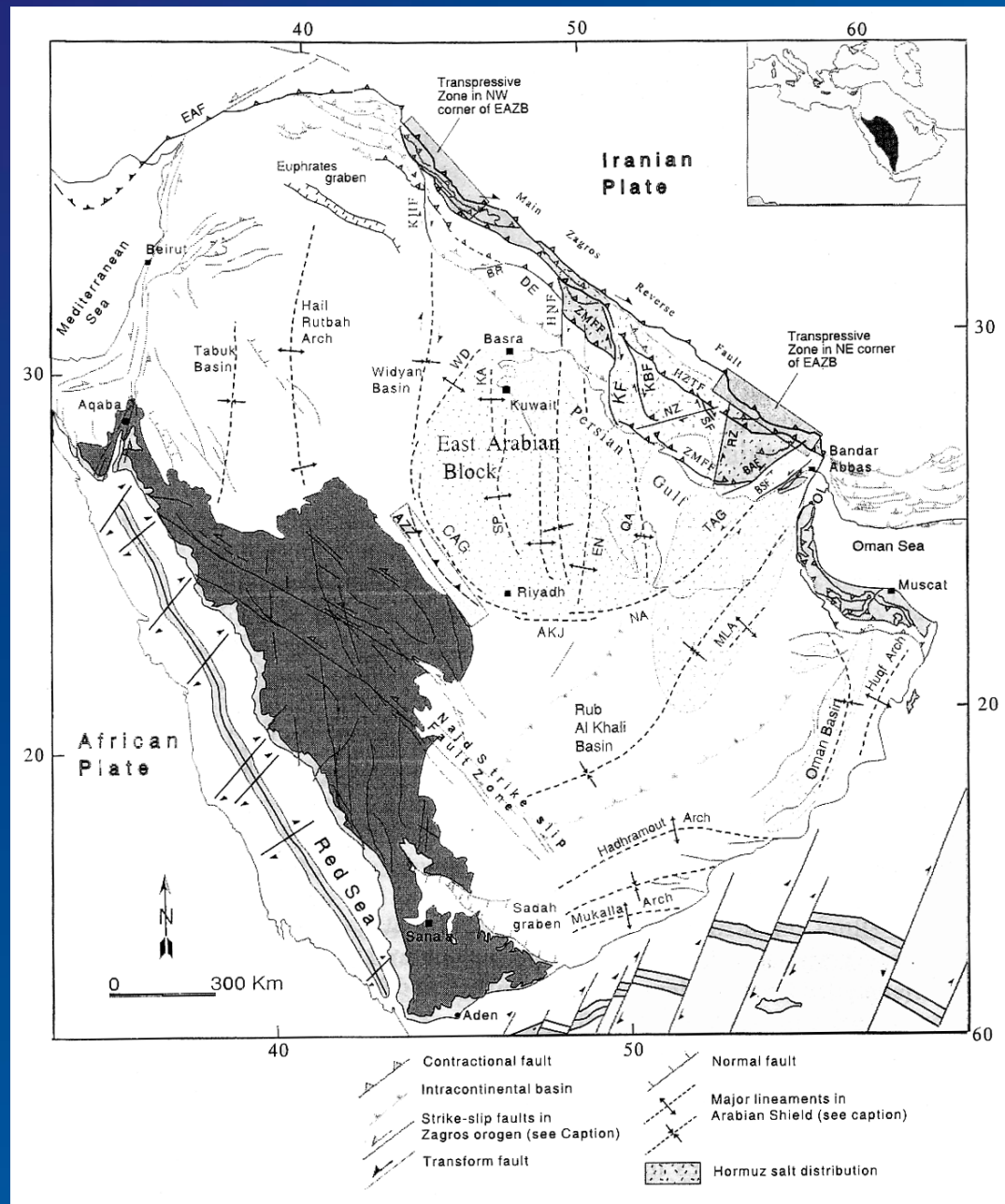


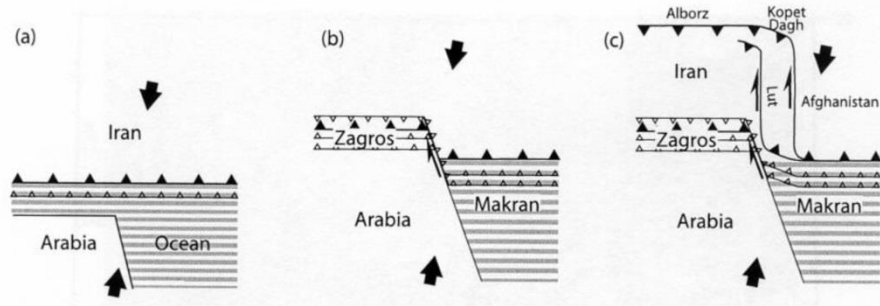
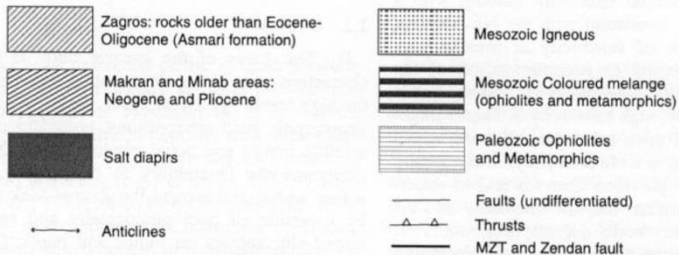
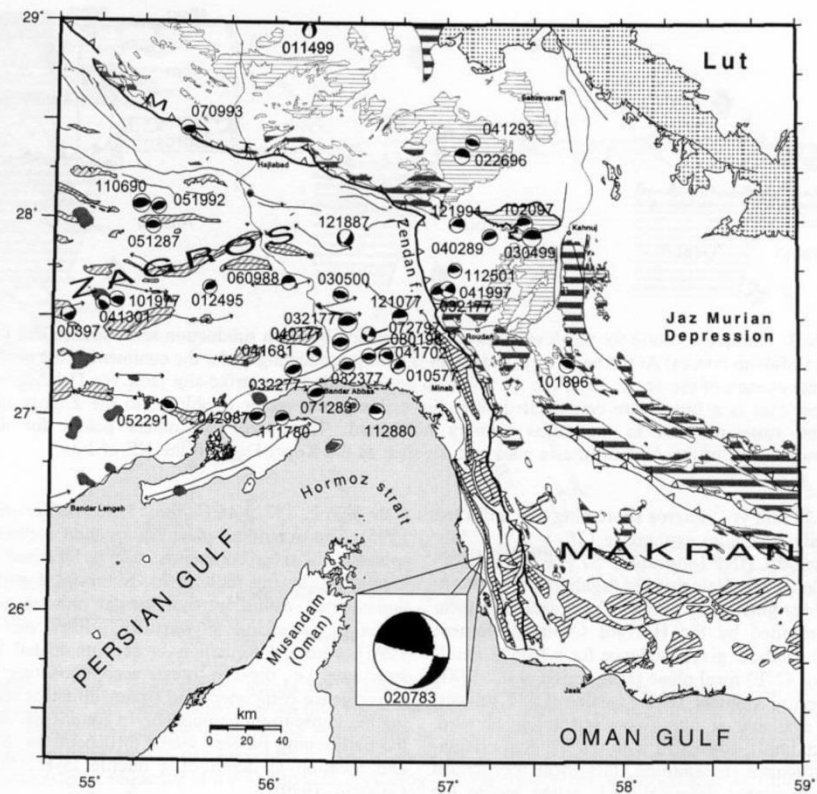
(Sepher and Cosgrove, 2005)



N-S basement faults
underlying the Zagros cover
inherited from
Panafrican orogeny

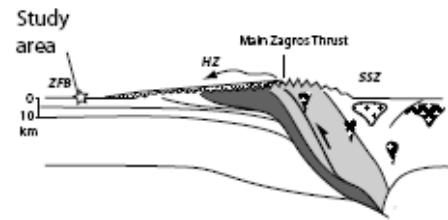
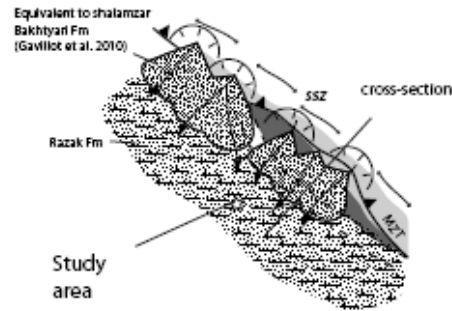
(Al Laboun, 1986; Beydoun,
1991; Berberian, 1995;
Weijermars, 1998;
Husseini, 2000;
Bahroudi and Talbot, 2003)



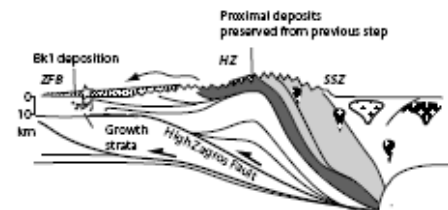
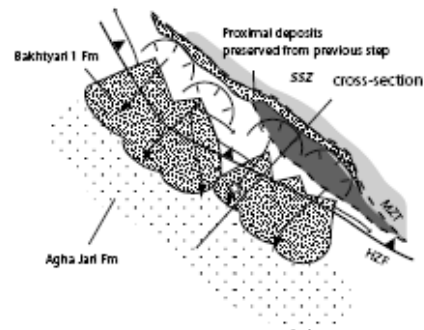


(Regard et al., 2004)

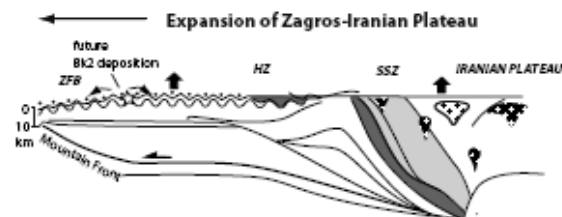
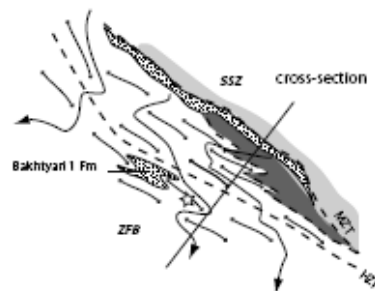
A) Early Miocene (19.7-16.6 Ma)



B) Early-Middle Miocene (16.6-13.8 Ma)



C) Late Miocene (<12.4 Ma)



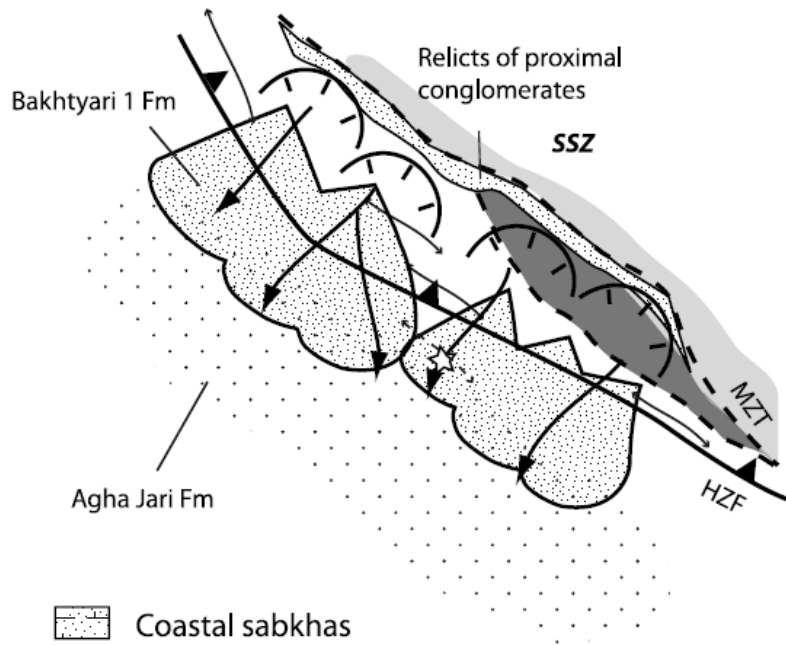
- Coastal sabkhas
- Alluvial fans
- Deltic environments



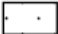
- Metamorphic mélange + Sanandaj-Sirjan HP belt
- Obducted complex
- Granite
- Gabbroic intrusion

(Khadivi et al., 2012)

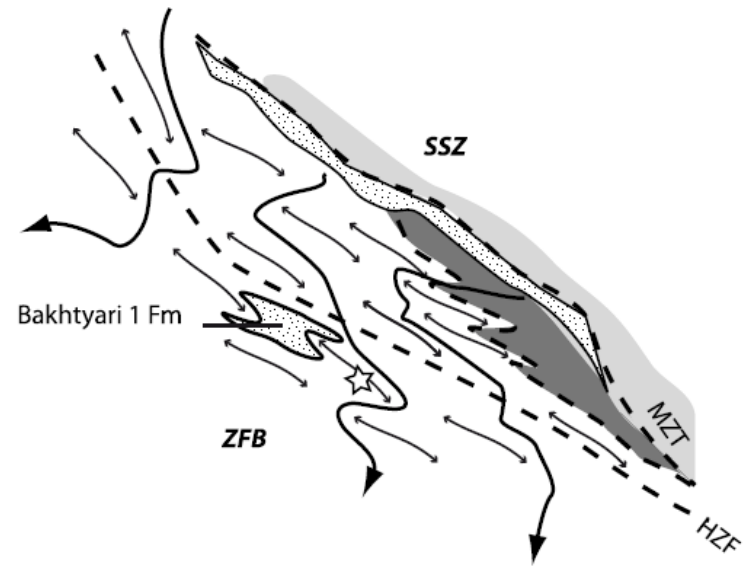
Drainage reorganisation from transverse to axial river network



Early-Middle Miocene (16.6-13.8 Ma)



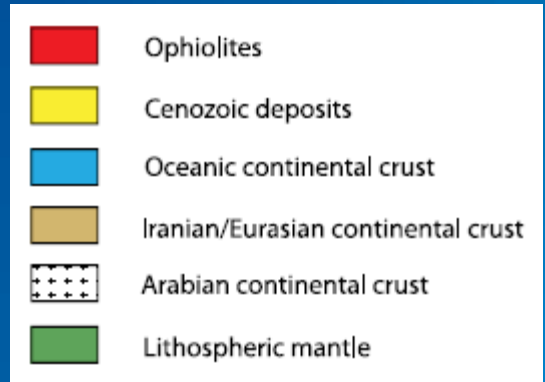
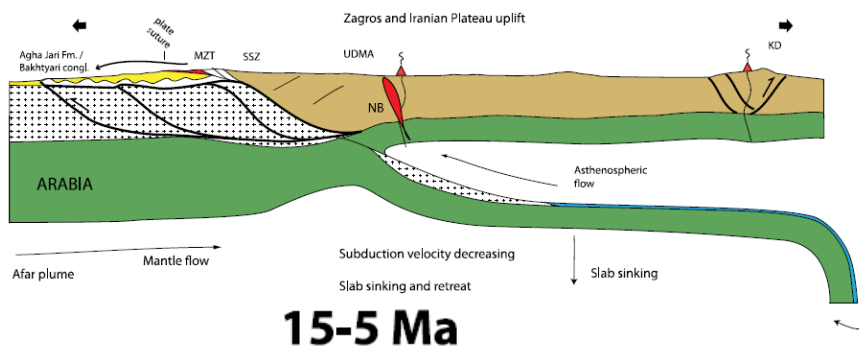
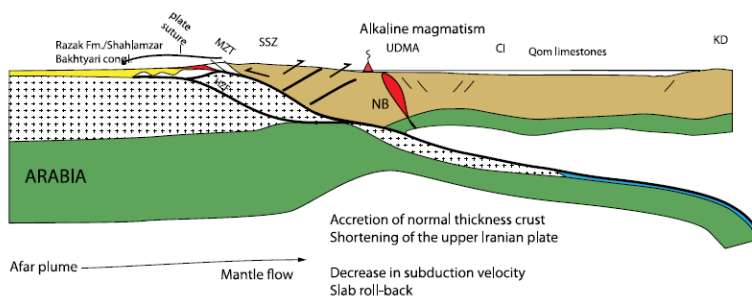
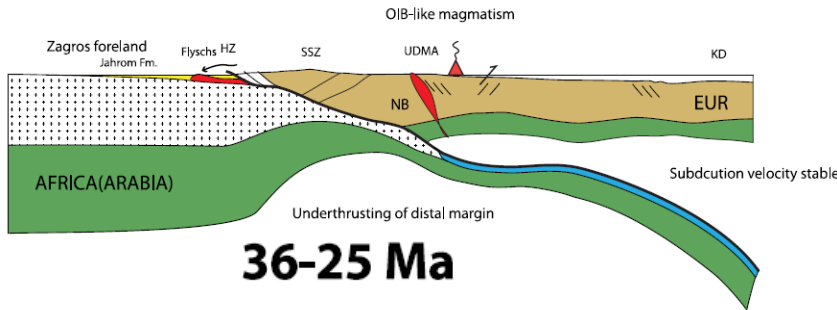
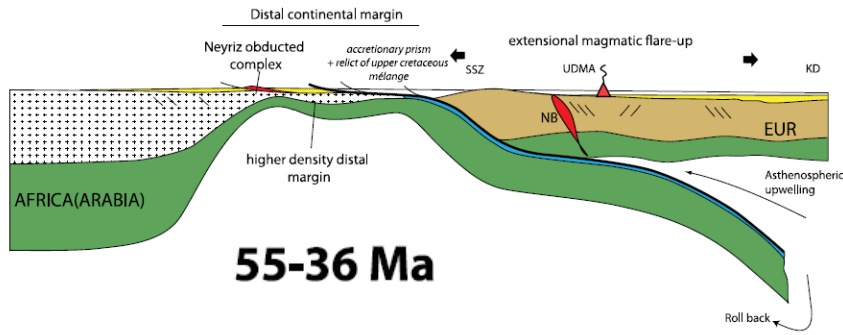
-  Coastal sabkhas
-  Alluvial fans
-  Deltaic environments

Late Miocene (<12.4 Ma)



-  Metamorphic mélange + Sanandaj-Sirjan HP belt
-  Obducted complex

Central Zagros



Deformation in the Zagros (1) : folding

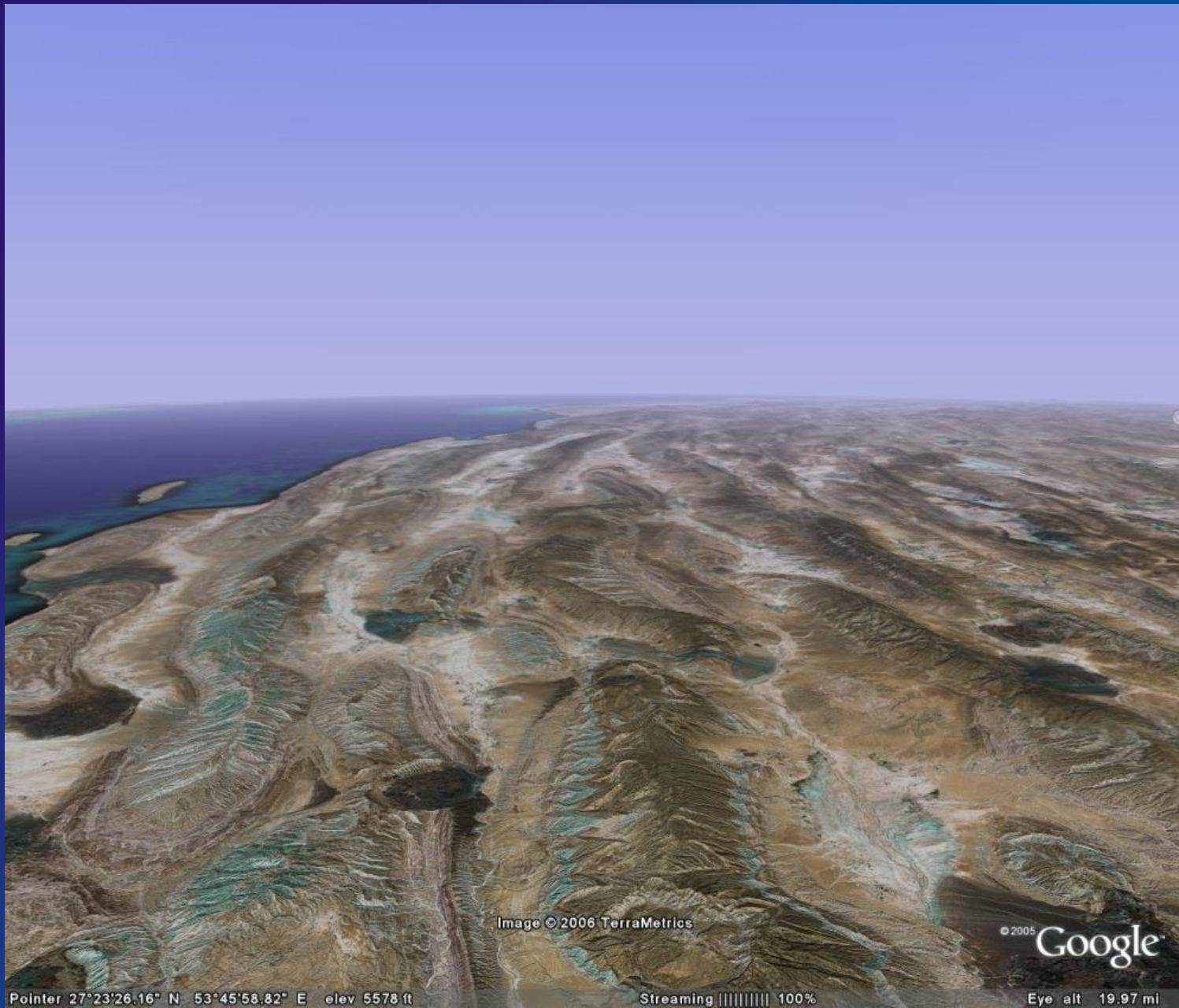


Image © 2006 TerraMetrics

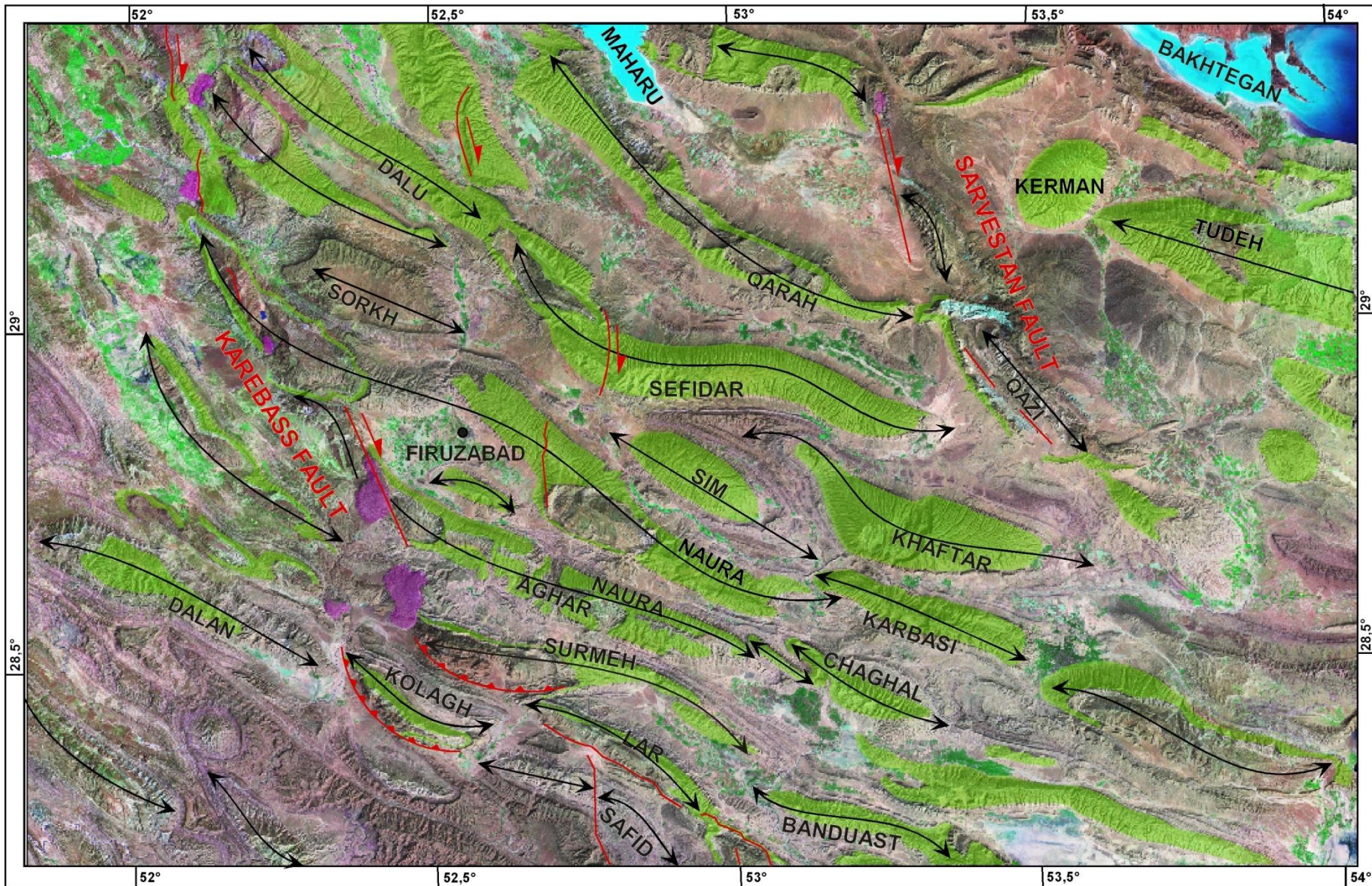
© 2005 Google

Pointer 27°23'26.16" N 53°45'58.82" E elev 5578 ft

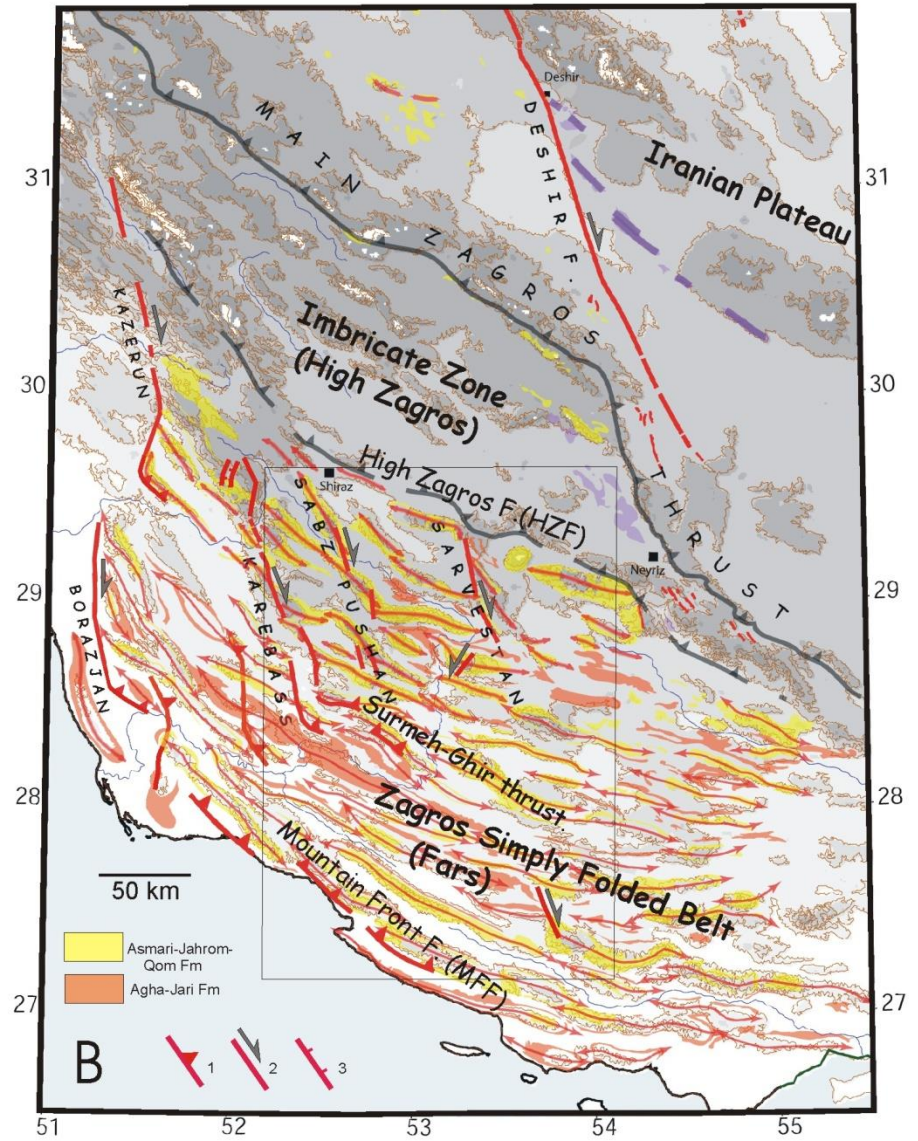
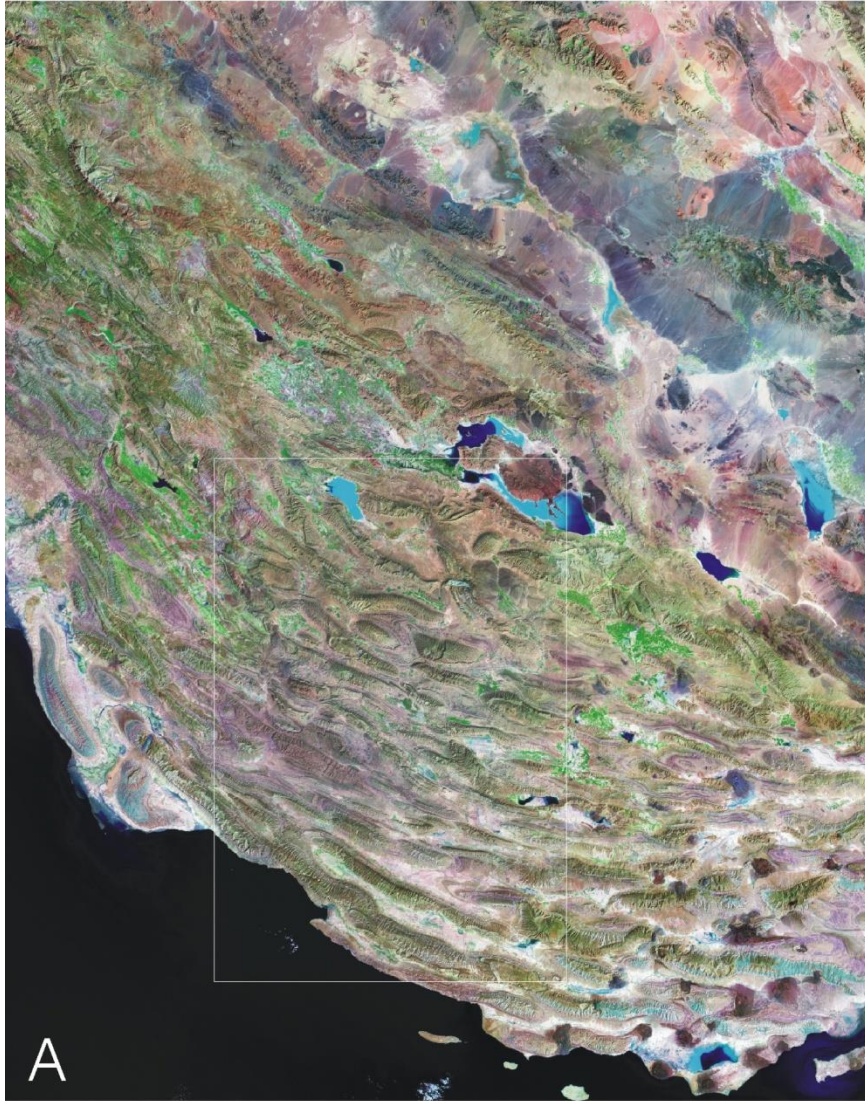
Streaming ||||| 100%

Eye alt 19.97 mi

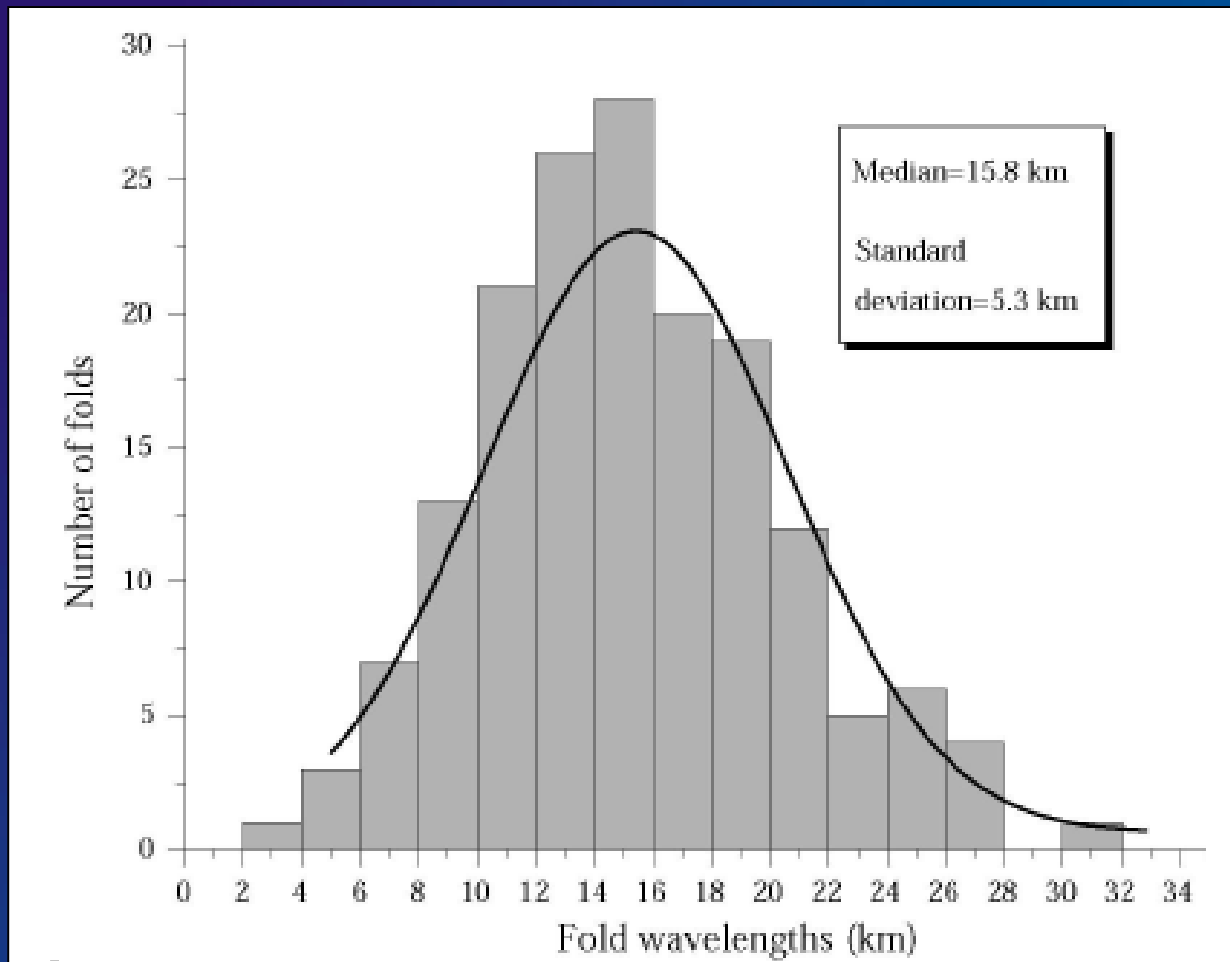




Fars



(Lacombe et al., 2006)



(Mouthereau et al, 2007a, b)





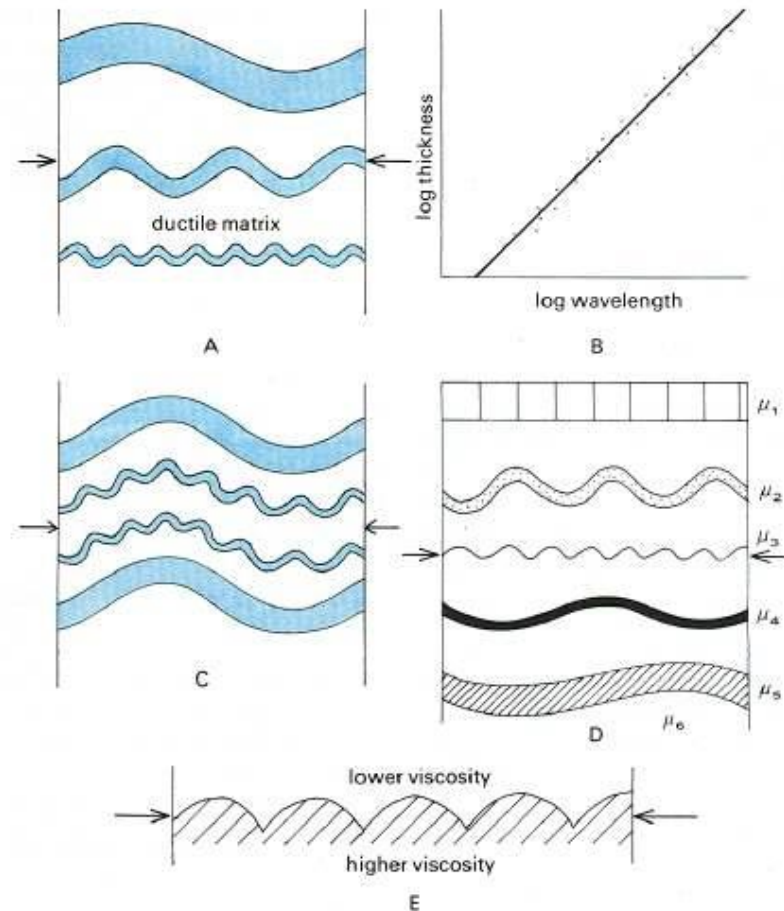




« buckle folds »

Development of this type of folds requires a significant contrast of competence between the folded strata (elastic or viscous) and the surrounding medium (viscous).

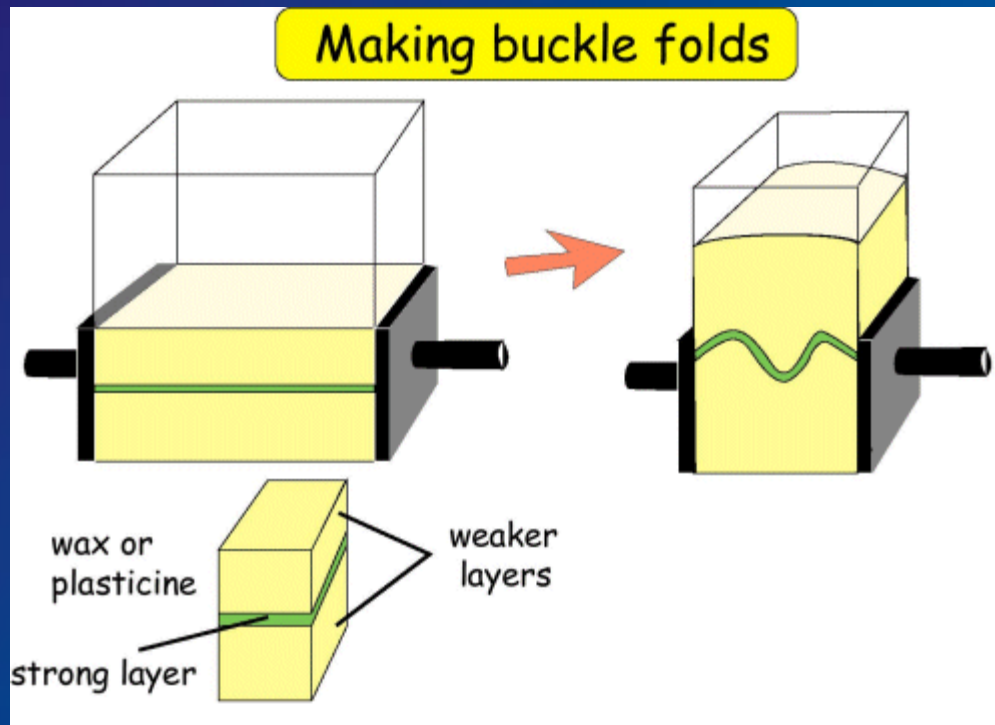
In this case, there is a direct relationship between the thickness of the competent strata and the wavelength of folding.



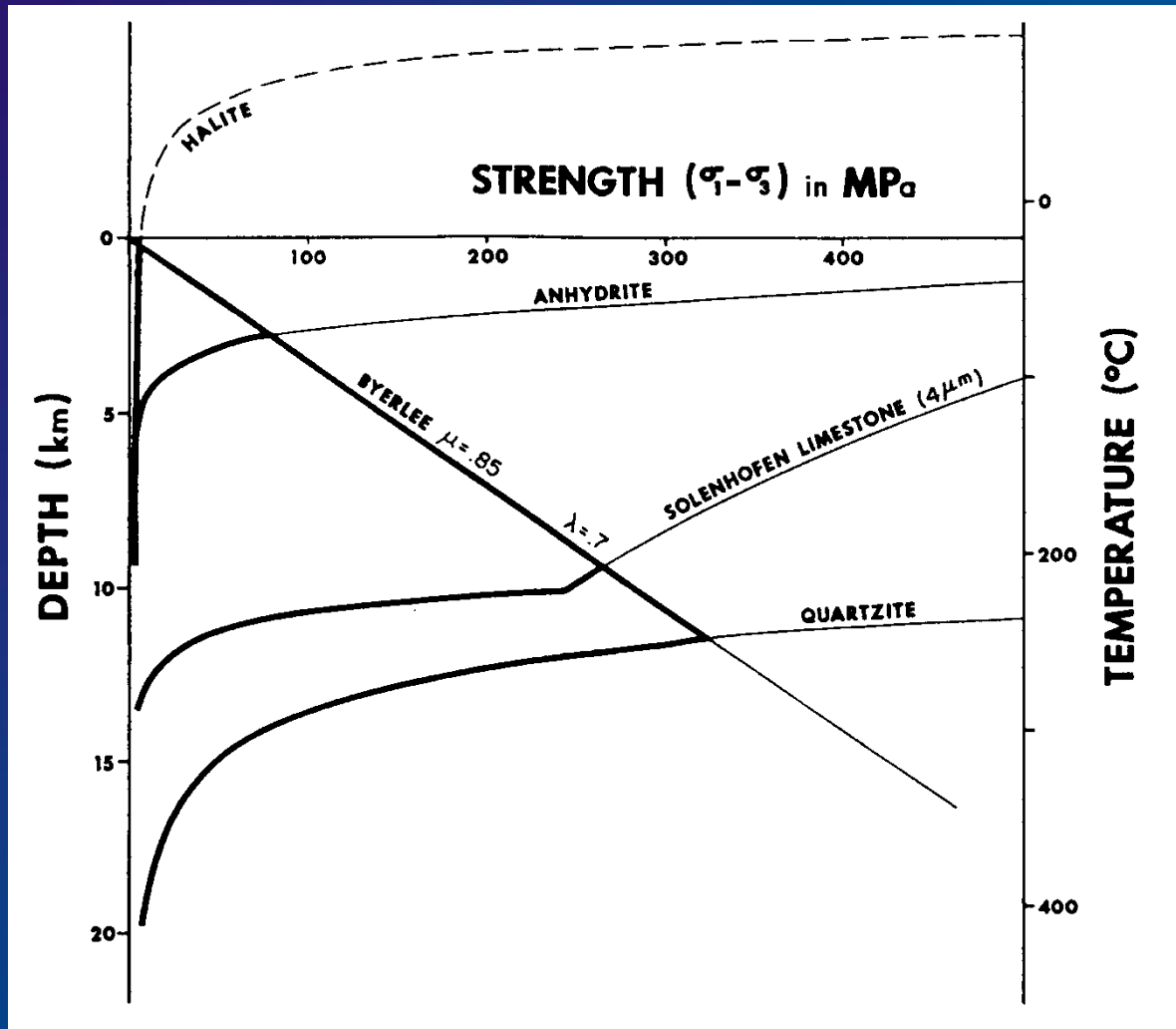
Influence of layer thickness and viscosity contrast on the wavelength of buckle folds. A, B. There is a linear relationship between log layer thickness and log buckle wavelength for widely separated layers of constant viscosity in a ductile matrix of much lower viscosity. C. Buckle folds of different wavelength may be superimposed if the layers are close enough to interfere. D. Buckle folding produced by a number of layers of different viscosity μ_1 - μ_5 and different thickness in a ductile matrix of much lower viscosity μ_0 . A, C and D are examples of disharmonic folding (see section 3.6). (After Ramberg, H. (1964) *Tectonophysics*, 1, 307-41.) E. Buckle folding of an interface between two thick layers of contrasting viscosity. The cusps point towards the material of higher viscosity (cf. mullion structure, see section 4.2 and Figure 4.8B).

« buckle folds »

Conditions : « pure shear »



Mechanical behaviour of evaporites



Wavelength L_w for viscous buckling

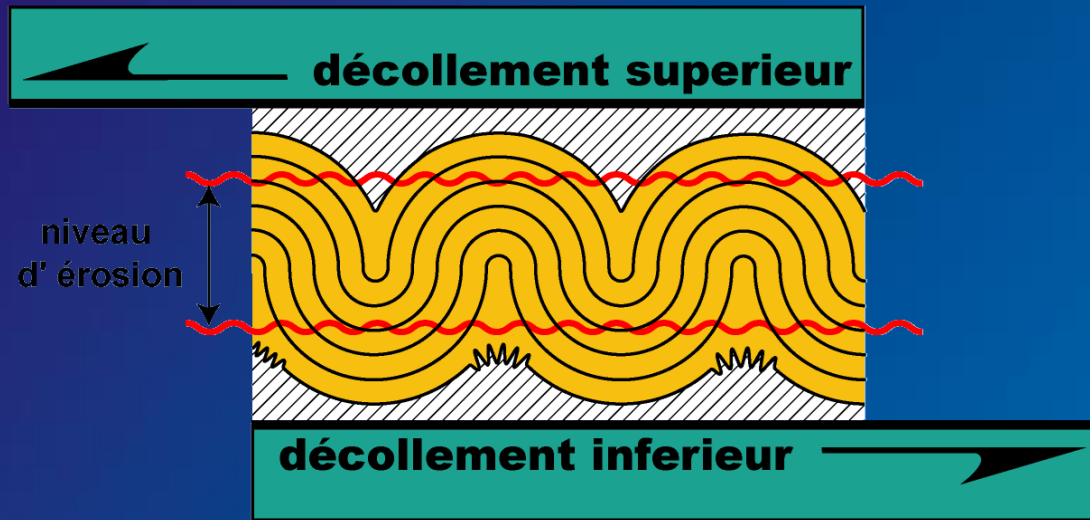


$$L_w = 2\pi H 6^{-1/3} \sqrt[3]{\eta_l / \eta_m}$$

Initial
thickness of
competent
strata

Viscosity
contrast
between
strata and
matrix

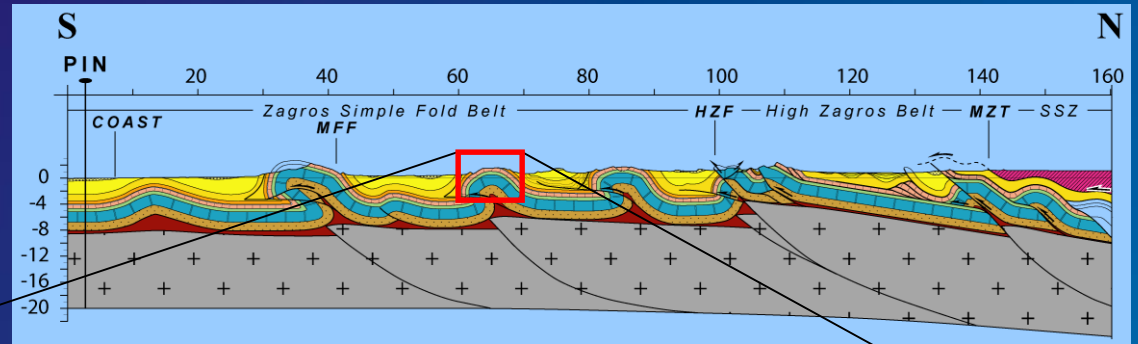
Outcrop scale



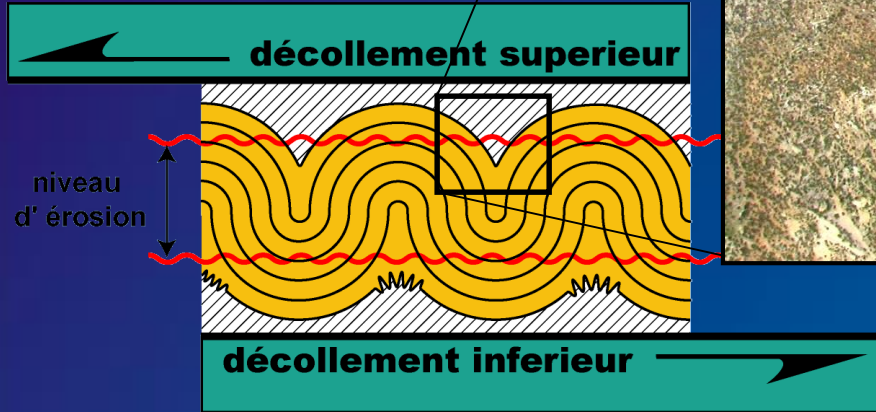
Dahlstrom (1969)

Concentric folding requires 2 décollement levels

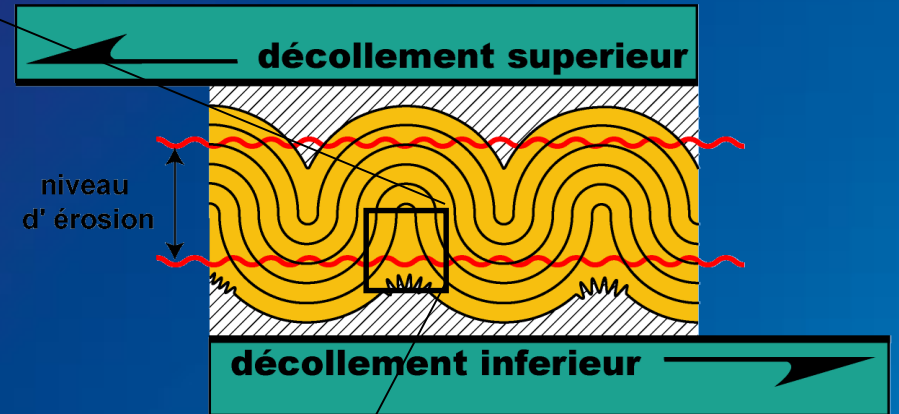
Décollement fold with typical geometry (eastern Zagros)
(Molinaro, 2004)



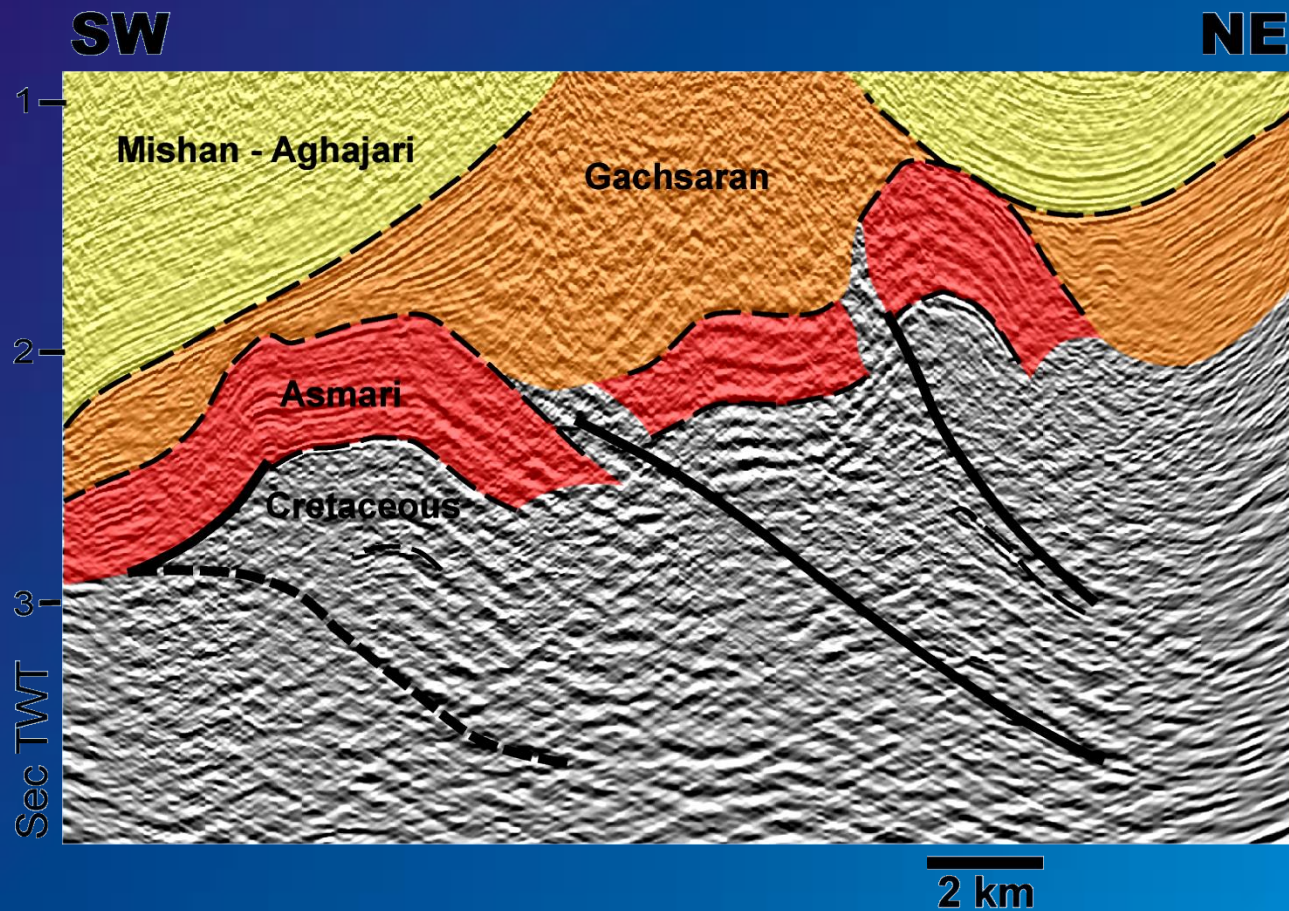
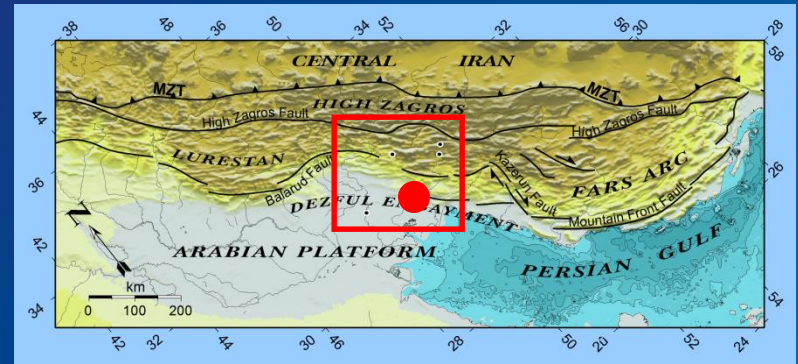
Syncline located just below the upper décollement (Gachsaran evaporites) (Sherkati, 2004)

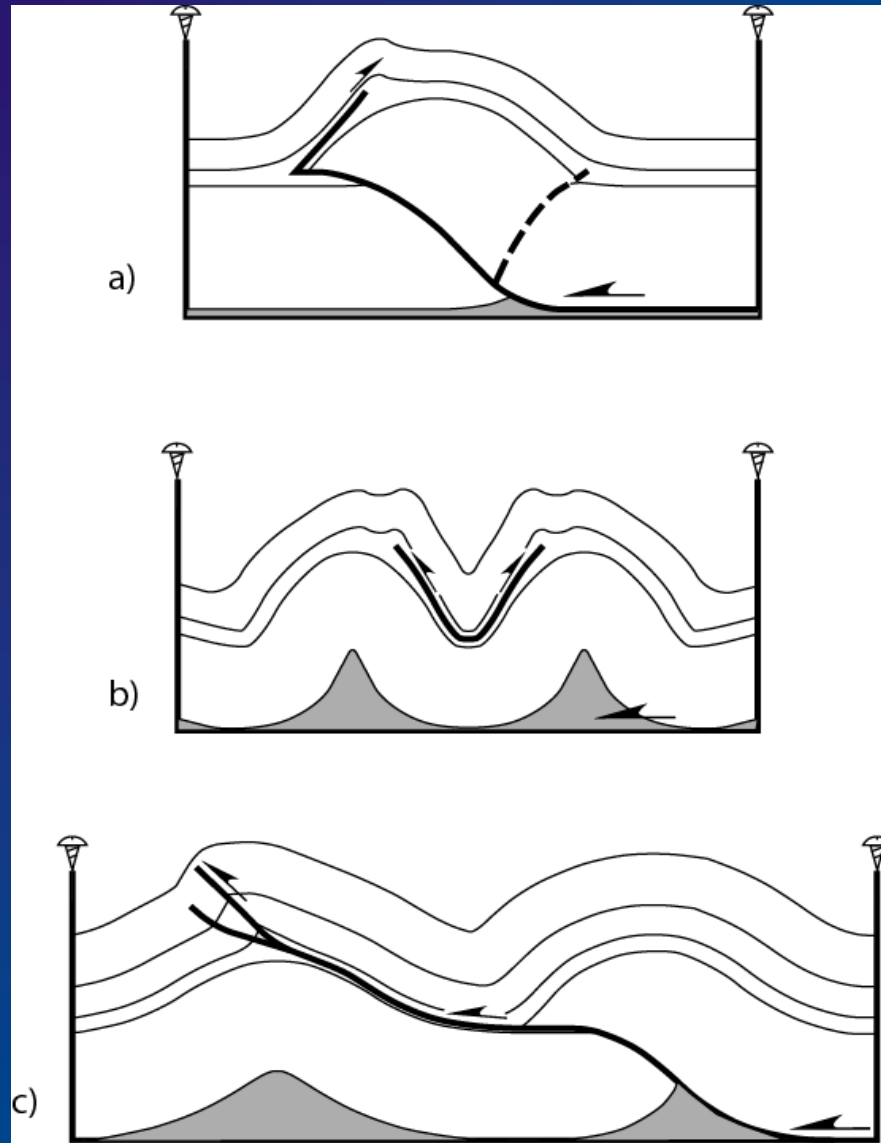


Anticline located just above the lower décollement (Kadjumi Fm) (Sherkati, 2004)



Complete decoupling across upper
décollement (Gachsaran salt)
(Sherkati, 2004)

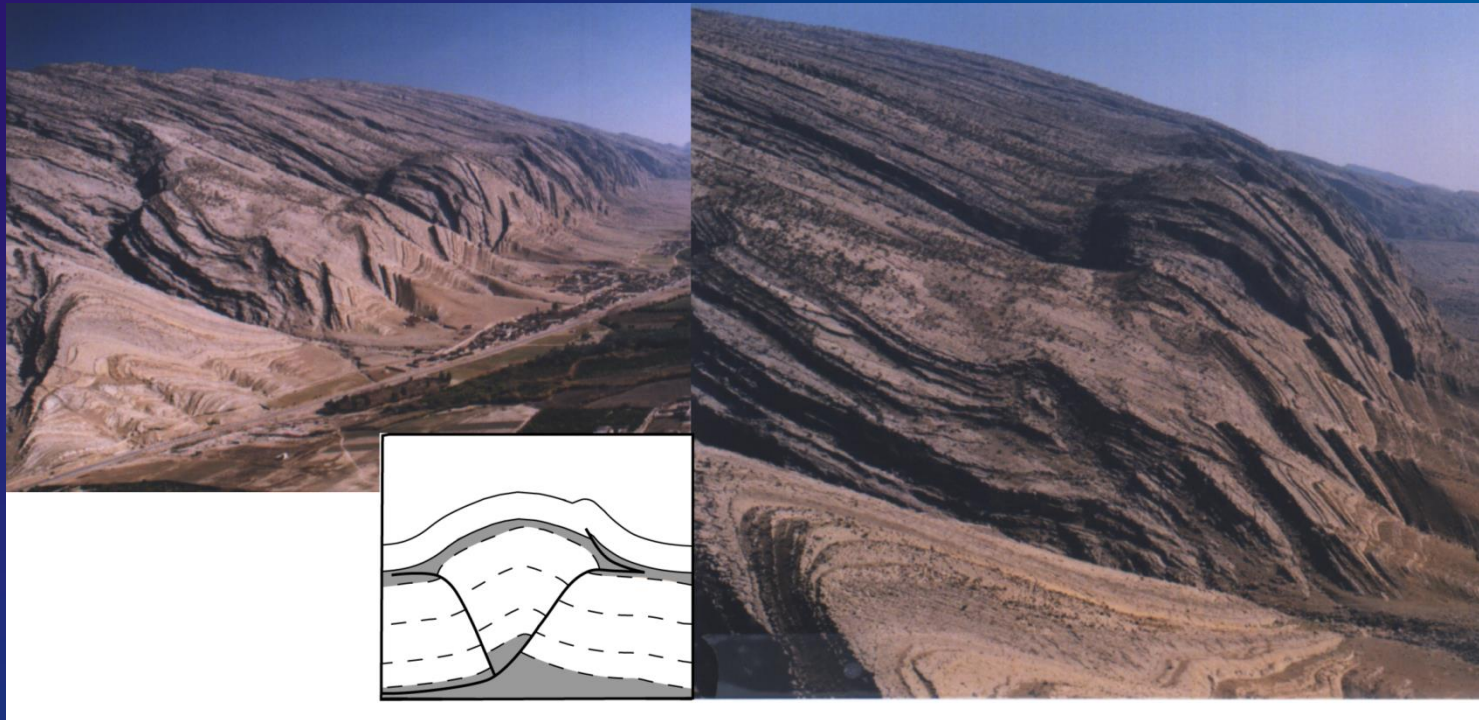




Role of intermediate décollement levels

a) et b): « rabbit-ear » folds

c): transmission of deformation from one fold to the other



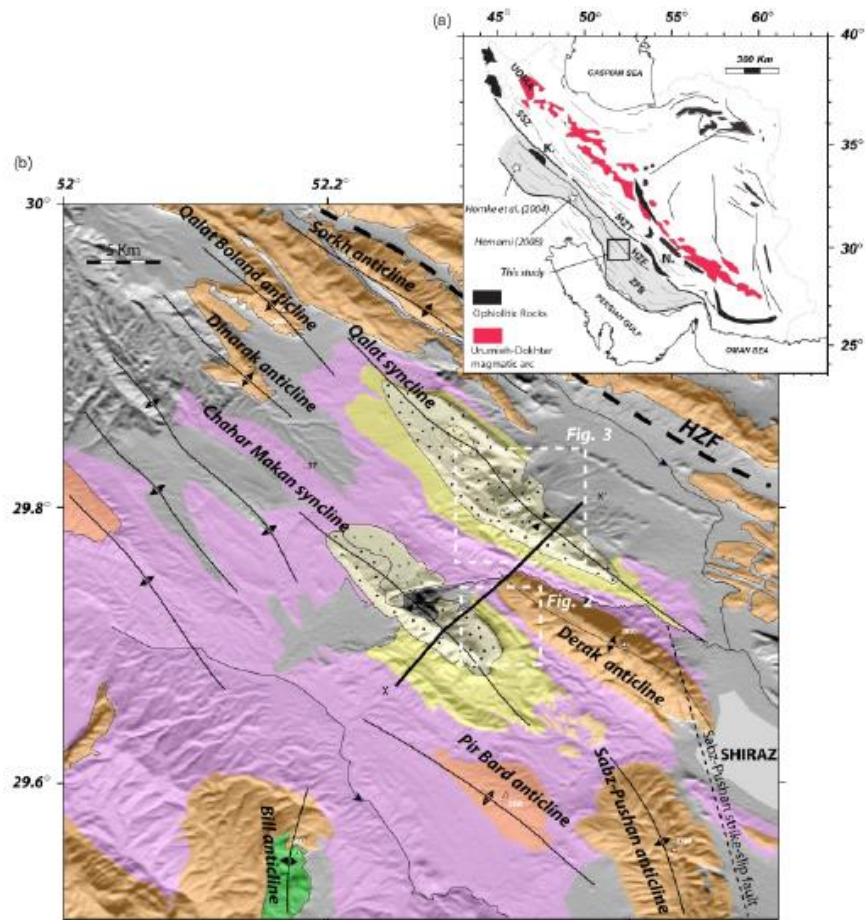
Example of « rabbit-ear » fold (central Zagros)

Upper Miocene : growth strata within upper Agha Jari Fm

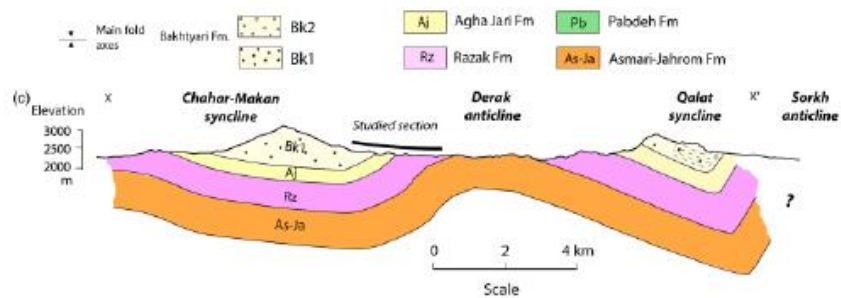


Plio-Pleistocene : Major post-folding unconformity
Regional uplift after deposition of Agha Jari Fm.

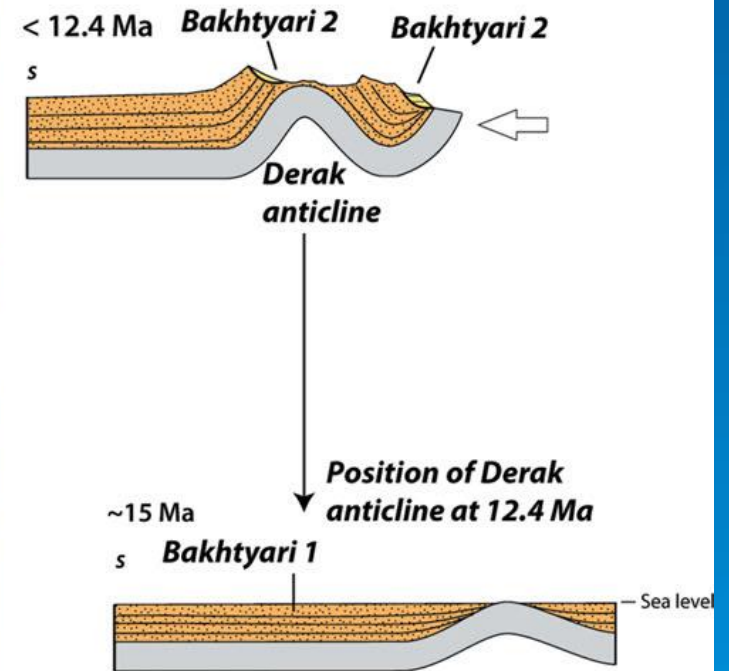
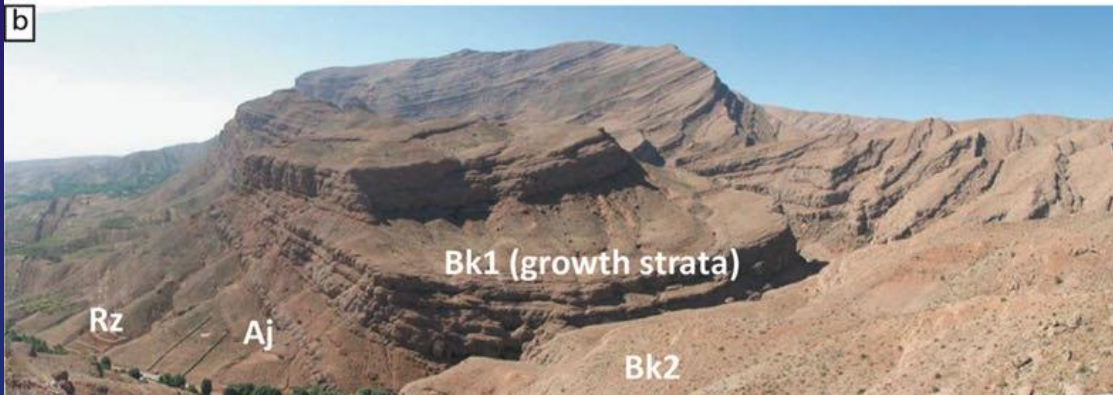




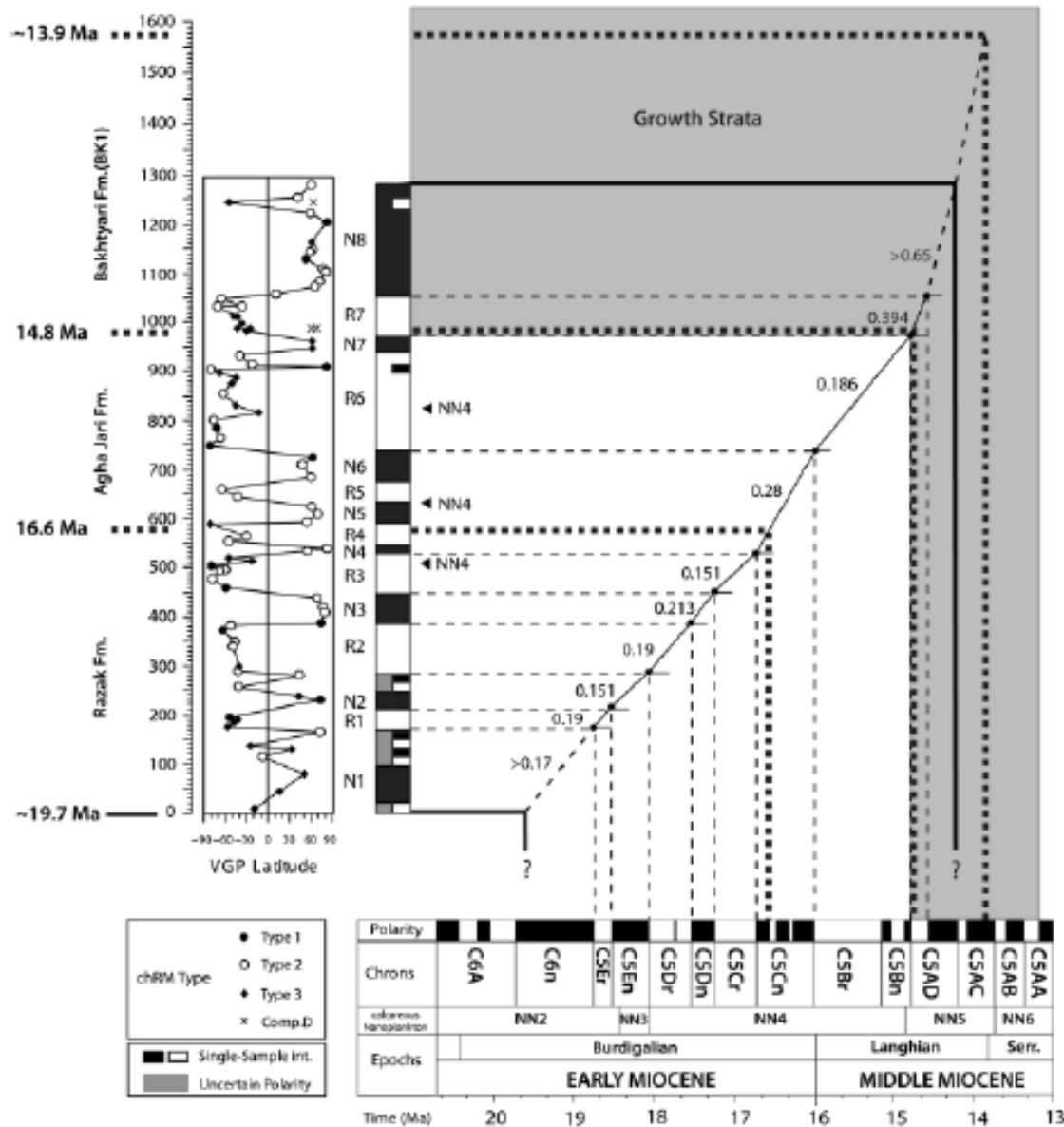
(Khadivi et al., 2010)



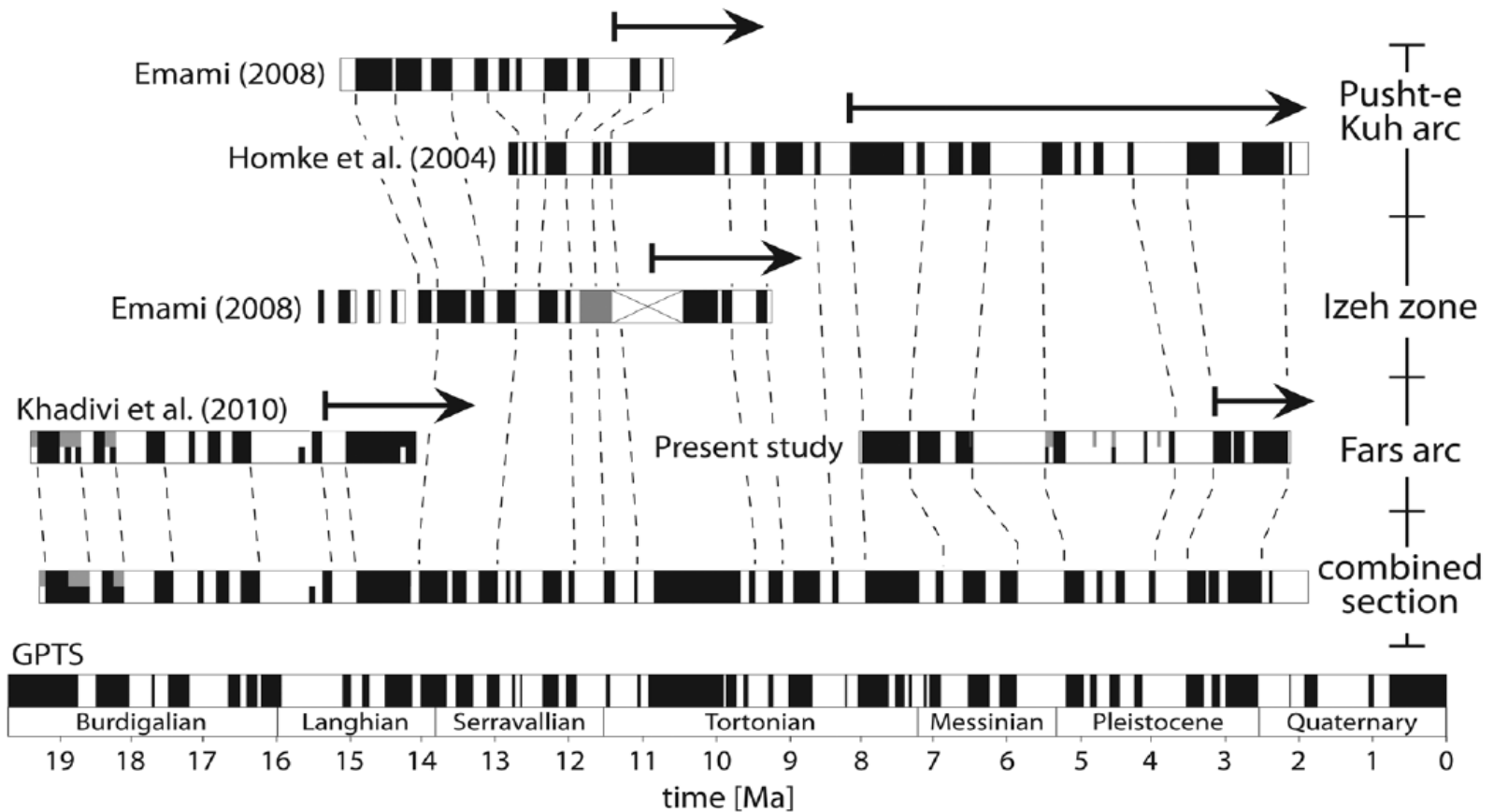
Fars



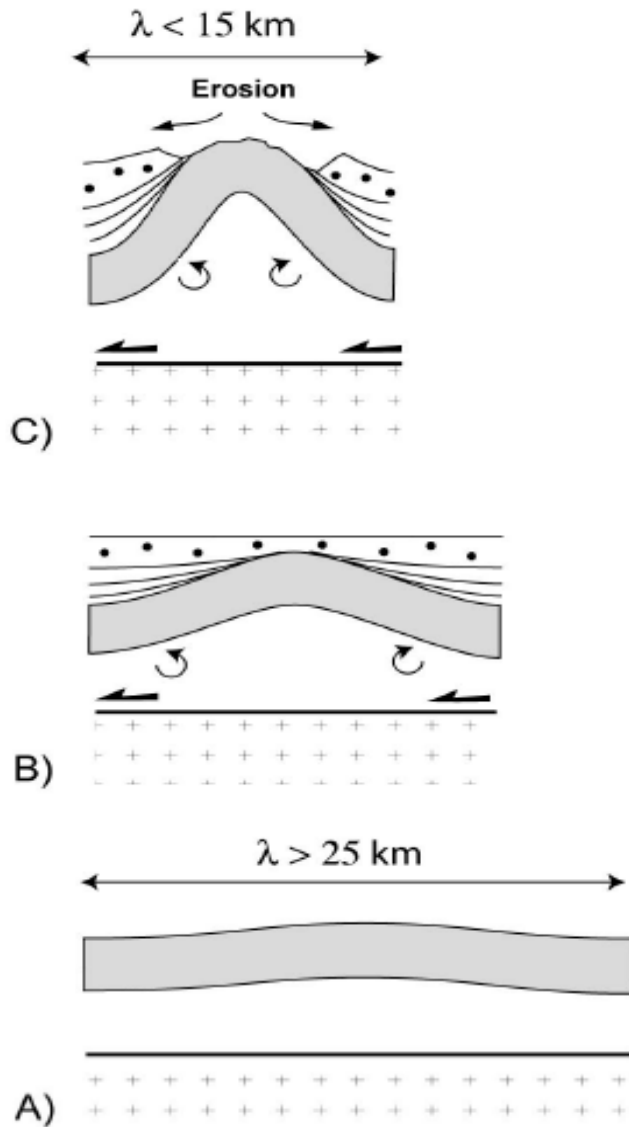
(Khadivi et al., 2010)



(Khadiji et al., 2010)



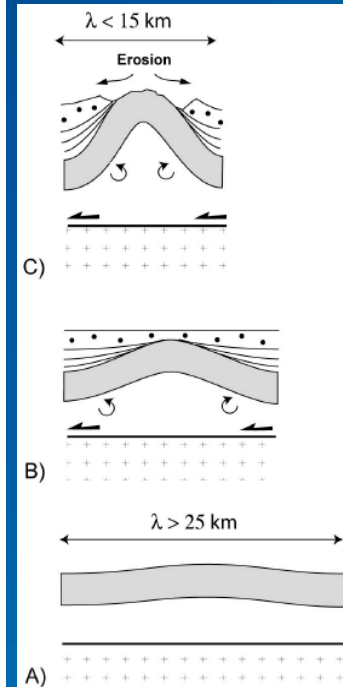
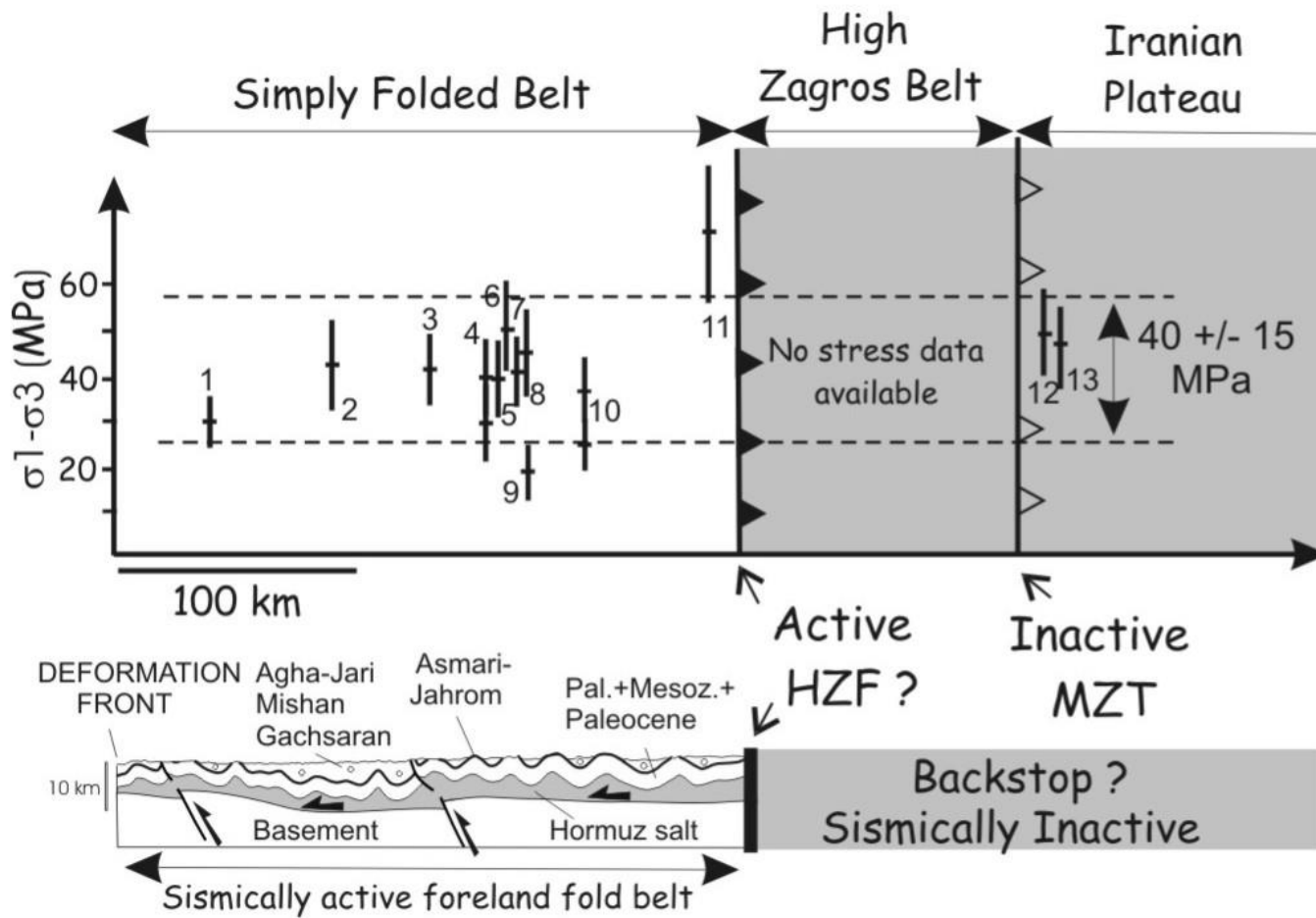
Combined magnetostratigraphic section of studies conducted in the Simply Folded Belt of the Zagros. Black arrows indicate onset of deformation inferred by progressive unconformities. Folding in the outer Pusht-e Kuh arc [Homke *et al.*, 2004] is triggered by the Mountain Front Flexure.



- Overall homogeneous fold wavelength;
- Homogeneously distributed shortening across the Simply Folded Belt;
- Initial rapid fold growth rate, then decrease relative to foreland subsidence;
- Folding under low differential stresses :

→ Buckling of the competent cover above the Hormuz salt

(Lacombe et al., 2007)



The relative homogeneity of differential stresses agrees with the homogeneously distributed shortening across the SFB, where no deformation gradient toward the backstop is observed in contrast to classical fold-thrust wedges

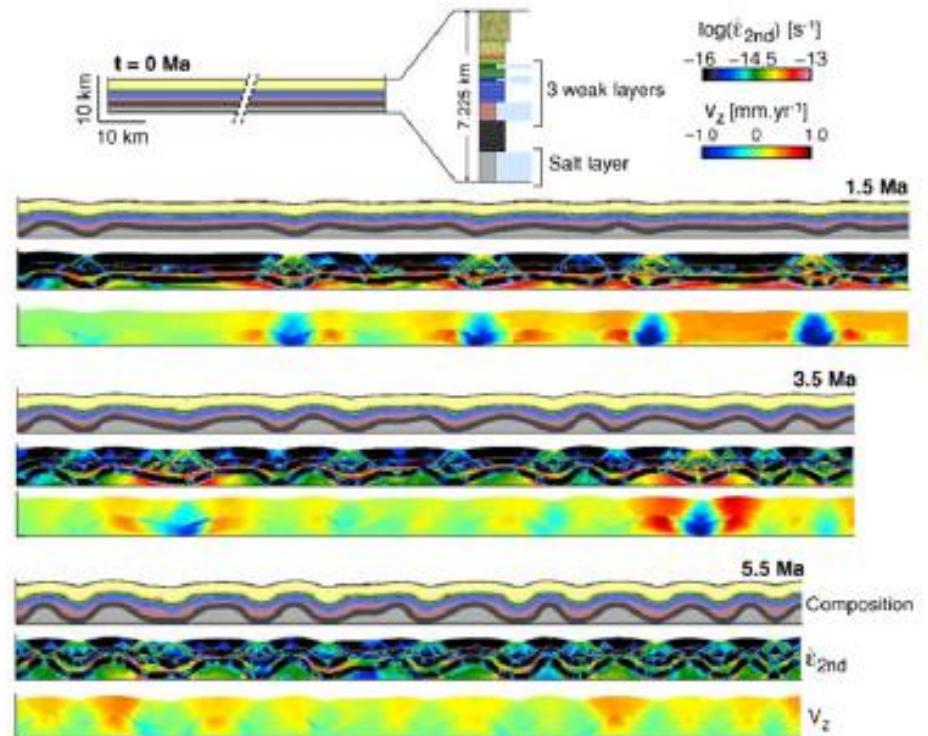
Both pre- and post-folding differential stresses are low --> folding likely occurred at low stresses; this favours pure-shear deformation and buckling of sedimentary rocks rather than brittle tectonic wedging.

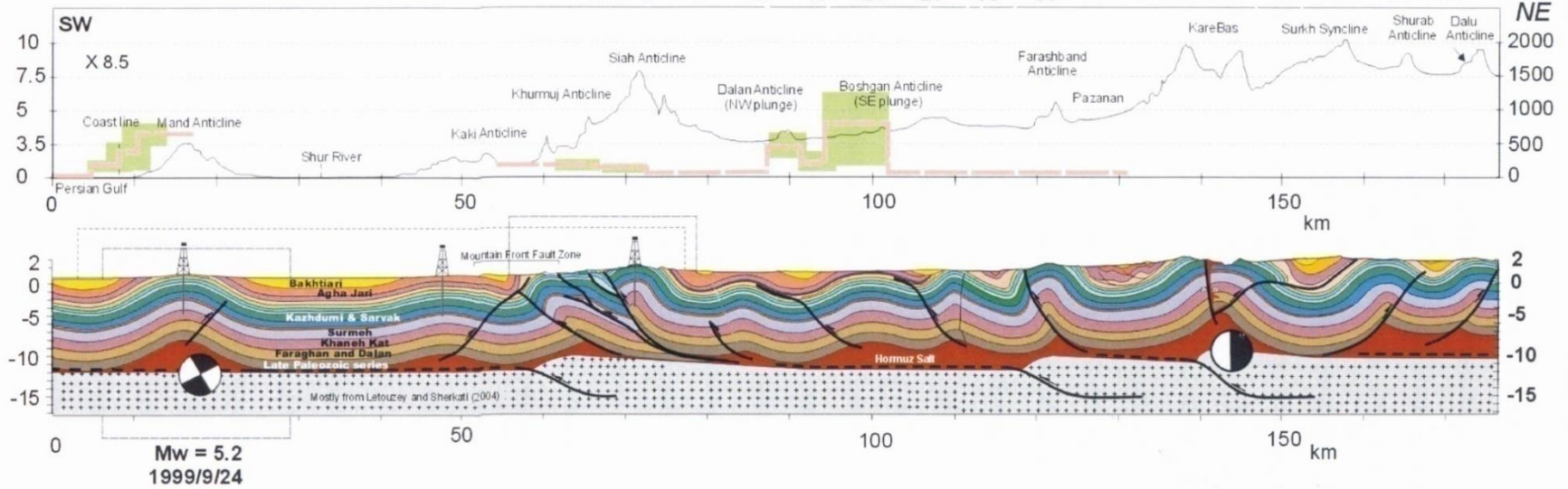
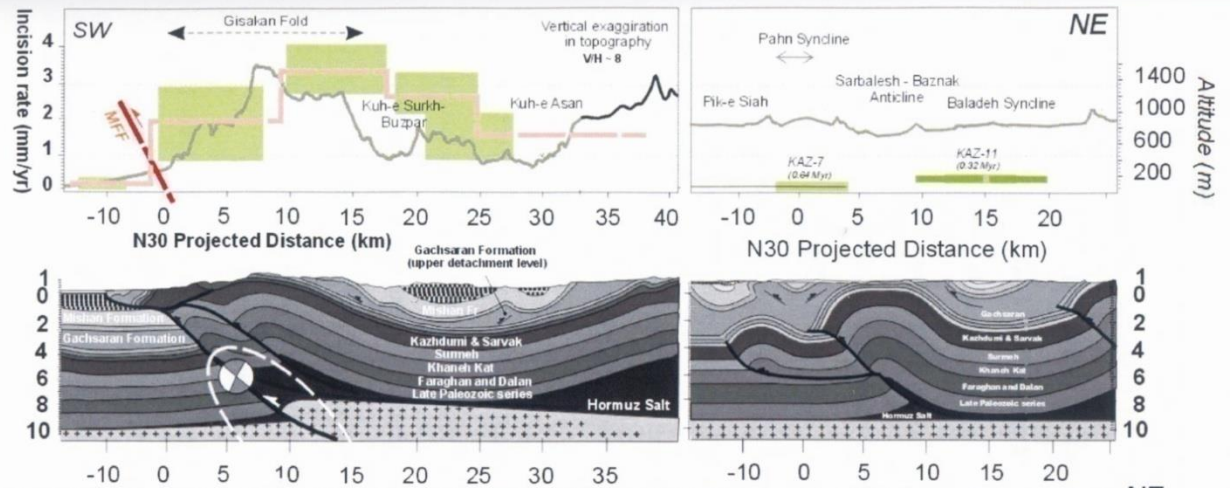
Mechanism of cover folding

Stratigraphy and mechanical layering (Fars region)

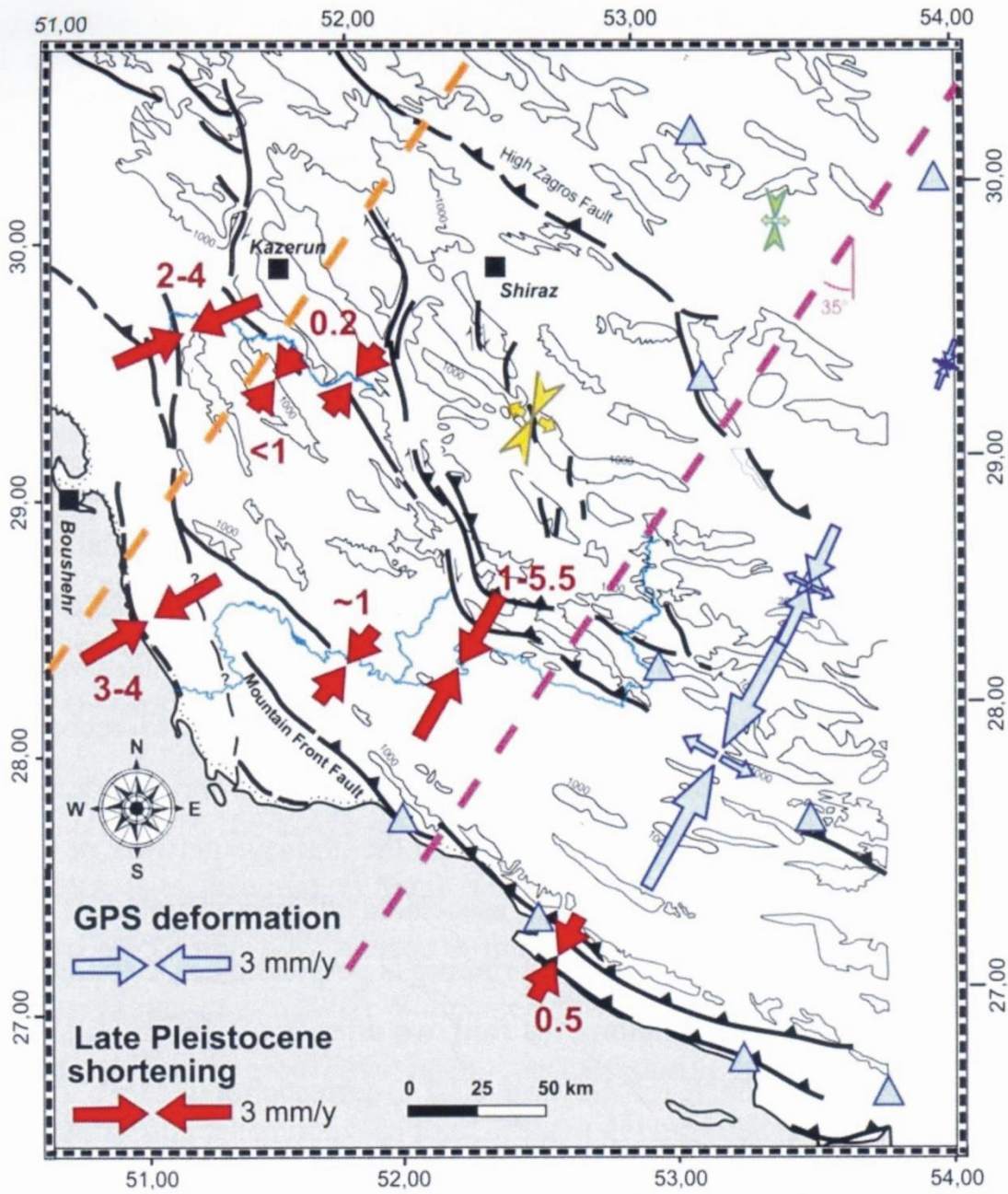


Mechanical modelling of cover folding





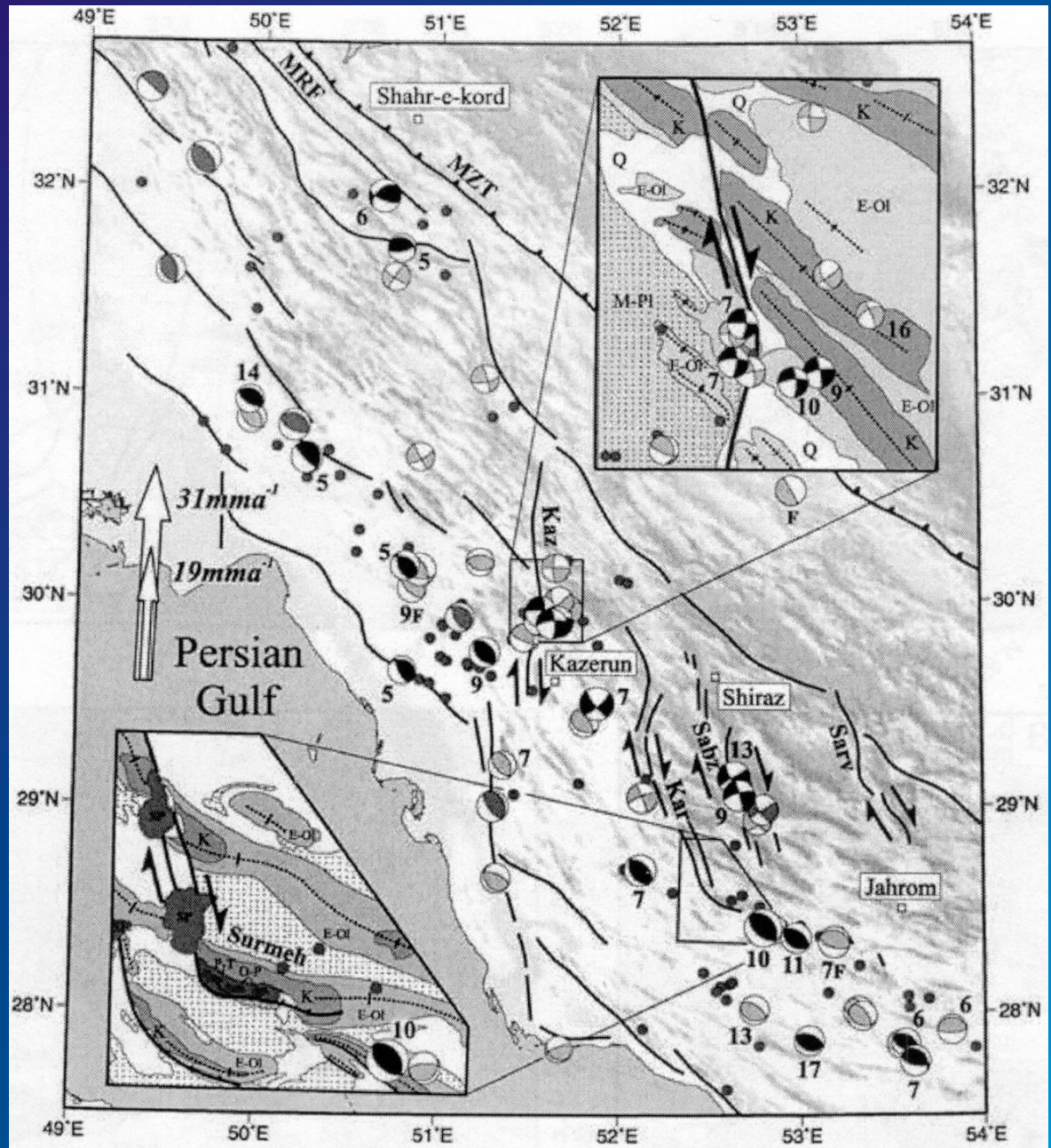
(Oveisi, PhD thesis, 2007)



Outer folds accommodate most of current shortening in the Zagros. Their growth over the last My can be accounted for either by thin-skinned tectonics, or by the activity of underlying basement faults. Cover and basement are mostly decoupled: this is in agreement with superimposed thin- and thick-skinned tectonics styles.

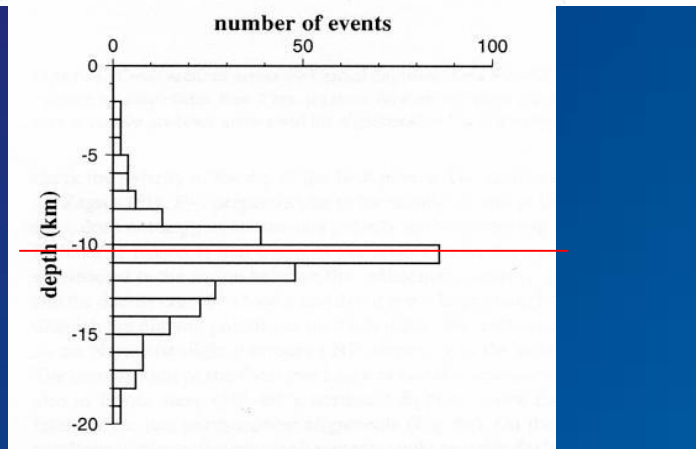
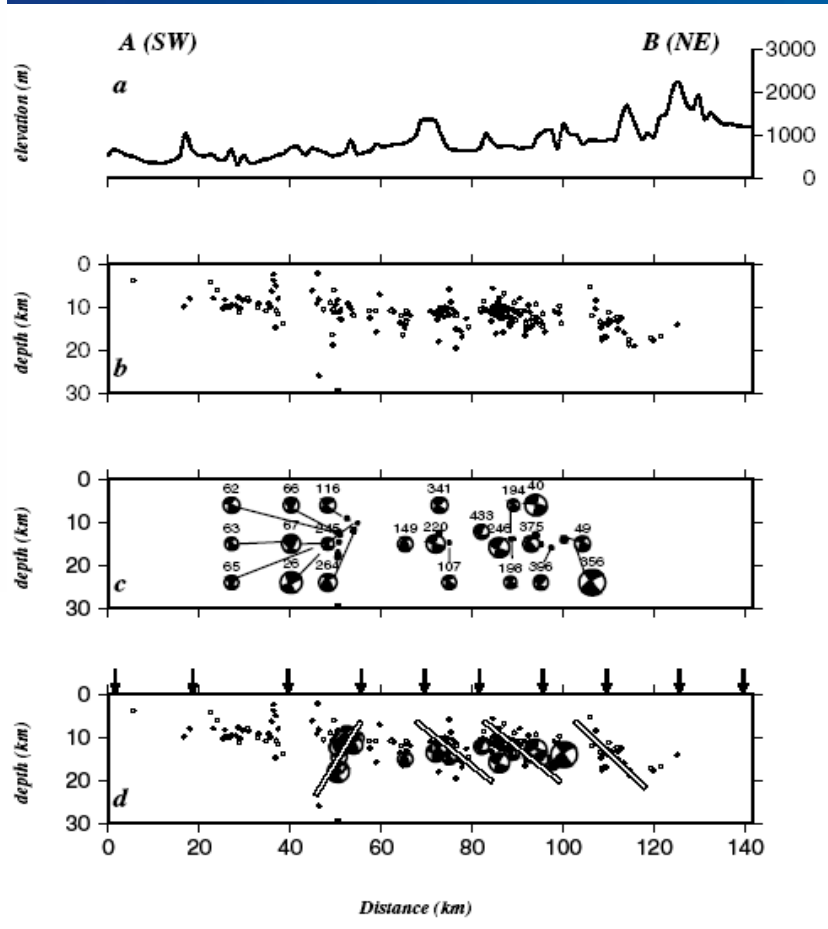
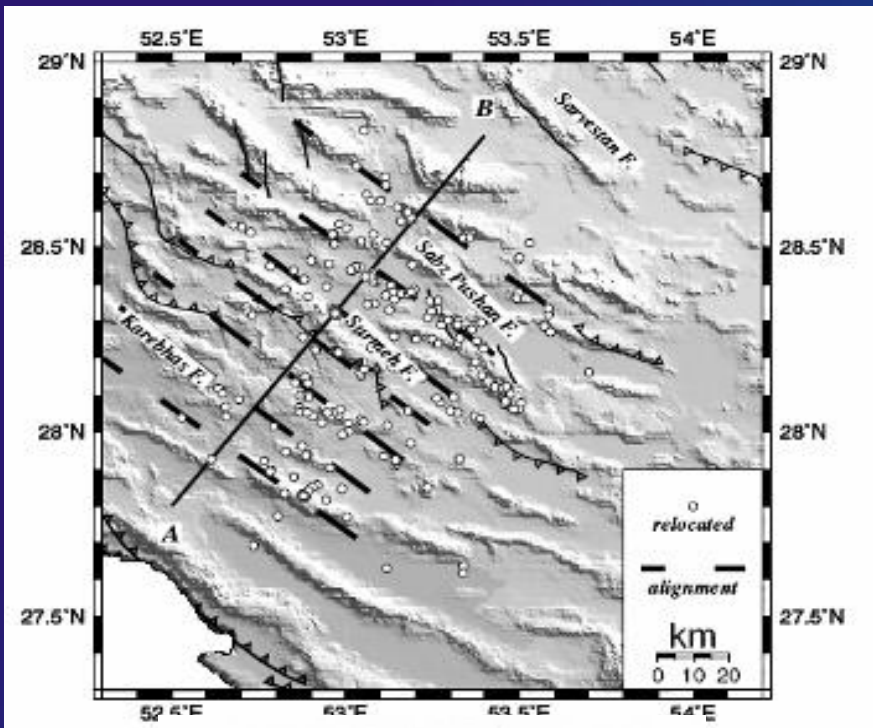
(Oveisi, PhD thesis, 2007)

**Deformation in the Zagros (2) :
earthquakes and seismic faulting**

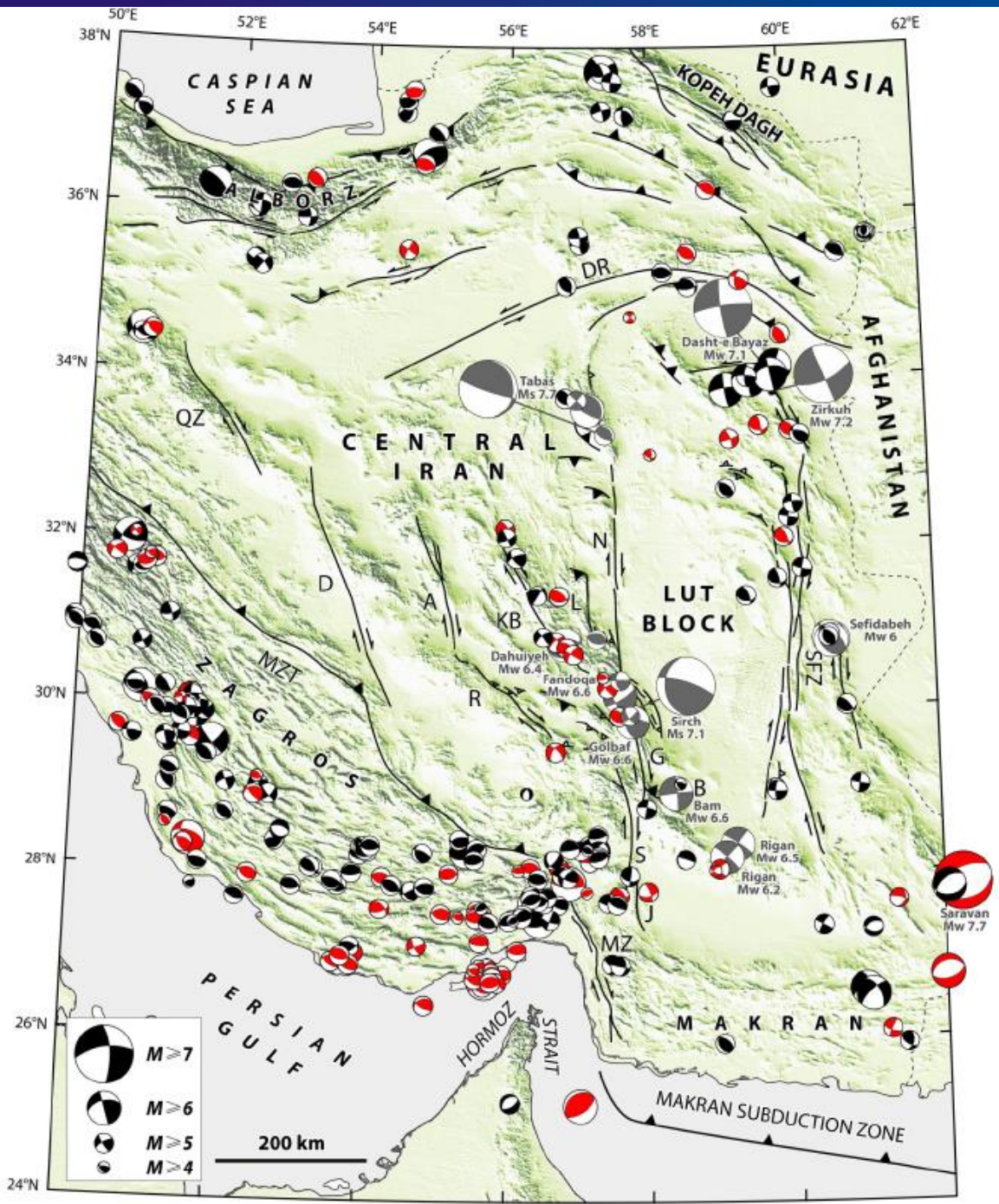


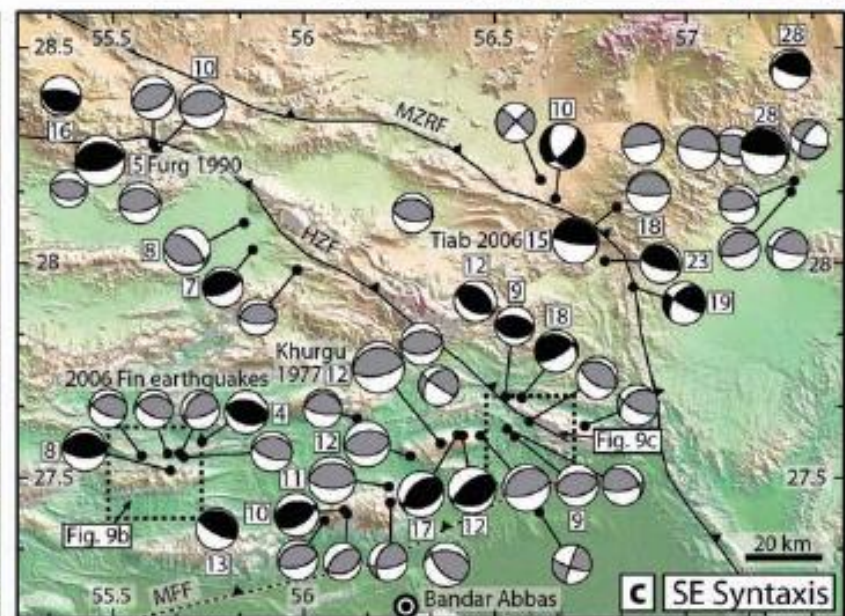
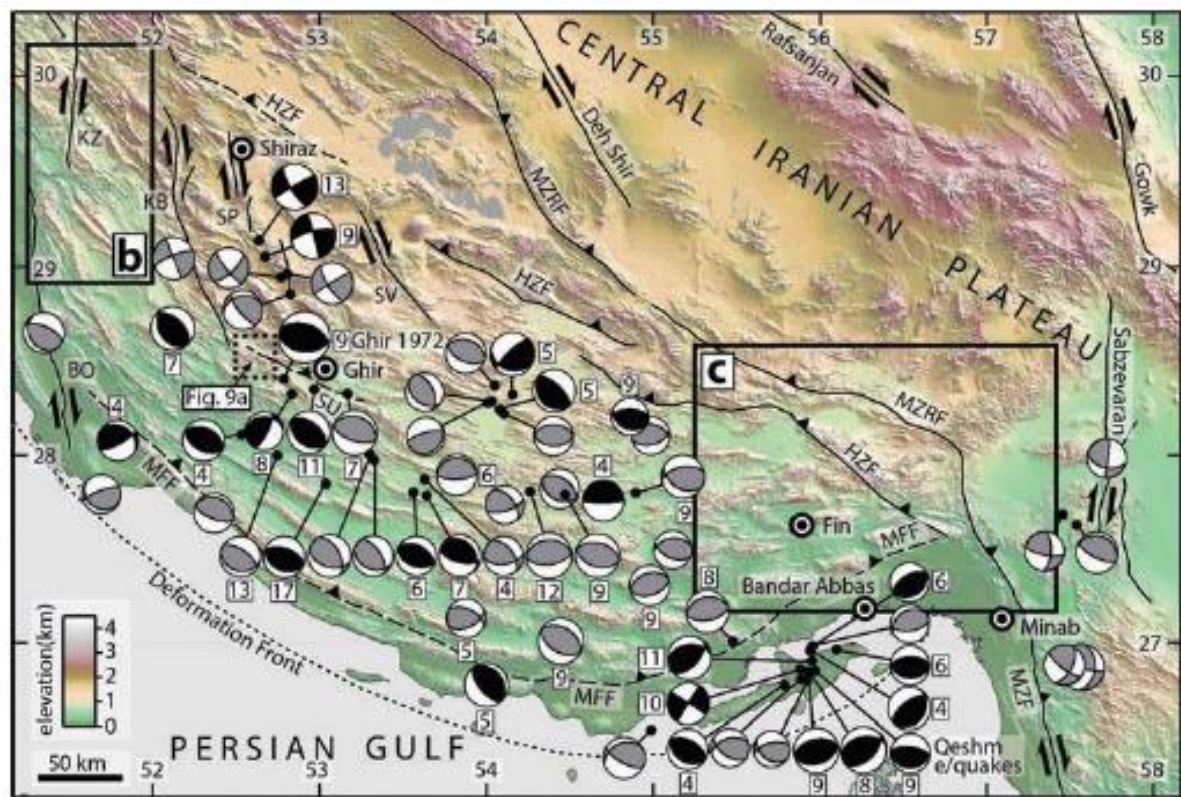
(Talebian and Jackson, 2004)

Localization of basement faults using microseismicity

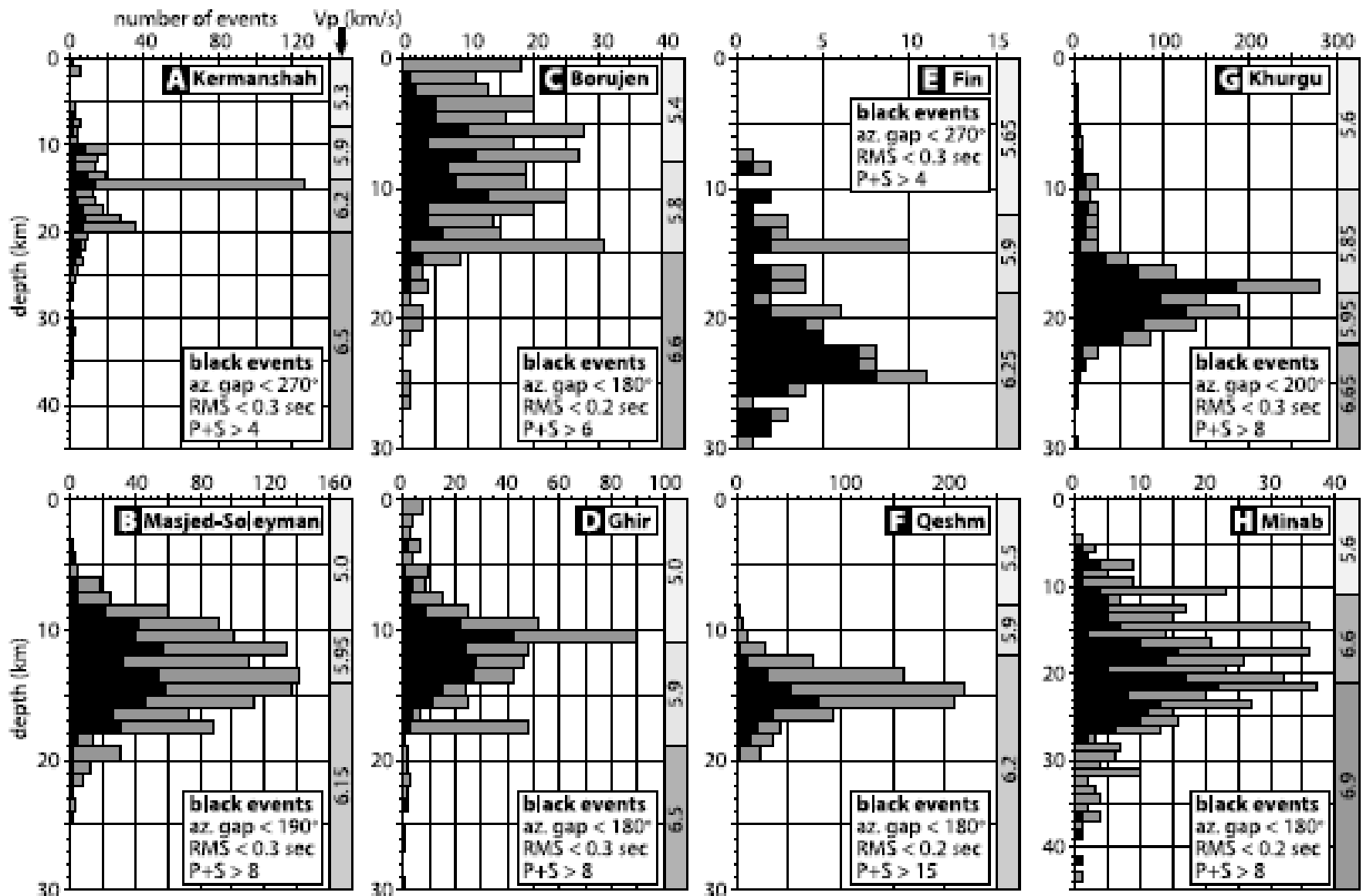


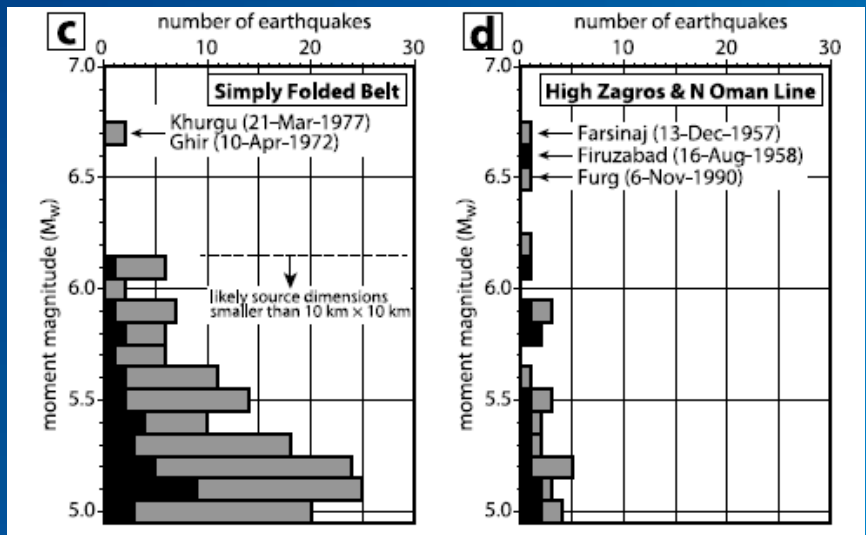
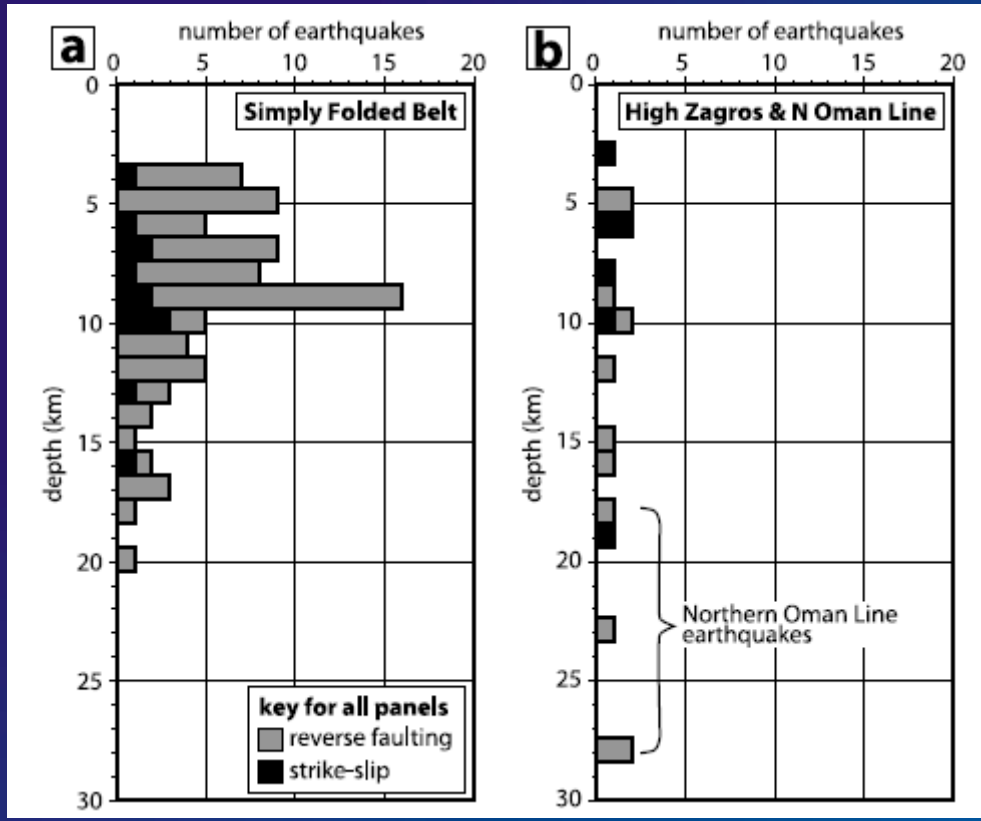
(Tatar et al. 2004).





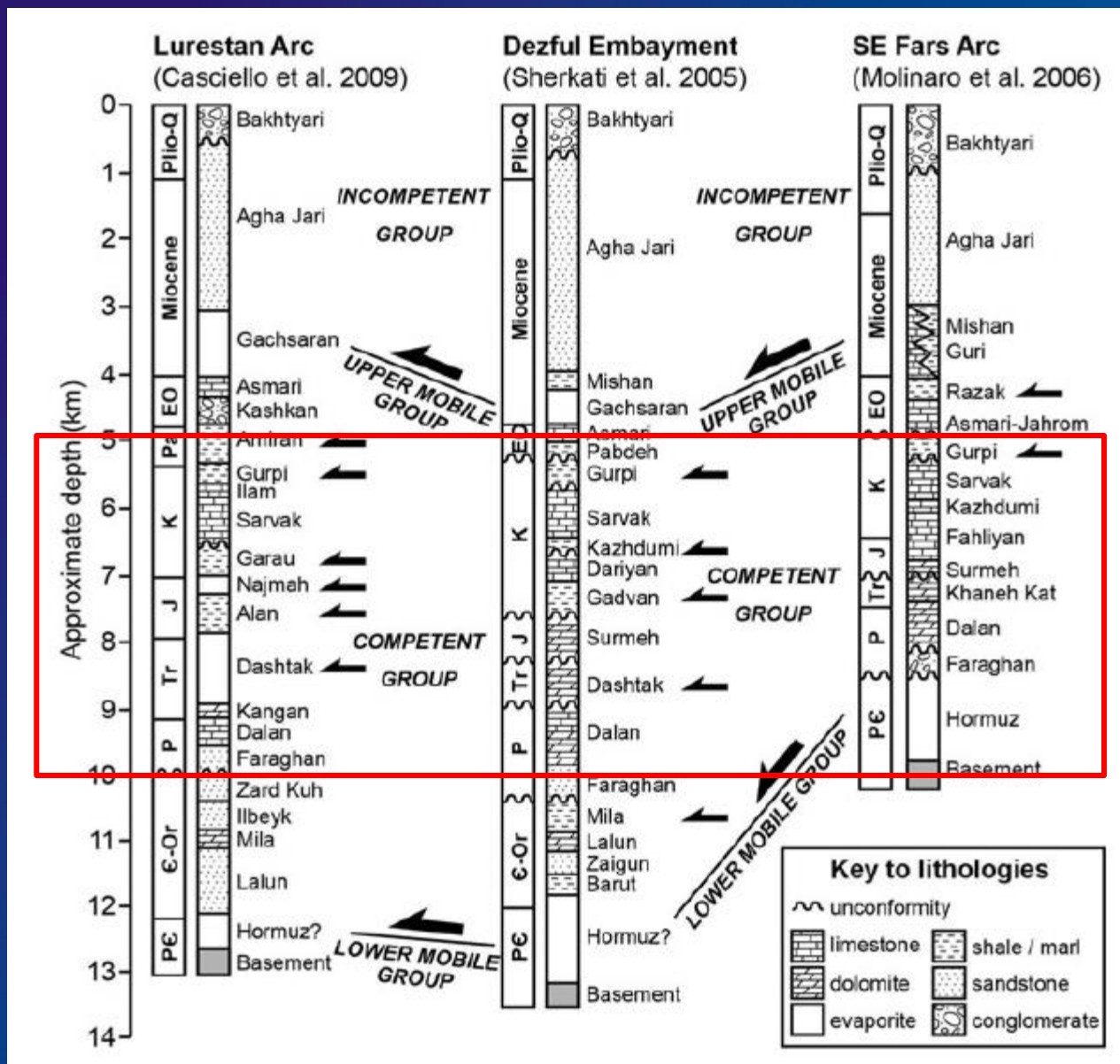
(Nissen et al., 2011)

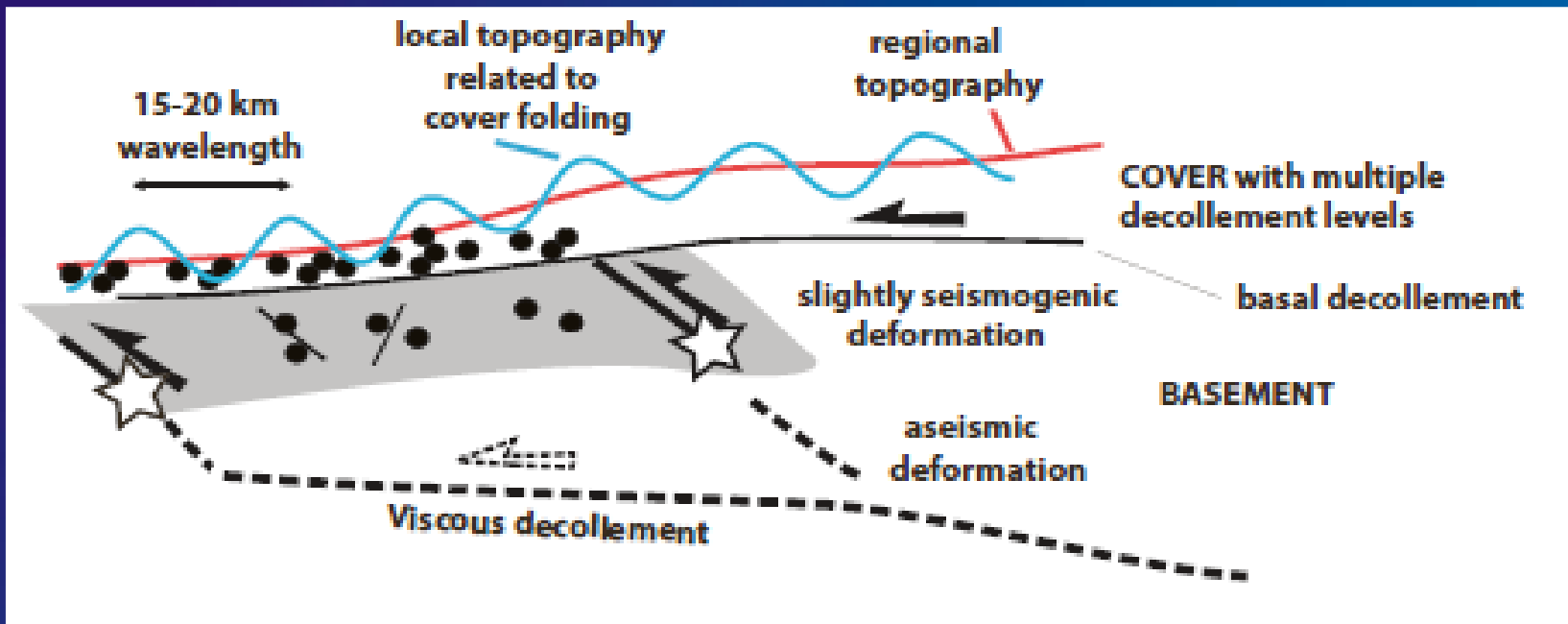




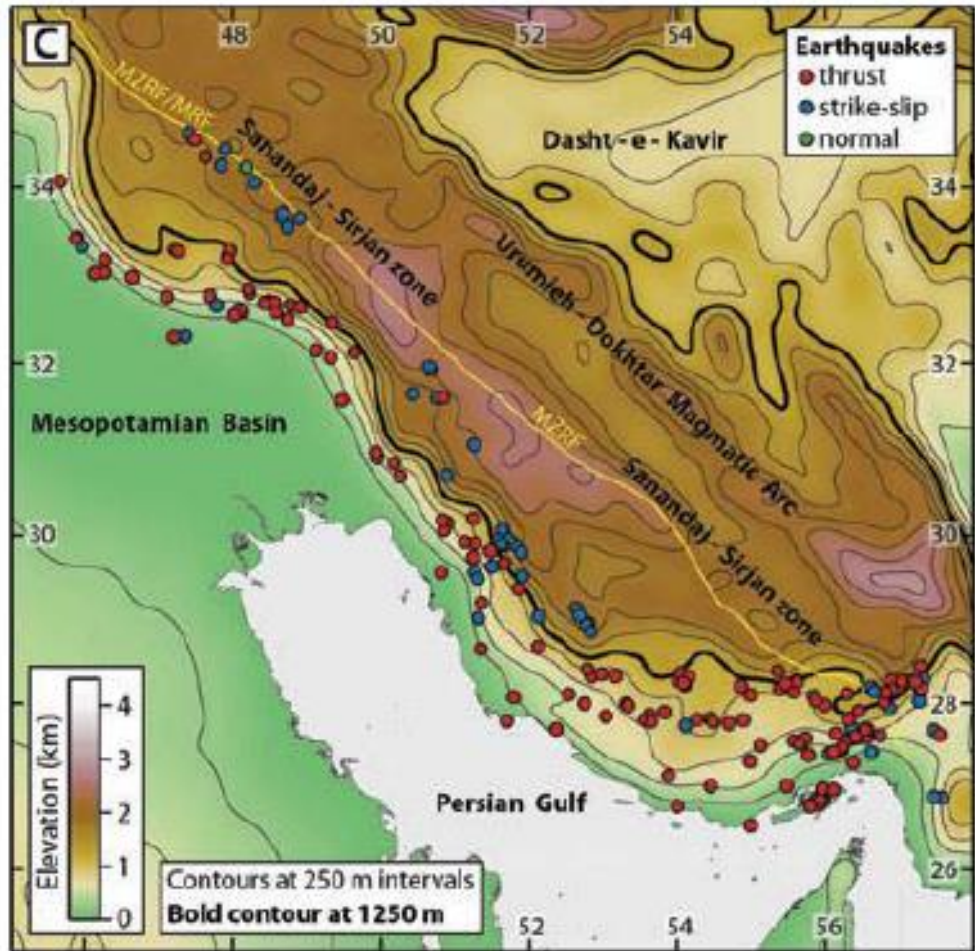
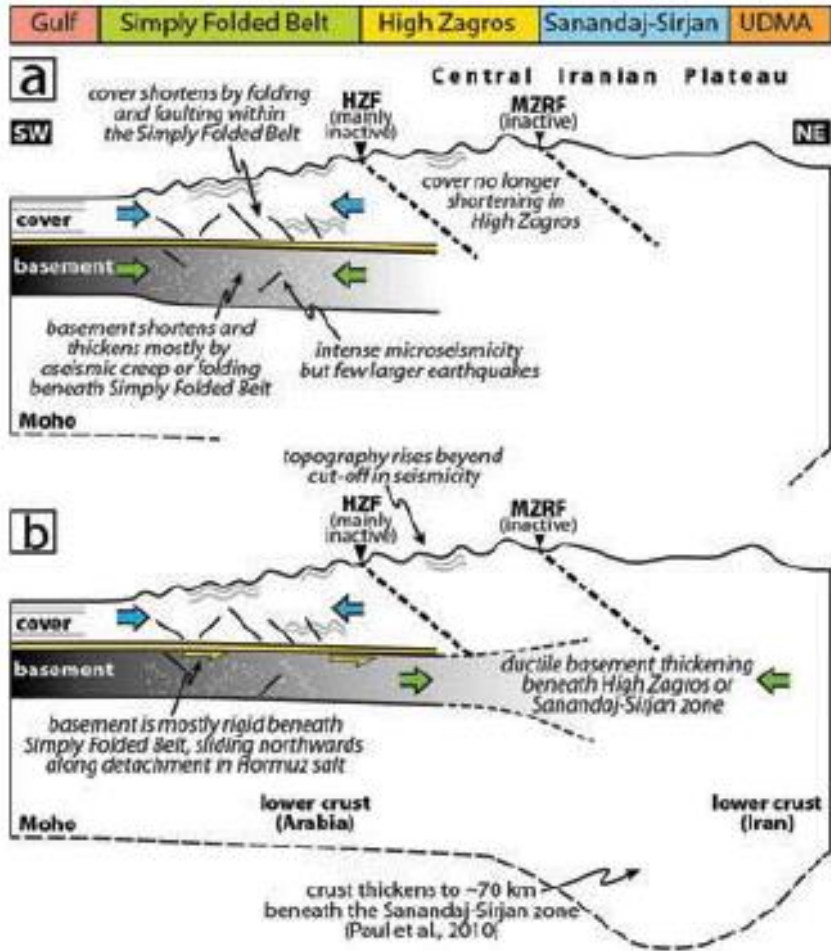
teleseismically recorded earthquakes

(Nissen et al., 2011)





(Mouthereau et al., 2012)



(Nissen et al., 2011)

**Deformation in the Zagros (3) :
meso-scale fracturing**

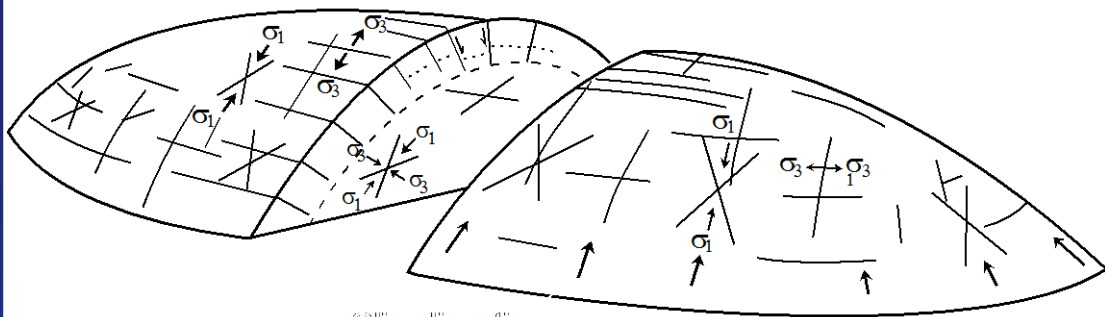
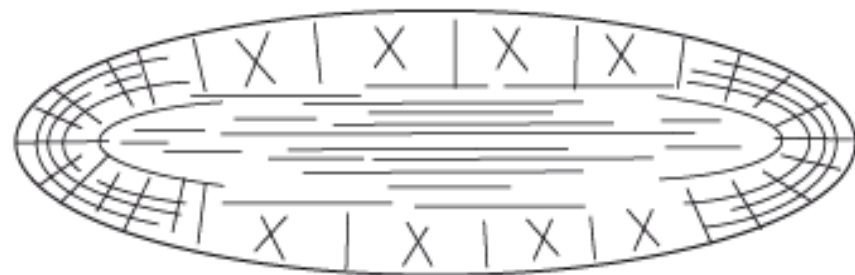
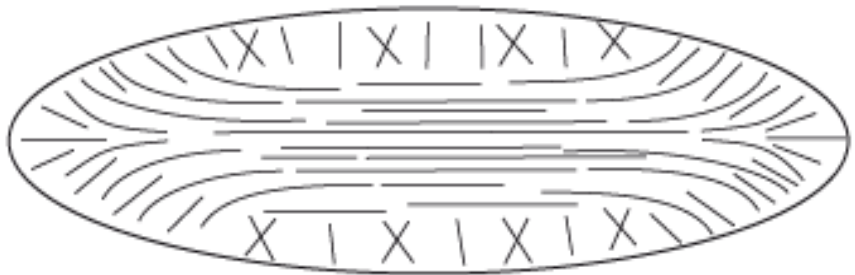
The study of fracture patterns and their possible genetic relationships to cover folding is of key importance in the Zagros.

Several giant oil fields are found, especially in the Dezful Embayment

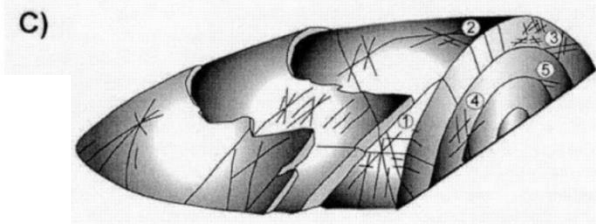
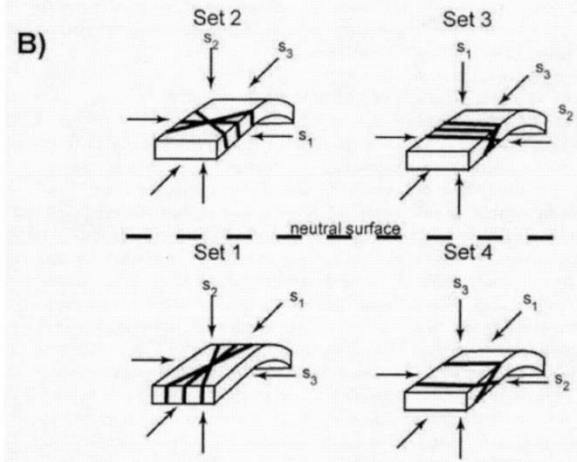
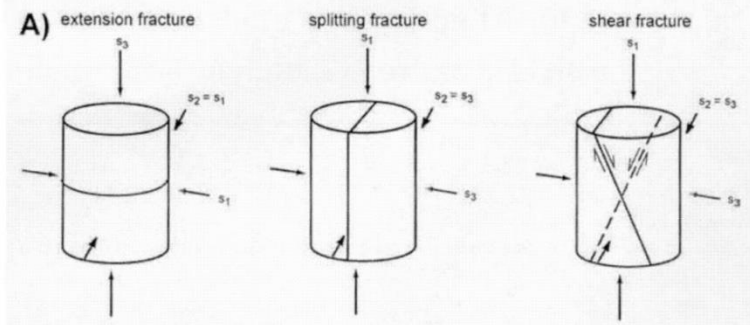
The Asmari Formation is an Oligocene-Early Miocene platform carbonate which is the most prolific oil reservoir in Iran, and it is commonly regarded as a classic fractured carbonate reservoir, with production properties that depend strongly on the existence of fracture networks

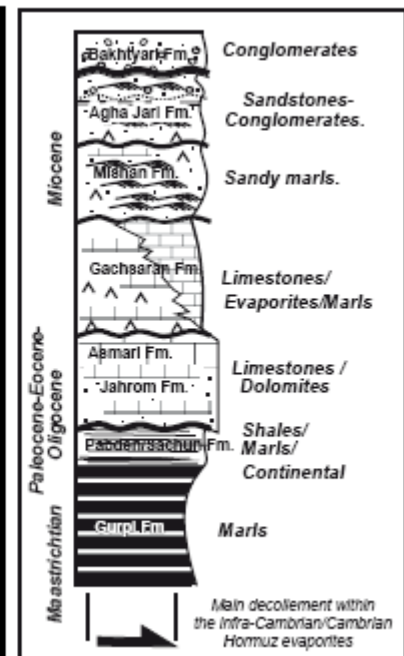
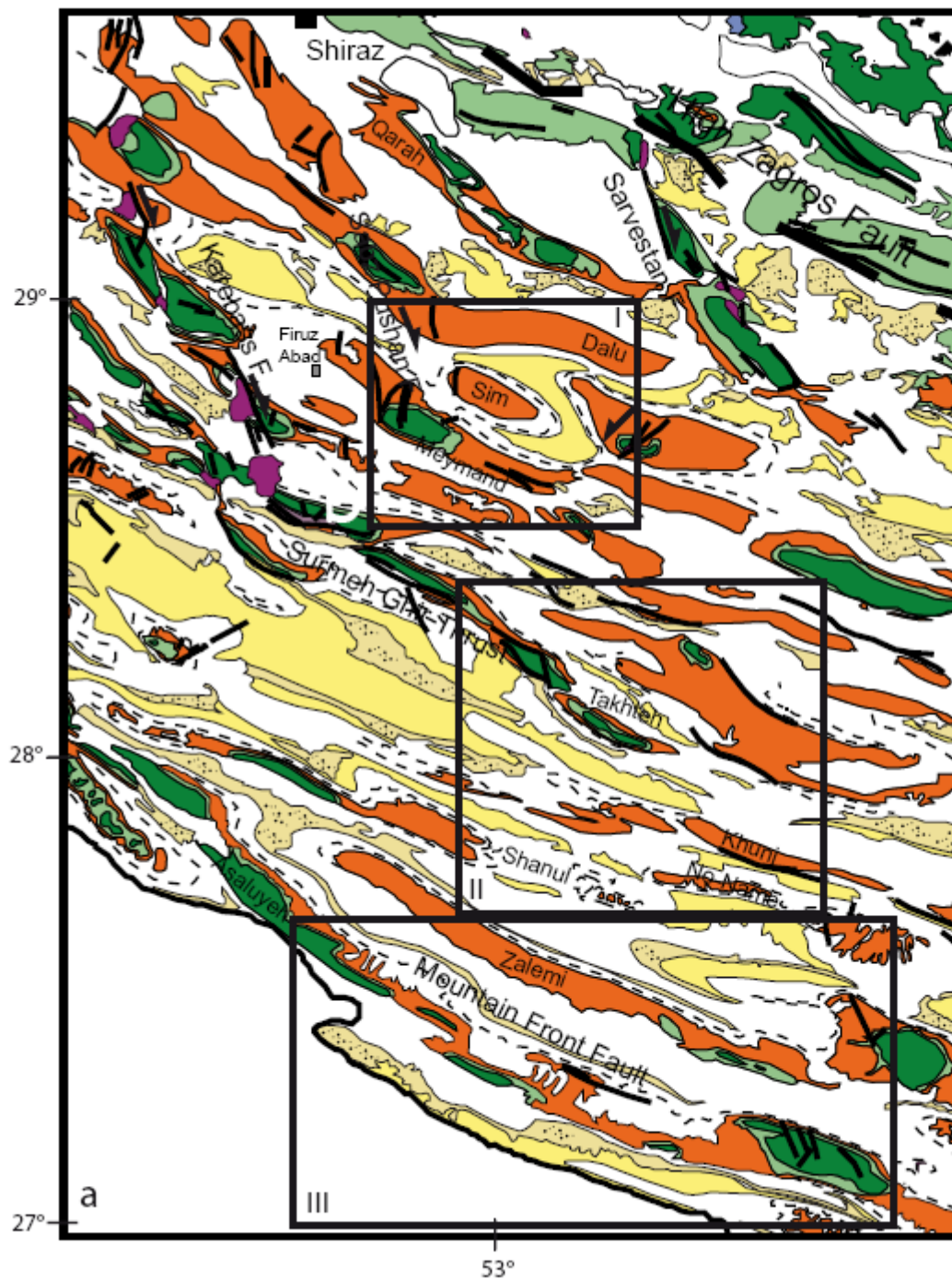
Fold geometry and kinematics have for a long time been recognized as the most important factors that control fracturing. Stearn & Friedman (1972) proposed a pioneering classification of fold-related fractures, including an axial extensional set running parallel to the fold axis, a cross-axial extensional set oriented perpendicular to the fold axis and two sets of conjugate shear fractures oblique to the fold axis with their obtuse angle intersecting the trend of the fold axis.

Since then, numerous studies have attempted to relate the development of meso-structures to either the structural domains of the fold or to quantitatively estimated curvature of strata



Slip direction





b

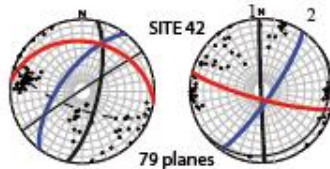
- Pliocene-Pleistocene**
Bakhtyari Fm + Labhari mb
- Miocene-Pliocene**
Fars Group (Gachsaran Fm, Mishan Fm including Gurpi mb, Agha Jari Fm)
- Eocene-Oligocene-L. Miocene**
(Jahrom Fm, Asmari Fm)
- Upper Cretaceous-Paleocene**
(Sarvak Fm, Gurpi Fm, Pabdeh Fm)
- Lower-Upper Cretaceous**
(Gadvan Fm, Darfyan Fm, Kazhdumi Fm)
- Jurassic**
(Surmeh Fm, Gotnia Fm, Fahliyan Fm)
- Triassic**
(Kahnet Kat Fm, Neyriz Fm, Dashtak Fm)
- Late Paleozoic and Permian**
(Faraghan and Dalan Fms)
- Upper Proterozoic-Middle Cambrian**
(Hormuz Fm)
- Neyriz ophiolites**





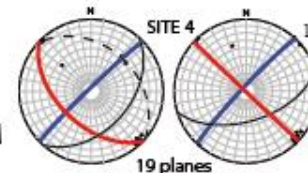


MEYMAND

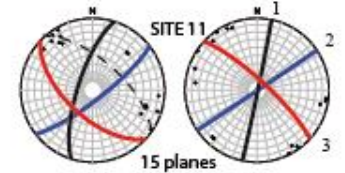


79 planes

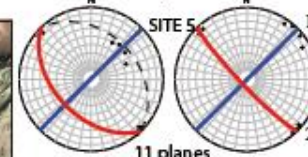
SIM



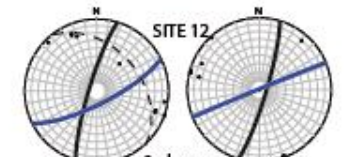
19 planes



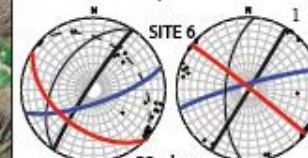
15 planes



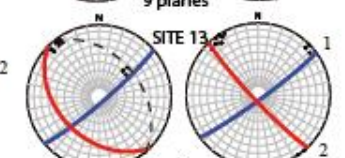
11 planes



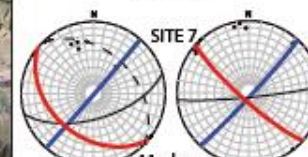
9 planes



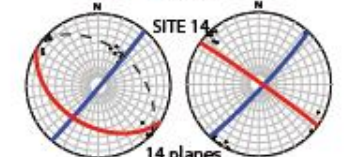
28 planes



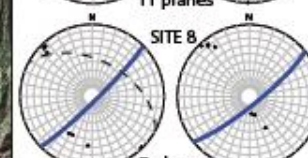
16 planes



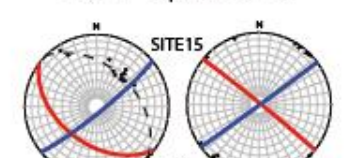
11 planes



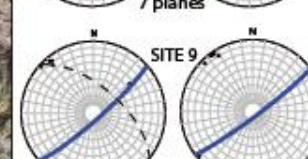
14 planes



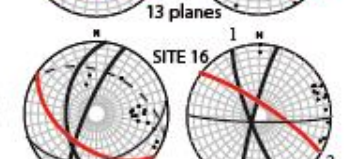
7 planes



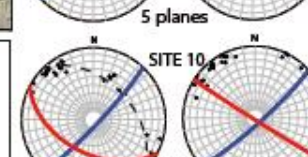
13 planes



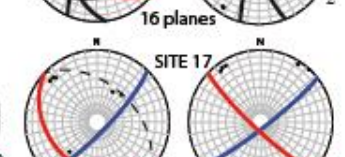
5 planes



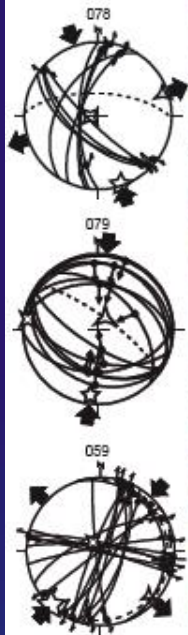
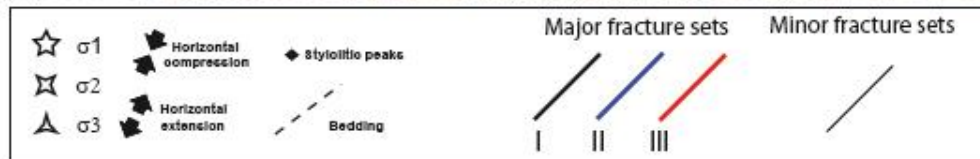
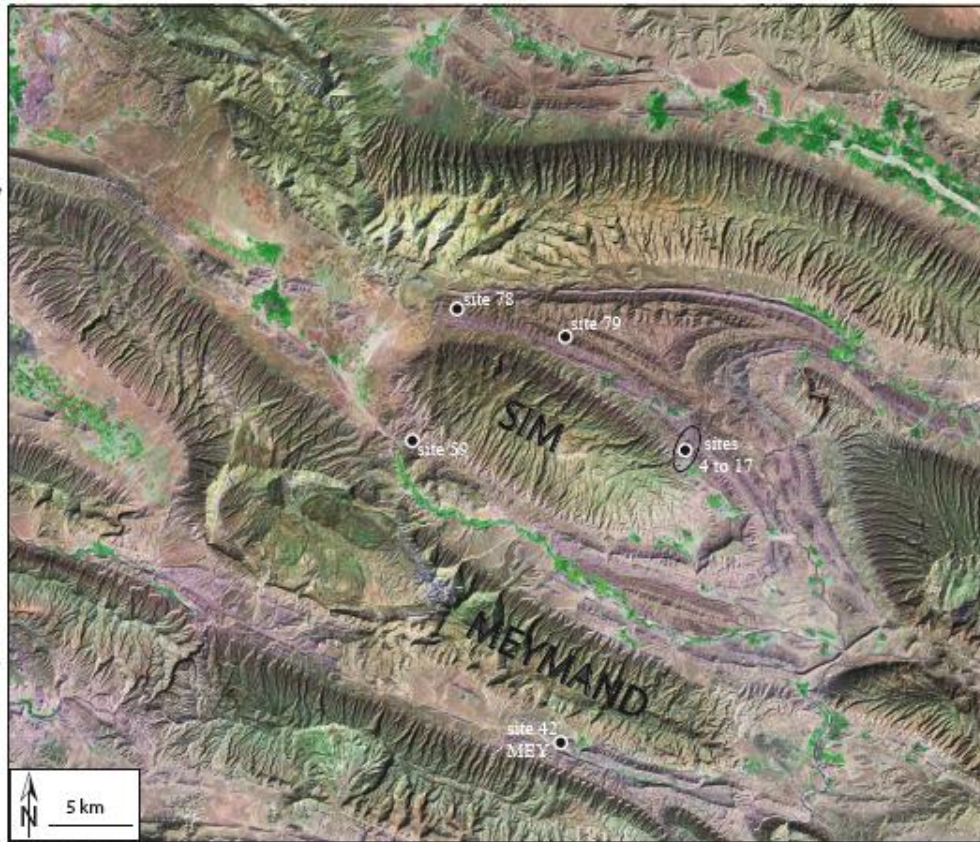
16 planes

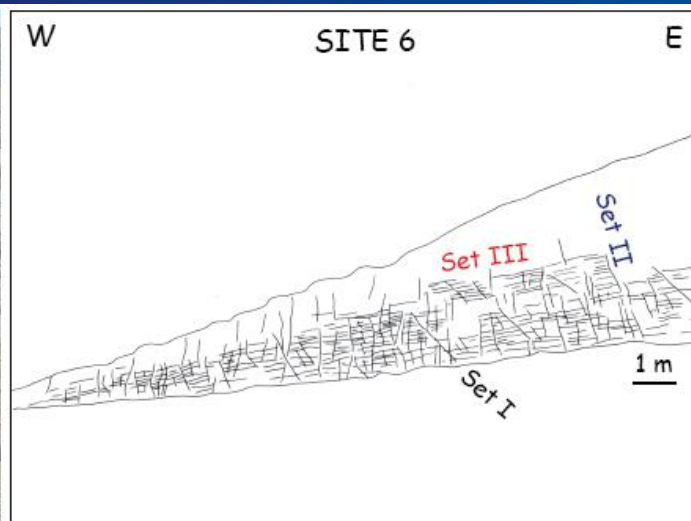


31 planes



7 planes

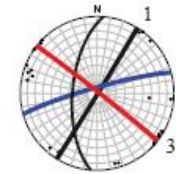
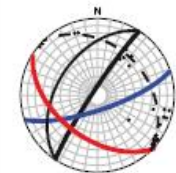
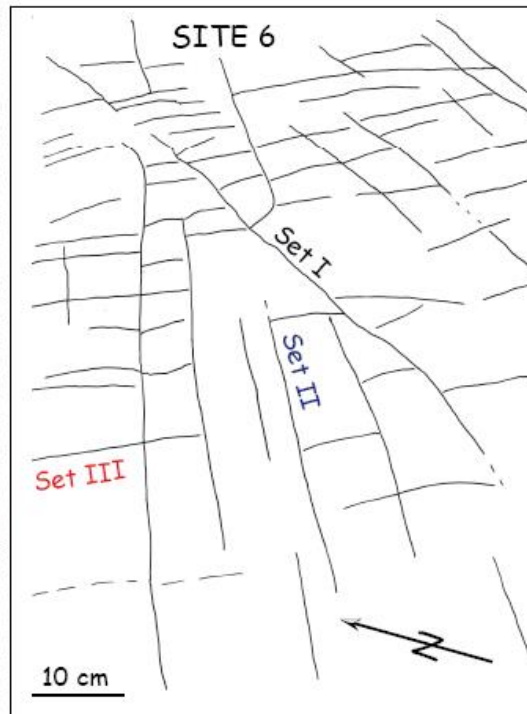




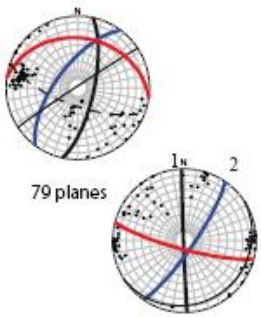
a

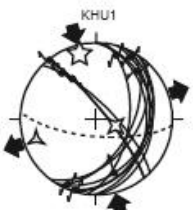
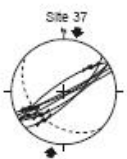
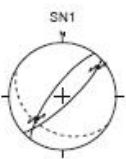
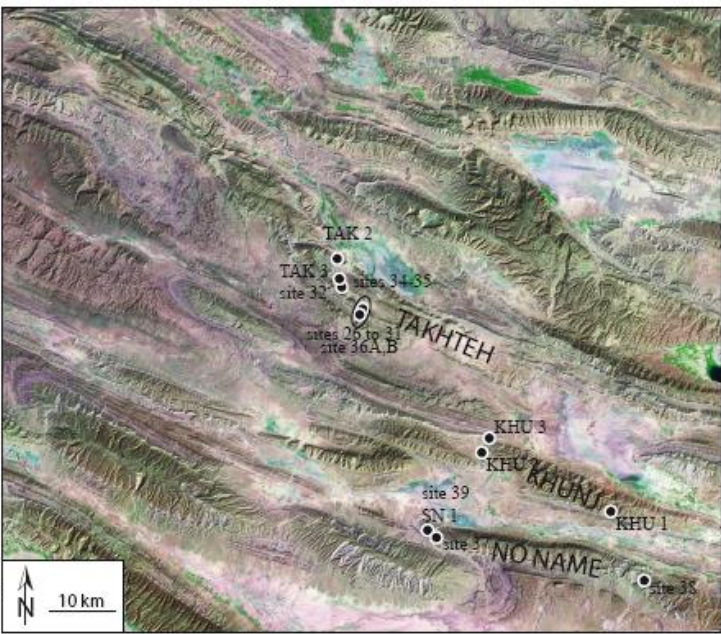
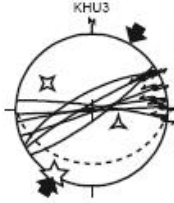
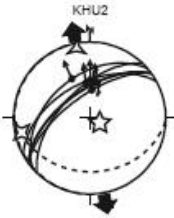
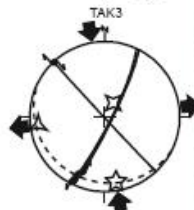
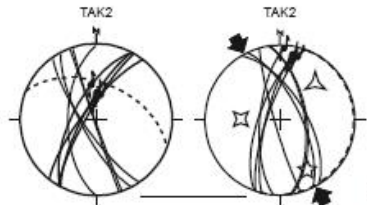


b

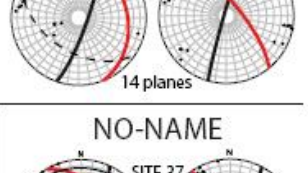
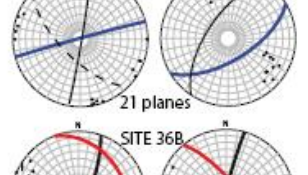
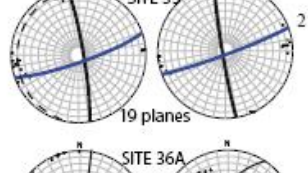
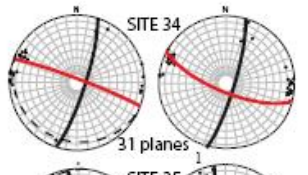
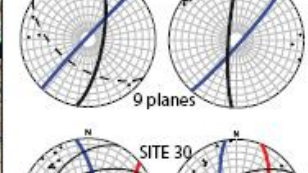
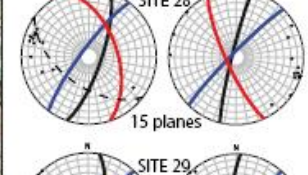
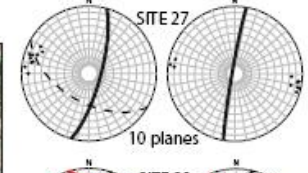
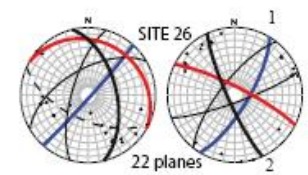


28 planes

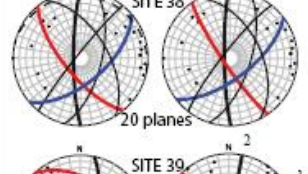
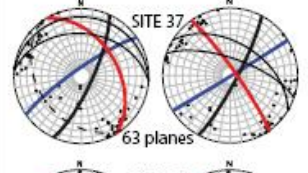




TAKHTEH



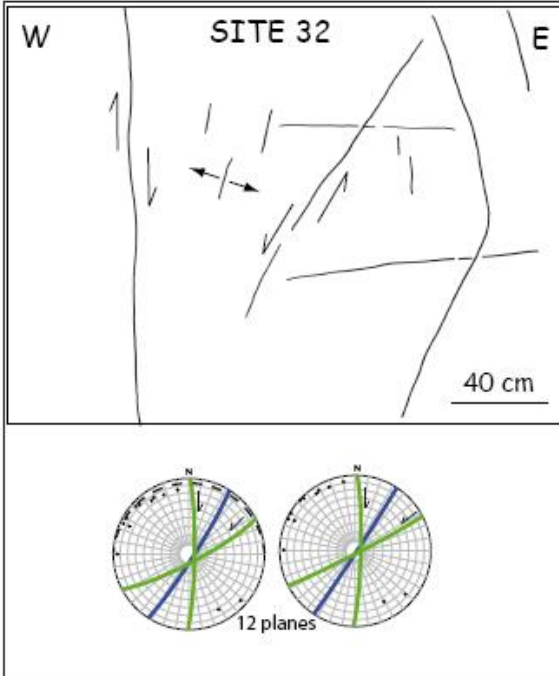
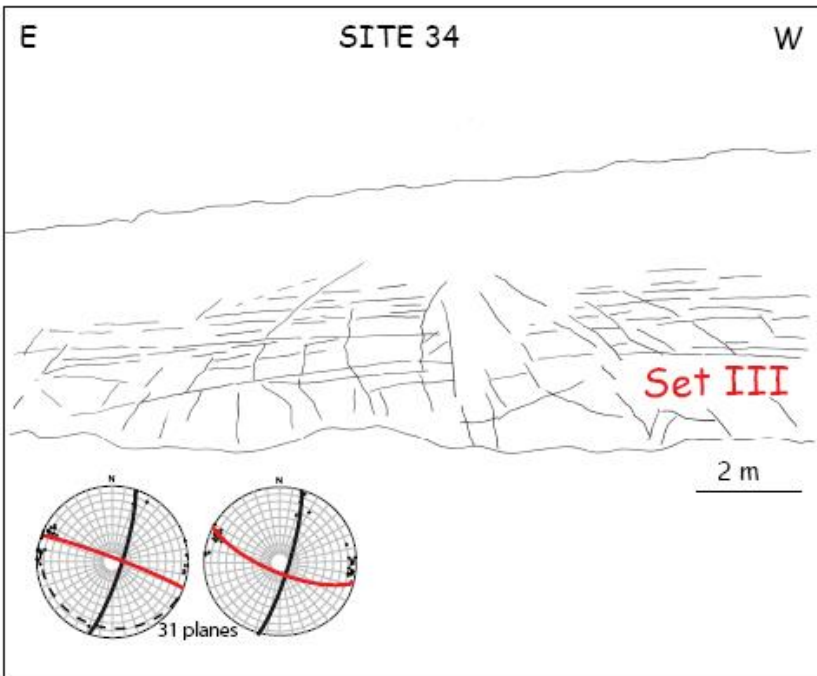
NO-NAME



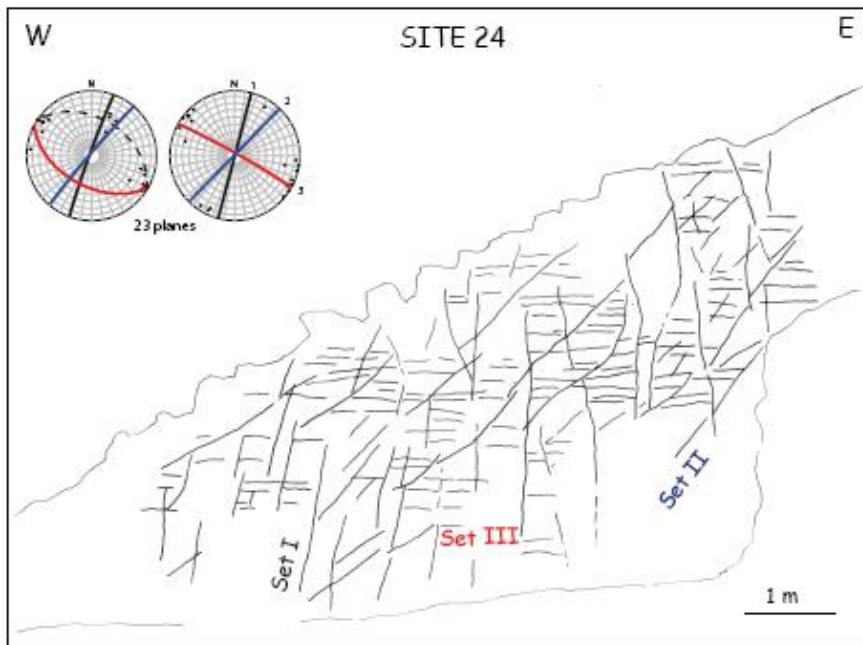
a



b



(Lacombe et al., 2011)



(Lacombe et al., 2011)

3 major sets in all the domains considered :

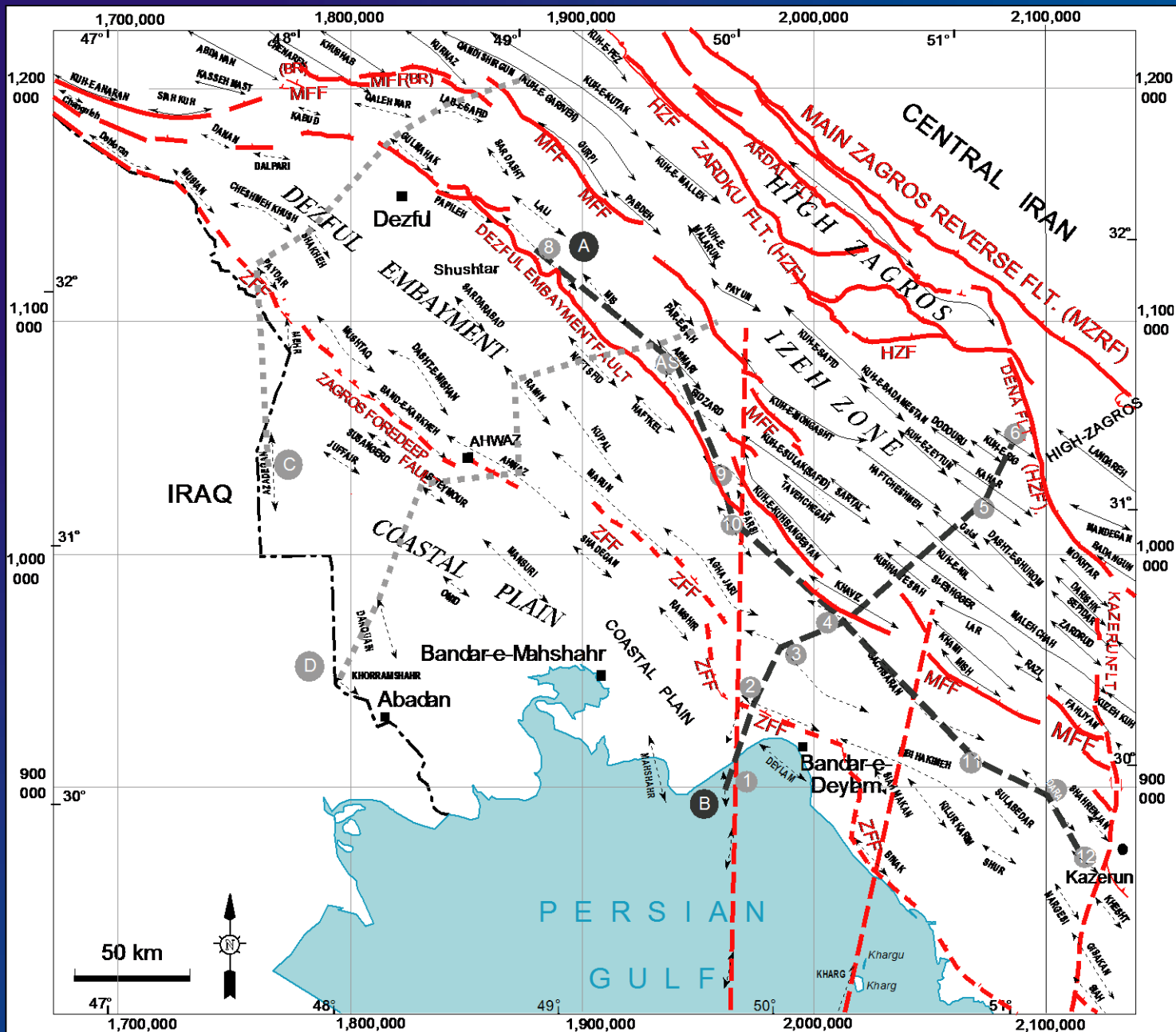
Set I is generally bed-perpendicular, and trends N-S to N020-030 after unfolding.
Set II is also bed-perpendicular, and strikes NE to ENE (N040 to N070) after unfolding.
Set III is bed-perpendicular and trends almost always parallel to the local fold axis
(E-W to NNW-SSE, mainly WNW-ESE).

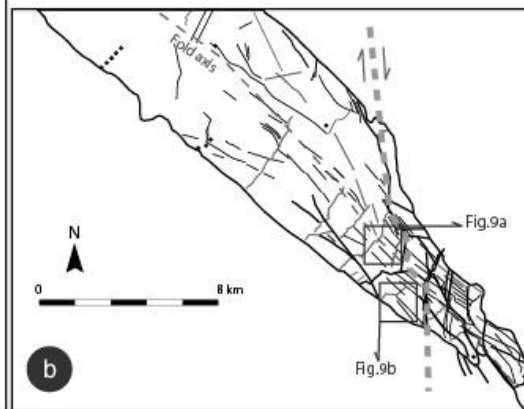
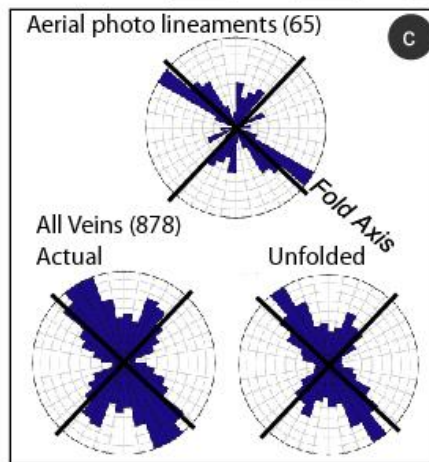
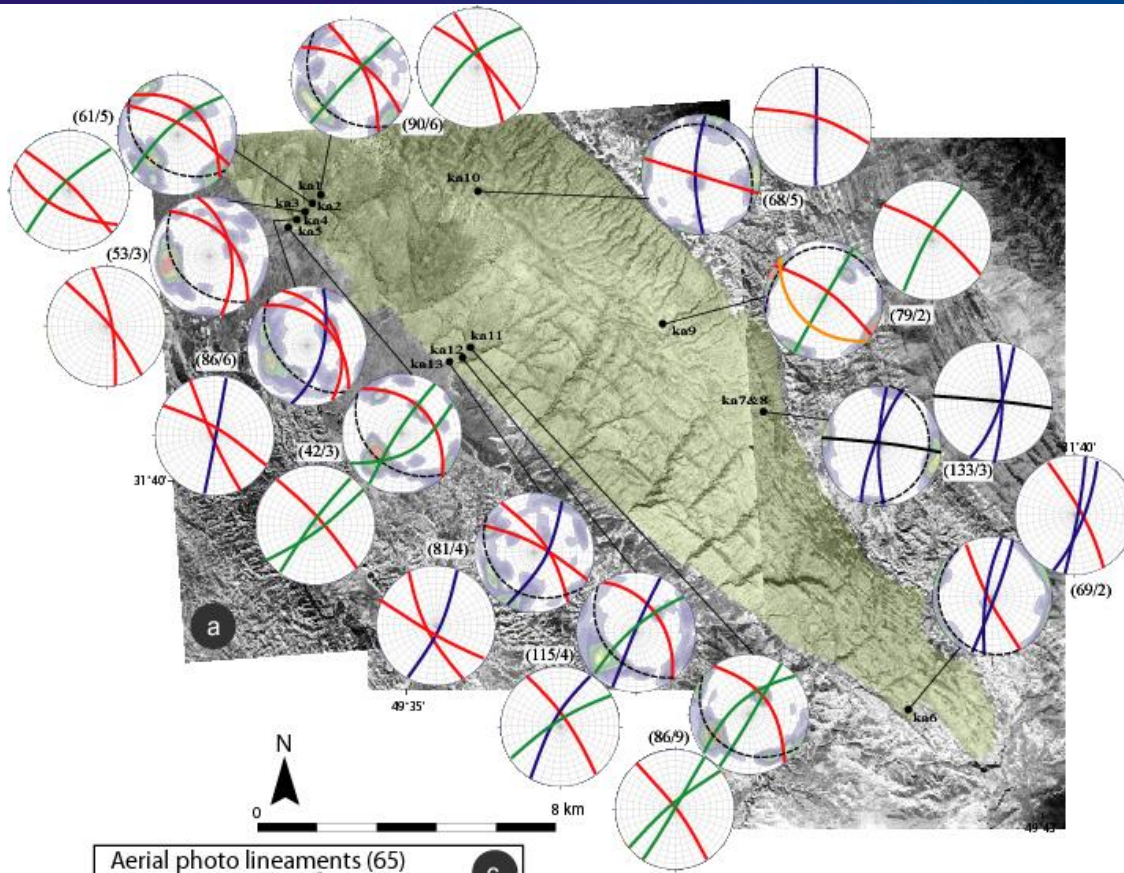
Set III fractures trending parallel to the fold axis and observed in most sites are interpreted as extensional axial fractures generated in response to the fold outer arc extension, hence typically fold-related.

Fracture sets, either bed-perpendicular (in most cases) or not strictly perpendicular, against which fractures of set III abut, were considered pre-tilting (or possibly syn-tilting if perpendicular to the fold axis, i.e. cross-axial).

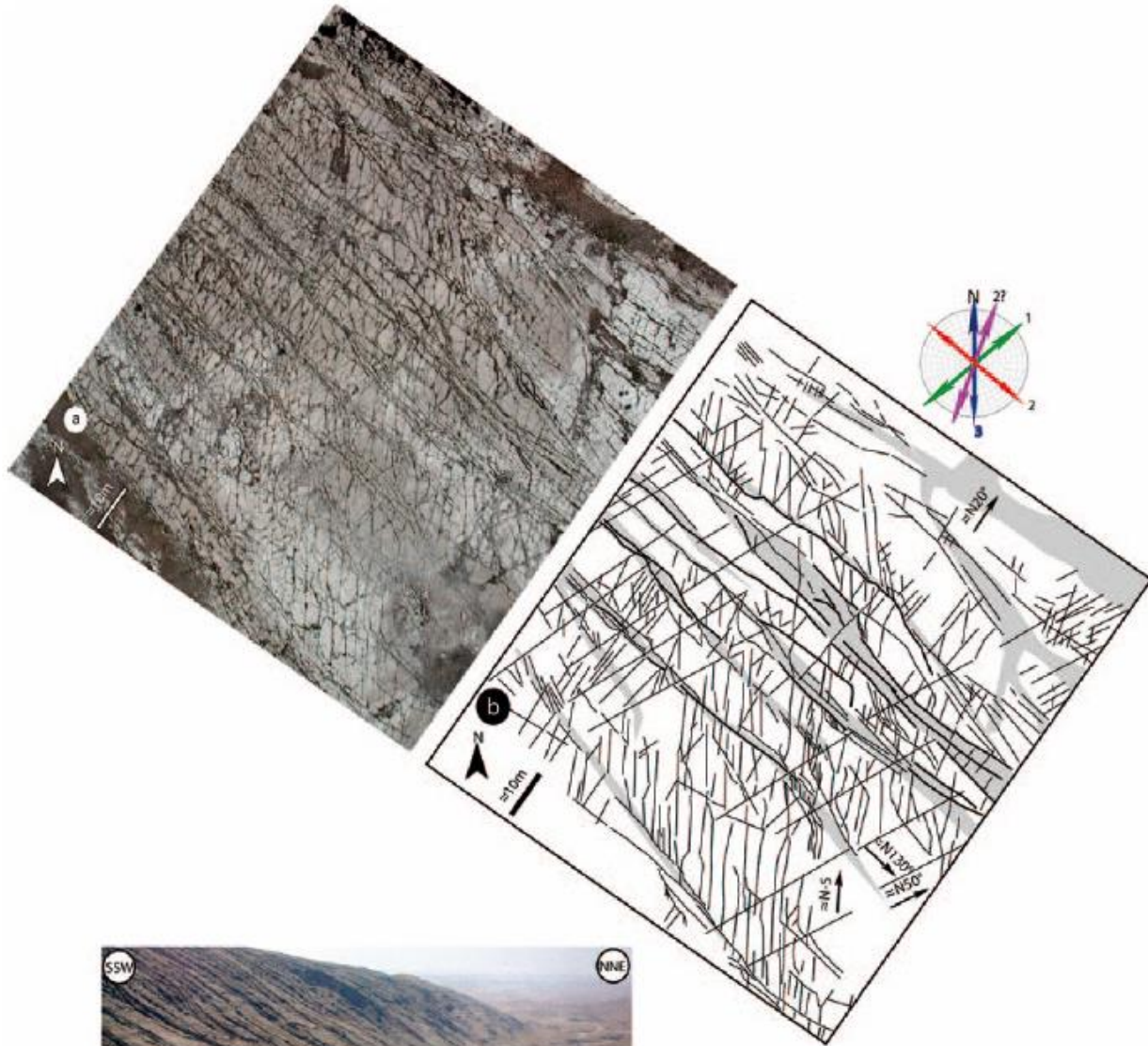
Among pre-tilting fractures, the distinction between pre-folding and early-folding fractures is based on the kinematic consistency with folding. While an early folding set formed during LPS in a consistent stress field (i.e. a fold-related extensional cross-axial set or oblique shear fracture set), a pre-folding set also predates bed tilting but may have originated in a different stress field (unrelated to folding).

Post-folding fractures are theoretically observed in a sub-vertical attitude and they cut across the tilted strata irrespective of the geometry of the fold if they originated from a later, different stress field. In our study, post-folding fracture sets have in their present attitude a trend similar to that of the early-folding fractures of set I after unfolding. They possibly reflect a late (post-tilting) stage of fracture development during late fold tightening.

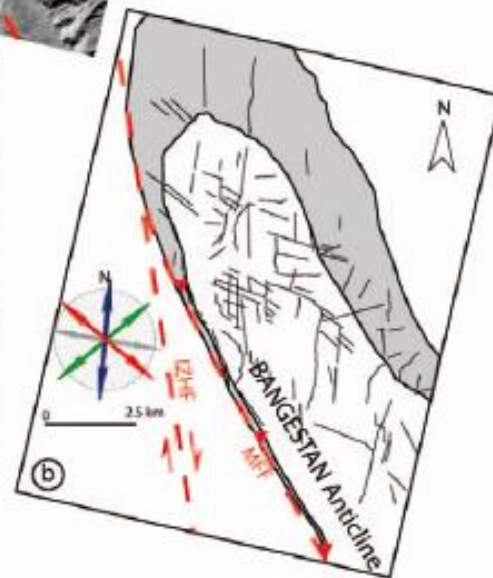
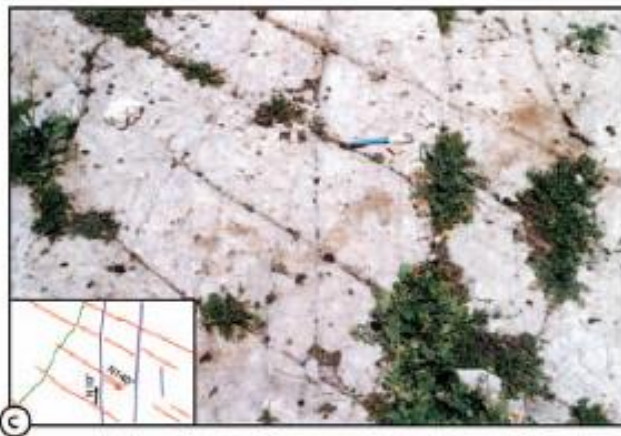
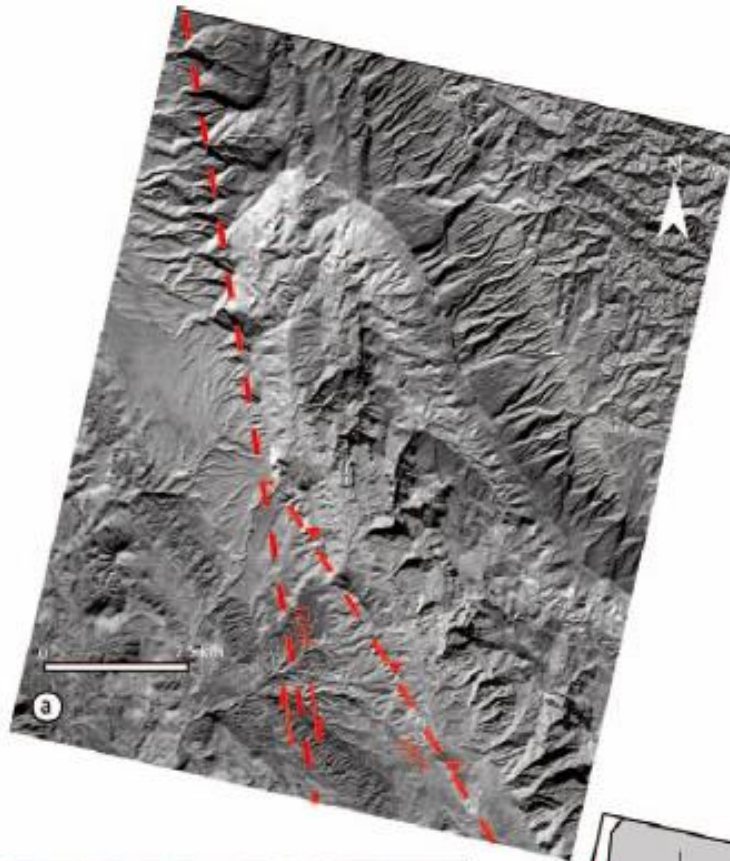




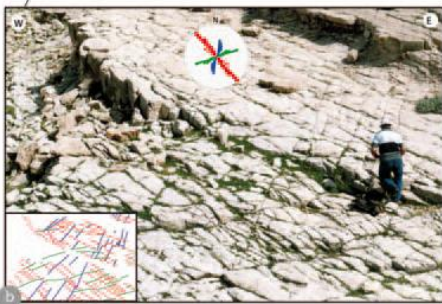
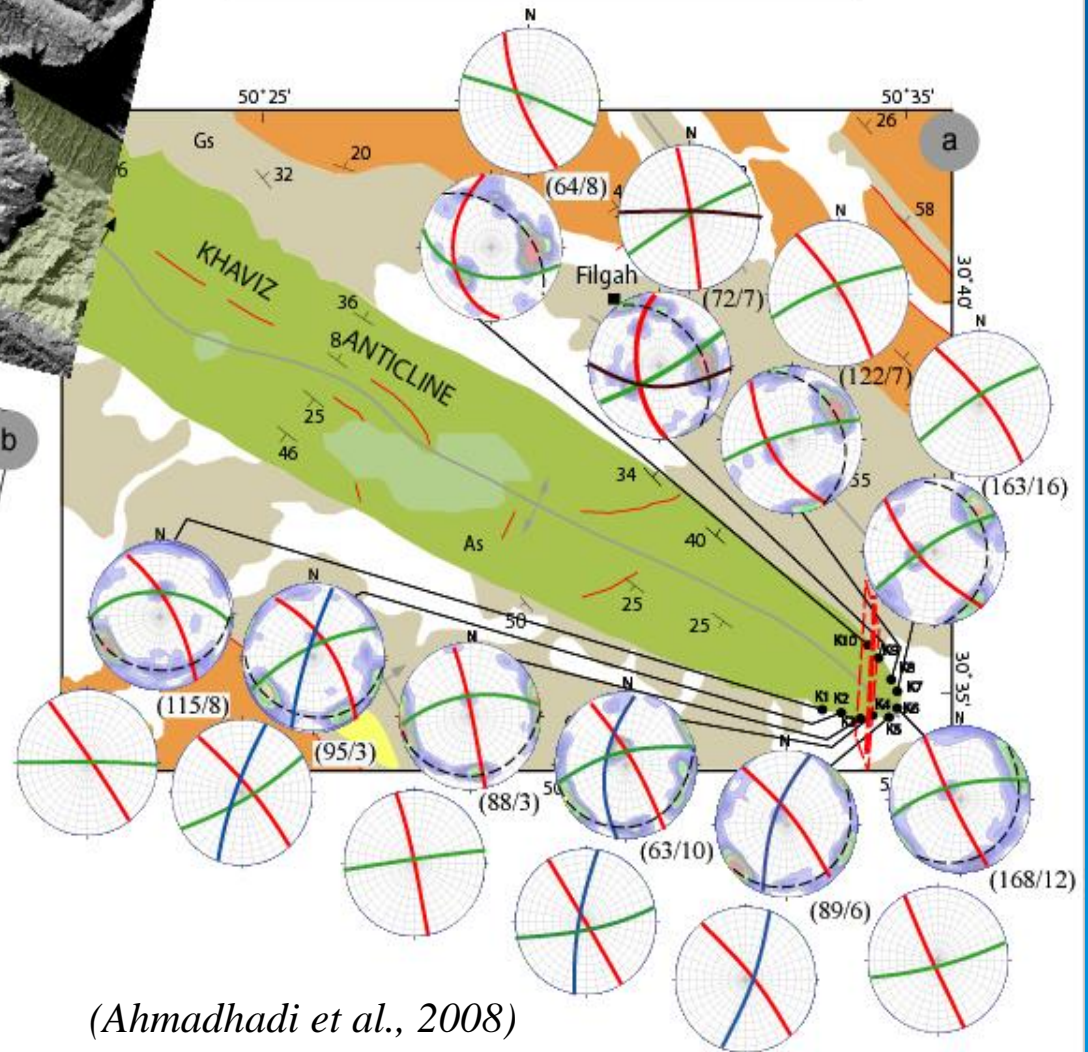
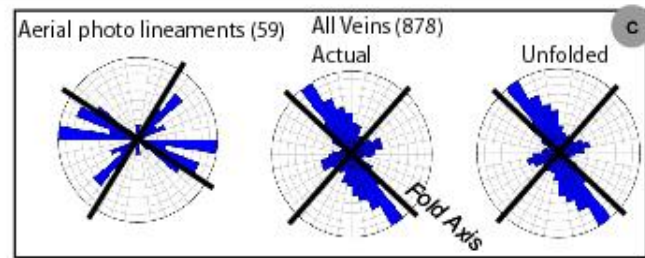
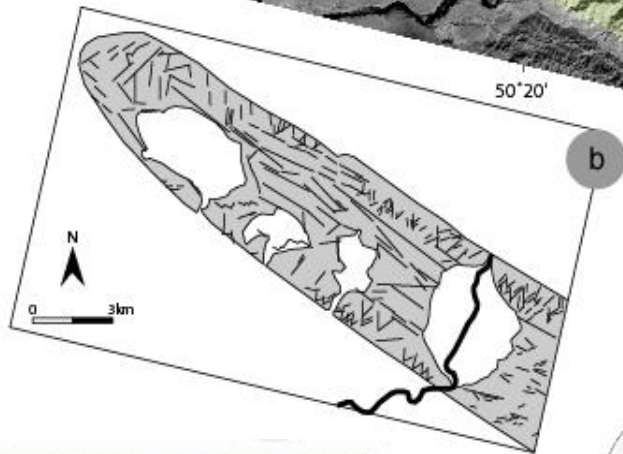
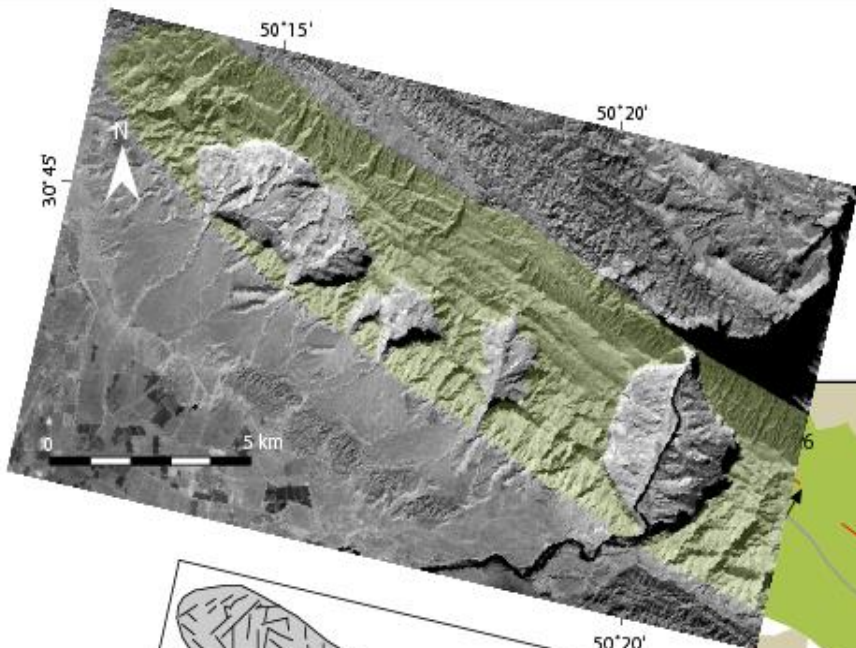
(Ahmadhadi et al., 2008)



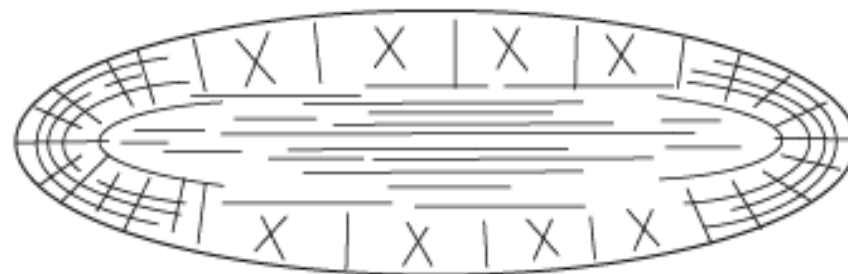
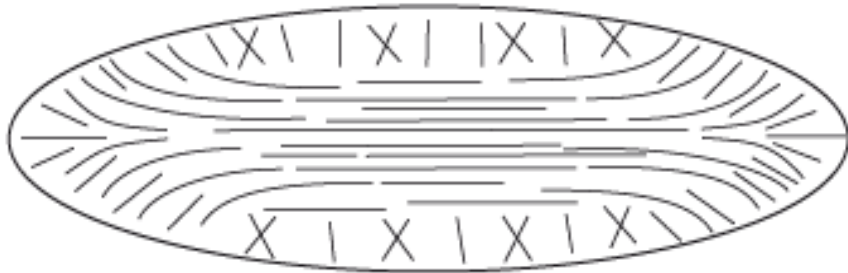
(Ahmadhadi
et al., 2007)



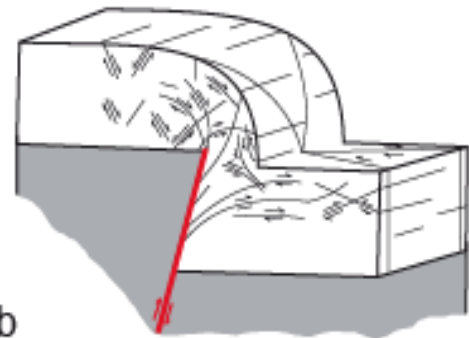
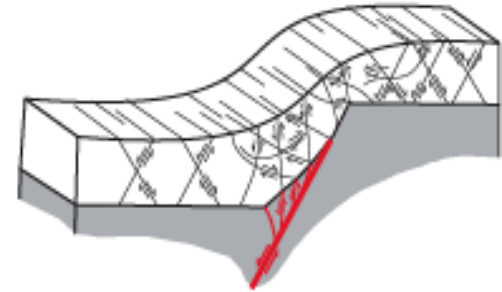
(Ahmadhadi
et al., 2007)



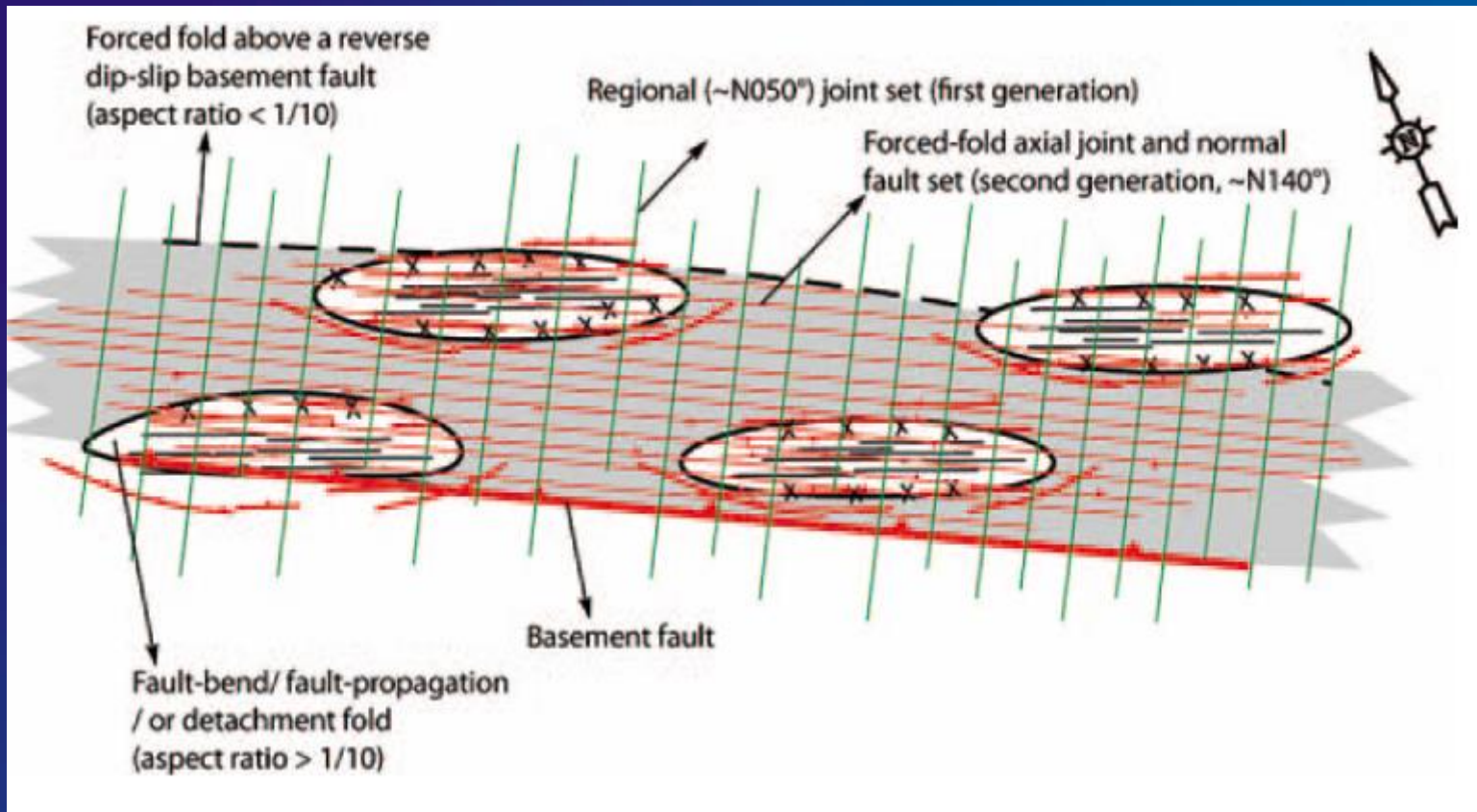
(Ahmadhadi et al., 2008)



a

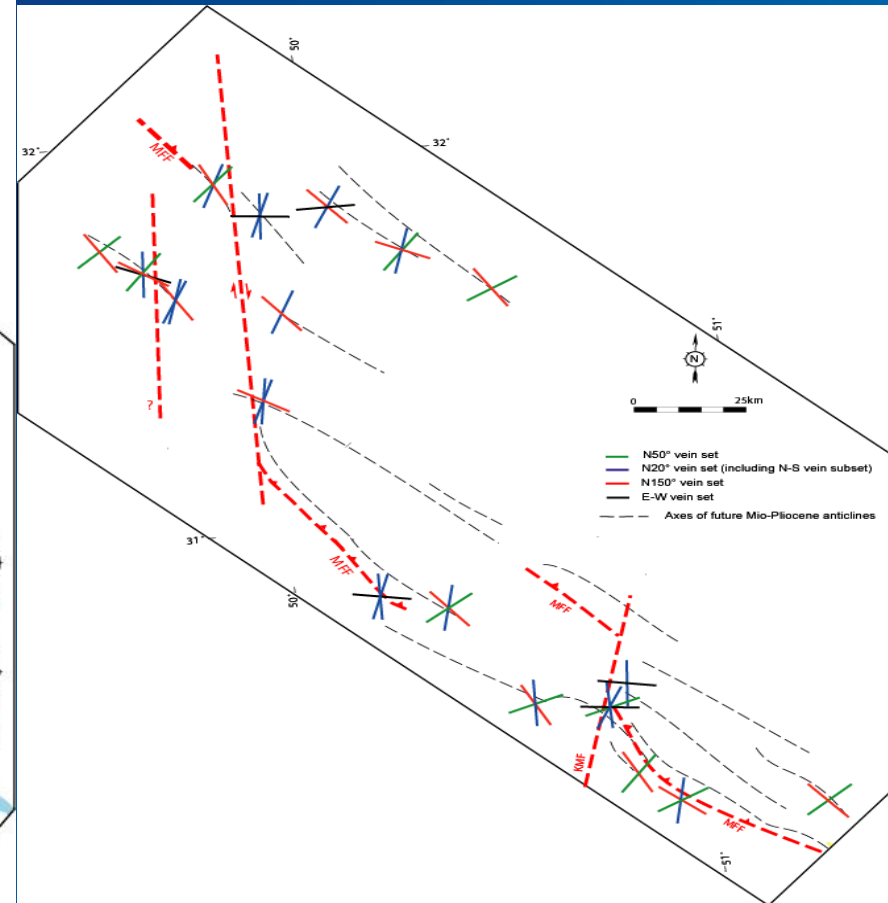
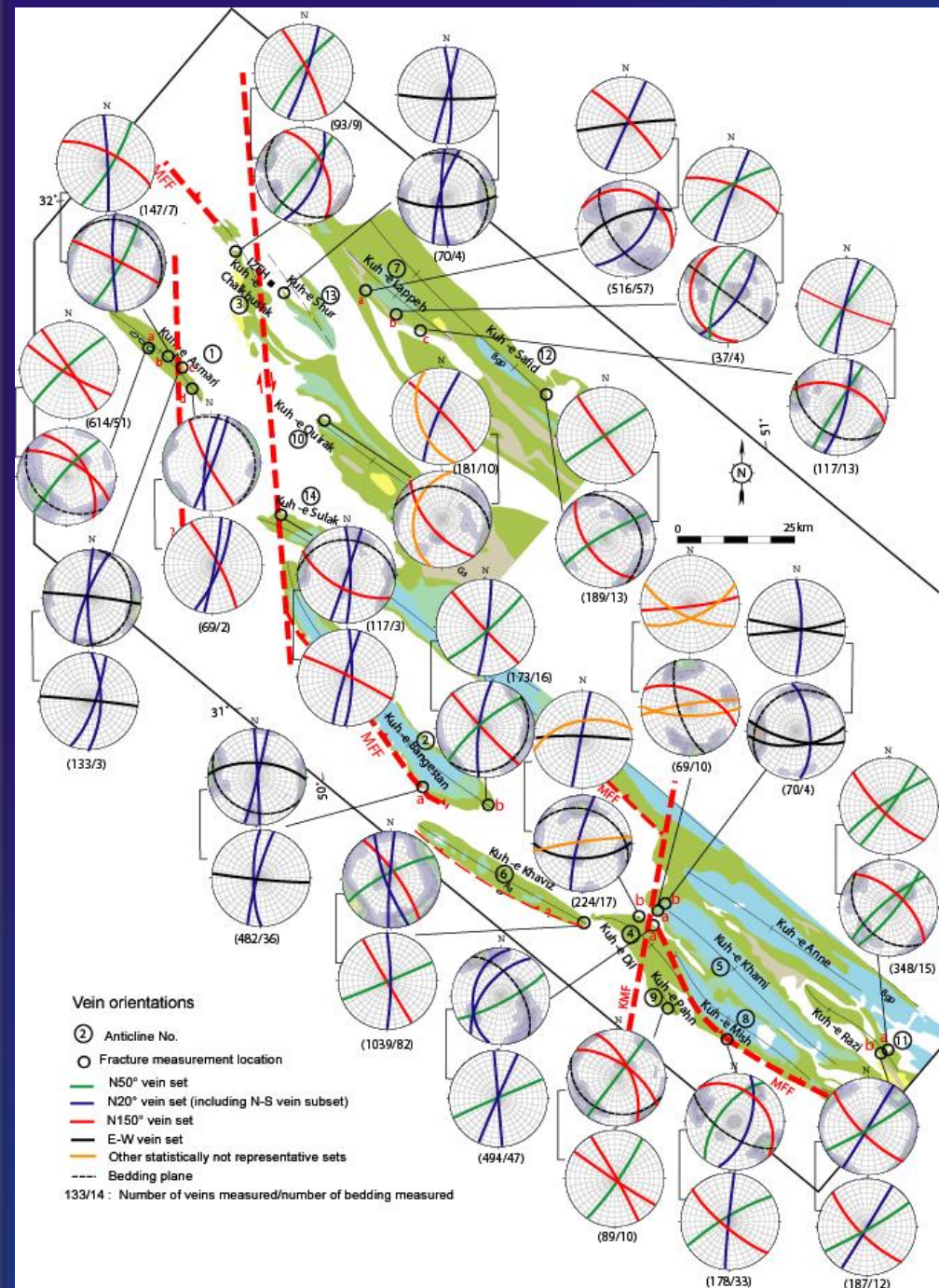


b

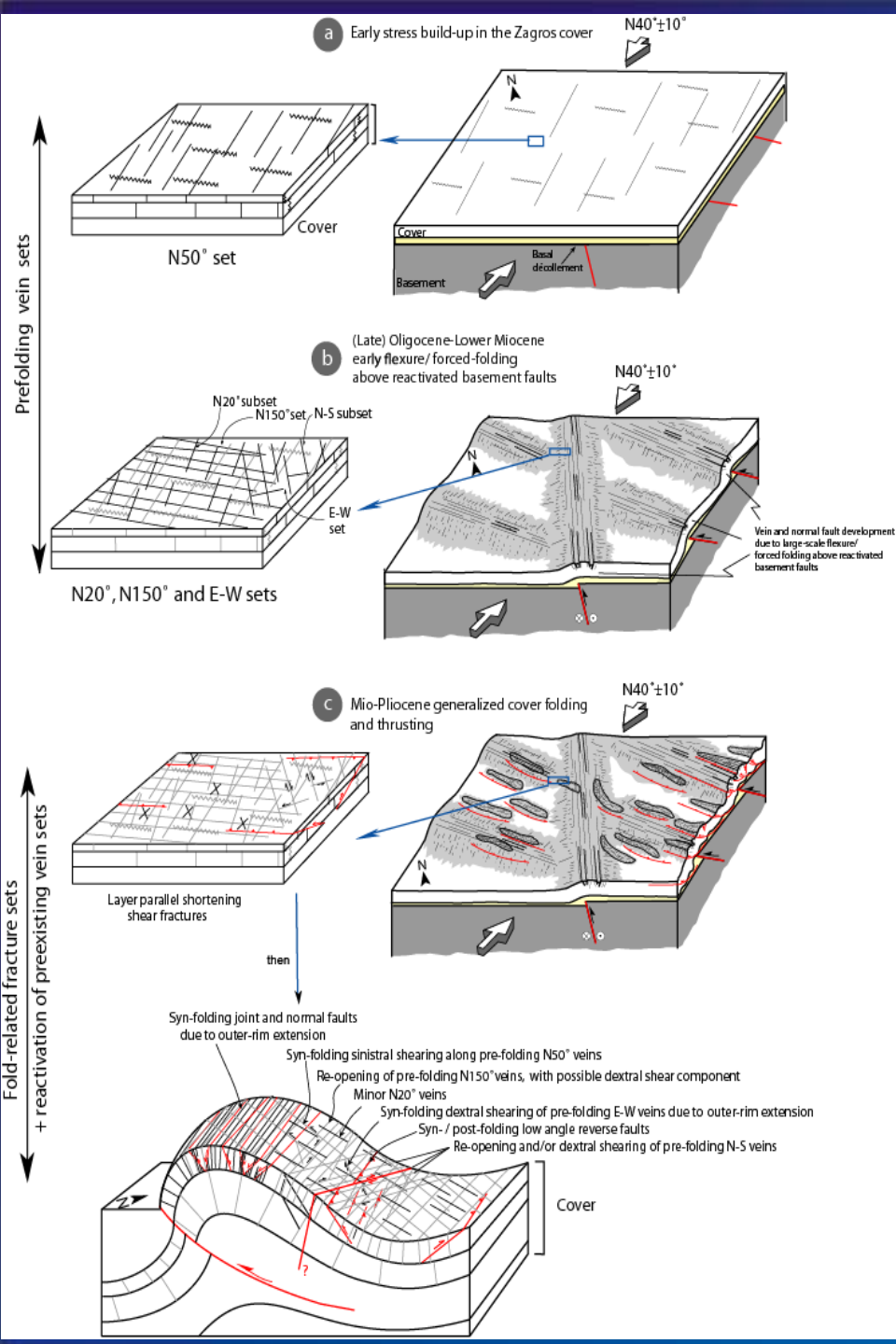


(Ahmadhadi et al., 2007)

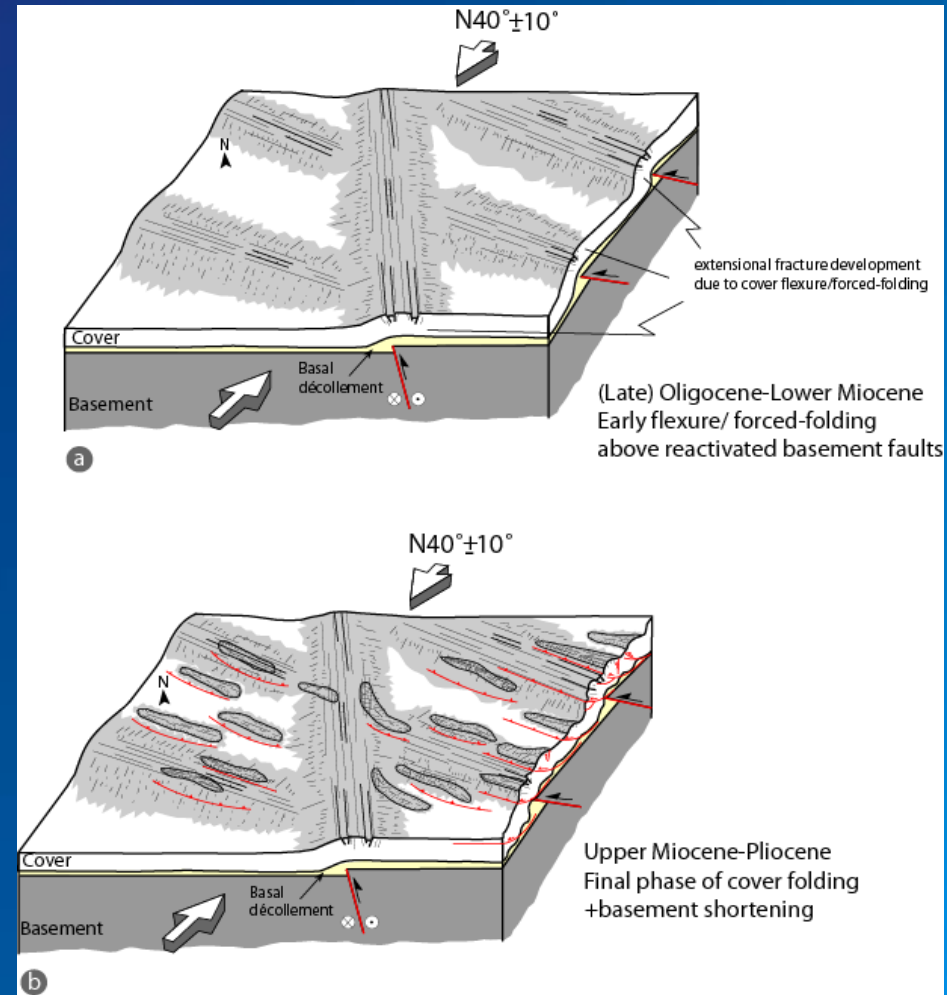
Specific occurrence of some prefolding vein sets in the vicinity of basement faults



(Ahmadhadi et al., 2008)



Onset of stress build-up

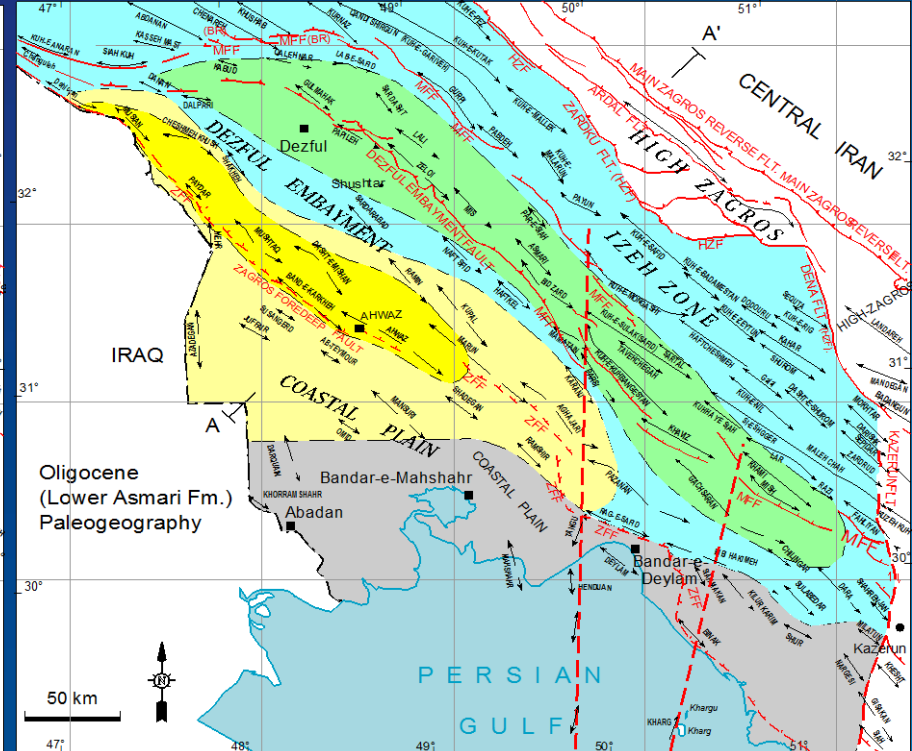
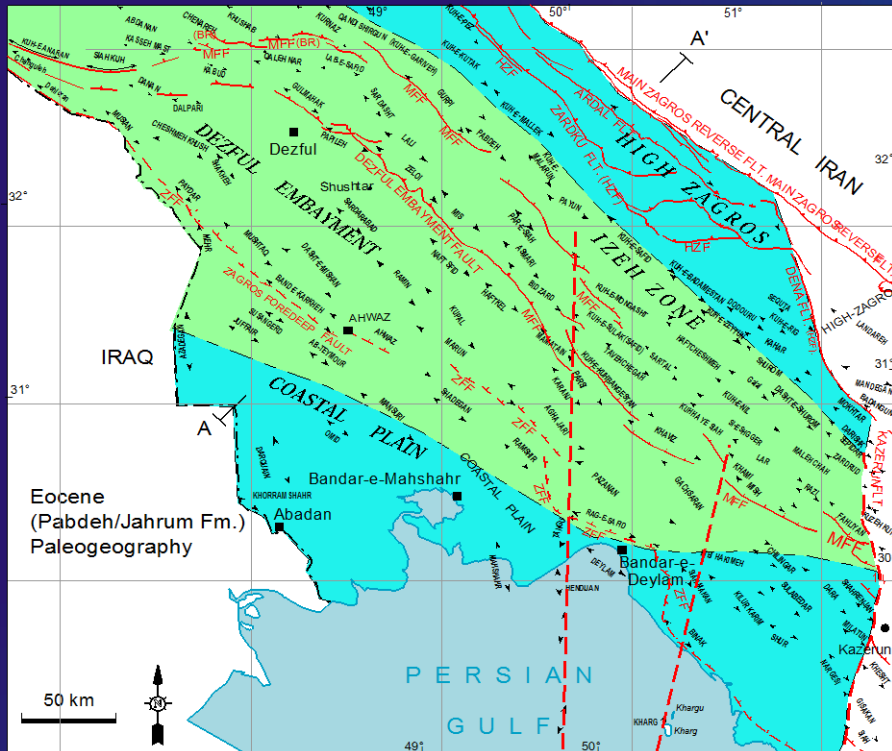


(Ahmadhadi et al., 2007;
Ahmadhadi et al., 2008)

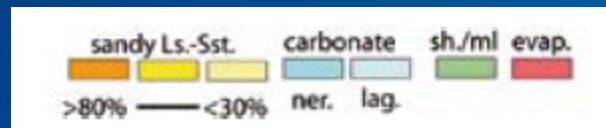
Basement structures and early basement block movements may therefore have an impact on fracture development in the overlying cover rocks.

The occurrence of some local compressional trends and related fracture sets was partly controlled by underlying deep-seated basement faults in the Zagros region. The transmission of orogenic stress through the faulted crystalline basement of the Zagros was probably heterogeneous and complex; deformation propagated in an irregular fashion through the basement and the cover leading to local stress perturbations, hence to a complex directional distribution and chronology of fractures in the cover.

Such a complexity should be taken into account in further studies of folded and fractured reservoirs.

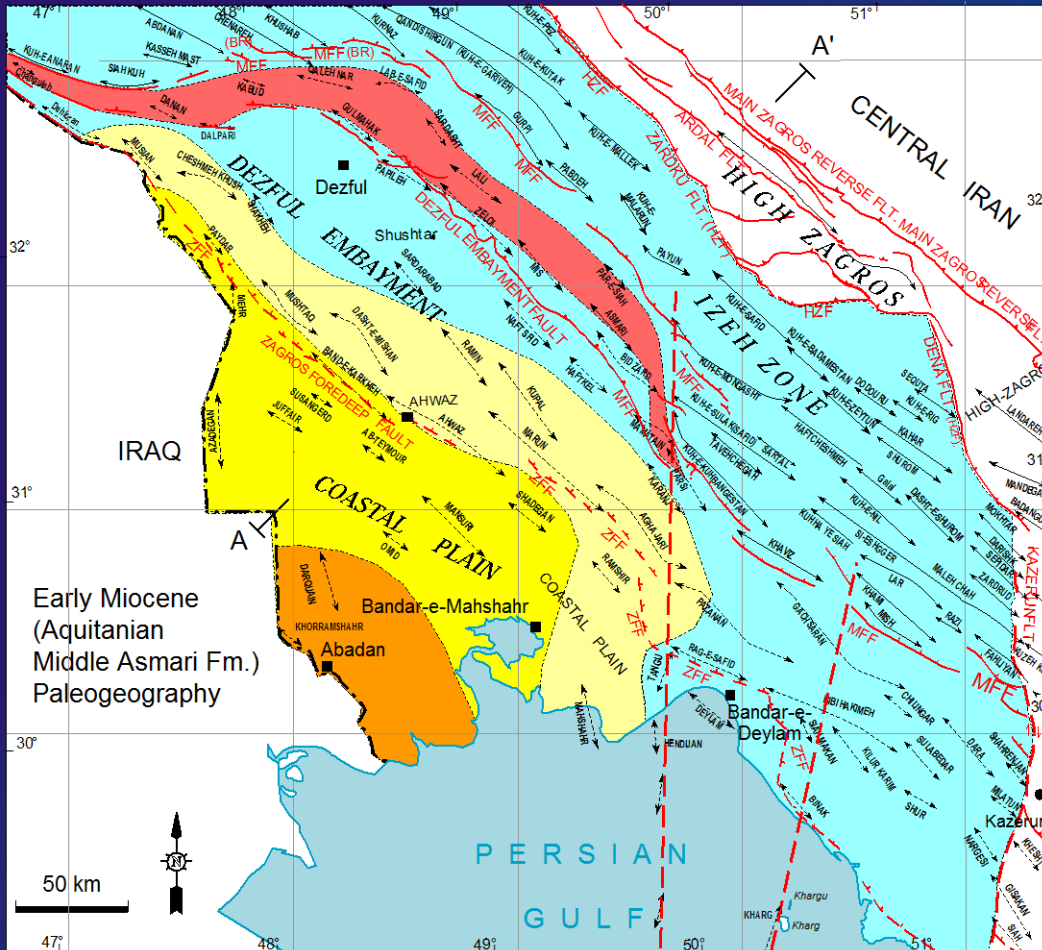


(Ahmadhadi et al., 2007)



During Eocene times, the Pabdeh basin covered a wide area from the south of the High Zagros fault toward the Zagros Foredeep Fault.

During the Lower Oligocene, progressive basin restriction and sedimentary flux progradation toward the depocenter of the previous Pabdeh basin - between the MFF to the north and the ZFF to the south - following the progradation of the carbonate platform and clastic facies of the Lower Asmari Formation suggest that the NW-SE trending basement faults were presumably reactivated

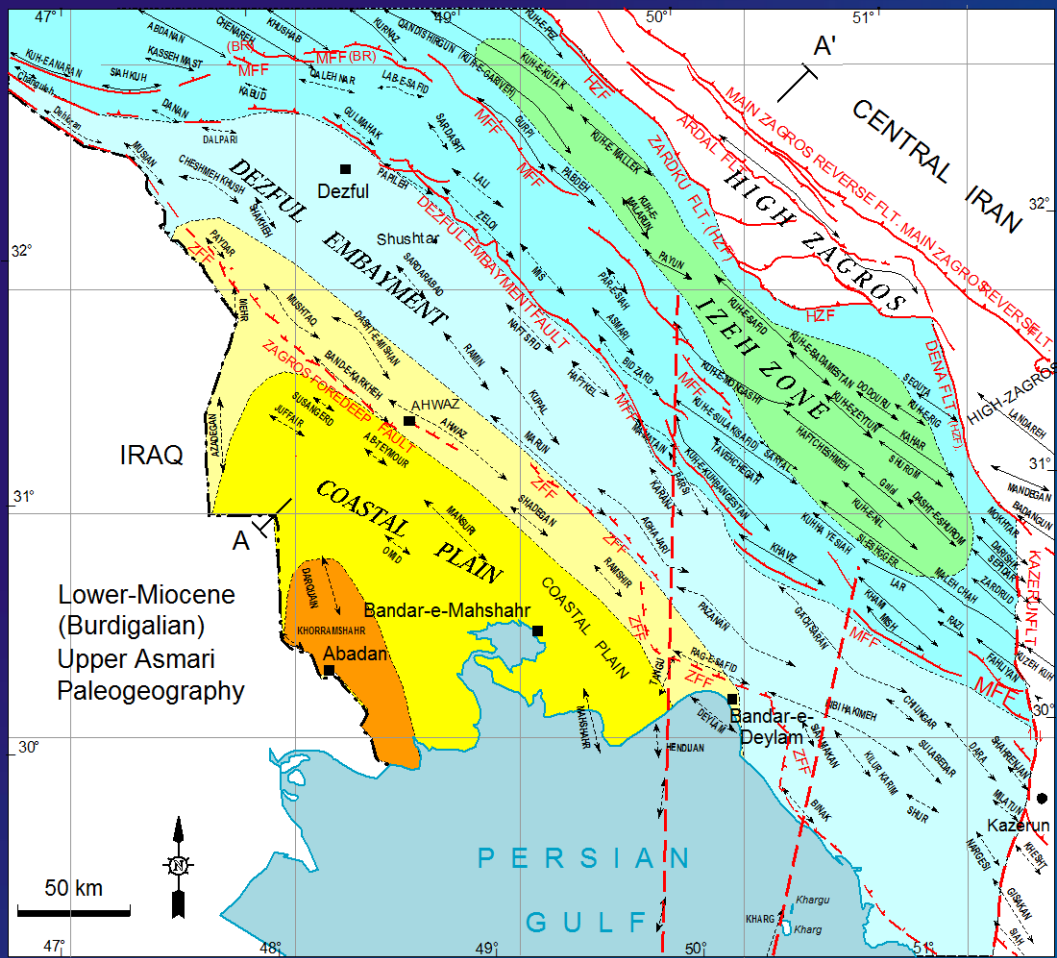


(Ahmadhadi et al., 2007)

The development of a long narrow evaporitic intra-basin (Kalhur Member) during the latest Oligocene-early Lower Miocene likely indicate an abrupt facies change (both laterally and vertically)

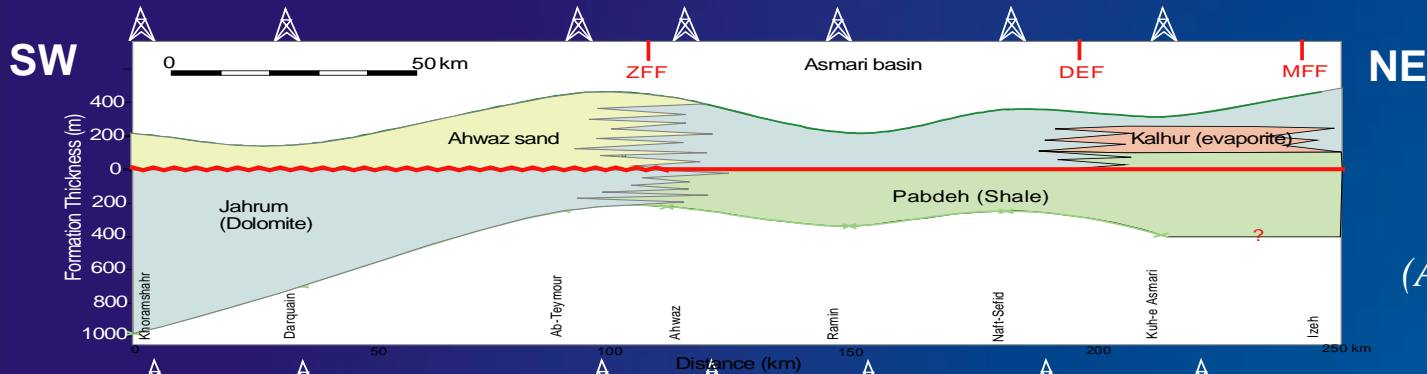
→ difficult to interpret simply by eustasy or any sedimentological process alone, without any tectonic control.

Rather :
 the localization of this intra-basin between the MFF to the north and the DEF to the south and the abrupt facies change from marls to evaporites suggests a direct relation between this restricted lagoon intra-basin and deep-seated basement faults.

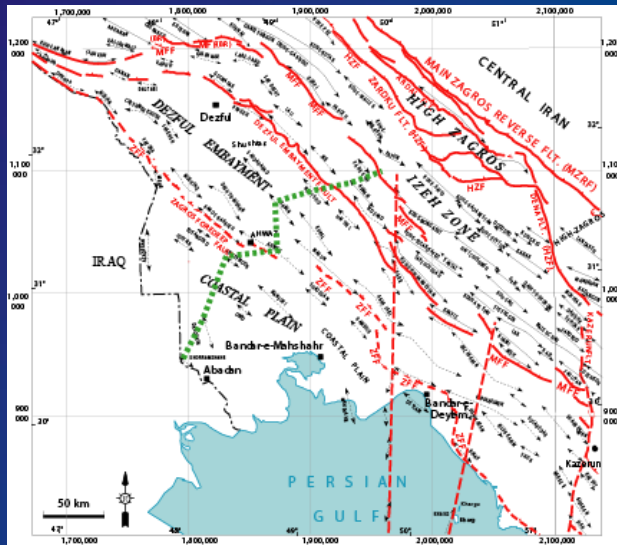
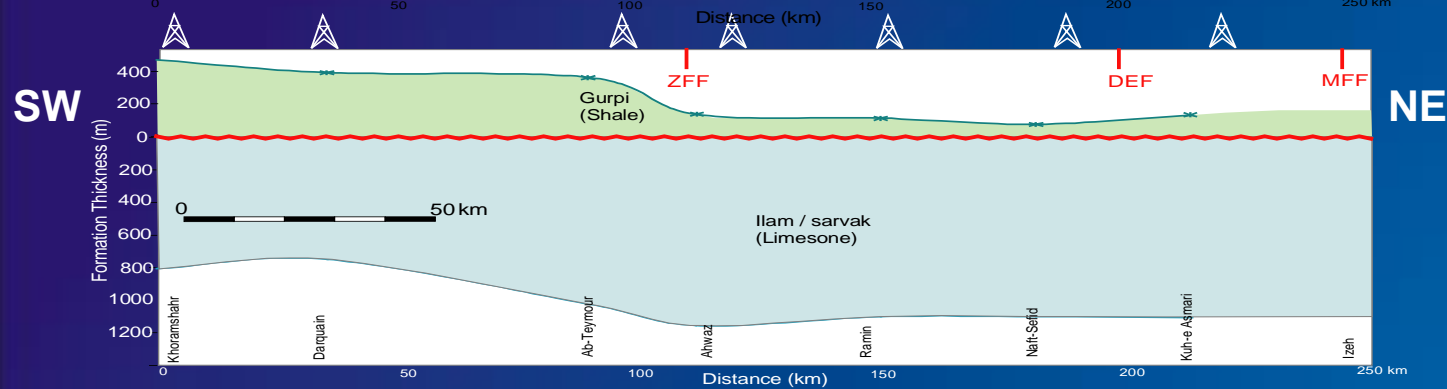


The Ahwaz/Ghar Member delta front, indicated by more than 30% of the sand content of the Asmari carbonate, formed just and parallel to the south of the ZFF.

During Burdigalian times, the Upper Asmari carbonates covered the entire basin with a hemipelagic facies toward the northern part of the Mountain Front Fault



(Ahmadhadi et al., 2007)



Transect based on the thickness variations of the main lithostratigraphical units (formations) with definite time lines (top and bottom) :

Both thickness and main facies variations within Pabdeh/Jahrum and Asmari formations coincide with the location of the main basement faults; this strongly suggests that these faults were reactivated during Pabdeh/Jahrum and Asmari deposition.

- Facies distribution and sub-basins development in the Central Zagros during Eo (?) - Oligocene - lower Miocene were likely controlled by the compressional reactivation of deep-seated basement faults
- Deformation in the region presumably started as soon as Eocene – Oligocene, with amplification of forced folding during Chattian/Aquitania (~30 – 22 Ma) and initiation of early vein sets within Asmari Fm

**Paleostress/shortening patterns in the Zagros belt :
AMS, calcite twins and meso-scale faulting**

Anisotropy of sedimentary rocks

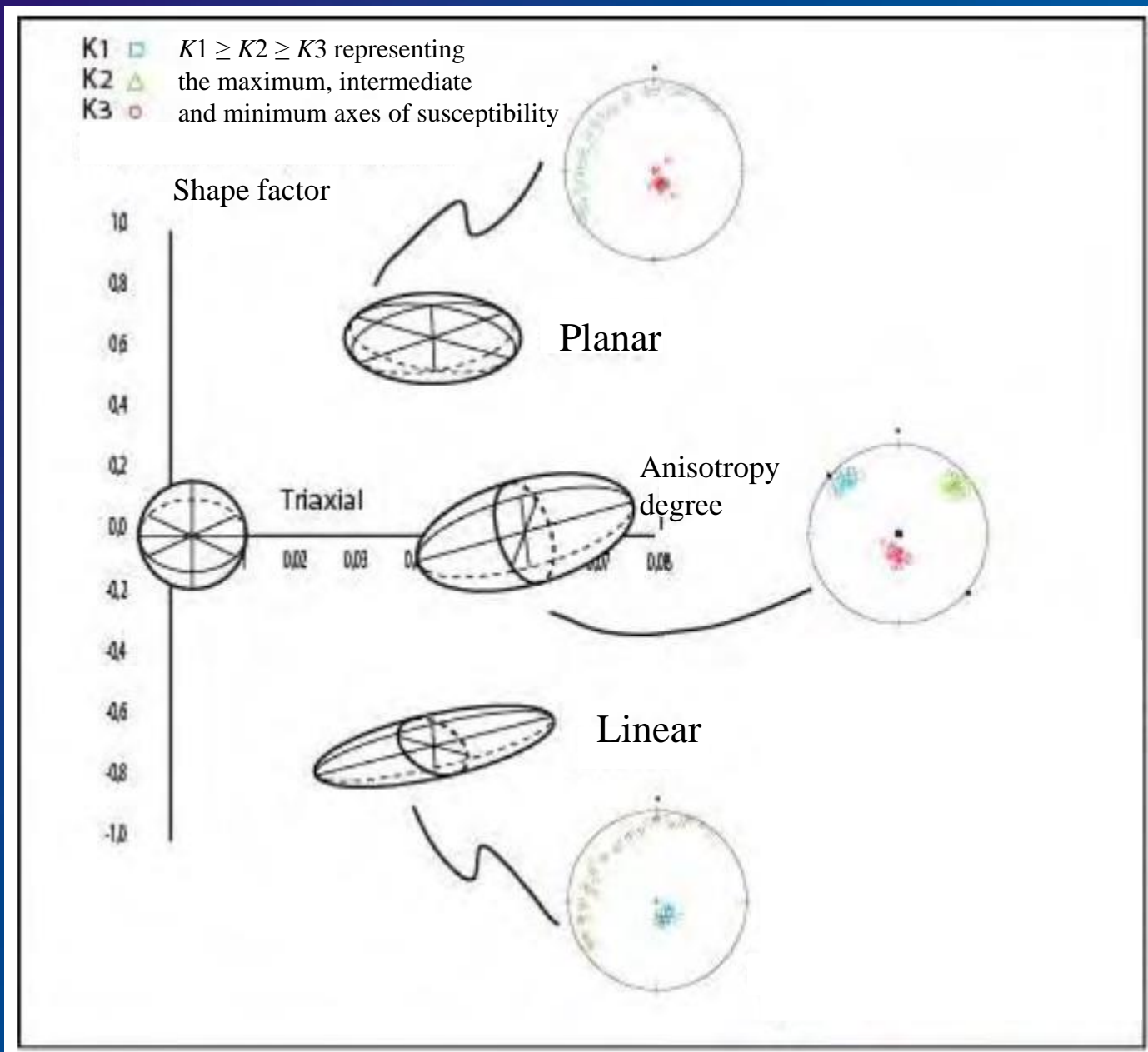
The anisotropic behaviour of sedimentary rocks with respect to a particular physical property (elasticity, magnetic susceptibility, electrical conductivity and permeability) is determined by both matrix properties and pore space distributions.

The matrix of a sedimentary rock can be anisotropic because of preferred mineral orientation, water currents during deposition or pressure solution in response to an anisotropic stress field during loading.

The pore space distribution can be anisotropic because of the sedimentation processes controlled by gravity, which often result in transversely isotropic rocks, depositional processes driven by water currents, and the presence of preferentially oriented cracks within or between the minerals

AMS

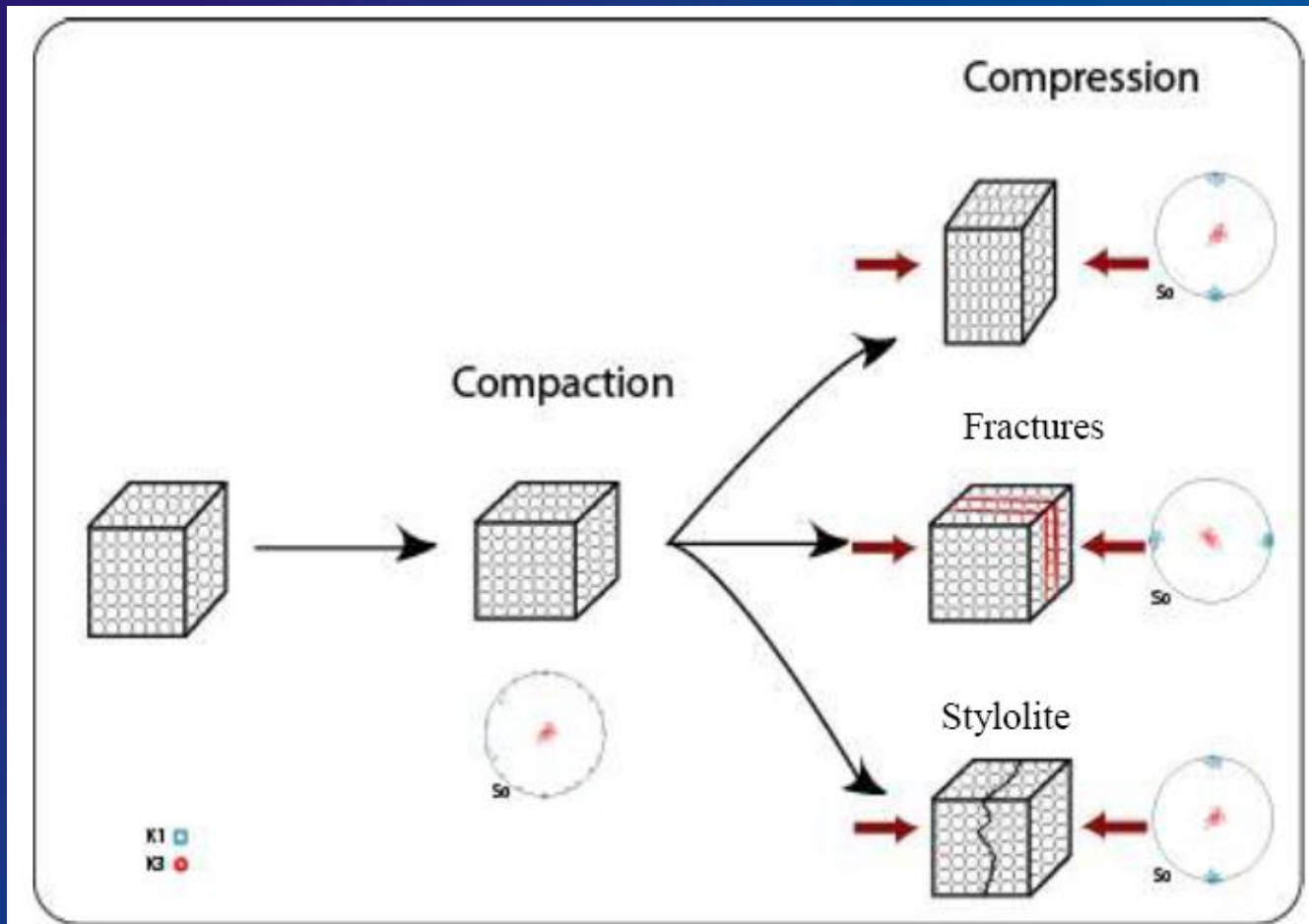
The measurement of AMS helps characterize penetrative tectonic fabrics in deformed rocks because AMS is sensitive to even slight preferred orientations of magnetic minerals.



In sedimentary rocks, magnetic susceptibility K_m originates primarily from three distinct sources: (1) the dominant diamagnetic minerals (quartz or calcite), (2) the paramagnetic minerals (clays and other Fe-bearing silicates) and (3) diluted ferromagnetic minerals (magnetite, hematite and pyrrhotite), depending on their relative proportion.

Generally, K_m ranges between low negative values and low positive values (from -10×10^{-6} SI to 10×10^{-6} SI). In Fe-bearing silicate rocks K_m covered susceptibilities up to $500-1000 \times 10^{-6}$ SI whereas ferromagnetically dominated rocks are generally characterized by values higher than 1000×10^{-6} SI. The lack of paramagnetic minerals tends to decrease the limit of influence of ferromagnetic fraction on magnetic susceptibility.

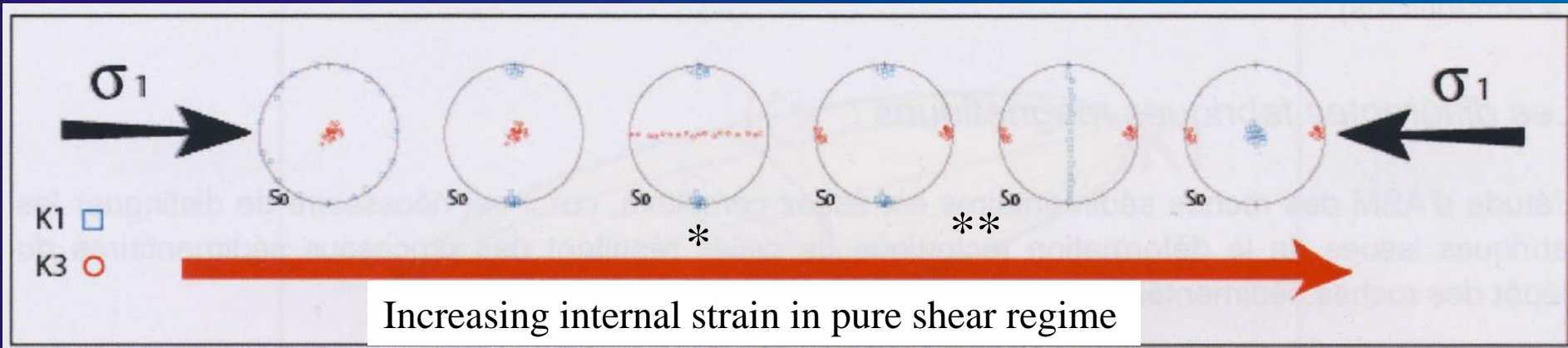
AMS



The interpretation of AMS fabrics is strongly dependent on the carrier of the magnetic signal

AMS

The magnetic fabric is typically defined using the orientation of either the magnetic foliation, that is, the plane containing the $K1$ and $K2$ axes when $K1 \approx K2 > K3$, or the magnetic lineation, that is, the direction of the $K1$ -axis.

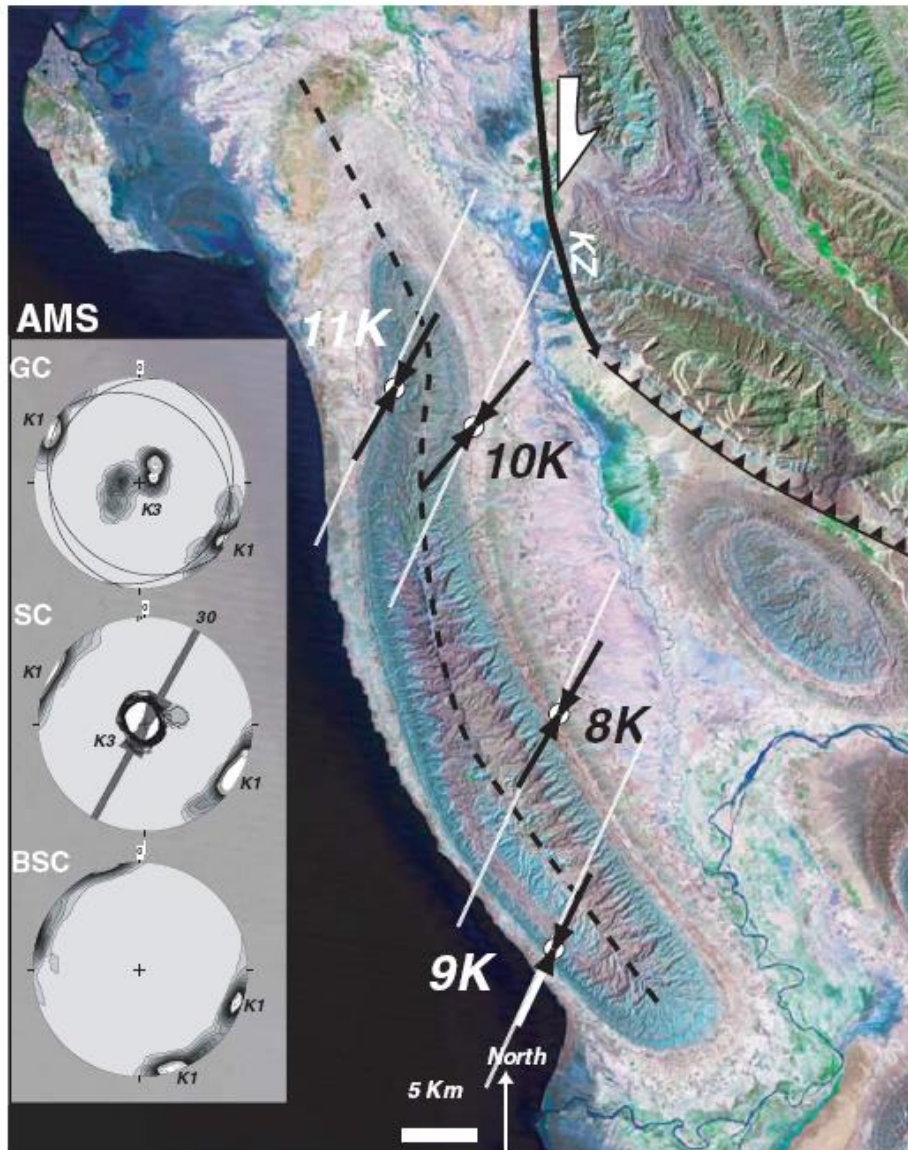


* Intermediate fabric : magnetic lineation $K1$ still contained within the bedding but clustered at right angle to the shortening direction, whereas the $K3$ is leaving the pole to bedding and exhibits a girdle distribution around $K1$.

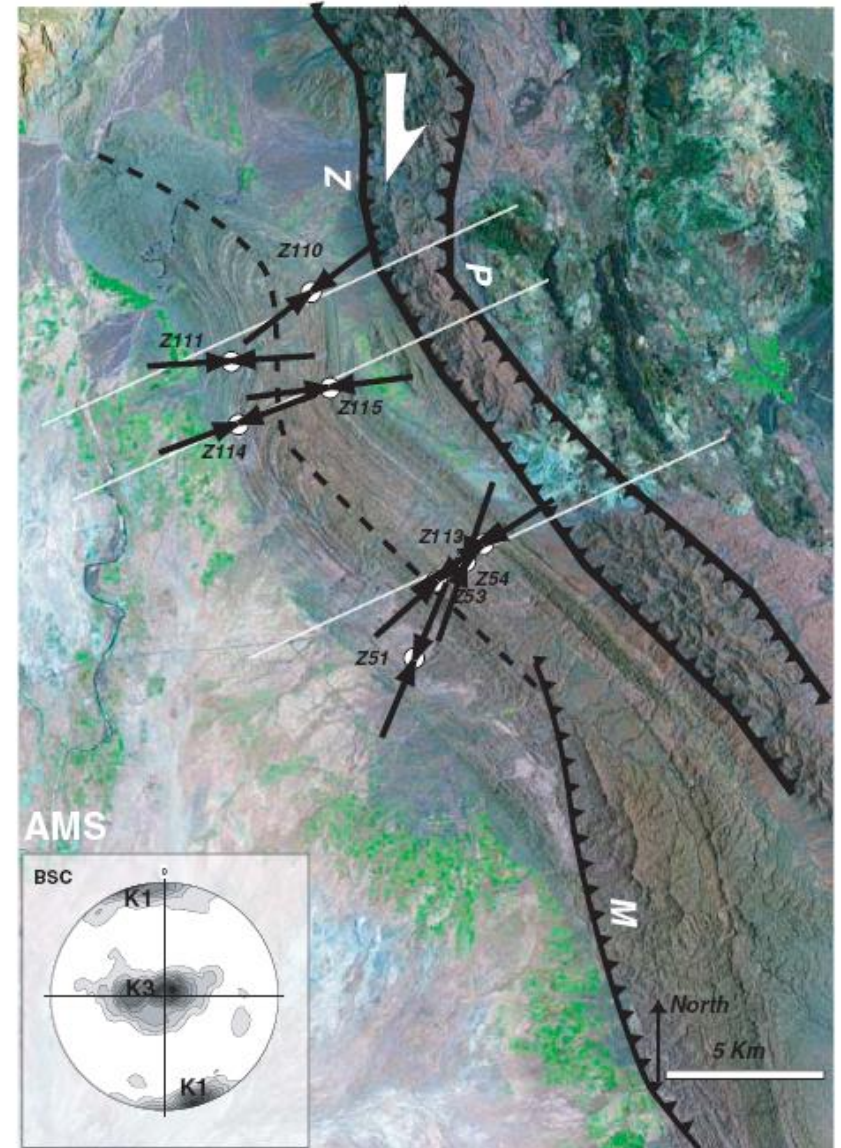
** Tectonic fabric characterized by $K3$ parallel to the shortening direction. $K1$ is either parallel to the intersection between the bedding and the incipient cleavage or exhibits a girdle around $K3$

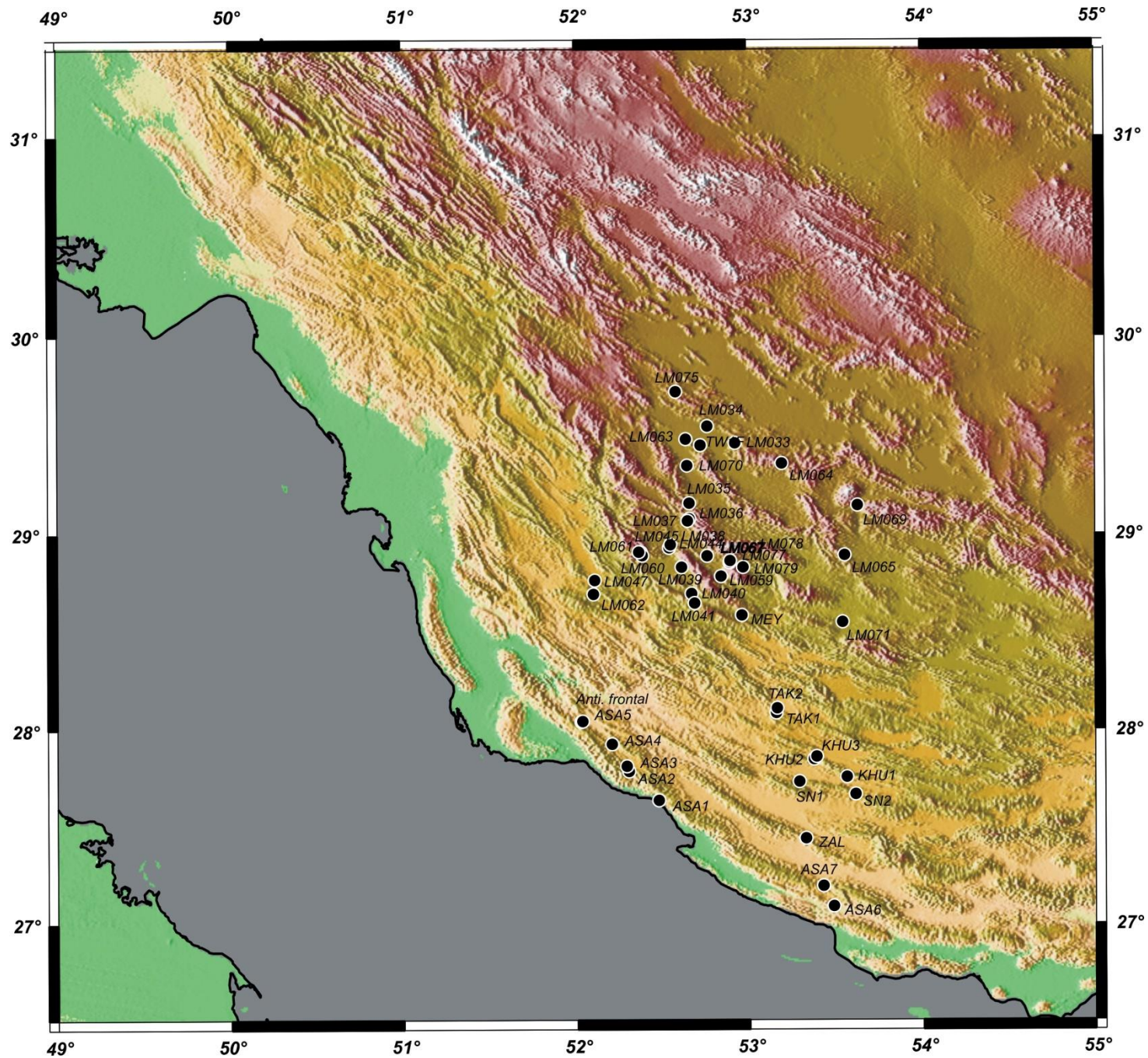
While the correlation between the orientations of principal AMS axes and principal strain axes tends to be very consistent, the correlation between the magnitudes of principal AMS axes and corresponding principal strain axes is not.

MAND anticline



MINAB anticline





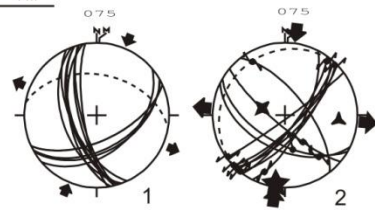


N

S

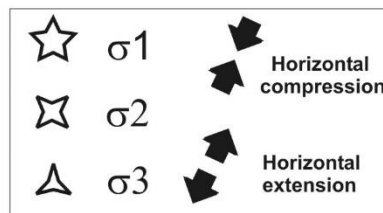
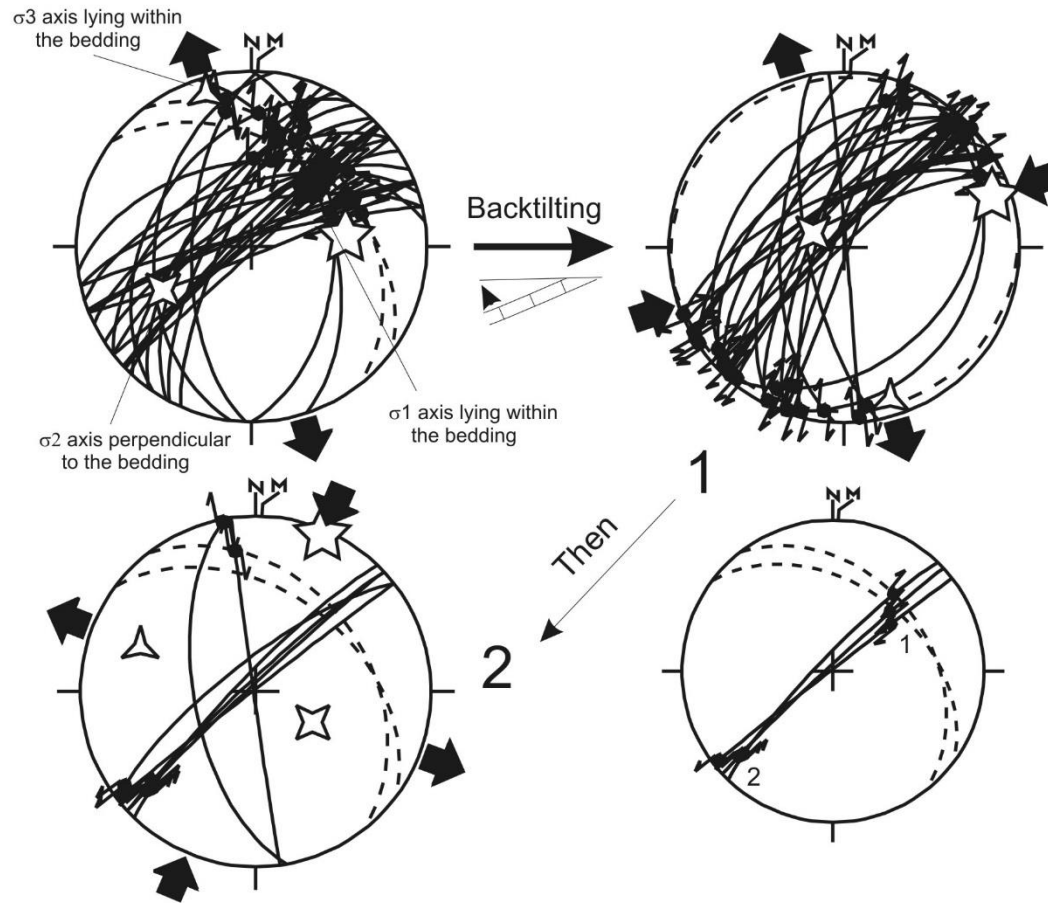


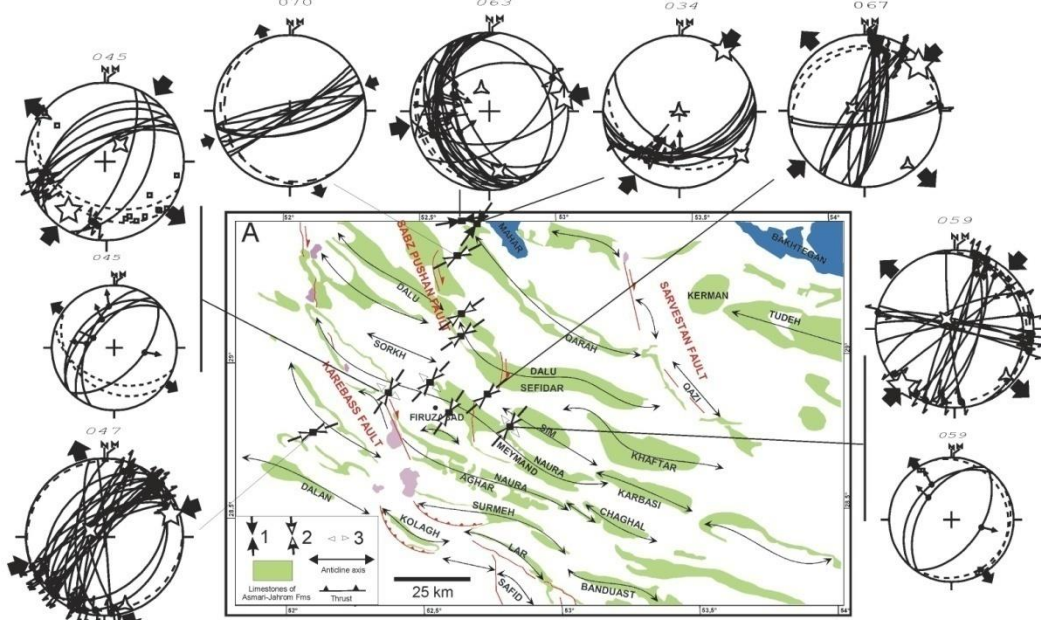
4 m



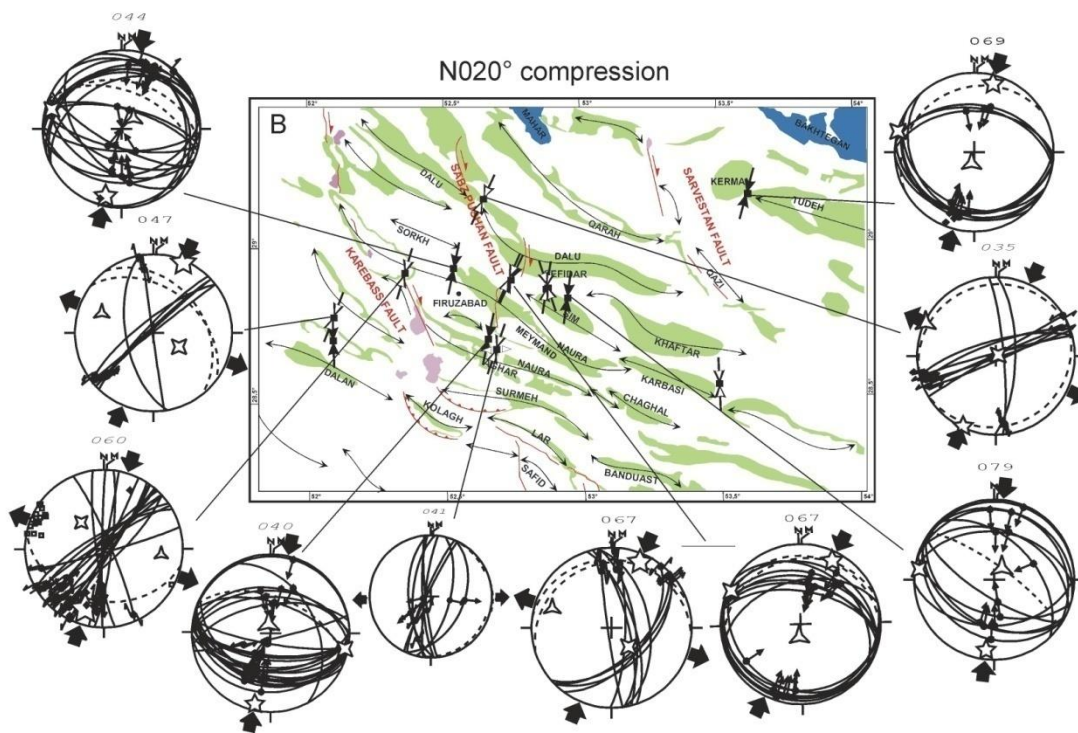
Hangingwall

Footwall



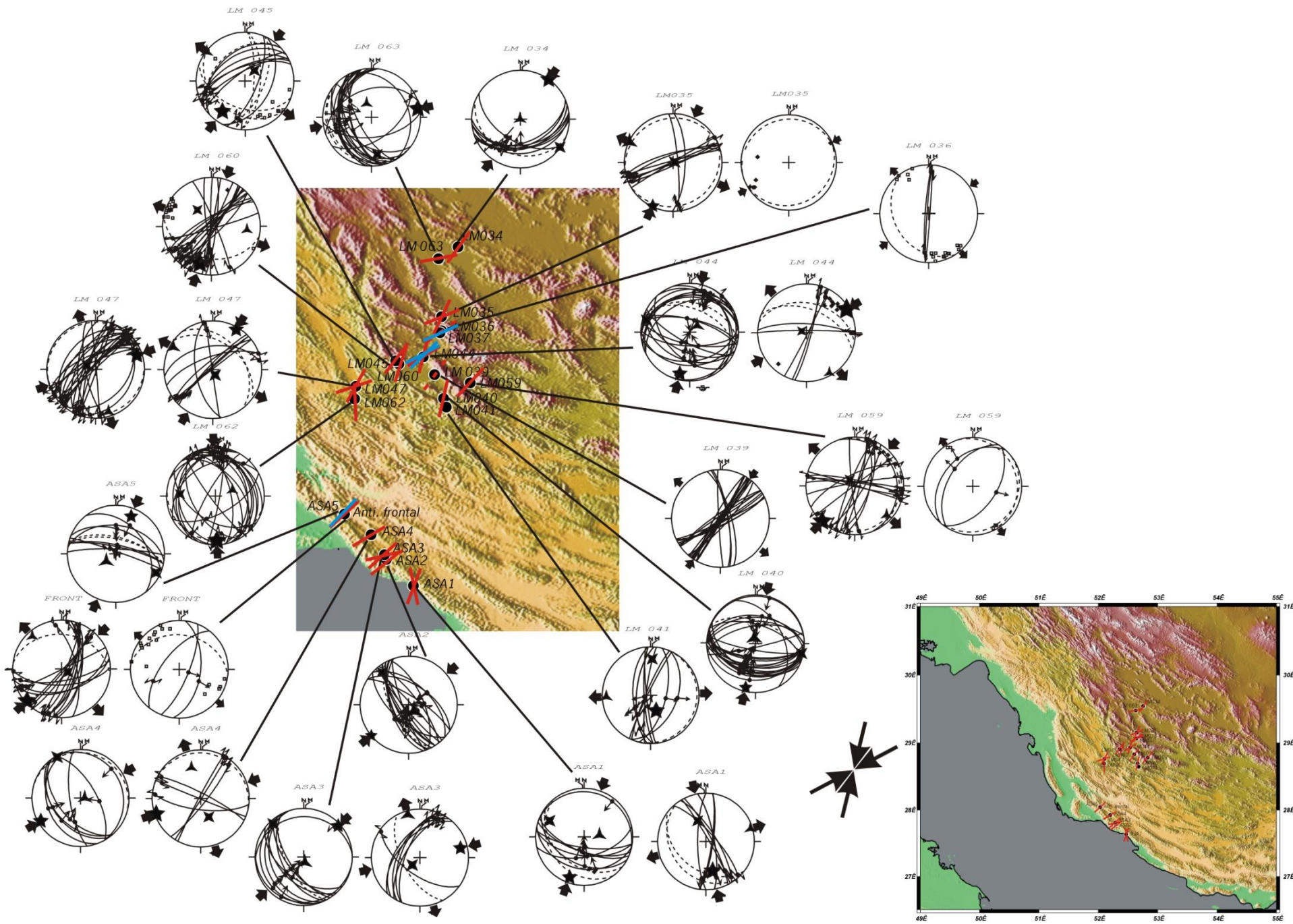


NE-SW compression

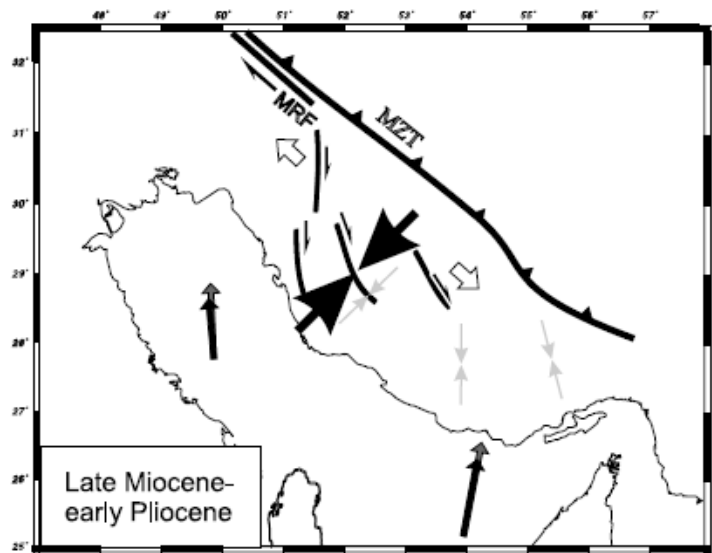


N020° compression

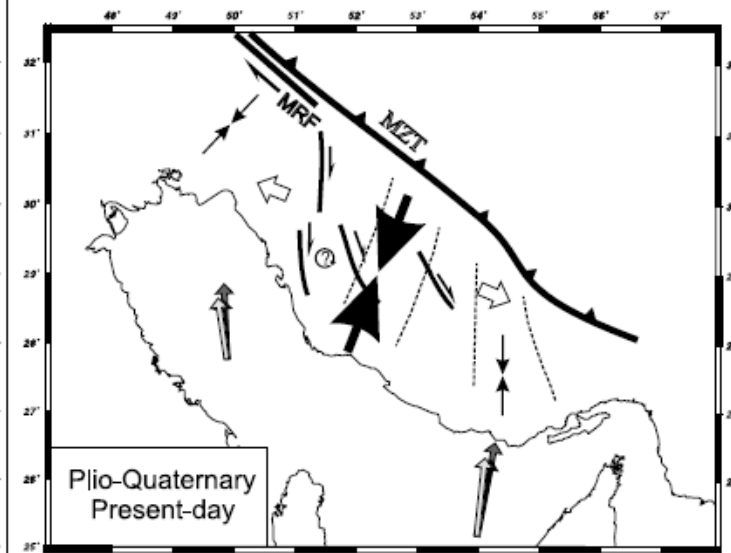
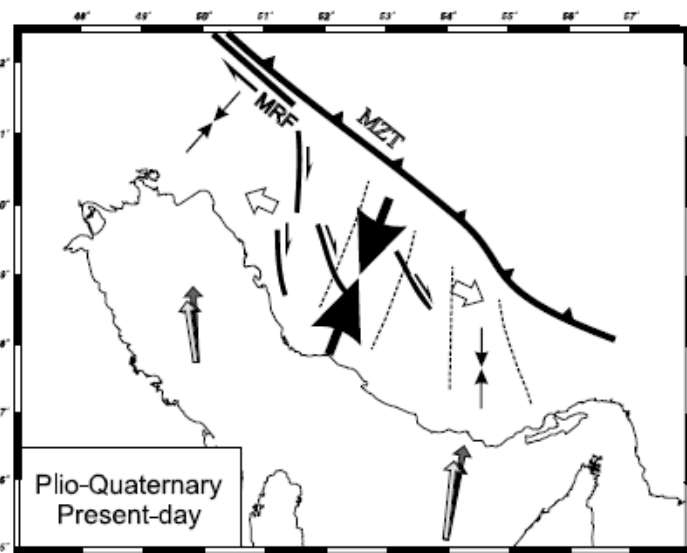
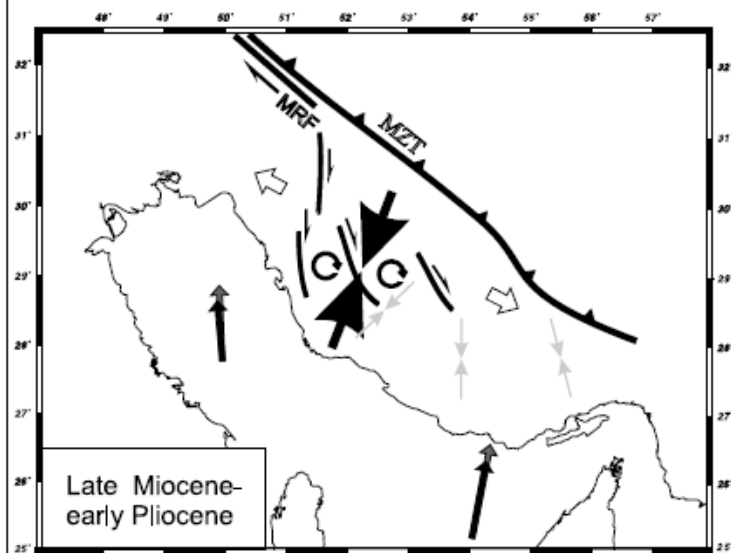
(Lacombe et al., 2006)



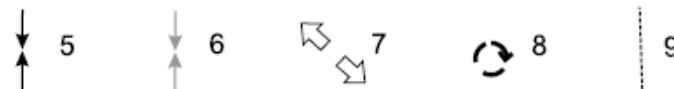
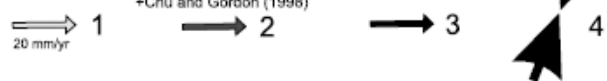
Scenario 1 : anticlockwise stress rotations



Scenario 2 : clockwise block rotations

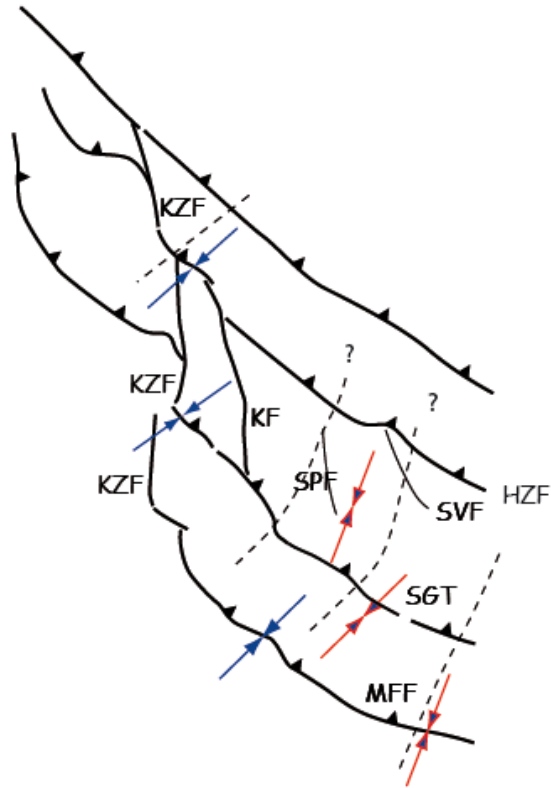


Vernant et al., 2004 Calais et al., 2003
+Chu and Gordon (1998) McQuarrie et al., 2003

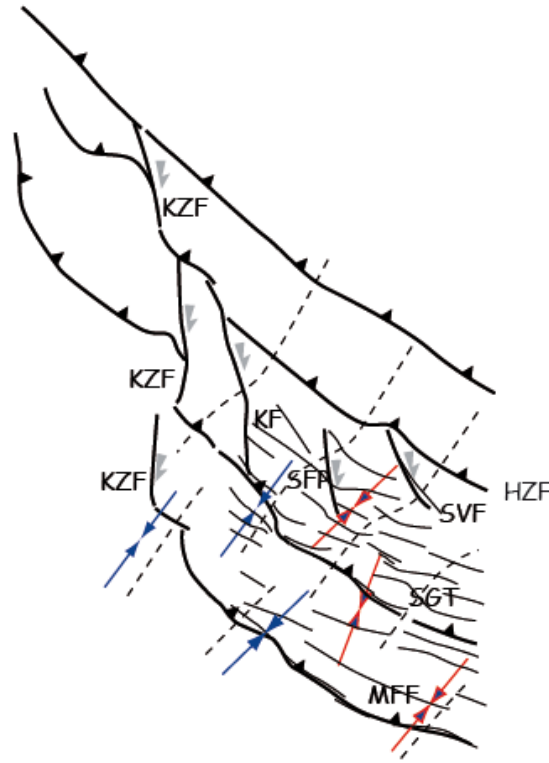


(Lacombe et al., 2006)

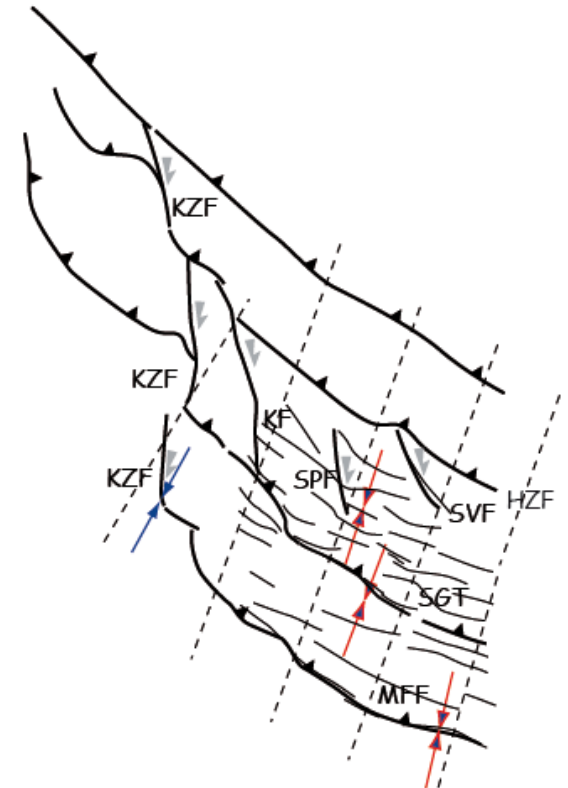
**Middle Miocene
pre-folding**

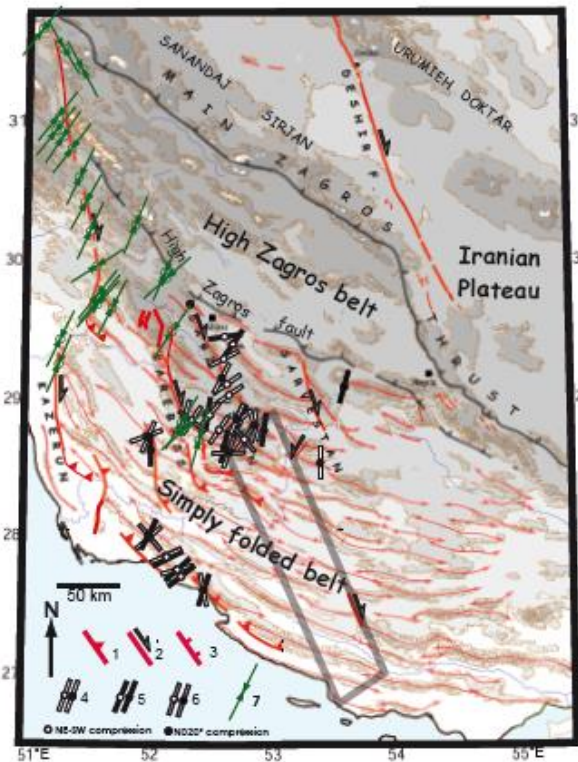


**Middle-late Miocene
early-folding to syn-folding**

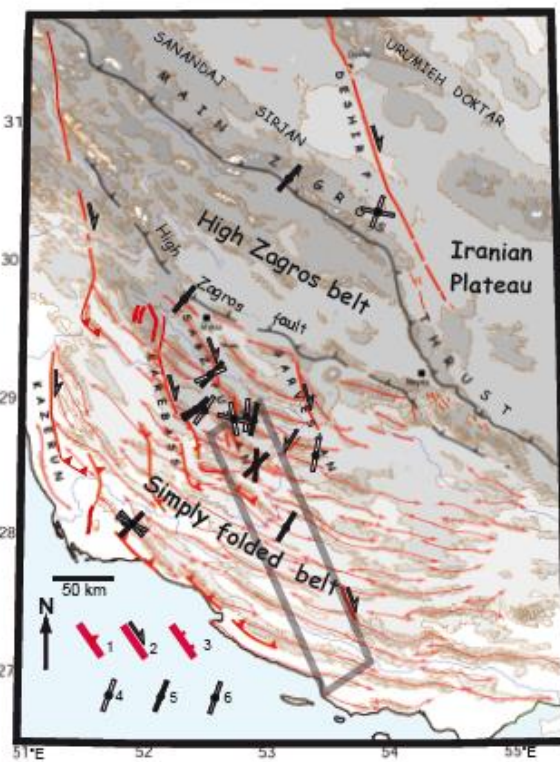


**Plio-Quaternary + Present-day
late to post-folding**

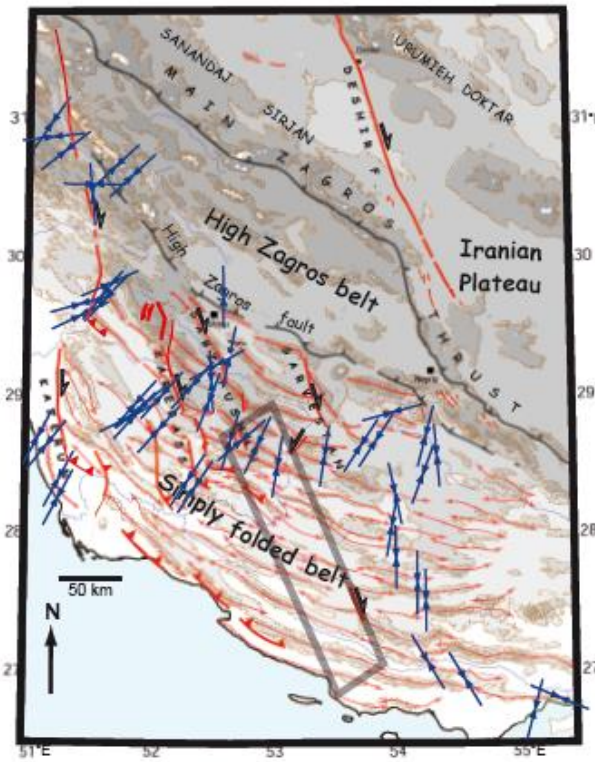




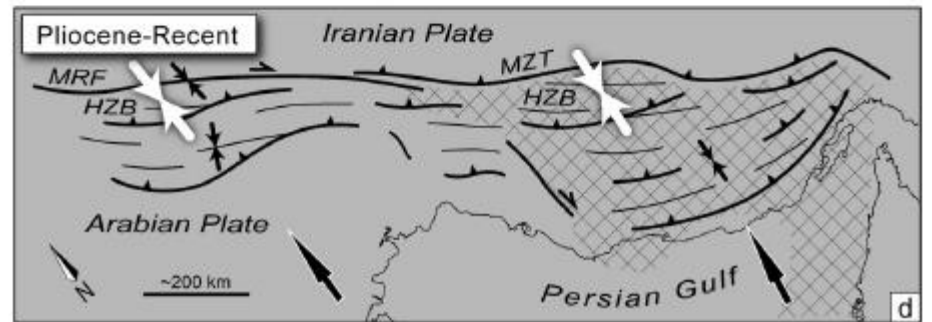
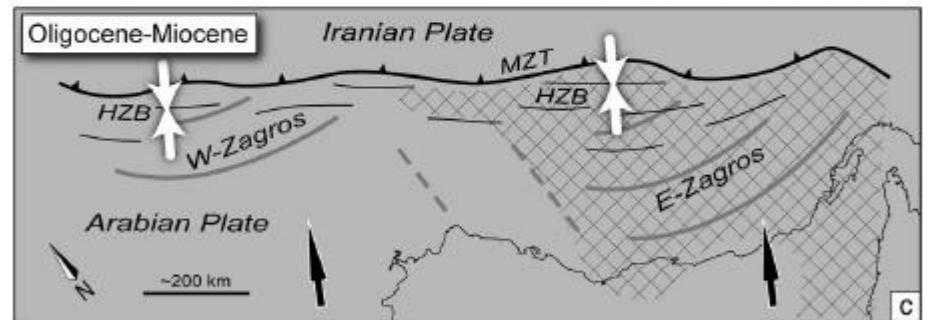
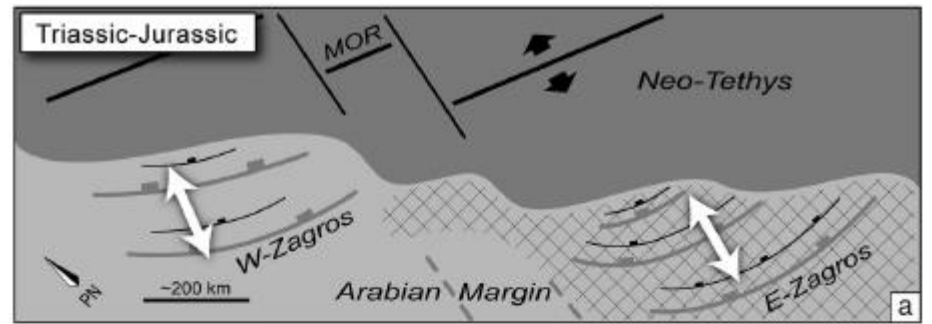
a



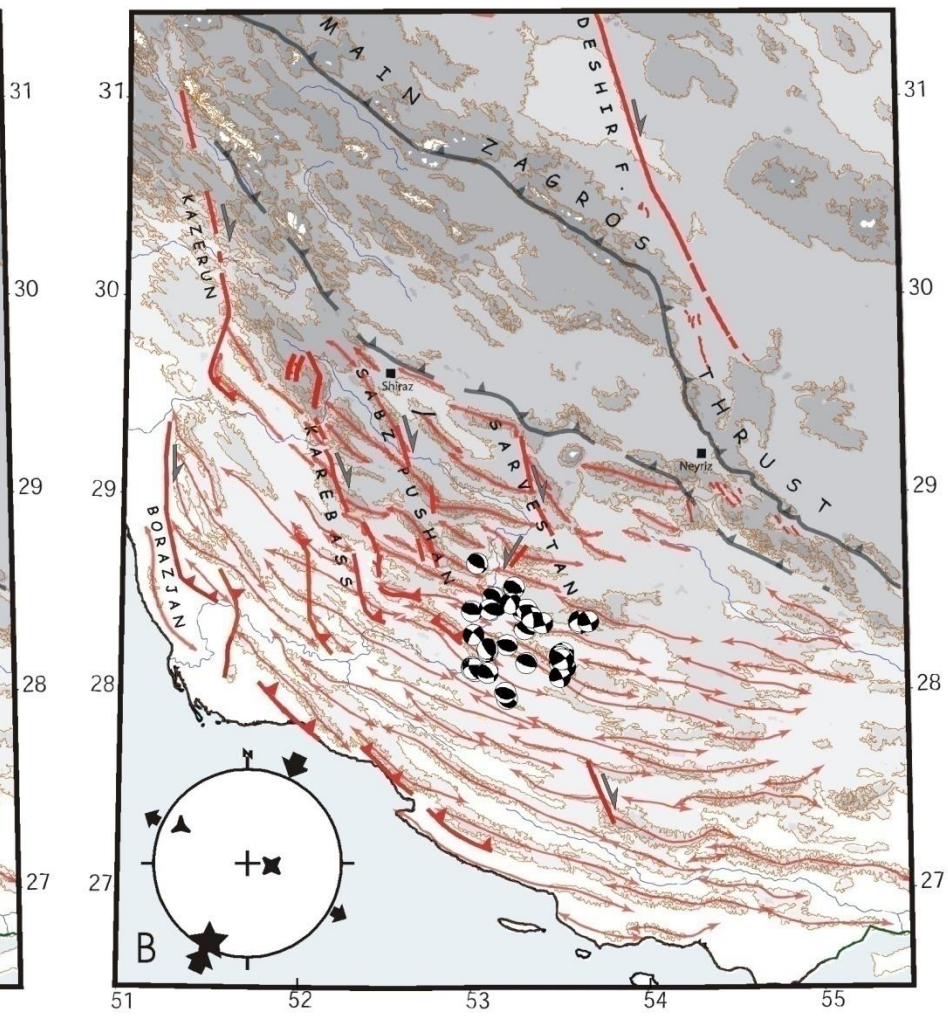
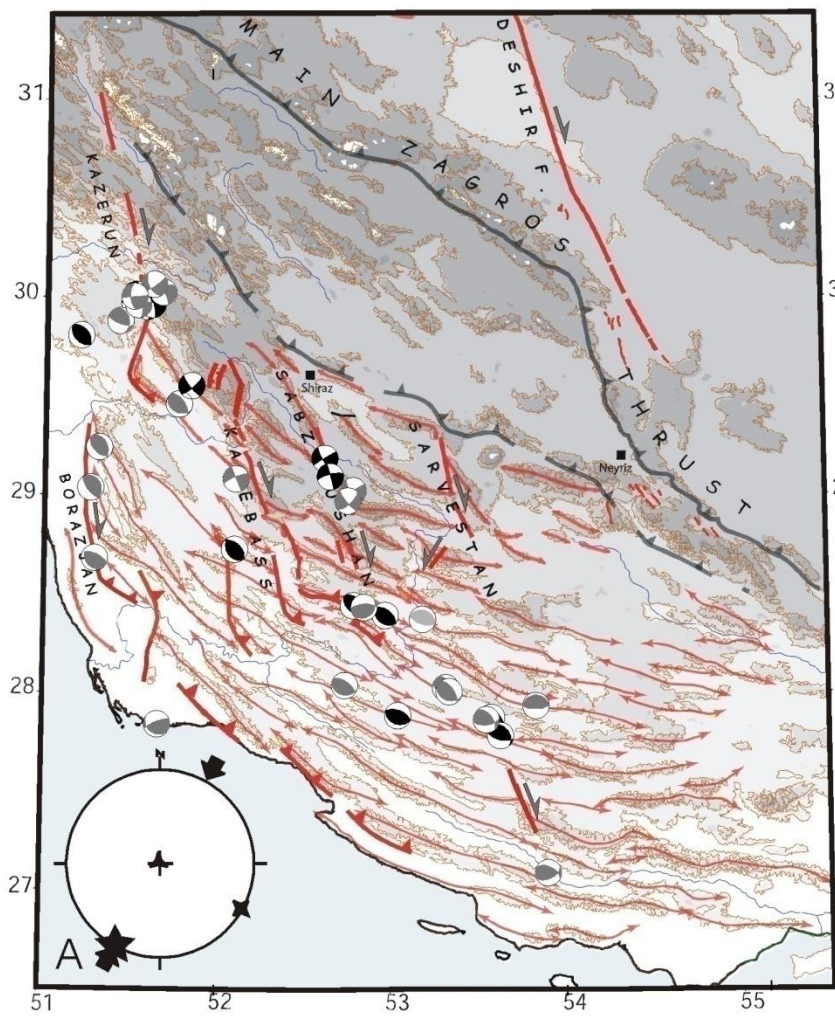
b



c



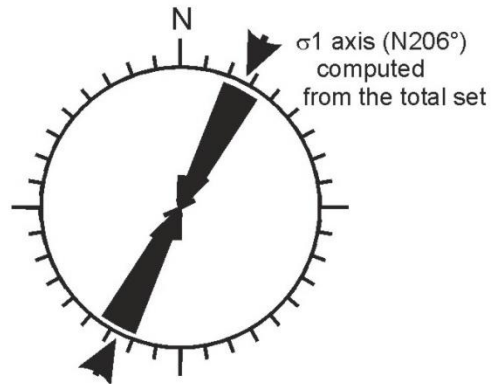
**Stress/shortening patterns in the Zagros belt :
earthquakes focal mechanisms and GPS measurements**



(Lacombe et al., 2006)

P-axes (total)

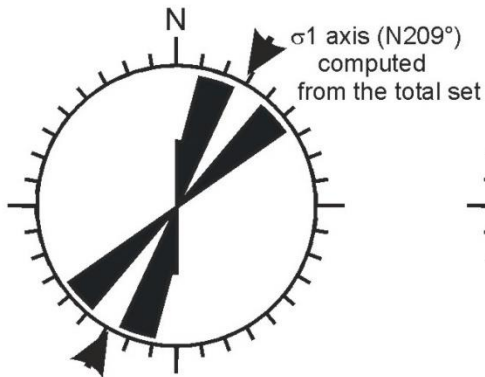
Tatar et al., 2004



Number of data = 50

P-axes (depth <8 km)

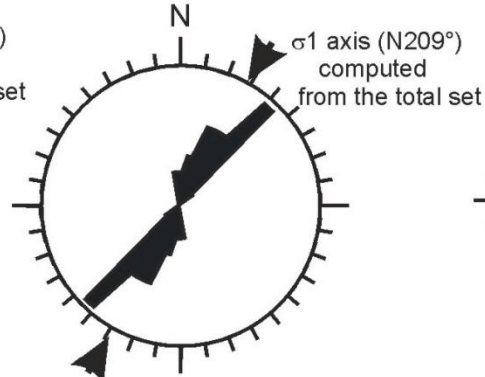
Talebian and Jackson, 2004



Number of data = 9

P-axes (depth >8 km)

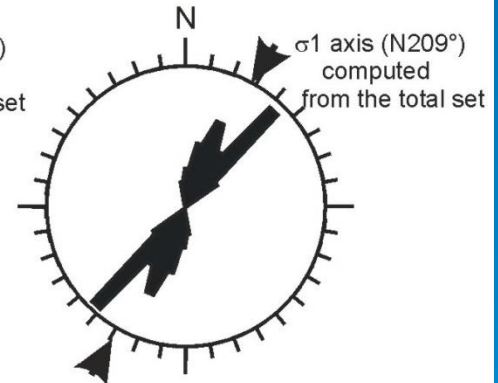
Talebian and Jackson, 2004



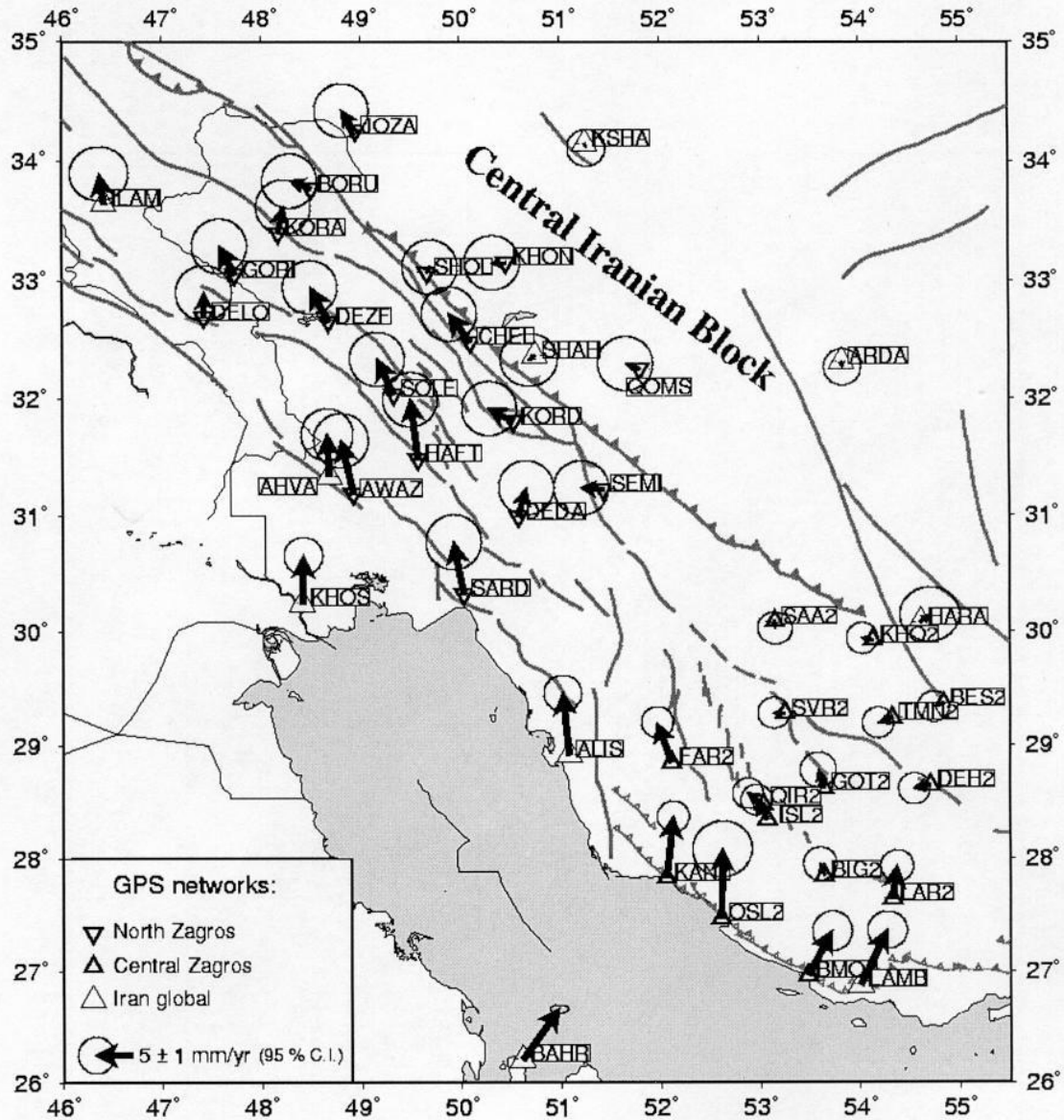
Number of data = 26

P-axes (total)

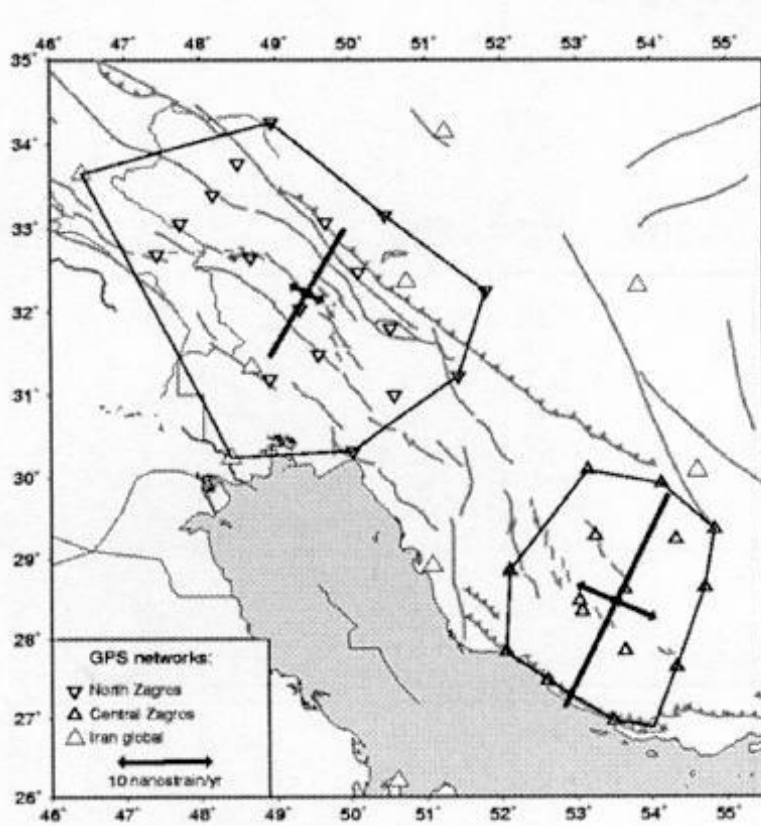
Talebian and Jackson, 2004



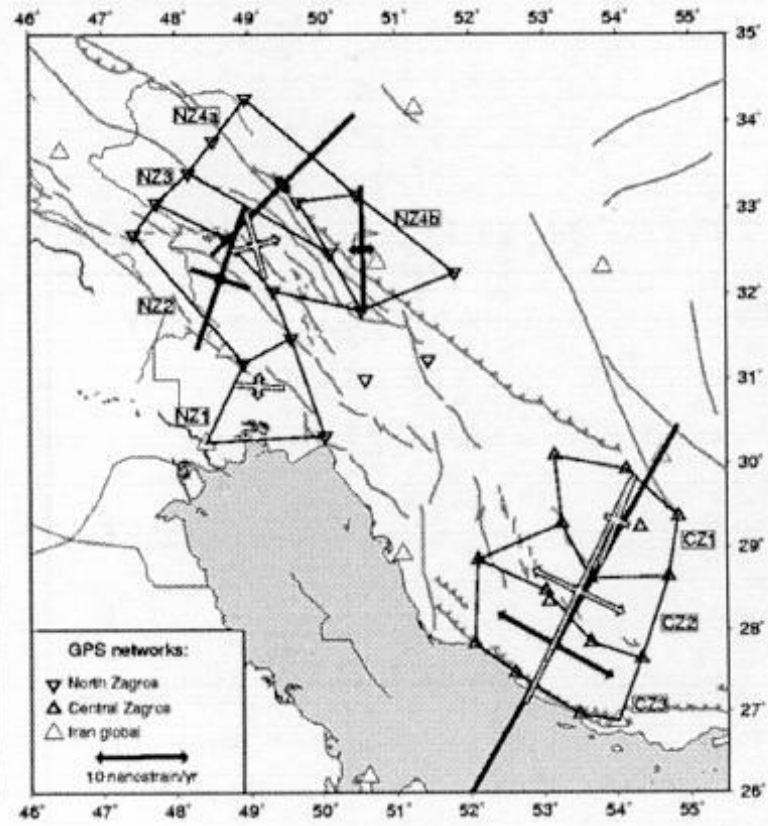
Number of data = 35



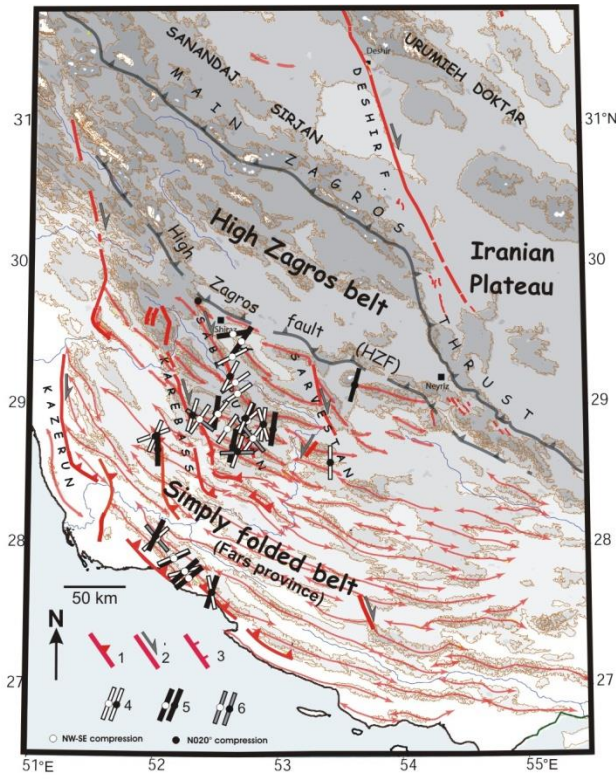
(Walpersdorf et al.,
2006)



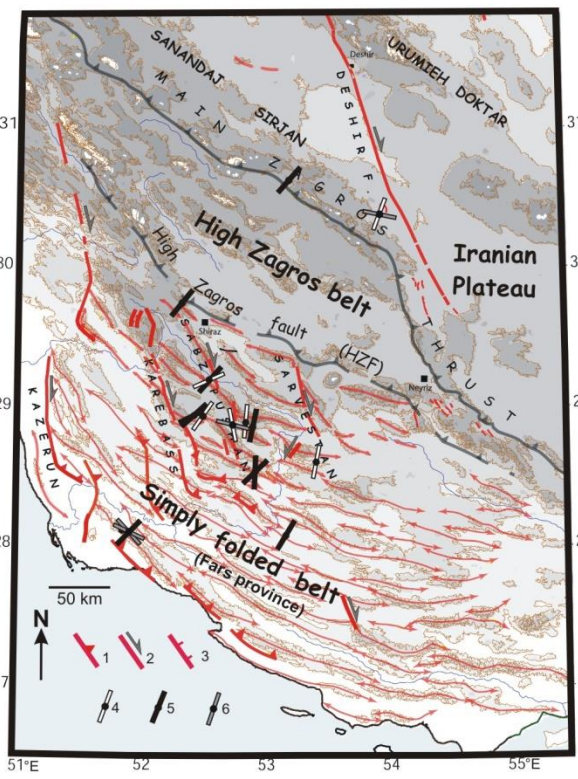
a)



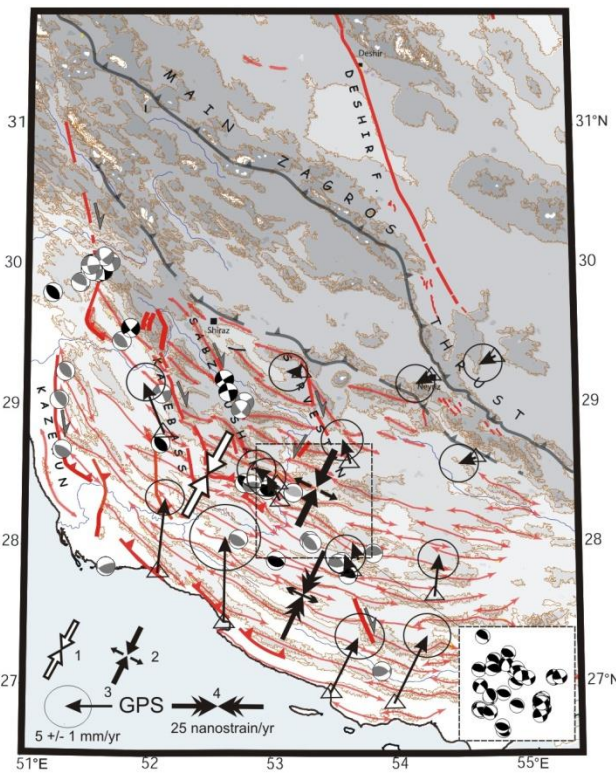
b)



Neogene compressional trends from fault slip data in the cover (Lacombe et al., 2006)



Neogene compressional trends from calcite twin data in the cover (Lacombe et al., 2007)



Current compressional trends from earthquake focal mechanisms in the basement (Lacombe et al., 2006) and GPS shortening rates (Walpersdorf et al., 2006)

→ Neogene collisional stresses consistently recorded at all scales
 → The salt-bearing Hormuz master decollement poorly decouples basement and cover stress fields

- The early stage of reactivation of basement faults likely marks the onset of collisional deformation and intraplate stress build-up in the Zagros basin. Basement-involved deformation started 25-15 Ma and predated the initiation of cover folding.
- This indicates far-field stress transmission from the Arabia-Central Iran plate boundary since late Oligocene-early Miocene , and therefore efficient mechanical coupling between the Arabian and Eurasian plates since that time.

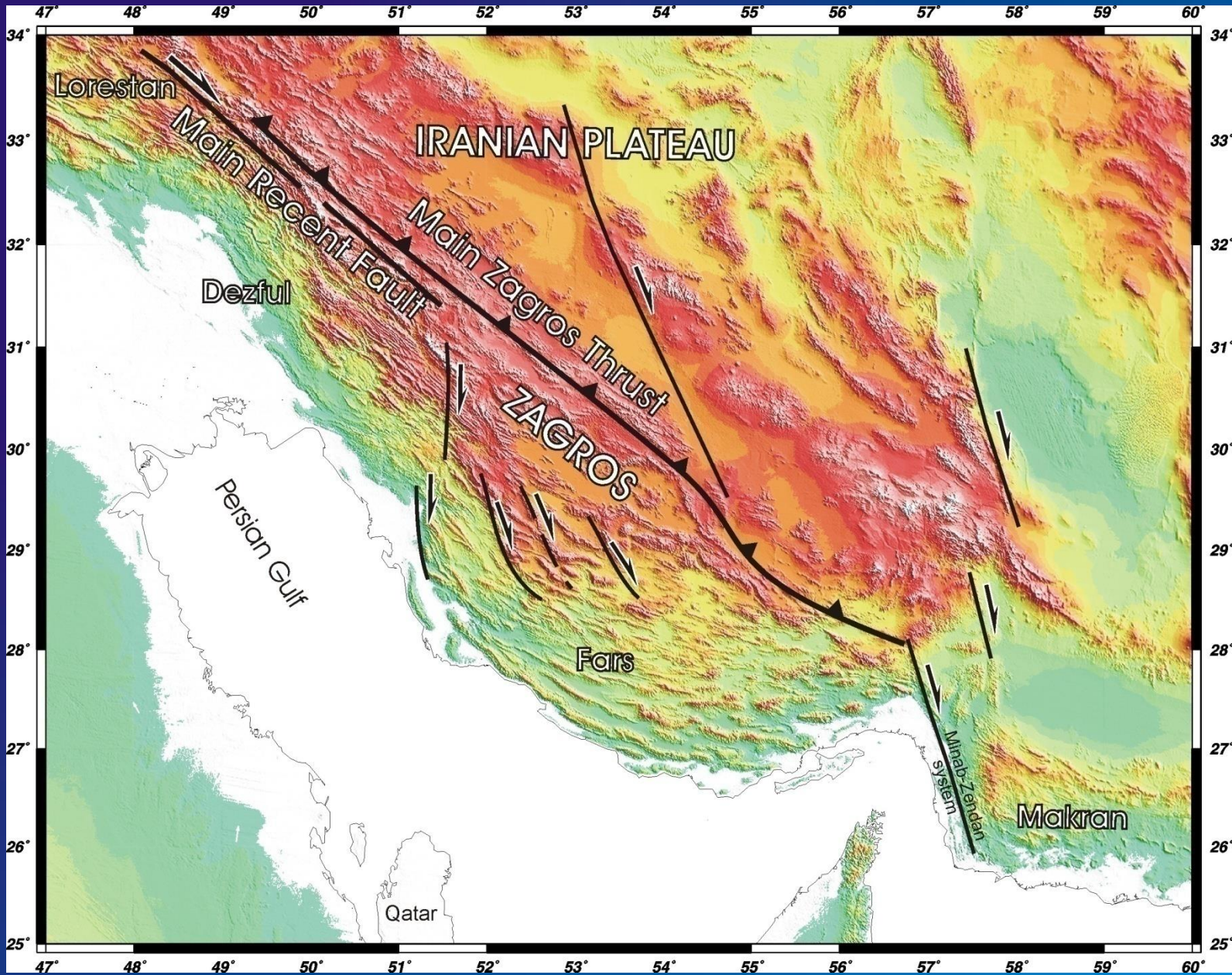
- The transmission of stress through the pre-fractured Arabian crystalline basement was however heterogeneous and complex, so the deformation front propagated in an irregular fashion through the basement and the cover.
- The sequence of deformation includes early inversion of basement faults, then more or less nearly coeval thin-skinned and thick-skinned tectonics.
- Beyond regional implications, this study also puts emphasis on the need of carefully considering pre-folding fracture development related to early reactivation of basement faults in models of folded-fractured hydrocarbon reservoirs.

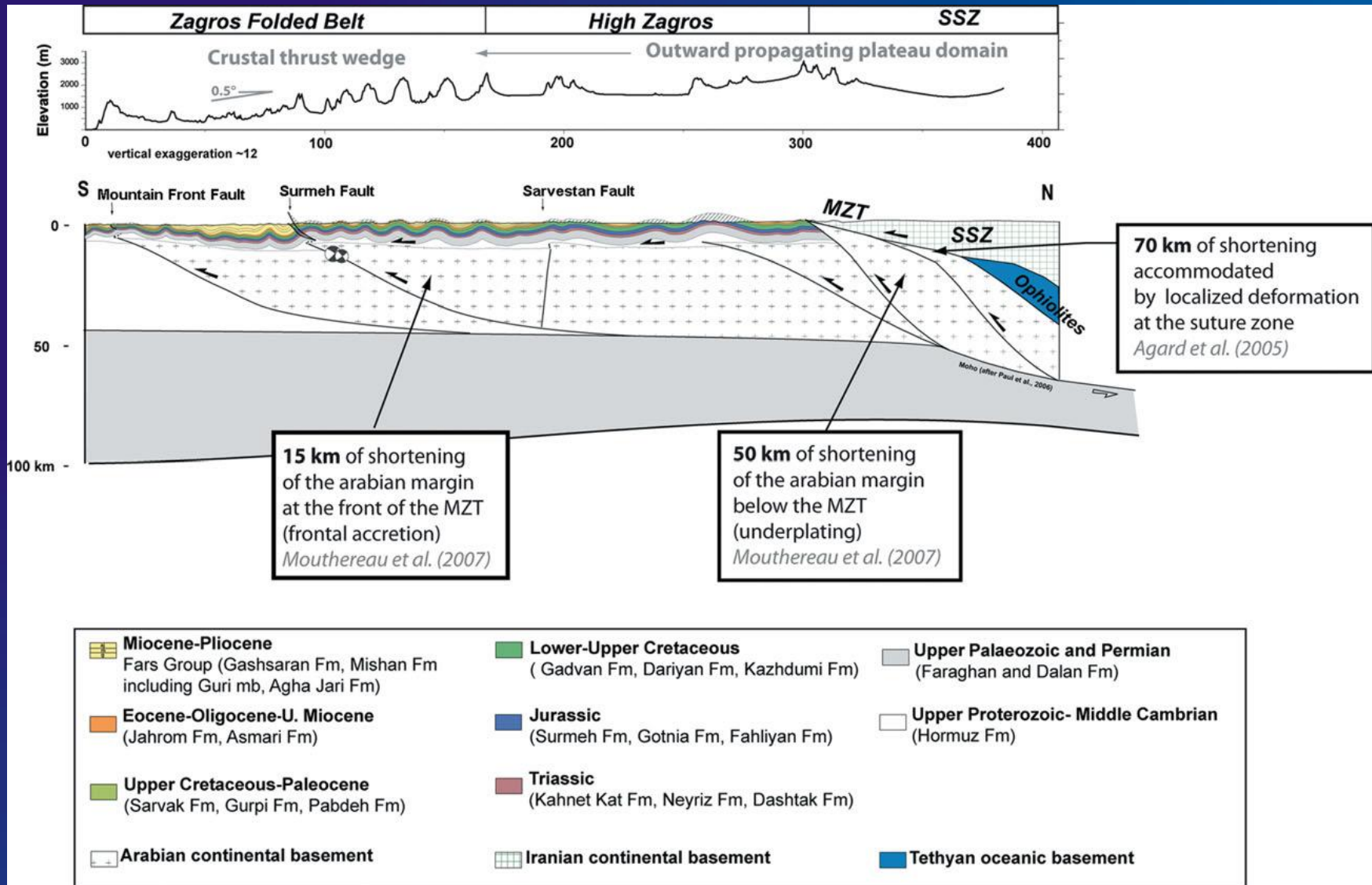
In contrast to other seismic regions of Iran (Alborz, Kopet Dagh), the seismicity in the Zagros is abundant but of low magnitude (only small to moderate earthquakes).

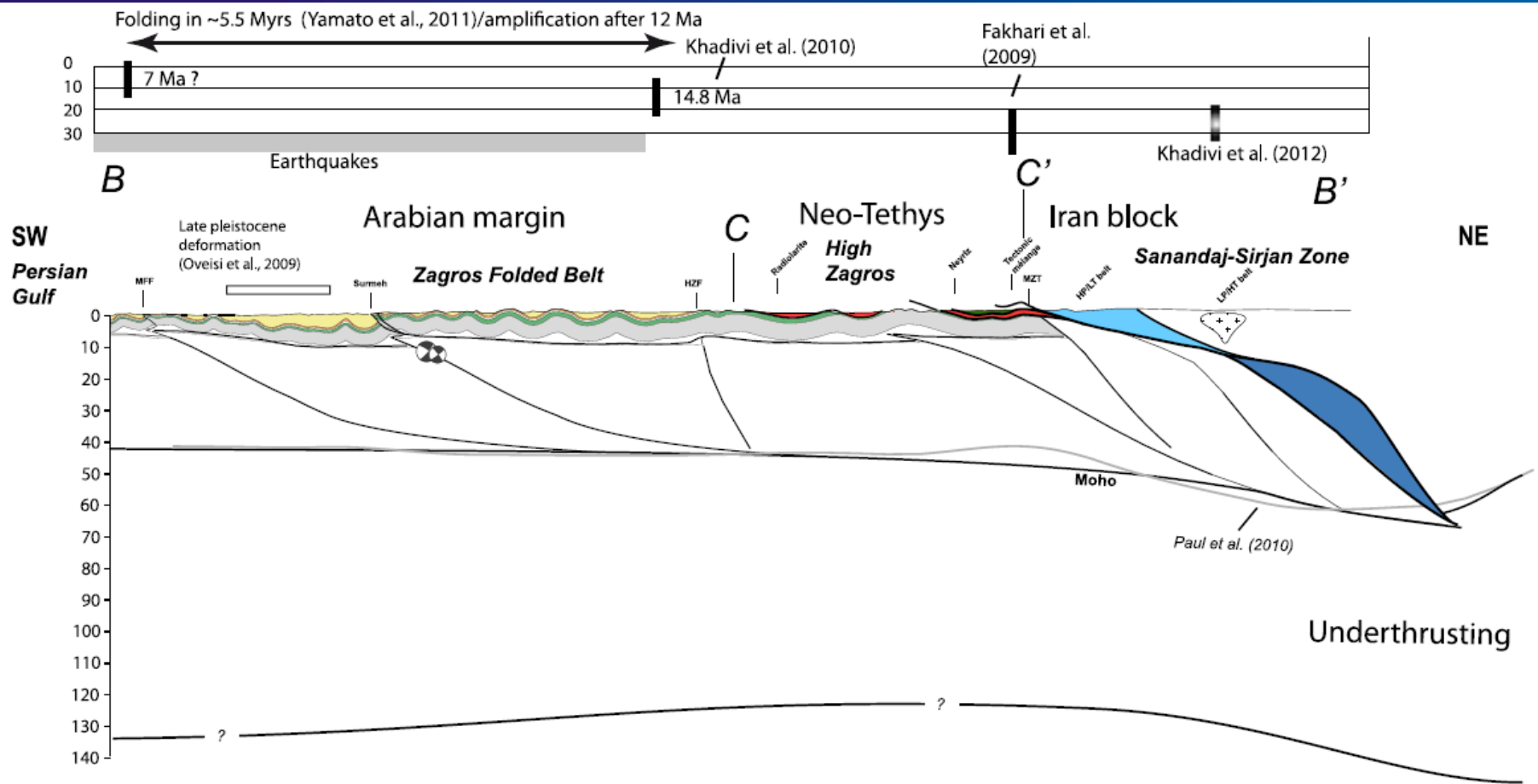
The comparison of seismic and geodetic strain rates indicates mainly aseismic deformation in the Zagros (Masson et al., 2005).

Cover is mainly decoupled from the basement (Hormuz salt); stress transfer from the basement to the cover may however occur during increasing strain rate (i.e., few large earthquakes).

**Crustal rheology, mechanics of folding
and the building of topography in the Zagros**

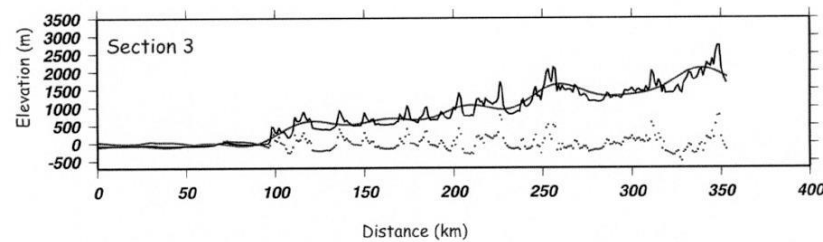
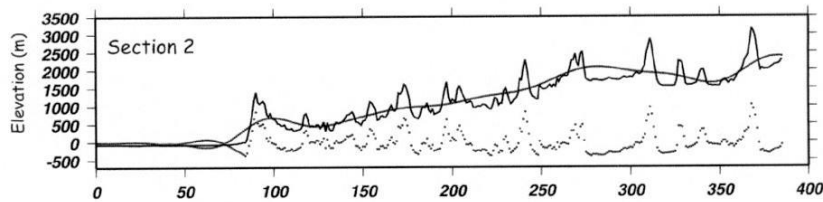
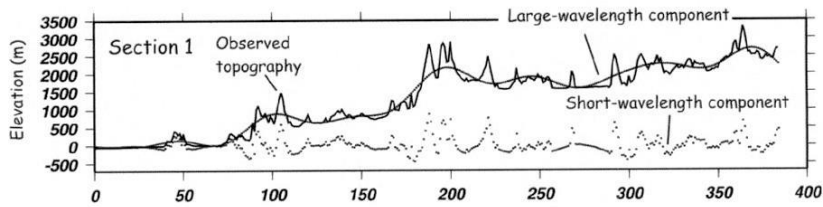
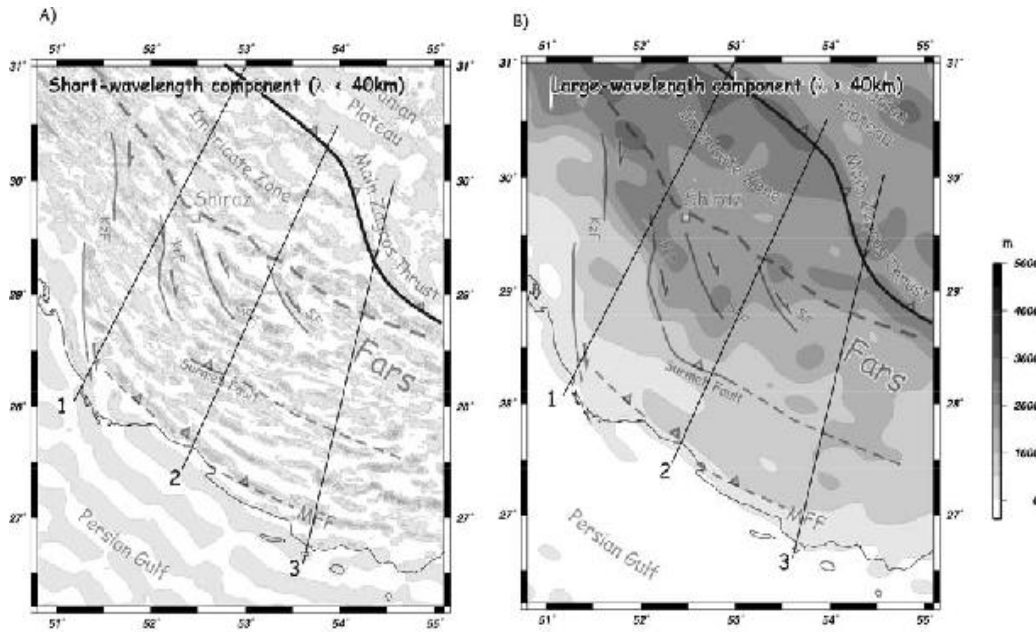




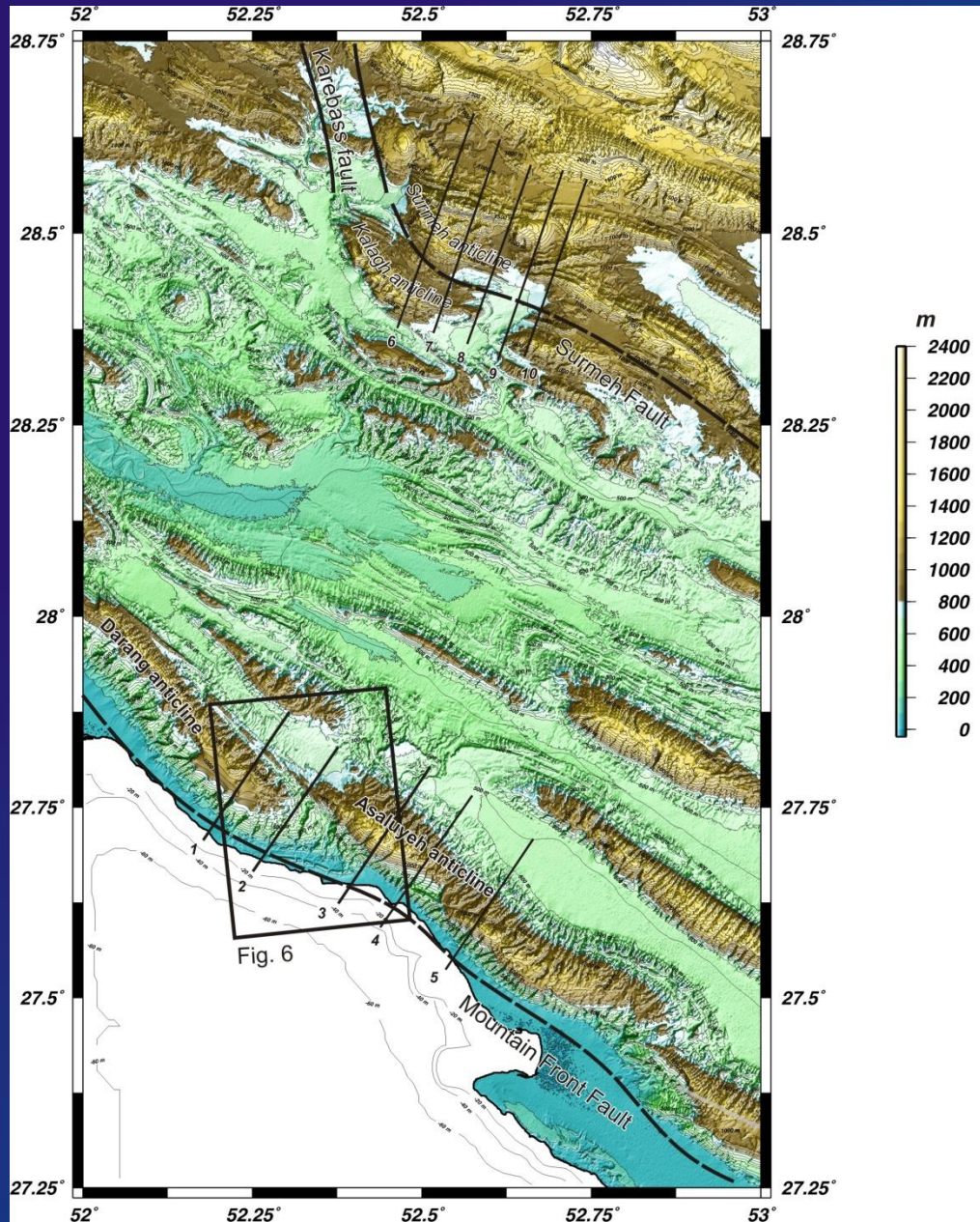


(Mouthereau et al., 2012)

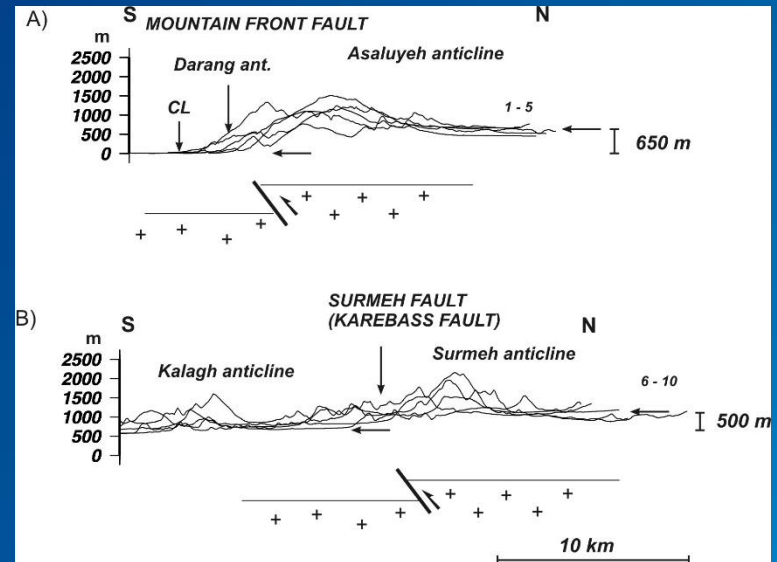
Analysis of topography



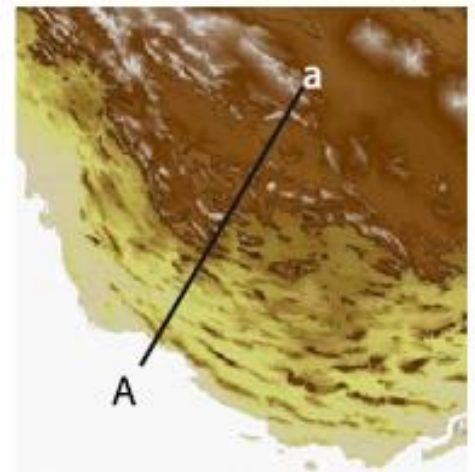
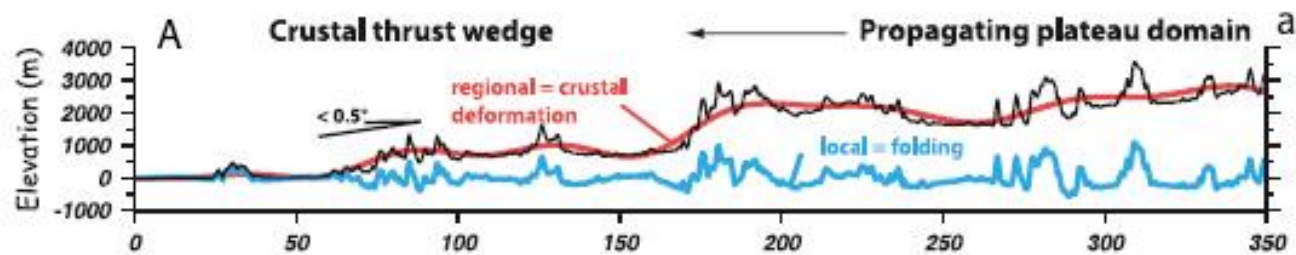
(Mouthereau et al., 2006)



(Mouthereau et al., 2006)

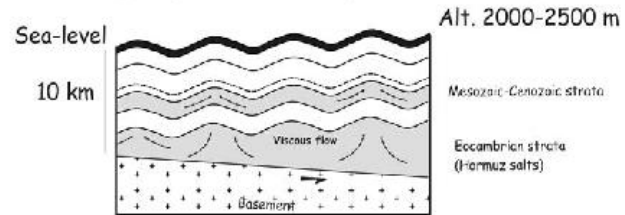


Wavelength components of the topography (Fars region, central Zagros)

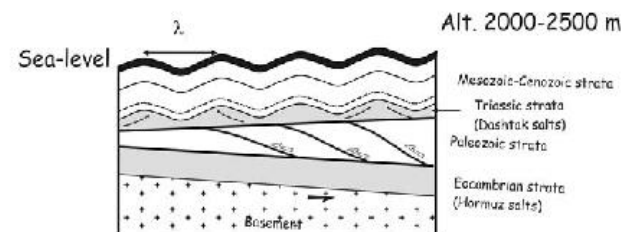
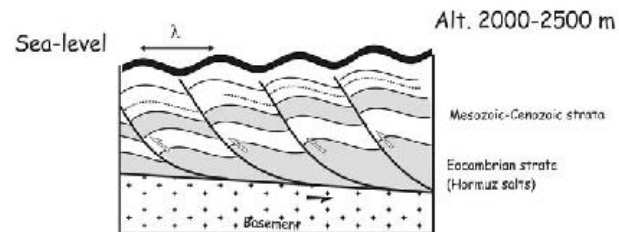


Mouthereau et al. 2012

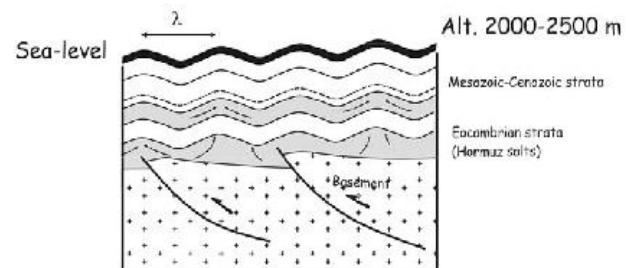
A) Wedge taper controlled by ductile thickening of salt



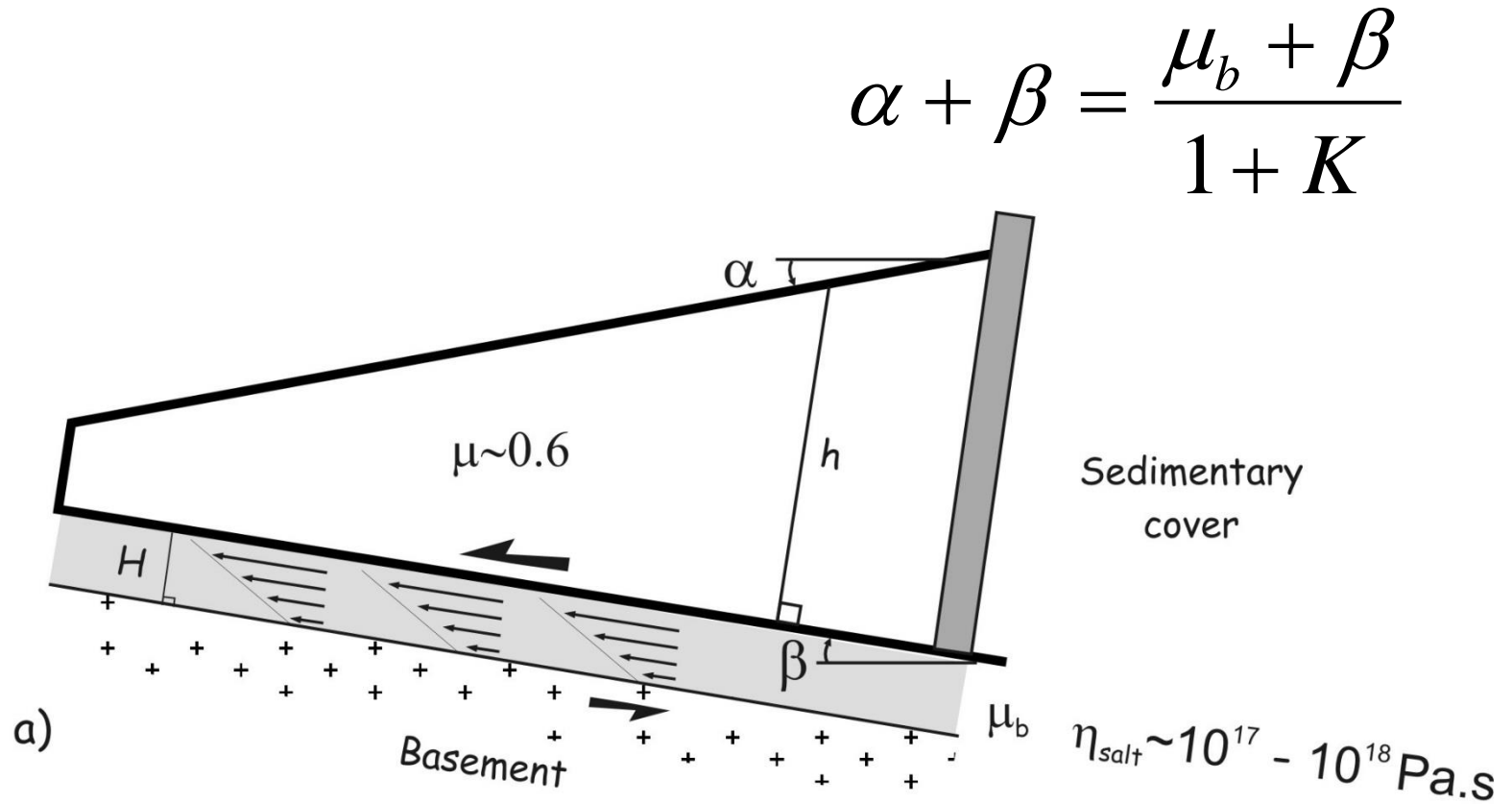
B) Wedge taper controlled by frictional behavior of sedimentary rocks



C) Wedge taper controlled by basement-involved faulting

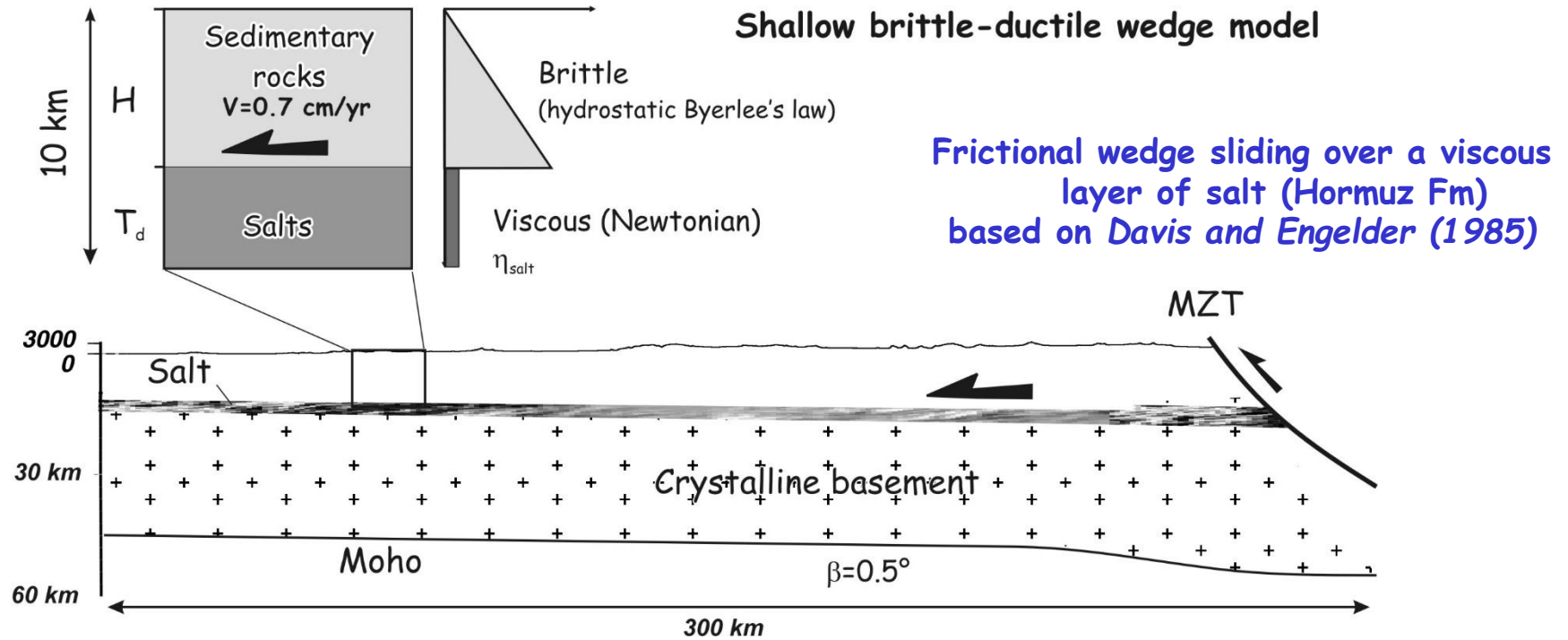


Wedge modelling



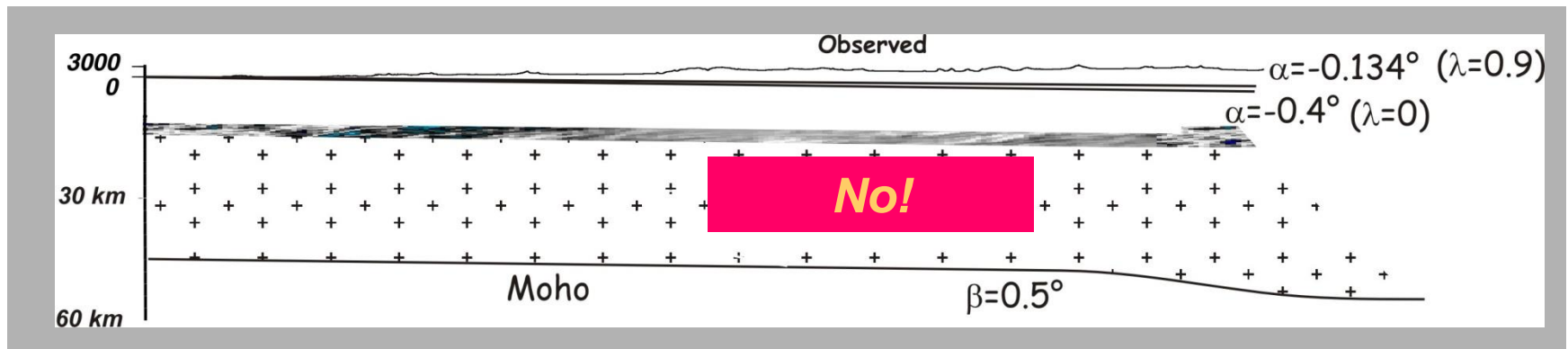
(Mouthereau et al., Geophys. J. Int., 2006)

Salt/cover wedge assumption

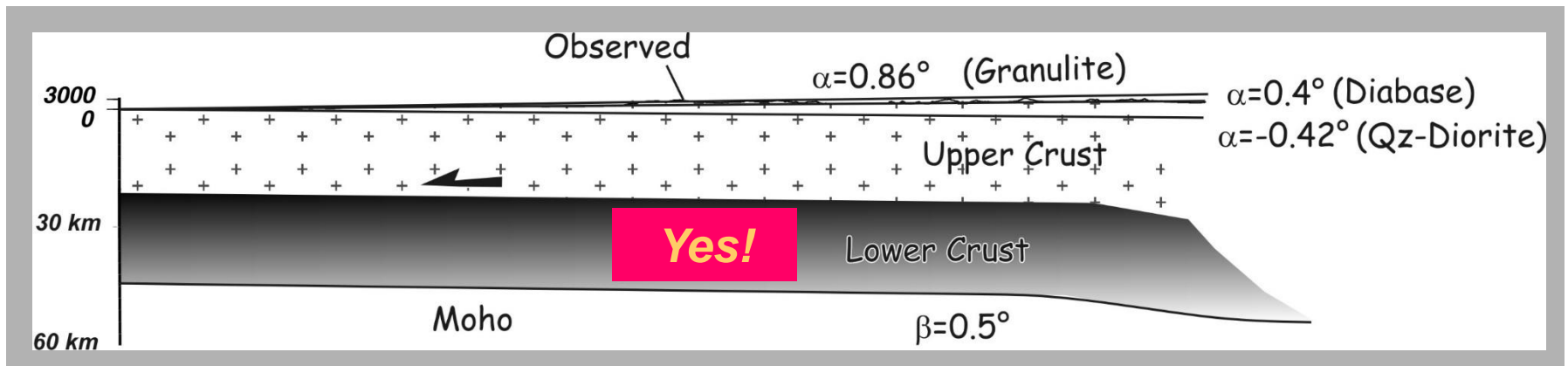
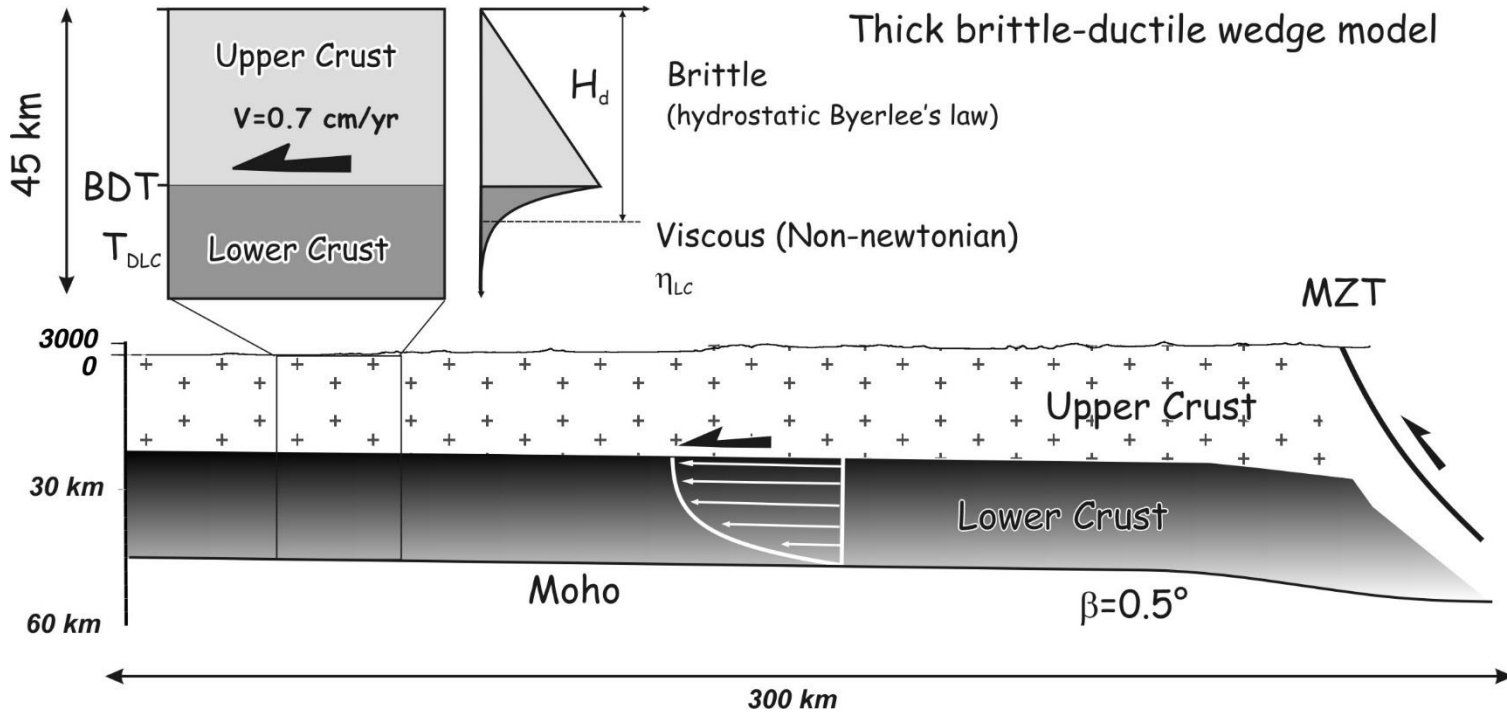


Viscosities 10^{17} to 10^{18} Pa.s (higher bounds)
Internal friction angles $30\text{-}40^\circ$

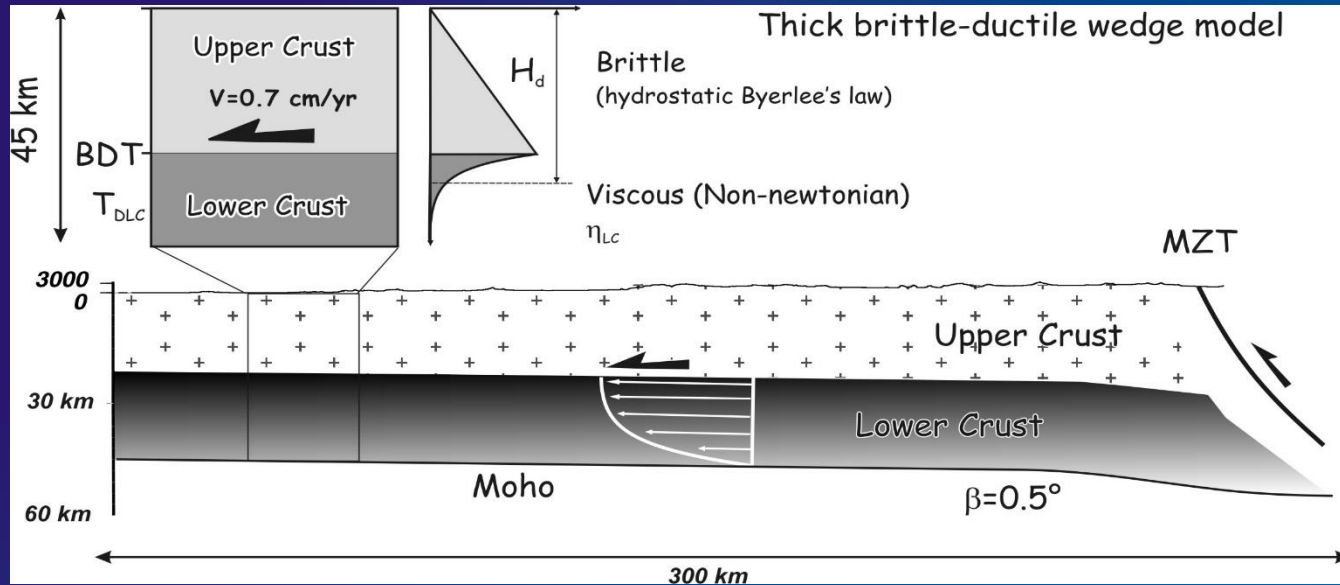
Salt thickness $0.5\text{-}1\text{-}2 \text{ km}$
Variable pore fluid ratio



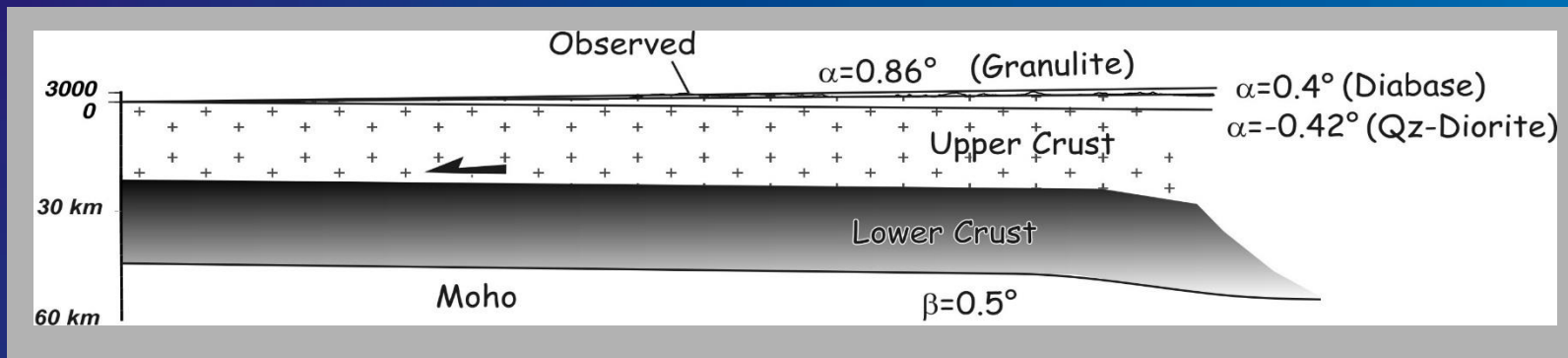
Crustal wedge assumption



Such a model involving a granitic lower crust with sufficient viscosity is able to reproduce the observed topography

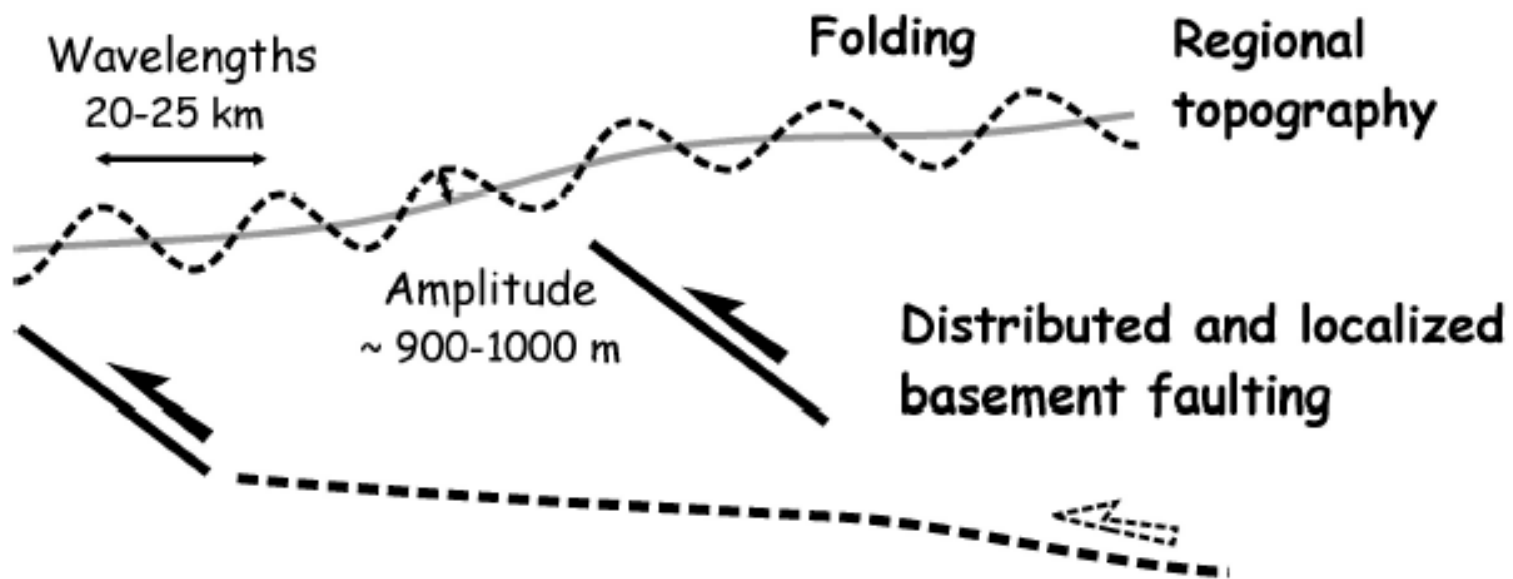


(Mouthereau et al., 2006)

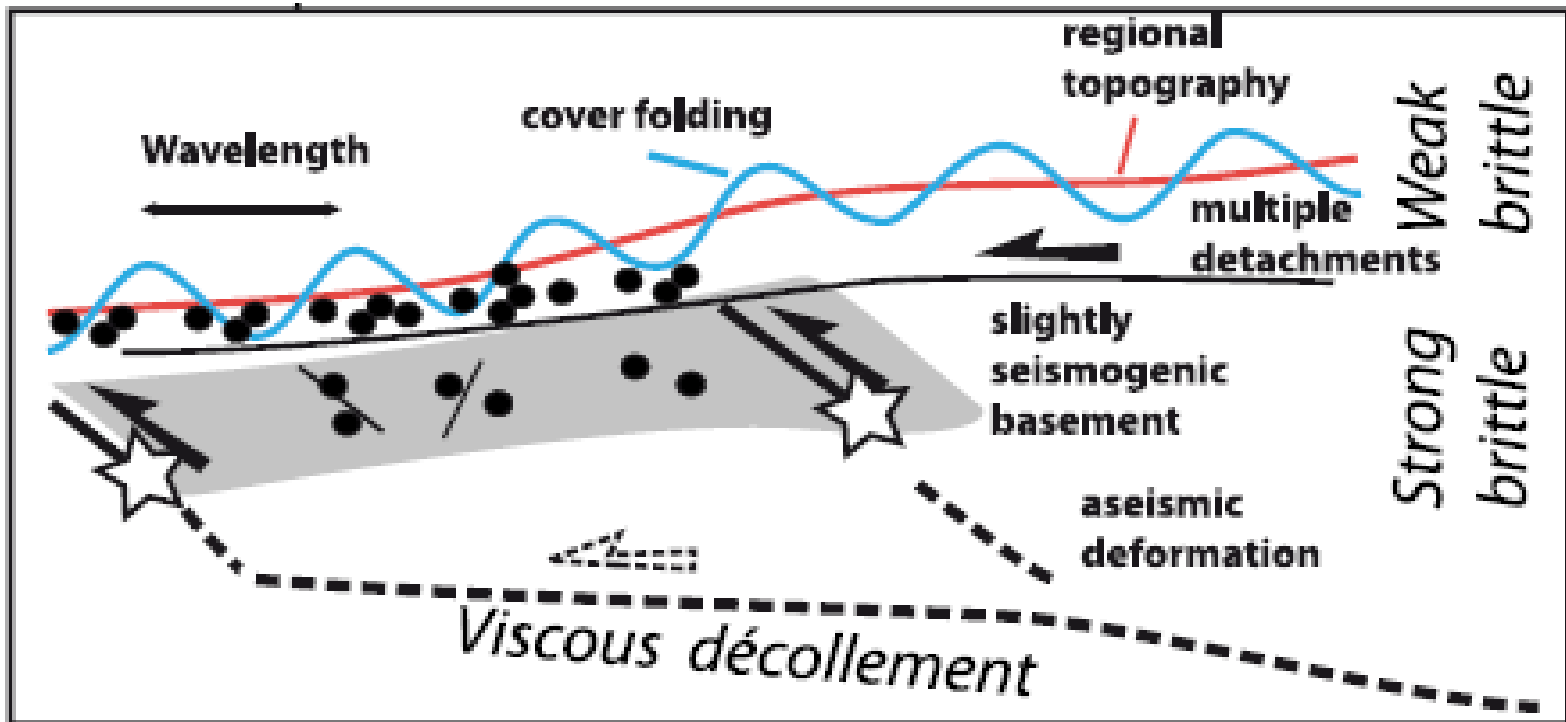


Analytical modelling of the Zagros wedge

→ salt is unable to sustain topography; only a model of critically-tapered brittle-viscous wedge involving the crystalline basement reproduces the observed topographic slopes across the Fars



(Mouthereau et al., 2007)



(Mouthereau et al., 2012)

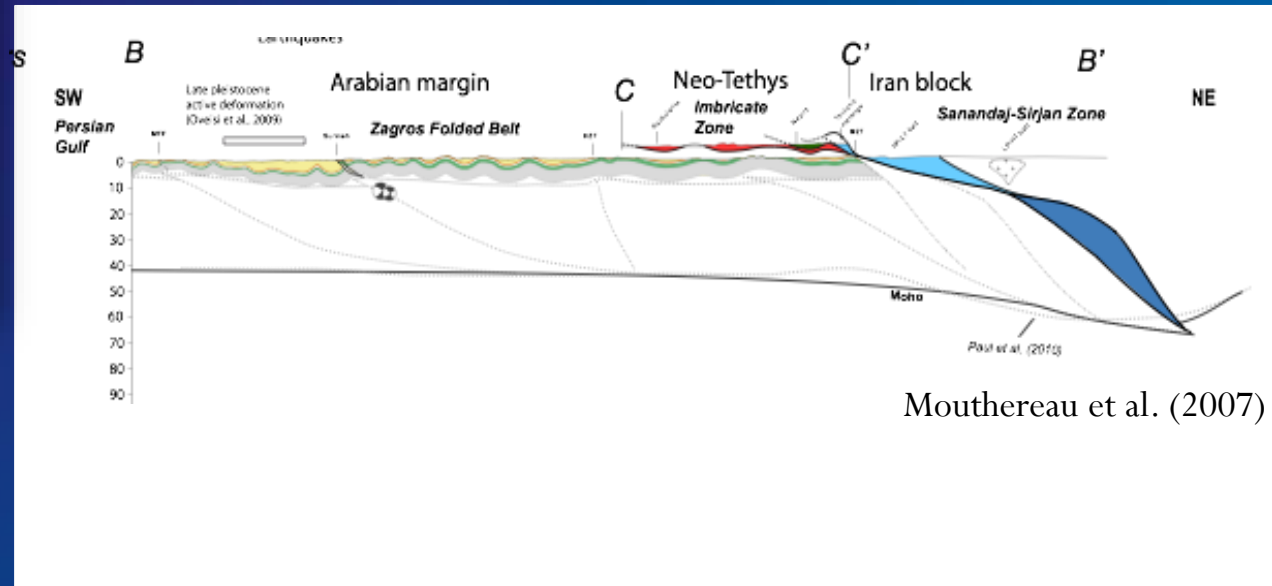
Zagros = superimposed thin-skinned and thick-skinned tectonics

Zagros : inverted Mesozoic rifted margin

Shortening : ~37 %

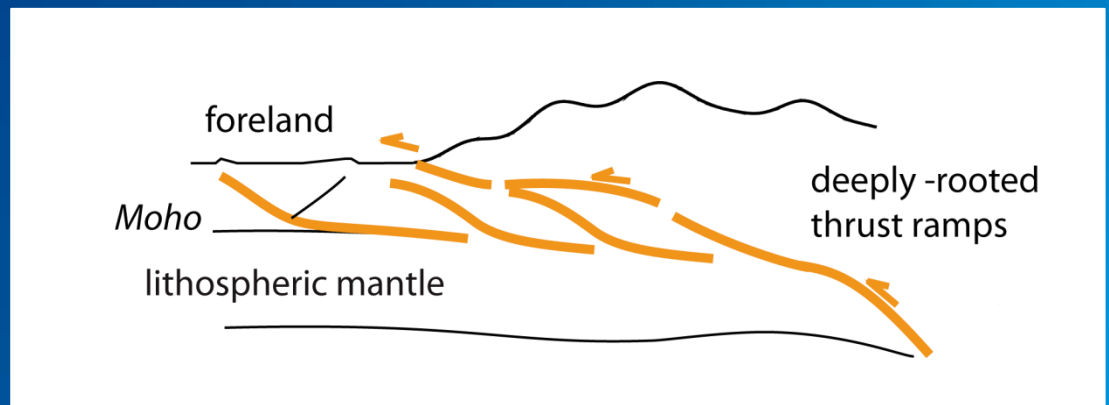


Convergence 7km/Ma
Erosion rate <2 km/Ma



style thick-skinned
"pure-shear"

Decoupling within
middle-lower crust
 $h \sim 15-20$ km





Thank you for your attention...

Suggested readings :

Ahmadhadi F., Daniel J.M., Azzizadeh M. & Lacombe O., 2008, Evidence for pre-folding vein development in the Oligo-Miocene Asmari Formation in the Central Zagros Fold Belt, Iran. **Tectonics**, 27, TC1016

Lacombe O., Mouthereau F., Kargar S. & Meyer B., 2006, Late Cenozoic and modern stress fields in the western Fars (Iran) : implications for the tectonic and kinematic evolution of Central Zagros. **Tectonics**, 25, TC1003

Lacombe O., Bellahsen N. & Mouthereau F., 2011, Fracture patterns in the Zagros Simply Folded Belt (Fars): New constraints on early collisional tectonic history and role of basement faults. In “Geodynamic evolution of the Zagros”, O. Lacombe, B. Grasemann and G. Simpson eds, **Geological Magazine**, 148, 940-963

Mouthereau F., Lacombe O. & Meyer B., 2006, The Zagros Folded Belt (Fars, Iran) : constraints from topography and critical wedge modelling, **Geophys. J. Int.**, 165(1), 336-356

Mouthereau F., Tensi J., Bellahsen N., Lacombe O., Deboisgrollier T. & Kargar S., 2007, Tertiary sequence of deformation in a thin-skinned/thick-skinned collision belt : the Zagros Folded Belt (Fars, Iran). **Tectonics**, 26, TC5006

Mouthereau F., Lacombe O. & Verges J., 2012. Building the Zagros collisional orogen: timing, strain distribution and the dynamics of Arabia/Eurasia plate convergence. **Tectonophysics**, 532-535, 27-60

Talebian, M.& Jackson J.A. , 2004. A reappraisal of earthquake focal mechanisms and active shortening in the Zagros mountains of Iran, **Geophys. J. Int.**,156, 506 – 526.